

Planning studies for a non-invasive treatment of atrial fibrillation with scanned ion beams

Planungsstudien zur nicht invasiven Behandlung von Vorhofflimmern mit gescannten Ionenstrahlen

Zur Erlangung des Grades eines Doktors der Naturwissenschaften (Dr. rer. nat.)
vorgelegte Dissertation von MSc Anna Maria Constantinescu aus Bukarest, Rumänien
April 23, 2014 — Darmstadt — D 17



Planning studies for a non-invasive treatment of atrial fibrillation with scanned ion beams
Planungsstudien zur nicht invasiven Behandlung von Vorhofflimmern mit gescannten Ionenstrahlen

Vorgelegte Dissertation von MSc Anna Maria Constantinescu aus Bukarest, Rumänien

1. Gutachten: Prof. Dr. Marco Durante
2. Gutachten: Prof. Dr. Christoph Bert

Tag der Einreichung:

Darmstadt – D 17

Summary

One treatment modality for atrial fibrillation, the most common cardiac arrhythmia, is radiofrequency catheter ablation in which fibrotic tissue is created around the pulmonary veins. The procedure has major drawbacks, a new treatment modality would hence be beneficial. This is the first *in silico* study for the feasibility of a non-invasive treatment of atrial fibrillation with scanned ion beams, which are successfully used in cancer radiotherapy. In collaboration with the Mayo Clinic (Rochester, Minnesota, USA) the first comparison between different irradiation techniques to cardiac target volumes was carried out in this work. In the presented results it was shown that the dose deposition to organs at risk could be drastically reduced compared to a potential non-invasive treatment of atrial fibrillation with photons. As a result of the actively applied ion beam, interference effects were observed when irradiating the moving cardiac volumes. The motion influences of respiration and heartbeat were studied individually and the resulting displacement was examined. To achieve a homogenous dose deposition in the moving target volumes, motion mitigation techniques (gating and rescanning) were successfully applied. The results will be validated in animal experiments at GSI in 2014.

Zusammenfassung

Eine Behandlungsmöglichkeit für Vorhofflimmern, der verbreitetsten Art von Herzrhythmusstörungen, ist Radiofrequenzablation mit Hilfe von Kathetern, bei der Narbengewebe um die Pulmonarvenen erzeugt wird. Dieser Eingriff hat schwerwiegenden Nachteile, so dass eine neue Behandlungsmöglichkeit wünschenswert wäre. Dies ist die erste *in silico* Studie, die die Durchführbarkeit einer nicht-invasiven Behandlungsmöglichkeit für Vorhofflimmern mit gescannten Ionenstrahlen untersucht. Diese werden erfolgreich in der Strahlentherapie von Tumoren eingesetzt. In dieser Arbeit wurde in Kollaboration mit der Mayo Clinic (Rochester, Minnesota, USA) der erste Vergleich zwischen verschiedenen Bestrahlungsarten von Zielvolumina im Herzen durchgeführt. In den Ergebnissen konnte gezeigt werden, dass die Dosisbelastung der umliegenden Risikoorgane im Vergleich zu einer potentiellen nicht-invasiven Behandlung von Vorhofflimmern mit Photonen drastisch reduziert werden konnte. Aufgrund des aktiv applizierten Ionenstrahls wurden Interferenzeffekte bei der Bestrahlung bewegter Herzvolumina beobachtet. Der Bewegungseinfluss von Atmung und Herzschlag wurden unabhängig voneinander untersucht und die resultierende Auslenkung erforscht. Um eine homogene Dosis in den bewegten Zielvolumen zu erreichen wurden bewegungskompensierende Methoden (gating und rescanning) erfolgreich angewandt. Die Ergebnisse sollen in Tierstudien, die 2014 an der GSI durchgeführt werden, validiert werden.



Publications related to this work

Peer-reviewed articles

Seregni M, Kaderka R, Fattori G, Riboldi M, Pella A, **Constantinescu A**, Saito N, Durante M, Cerveri P, Bert C, Baroni G: Tumor tracking based on correlation models in scanned ion beam therapy: an experimental study; *Phys Med Biol*; 58(13); 2013

Graeff C, **Constantinescu A**, Lüchtenborg R, Durante M, Bert C: Multigating: 4D optimized beam tracking in scanned ion beam therapy; *Technol Cancer Res Treat.*; Epub ahead of print DOI: 10.7785/tcrexpress.2013.6002772013; 2013

Fattori G, Saito N, Seregni M, Kaderka R, Pella A, **Constantinescu A**, Riboldi M, Steidl P, Cerveri P, Bert C, Durante M and Baroni G: Commissioning of an integrated platform for time-resolved treatment delivery in scanned ion beam therapy by means of optical motion monitoring; *Technol Cancer Res Treat.*; Epub ahead of print DOI: 10.7785/tcrexpress.2013.600275; 2013

Lehmann HI, Richter D, Prokesch H, Graeff C, Prall M, Simoniello P, Fournier C, Bauer J, Kaderka R, Weymann A, Szabo G, Sonnenberg K, **Constantinescu A**, Johnson SB, Haberer T, Debus J, Durante M, Bert C and Packer DL: AV node Ablation in Langendorff-perfused Porcine Hearts Using Carbon Ion Particle Therapy: Methods and an In vivo Feasibility Investigation for Catheter-free Ablation of Cardiac Arrhythmias; submitted to *Circulation*; April 2014

GSI scientific reports

Constantinescu A, Lüchtenborg R, Durante M, Bert C: Experimental validation of motion phase interpolation when tracking a moving tumor with a scanned ion beam; *GSI Scientific Report 2011*, 541

Constantinescu A, Lehmann HI, Graeff C, Packer D, Durante M, Bert C: Influence of cardiac motion on pulmonary veins for the non-invasive treatment of atrial fibrillation with a scanned carbon ion beam; *GSI Scientific Report 2012*, 472

Constantinescu A, Lehmann HI, Graeff C, Packer D, Durante M, Bert C: Influence of cardiac motion on porcine AV node for the non-invasive treatment of atrial fibrillation with a scanned carbon ion beam; *GSI Scientific Report 2013*

Articles

Tami Freeman: Carbon ions tackle atrial fibrillation; medicalphysicsweb.org; June 20; 2013

Conference contributions

Constantinescu A, Blanck O, Durante M, Bert C (2012). Non-invasive treatment of atrial fibrillation with a scanned carbon ion beam; *Radiotherapy and Oncology*, 102 (Supplement 1); S215. Oral presentation

Constantinescu A, Blanck O, Durante M, Bert C (2012). Non-invasive treatment of atrial fibrillation with a scanned carbon ion beam; *DPG spring meeting*. Oral presentation

Constantinescu A, Lehmann HI, Graeff C, Packer DL, Durante M and Bert C (2013). Planning studies for non-invasive isolation of the pulmonary veins with a scanned carbon ion beam; *HRS Scientific Meeting*. Oral presentation

Constantinescu A, Lehmann HI, Graeff C, Packer DL, Durante M and Bert C (2013). Planning studies for non-invasive isolation of the pulmonary veins with a scanned carbon ion beam; *PTCOG 52*. Oral presentation

Constantinescu A, Lehmann HI, Graeff C, Packer DL, Durante M and Bert C (2013). Non-invasive treatment of atrial fibrillation with a scanned carbon ion beam; *Particle Radiosurgery: A new Frontier in Physics in Medicine*. Poster presentation

Constantinescu A, Lehmann HI, Graeff C, Packer DL, Durante M and Bert C (2014). Catheter-free ablation of atrial fibrillation: further planning studies in patient data using a scanned carbon ion beam for pulmonary vein isolation; *HRS Scientific Meeting*. Moderated poster presentation

Contents

Motivation	11
1. Introduction - research background and fundamentals	13
1.1. Physical and biological basics of radiotherapy	14
1.1.1. Dose	14
1.1.2. Interaction of radiation with matter	14
1.1.3. Radiobiology	21
1.2. Radiotherapy	24
1.2.1. Photon therapy	24
1.2.2. Carbon therapy	25
1.2.3. Treatment planning	30
1.2.4. Organ motion in radiotherapy	32
1.3. Atrial fibrillation	40
1.3.1. Heart's conduction system	41
1.3.2. Types of atrial fibrillation	43
1.3.3. Possible causes for atrial fibrillation and risk factors	44
1.3.4. Treatment modalities	45
2. Irradiation of pulmonary veins under influence of respiration in human data	53
2.1. Material and methods	54
2.1.1. Treatment planning input data	54
2.1.2. Treatment planning parameters	55
2.1.3. Treatment planning studies	57
2.1.4. Analysis	57
2.2. Results	58
2.2.1. Motion assessment of respiration	58
2.2.2. Motion mitigation techniques for respiration	62
2.3. Discussion	73
2.4. Conclusion	75

3. Irradiation of pulmonary veins under influence of heartbeat in human data	77
3.1. Material and methods	78
3.1.1. Treatment planning input data	78
3.1.2. Treatment planning parameters	79
3.1.3. Treatment planning studies	81
3.1.4. Analysis	81
3.2. Results	83
3.2.1. Beam direction	83
3.2.2. Safety margin limitations	90
3.2.3. Motion assessment of heartbeat	96
3.2.4. Motion mitigation techniques for heartbeat	100
3.3. Discussion	107
3.3.1. Dose to critical structures	107
3.3.2. Beam channel directions and safety margins	109
3.3.3. Movement of PVs in cardiac cycle	110
3.3.4. Rescanning as motion mitigation technique	111
3.4. Conclusion	112
4. Irradiation of cardiac target volumes in porcine data	113
4.1. Material and methods	114
4.1.1. Treatment planning input data	114
4.1.2. Treatment planning parameters	115
4.1.3. Treatment planning studies	116
4.1.4. Analysis	116
4.2. Results	117
4.2.1. Motion directions and magnitude	117
4.2.2. Dose to organs at risk when irradiating the AV node	125
4.2.3. Motion mitigation techniques for AV node irradiation	126
4.3. Discussion	133
4.3.1. Movement of cardiac target volumes in cardiac cycle	134
4.3.2. Dose to organs at risk for the irradiation of AV node	135
4.3.3. Rescanning as motion mitigation technique for AV node irradiation	136
4.4. Conclusion	137
5. Discussion	139
5.1. Dose deposition	140
5.1.1. Dose to target area	140
5.1.2. Dose to OAR	141

5.1.3. Dose to OAR: Comparison to photons	143
5.2. Treatment planning of cardiac target volumes with scanned ions	150
5.2.1. Motion of cardiac volumes	150
5.2.2. Contrast enhanced CT scans	152
5.2.3. Motion mitigation techniques	152
6. Conclusion and outlook	155
A. Appendix of chapter 2	159
A.1. Motion of PV due to respiration	159
A.2. Values of dose analysis parameters for all patients	165
B. Appendix of chapter 3	189
B.1. Motion of PV due to heartbeat	189
B.2. Values of dose analysis parameters for all patients	192
C. Appendix of chapter 4	203
C.1. Motion of target volumes in contrast enhanced CT scans	203
C.2. Motion of AV node in native CT scan	209



List of Abbreviations

3DCRT	three dimensional conformal radiotherapy	LET	linear energy transfer
4DCT	time resolved computed tomography	LR	left-right
AF	atrial fibrillation	LV	left ventricle
AP	anterior-posterior	MDACC	MD Anderson Cancer Center
AV	atrioventricular	MLC	multileaf collimators
CNAO	Centro Nazionale di Adroterapia Oncologica	MP	motion phase
CT	computed tomography	MRI	magnetic resonance imaging
CTV	clinical target volume	NIRS	National Institute of Radiological Sciences
CTI	cavotricuspid isthmus	OAR	organ at risk
D5-D95	measure for dose homogeneity	PET	positron emission tomography
DKFZ	Deutsches Krebsforschungszentrum	PMMA	polymethyl methacrylate
DSB	double strand breaks	PSI	Paul Scherer Institut
DVH	dose volume histogram	PTV	planning target volume
ECG	Electrocardiograph	PV	pulmonary vein
FWHM	full width at half maximum	RA	right atrium
GSI	GSI Helmholtzzentrum für Schwerionenforschung GmbH	RBE	relative biological effectiveness
GTV	gross tumor volume	RCA	right coronary artery
GyE	Gray equivalent	RTOG	Radiotherapy Oncology Group
HIT	Heidelberg Ion-Beam Therapy Centre	RV	right ventricle
HU	Hounsfield unit	SA	sinoatrial
IES	iso-energy slice	SI	superior-inferior
IM	internal margin	SBRT	stereotactic body radiotherapy
IMPT	intensity modulated particle therapy	SFUD	single field uniform dose
IMPT(OAR)	IMPT with included OAR	SOBP	spread out Bragg peak
IMRT	intensity modulated radiotherapy	SPV	superior pulmonary vein
IPV	inferior pulmonary vein	SSB	single strand break
ITV	internal target volume	TRiP	treatment planning for carbon ion radiotherapy
LA	left atrium	V95	volume which received at least 95% of the target dose (dose coverage)
LCA	left coronary artery	V107	volume which received at least 107% of the target dose (over dosage)
LEM	local effect model		



Motivation

Atrial fibrillation is the most common cardiac arrhythmia [ESC10, CE09]. One out of four people over forty are estimated to suffer from this condition in the course of their lifetime. While genetics play a role in the development of atrial fibrillation in younger patients, age is an important risk factor for this cardiac arrhythmia and the prevalence is estimated to double in the next fifty years due to aging of society. In atrial fibrillation, an unorganized atrial activity leads to a quivering motion and hence the heart is not able to sustain a healthy pumping rhythm. This is not in itself life threatening but it alters the quality of life of the patients and increases the risk of the patients to suffer a stroke [Ben98, Wol91].

A typical treatment modality for atrial fibrillation is catheter ablation. Based on the landmark paper by Haissaguerre et al. [Hai98], where electrical signals causing atrial fibrillation were found to originate from the pulmonary veins in 97% of the studied cases, it is assumed that atrial fibrillation is triggered and sustained by the same anatomical site in the majority of patients. With catheter ablation flexible catheters are inserted into the patient to deposit radiofrequency energy around the junction between pulmonary veins and atria. This creates a scar which inhibits the signal propagation from the pulmonary veins into the heart's conduction system. Catheter ablation requires the anesthetization of the patient for multiple hours while it offers only a limited treatment success rate. Major complications and even death may occur due to this procedure [Cap05, Cap10]. Alternative treatment modalities are thus warranted.

Radiosurgery has the potential to become a new technique for such a treatment [Ber12]. In a study by Sharma et al. [Sha10] it was demonstrated that the irradiation of various target sites in the heart with a focused photon beam changed the electrical pathway of the heart's conduction system. Based on the experience gained in cancer radiotherapy an improved treatment outcome for such a deep seated target is expected for carbon ions. Compared to photons, particles like carbon ions deposit their energy in a defined area at the end of their particle track, the so called Bragg peak [Wil46]. This enables to deposit a high dose to the target while sparing the surrounding tissue [Kra00]. The physical and biological properties of carbon ions, combined with the active beam delivery and beam shaping [Hab93], led to successful clinical results in treatment of deep seated, static tumors in the GSI pilot project from 1997 to 2009 [Schu07]. Based on the convincing treatment outcome other centers like the Heidelberg Ion-Beam Therapy Center (HIT) and CNAO (Centro Nazionale di Adroterapia Oncologica) were built, where patients are now treated with scanned carbon ion beams on a regular basis [PTCOG13, Loe13].

Scope of this work

This is the first *in silico* survey to study the feasibility of a non-invasive treatment modality for atrial fibrillation with carbon ion radiosurgery [Ber12]. Thereby the irradiation of ablation sites in the junction between pulmonary veins and atria will be studied in human data. Another potential ablation site for atrial fibrillation, the AV node, will be studied in porcine data sets. A single fraction dose of 25Gy will be applied on the cardiac target volumes.

When intending to irradiate non-static targets interference effects between target motion and the actively applied ion beam cause local under and over dosages [Phi92, Ber08]. In order to deposit a homogenous dose in the target area, motion mitigation techniques are needed. Different motion mitigation techniques will be used in this dissertation. The interrupted irradiation during a selected part of the motion cycle (gating) [Kub96] as well as the repeated scanning of the same slice with a reduced dose so that averaging effects cause a homogenous dose deposition in the target volume (rescanning) [Phi92] will be analyzed. For the feasibility of a non-invasive treatment modality for atrial fibrillation with carbon ions, two independent motion influences have to be considered. On the one hand the heart beat, a fast but small amplitude motion, and on the other hand the respiration of the patient, a typically slow motion with big amplitude. Respiration and heartbeat gated CTs of human patients will be studied and the resulting treatment planning studies will be presented. In preparation for animal studies planned at GSI in the summer of 2014 treatment plan results for porcine data will also be investigated.

The structure of this dissertation is as follows. Chapter 1 will give an overview over the physical and biological fundamentals of radiotherapy. Different radiotherapy applications will be presented and a special emphasis will be given on the treatment of moving targets. Furthermore, the cause of atrial fibrillation and its resulting risk factors will be presented. Currently existing therapies and the potential benefit of a non-invasive treatment modality will be discussed. In chapter 2 the influence of the respiratory motion on pulmonary veins ablation sites in humans will be discussed. The feasibility to use gating as motion mitigation technique for this case will be investigated. In chapter 3 the displacement of the pulmonary veins ablation site due to heartbeat will be examined in human data. Rescanning will be studied as motion mitigation technique for this motion component. In preparation for the planned animal experiments, which will be carried out as a first experimental feasibility study in the summer of 2014 at GSI, chapter 4 will discuss an AV node ablation with carbon ions in porcine data. The underlying heartbeat motion will be studied and rescanning as motion mitigation technique will be utilized. Discussion of the overall results will be given in chapter 5, while chapter 6 will conclude the findings and give a short outlook on future directions.

1 Introduction - research background and fundamentals

Contents

1.1. Physical and biological basics of radiotherapy	14
1.1.1. Dose	14
1.1.2. Interaction of radiation with matter	14
1.1.3. Radiobiology	21
1.2. Radiotherapy	24
1.2.1. Photon therapy	24
1.2.2. Carbon therapy	25
1.2.3. Treatment planning	30
1.2.4. Organ motion in radiotherapy	32
1.3. Atrial fibrillation	40
1.3.1. Heart's conduction system	41
1.3.2. Types of atrial fibrillation	43
1.3.3. Possible causes for atrial fibrillation and risk factors	44
1.3.4. Treatment modalities	45

Radiosurgery has the potential to become a new and non-invasive treatment modality for atrial fibrillation (AF), the most common cardiac arrhythmia. Irradiation with photons is known to alter the electrical pathway of the heart's conduction system [Sha10]. Based on the experience gained in cancer radiotherapy promising results are expected by the usage of scanned carbon ion beams. In order to explain the underlying physical and biological differences between carbon ions and photons as well as other ions (e.g. protons), and also the resultant benefits of carbon ions when irradiating a deep seated target, the physical and radiobiological fundamentals will be explained in the first section of this chapter. In the second section the difference in radiotherapy application will be outlined, with special emphasis on the irradiation of moving targets. In the last section the basics of the heart's conduction system will be presented. Abnormalities, risk factors and underlying mechanisms causing cardiac arrhythmia in general and especially atrial fibrillation will be explained. The currently existing treatment modalities

for atrial fibrillation, as well as their limitations and risk factors will be presented in order to motivate the benefits of a non-invasive treatment modality.

1.1 Physical and biological basics of radiotherapy

The usage of radiation for medical purposes is almost as old as its detection. Shortly after W.C. Roentgen discovered X-rays in 1895 it was first used for the treatment of a cancer patient [Hal06]. With the development of accelerators and the resulting study of ion energy deposition profiles particles were connected to their therapeutic implications and benefits [Wil46]. In the following the physical and biological fundamentals of radiotherapy will be presented.

1.1.1 Dose

The dose D is defined as the deposited energy per unit mass [ICRU93]:

$$D = \frac{dE}{dm}; \quad [D] = 1\text{Gy} = 1\frac{\text{J}}{\text{kg}} \quad (1.1)$$

The magnitude of the deposited dose in a material depends, among other factors, on the used particle type, as they underlie different physical interaction mechanisms, which will be explained in the following.

1.1.2 Interaction of radiation with matter

Photons and ions interact differently with matter, resulting in different depth-dose-profiles (see figure 1.1). In the energy range used for radiotherapy, photons deposit their highest local dose shortly after entering the material while ions display an inverse depth-dose-profile. Thereby most of their energy is deposited in a defined area at the end of the particle track, the so-called Bragg Peak region, which is beneficial when irradiating a deep seated target as the dose to the surrounding normal tissue can be drastically reduced. Even though the interaction mechanisms for the energy deposition of photons and ions occurs primarily through secondary electrons, the underlying processes differ.

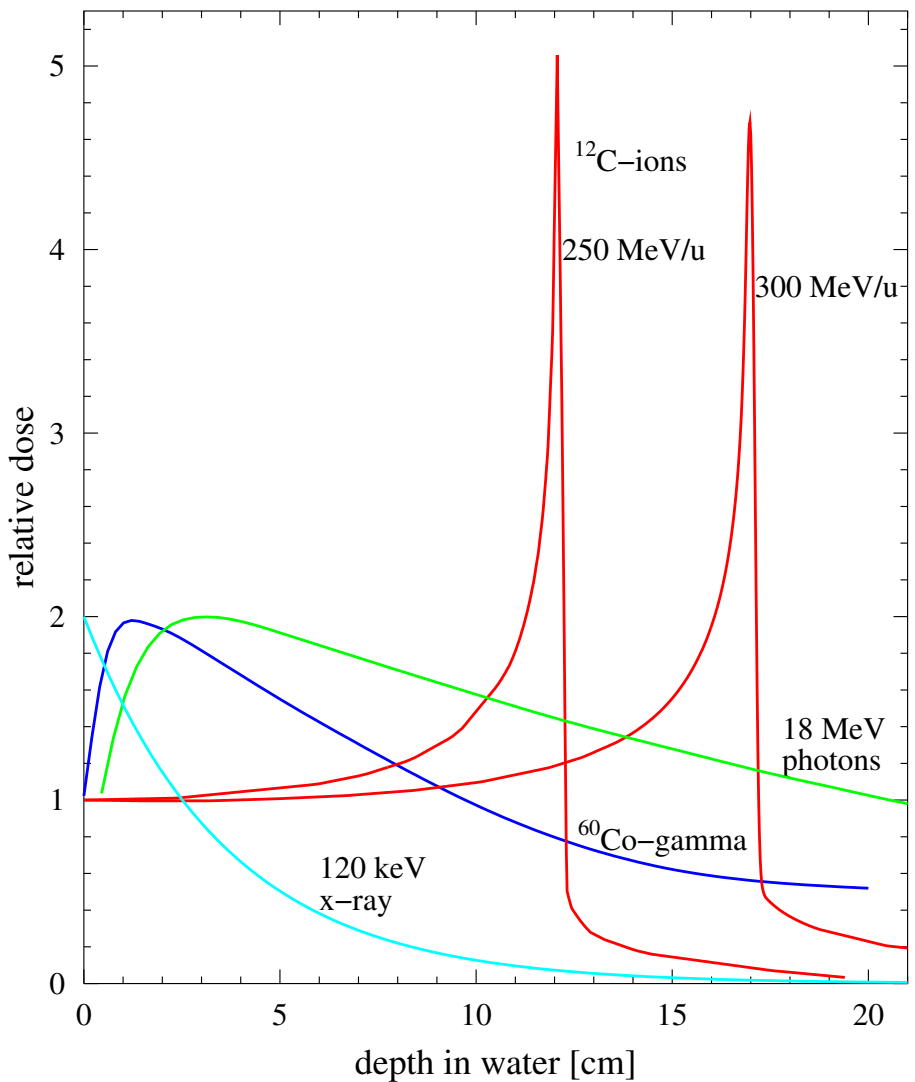


Figure 1.1.: Depth dose distributions of photons and carbon ions at different energies. Photons display an exponential decrease after a certain build up. Ions on the other hand interact differently with matter, resulting in an increased dose deposition at the end of the particle track, the Bragg peak. Figure taken from [Sch10]

Interaction of photons with matter

Photons undergo different processes when passing matter, like coherent scattering or Rayleigh scattering, photoelectric effect, Compton scattering and pair production. The probability for each process depends on one hand on the energy of the primary photons as well as on the atomic number of the absorbing material, while the strength of these dependencies varies in turn on the different processes [Lil06]. The overall decrease of the photon beam intensity when passing a material can be described by the following formula:

$$I = I_0 \cdot e^{-N\sigma x} = I_0 \cdot e^{-\mu x} \quad (1.2)$$

where I_0 represents the intensity of the incident photon, x the depth of the material in units of length, N the atomic density of the material and μ is the attenuation coefficient. The latter is directly related to the overall cross section σ , which is a measure of the probability of the occurrence of an interaction mechanism. It has contributions from all single interaction processes.

$$\sigma = \sigma_{\text{rayleigh}} + \sigma_{\text{photoelectric}} + Z\sigma_{\text{compton}} + \sigma_{\text{pairproduction}} \quad (1.3)$$

In the energy range of radiotherapy (between 100 keV and 25 MeV) the dominating process is Compton scattering [Alp98]. The attenuation of the photon beam results thus in the following way: The Compton electrons are scattered in a strongly forward direction, leading to a build up effect in deeper layers of the material. The maximum of the depth-dose profile is reached when the electrons are completely stopped at a certain depth, which is called the mean electron range (and is dependent on the initial photon energy). Afterwards the dose deposition decreases exponentially (see eq. 1.2).

Interaction of ions with matter

Interaction of ions with matter occurs via one of the following processes: elastic coloumb scattering from target nuclei (nuclear stopping) and inelastic collision with target electrons (electronic stopping). In the mildly relativistic region used in radiotherapy (energies of less than 500MeV/u) the total stopping power of ions is dominated by electronic stopping, resulting in ionization and excitation of the target atoms. The Bethe-Bloch formula [Bet30, Blo33], describing the mean rate of energy loss of relativistic ions, can thus be corrected for low particle energies [Nak10], resulting in the following approximation:

$$-\left\langle \frac{dE}{dx} \right\rangle = \frac{4\pi N_e z_{eff}^2}{m_e v^2} \left(\frac{e^2}{4\pi\epsilon_0} \right)^2 \left[\ln \left(\frac{2m_e v^2}{I} \right) + \text{correction} \right] \quad (1.4)$$

where N_e is the materials electron density, e and m_e are the charge and mass of an electron, ϵ_0 the electrical field constant and I the mean excitation energy of the absorber material. The effective projectile charge z_{eff} can be approximated by the Barkas formula [Bar63], where β is the projectile speed in units of c :

$$z_{eff} = z \left(1 - e^{-125\beta z^{2/3}} \right) \quad (1.5)$$

The main dependencies of the mean rate of energy loss can be seen in equation 1.4. It is proportional to z_{eff} and inversely proportional to v^2 . The overall depth dose distribution can thus be understood in the following way: in the beginning the particles have a high energy and thus high velocity, causing the dose deposition to be small. While passing the material, the velocity of the projectile decreases, causing the energy deposition to increase. At low particle energies, close to the particle range, target electrons are collected hence causing z_{eff} to decrease, leading to a decrease in dose deposition. The position of the maximum specific energy loss around the particle range is known as Bragg peak.

Range straggling and lateral scattering

Even though electronic stopping via inelastic collisions with target electrons is the main interaction process in the therapeutic energy range, elastic Coulomb scattering from target nuclei is still occurring and represents the main reason for lateral scattering. In an analytical approximation by Molière [Mol48], the angular spread of the overall deflection in a material has been described. It is on one hand dependent on the mass of the target nuclei, where a higher mass causes a larger angular spread for the same material thickness. And on the other hand it is inversely proportional on the momentum of the projectile, causing carbon ions to have a smaller lateral deflection than e.g. protons. Experimental validation comparing carbon ions to protons having the same range in water (15.6cm, 150MeV protons and 285MeV/u ^{12}C ions) resulted in an approximately three times smaller angular spread [Sch10].

Range straggling is caused by the statistical fluctuations of single electronic stopping events. In case of large number of collisions or thick layers of material these fluctuations can be approximated by a Gaussian probability distribution [Bor40] [Ahl80, Ric12]. This leads to an inverse proportional dependence between the ratio of the straggling width σ_R with the mean range R and the square root of the ion mass M ($\sigma_R/R \propto 1/\sqrt{M}$). This results in a smaller range scat-

tering for heavier ions. Experimentally, the ratio between the straggling width and the mean range was found to be 3.5 smaller for carbon ions compared to protons [Sch10].

Nuclear fragmentation

At large penetration depths, when the projectile ions have lost most of their energy, projectile fragmentation processes start to be relevant for ions heavier than protons. Mostly lower Z fragments are produced, which move with approximately the same velocity and in the same direction as the primary ions. This causes dose tails behind the Bragg peak position (see figure 1.2). Thus the resulting depth-dose distribution is actually the sum of the energy deposition of the projectiles and the resulting fragments.

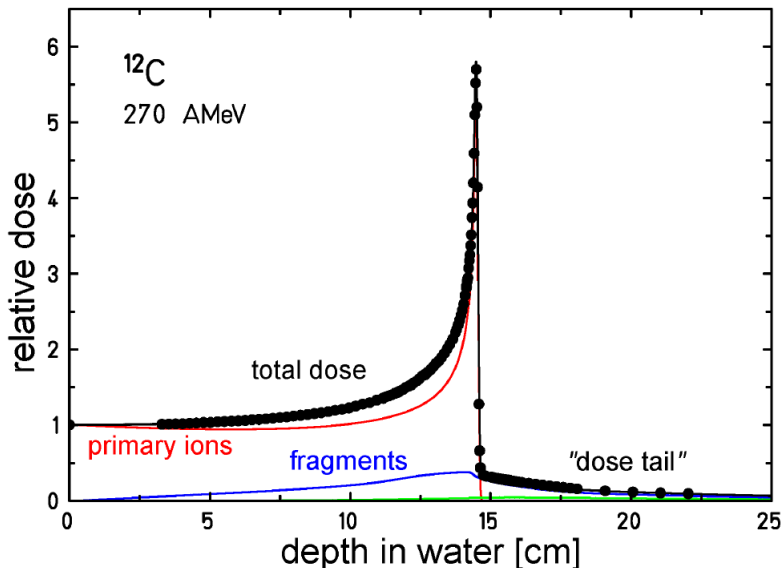


Figure 1.2.: Depth dose distribution of carbon ions. Besides of the energy deposition of the primary ions (red), the produced fragments (blue curve) contribute to the overall dose deposition (black) and are especially visible in the dose tail behind the Bragg peak. Figure taken from [Gro04]

Nevertheless, the produced fragments also offer the chance for PET (Positron Emission Tomography) monitoring, without additional radiation exposure for the patient. As peripheral collisions are more frequent than central ones [Kra00] isotopes like ^{11}C and ^{10}C are often produced when ^{12}C ions penetrate through tissue. Both isotopes are β^+ emitters. They annihilate with electrons in the human body, producing two γ -rays which travel in opposite directions.

Track structure

For inelastic collisions with atomic target electrons, only about 20% of the initial projectile energy is used to overcome the electron binding energy [Kra92]. A high amount of energy is transformed into the kinetic energy of the secondary electrons, the so-called δ -electrons. These δ -electrons can in turn emerge from the primary particle trajectory and undergo frequent elastic and inelastic scattering. If their energy is sufficiently high they can induce further ionization in more distant locations, leading to a high number of additional electrons. The radial dose fall off is approximated by a $1/r^2$ law, illustrating that the radial dose quickly falls off with larger radial distance r [Cha76, Kat99, Ric12]. The range of the δ -electrons is restricted to a maximum value according to the kinematics of the collision between projectile and target electron. Empirically this can be described by a power law [Kie86], where E is energy of the primary ion:

$$r_{max} \propto E^{1.7} \quad (1.6)$$

As stated by the Bethe equation (1.4), the energy deposition of the primary ions is dependent on the used ion species and their energy. This results in a higher stopping power for higher Z primary ions as well as an increased stopping power for smaller energies. Hence carbon ions have a much higher δ -electron output than e.g. protons. Furthermore with decreasing energy of carbon ions, the δ -electron output increases. This can be seen in figure 1.3. The higher ionization density produced by δ -electrons is also the reason for the difference in induced biological damage.

Linear Energy Transfer LET

The critical measure for the energy deposition of the δ -electrons is the linear energy transfer (LET). It is defined as the locally deposited energy to the medium (average energy deposited per unit length of track [Hal06]) and in radiobiology is given in keV/ μ m. Sparsely ionizing radiation (such as photons, protons and fast ions) have a low LET, while slow ions are densely ionizing and hence have a high LET.

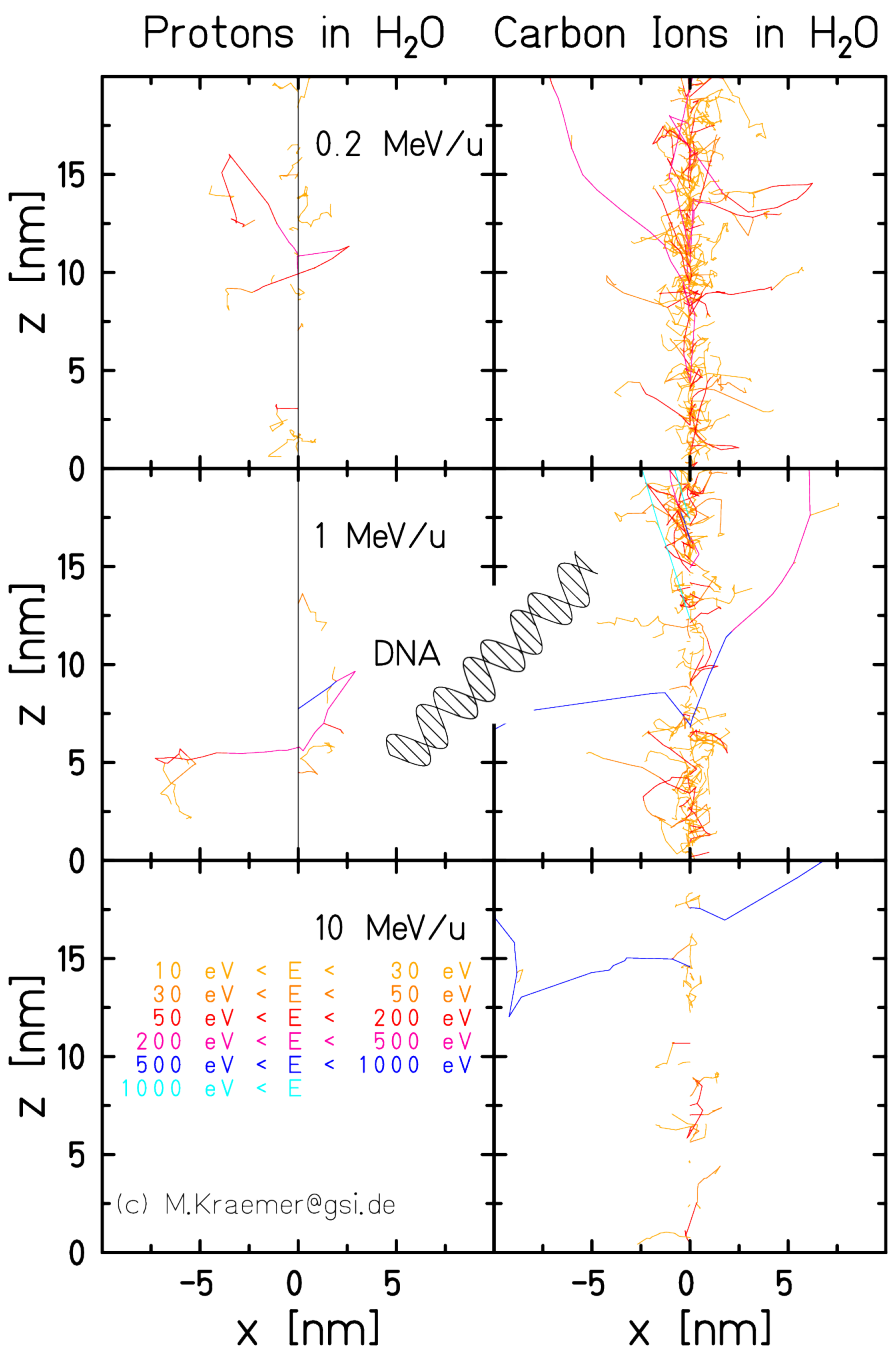


Figure 1.3.: Microscopic track structure of protons (left side) and carbon ions (right side) at different energies. Protons and high energy carbon ions are low LET radiation and hence sparsely ionizing. Low energy carbon ions on the other hand are high LET radiation and hence densely ionizing. For comparison the size of the DNA is displayed. Figure courtesy of Michael Krämer.

1.1.3 Radiobiology

It was described in the previous section that both, photons and ions, are ionizing radiation producing δ -electrons which in turn can cause subsequent ionizations. These ionizations attack the carrier of the genetic information, the DNA, of the irradiated cells and hence causes them to stop to proliferate. The biological background of these processes will be described in this section. Furthermore the enhanced biological effect of ions compared to photons will be explained. This is one of the potential benefits expected from a non-invasive irradiation of atrial fibrillation with carbon ions compared to photons.

Impact of radiation on cells

In eukaryotic cells, meaning cells that contain a cell nucleus, the genetic information is stored in the DNA (desoxyribonucleic acid), making it therefore the critical target in radiotherapy. DNA is made of two sugar and phosphate backbones and four different base pairs (adenine A, cytosine C, guanine G and thymine T), which bind in a defined way (A with T and C with G) and thus form the double helix structure with a distance between the two strands of about 2 nm. The genetic information is encoded in the sequence of the base pairs. Ionizing radiation can destroy the described structure of the DNA, either by direct or indirect action [Hal06].

As can be seen in figure 1.1.3 direct effects are caused by the destruction of molecular bonds of the DNA itself through any form of radiation. This process is considered the dominant effect if radiation with a high LET is used. Indirect action means that free radicals are produced by the ionizing radiation, which then in turn can damage the DNA. This phenomenon is predominant when sparsely ionizing radiation (low LET, like photons) are used and interact with molecules in the cell, particularly water.

Both mechanisms can cause either single strand breaks (SSB) or double strand breaks (DSB) (see figure). SSB means that only one of the strands is destroyed, leaving the complementary base on the other strand intact and thus enabling a fast repair if the SSBs occur at a certain distance from each other. DSBs or clustered SSBs are more complex and can cause the breakage of the chromatin. But even these damages are usually steadily repaired. The repair mechanisms only start to fail when the DSBs accumulate to local lesions. Changes in the original DNA material is the result. Depending on the produced damage mutations, carcinogenesis or cell death can be the result. Cell death can occur in different pathways. Apoptosis is the controlled self-inactivation of the cell due to DNA damage and the preferred pathway in radiotherapy. Uncontrolled cell death, necrosis, typically causes severe reactions of the immune system, leading to e.g. inflammation.

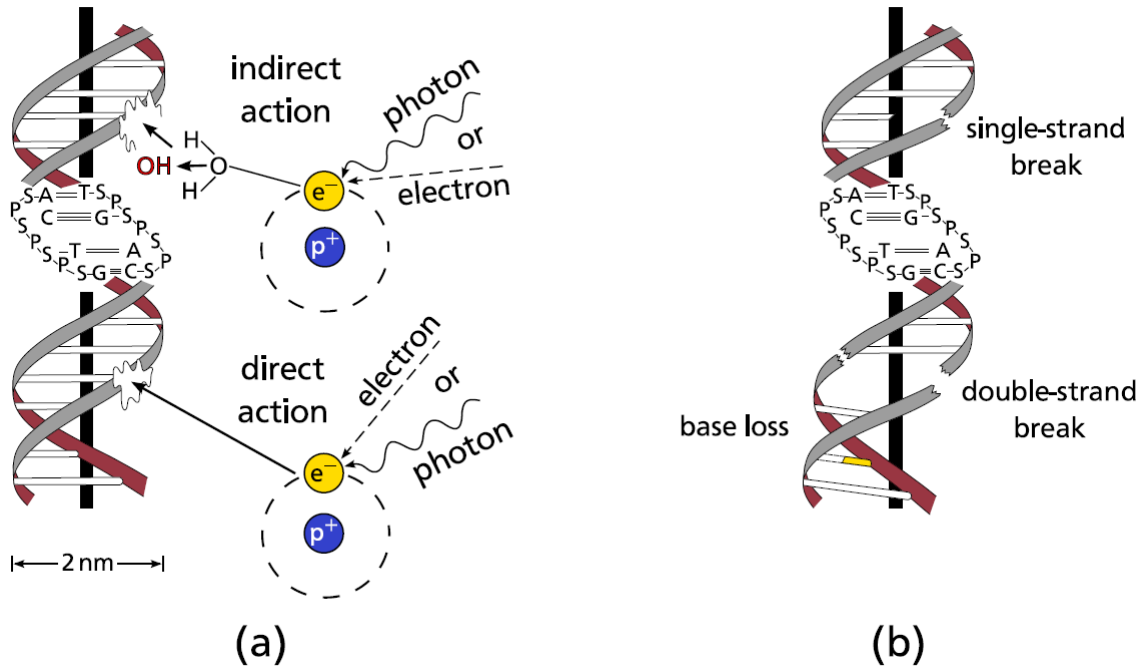


Figure 1.4.: On the left side (a) direct and indirect radiation damages are illustrated. On the right side (b) single strand breaks and double strand breaks are visualized. Figure taken from [Ric12]

Relative Biological Effectiveness RBE

As outlined, at the same dose level radiation the damage depends on the LET. This means that the induced biological effect is, amongst others, dependent on the energy and type of radiation. This is described in the relative biological effectiveness (RBE), which is defined as follows:

$$RBE = \left. \frac{D_{photon}^{ref}}{D_{ion}} \right|_{\text{isoeffect}} \quad (1.7)$$

D_{photon}^{ref} is the absorbed photon dose necessary to induce a certain isoeffect and D_{ion} is the absorbed dose of ions at a defined energy which leads to the same effect. Comparison of RBE values are valid only for the same effect and biological endpoint and by using the same reference radiation. This idea is used in the local effect model (LEM) at GSI for the prediction of the RBE. By assuming that the biological effect is independent of the specific radiation type but rather dependent on the energy deposition distribution in small sub volumes of the cell nucleus, RBE predictions are computed in relation to the known biological response of photons [Krae03, Fried13]. Weighting the physically absorbed dose with the RBE results in the biological dose in units of Gray equivalent (GyE).

The RBE depends on multiple parameters, like the endpoint, the irradiated tissue and its repair mechanism, the particle type, the used dose level and the LET. The dependence between RBE and LET is illustrated in figure 1.5. In case of x-rays (sparsely ionizing) the probability of an induced DSB is low and in general more than one track would be required to induce DSBs, resulting in a small RBE. Irradiation with a LET around $100\text{keV}/\mu\text{m}$ on the other hand is optimal in producing a biological effect, as the density of ionization coincides with the diameter of the DNA double helix of about 2nm . Thus radiation with this LET has the highest probability to induce a biological damage with DSBs. More densely ionizing radiation ($\text{LET} > 200\text{keV}/\mu\text{m}$) produces many DSBs, leading to ionization events which are closer together than needed. The RBE consequently decreases again, an effect known as overkill effect.

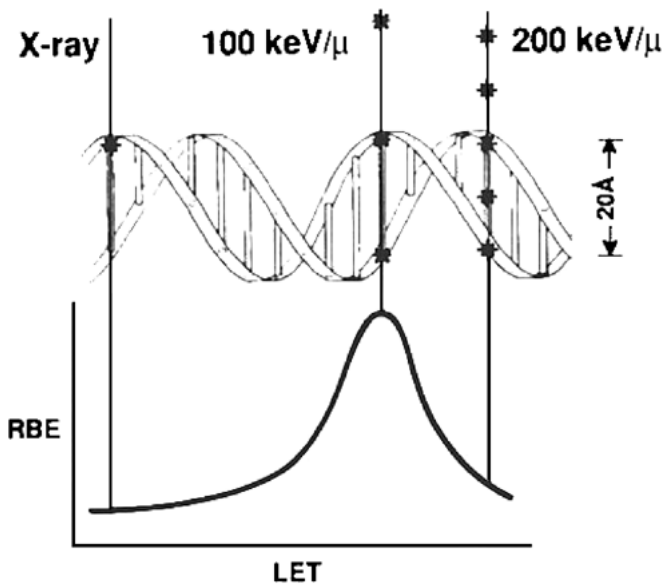


Figure 1.5.: Photon radiation with a LET of $100\text{keV}/\mu\text{m}$ has the biggest RBE for cell killing due to the fact that average separation between ionizing events coincides with the diameter of the DNA double helix (2 nm). Figure taken from [Hal06]

Concerning the increased biological effectiveness of ions it can be stated that it is only of advantage if the RBE is more pronounced in the target tissue compared to the normal tissue in the entrance channel. While protons exhibit an almost constant RBE throughout the energy deposition (a constant value of $\text{RBE} = 1.1$ is used), for ions heavier than oxygen the location for the highest RBE moves towards the proximal region of the depth-dose profile, starting to coincide with the plateau region [Kra00]. For carbon ions on the other hand the position of the highest RBE value coincides with the Bragg peak region, enhancing the possibility of a beneficial treatment outcome.

1.2 Radiotherapy

The conventional method for radiotherapy remains the irradiation with photons. Nevertheless, the biological and physical properties of ions (which were described in the previous section) result in advantages for radiotherapy, especially when treating deep seated targets. As a result, more and more ion facilities are opened worldwide, treating an increasing number of patients with protons and carbon ions [Loe13]. In this section the state of the art in treating static tumors with photon and carbon ion therapy will be summarized. Afterwards organ motion and the resultant difficulties, as well as approaches for motion mitigation will be presented.

1.2.1 Photon therapy

As can be seen in figure 1.1, a treatment of deep seated targets with photons can be carried out more effectively the higher the photon energy. Over the decades, different photon emission techniques were developed which allowed for higher photon energies. Currently, photons in the energy range of (6-25)MeV [Ber06] are used. The photons are produced with the help of linear accelerators, which are used to shoot accelerated electrons on a target, thereby emitting bremsstrahlung which is then used for radiotherapy.

Not only the used photon energy spectrum but also the application techniques developed over the last decades [Buc05]. Two dimensional (**2D**) radiotherapy was based on radiographies and was carried out with a single beam, which was applied from one to four different directions, usually as opposing lateral fields. As the imaging techniques advanced the treatment became also more conformal. CT scans enabled axial anatomy and tumor visualization in three dimensions. Hence in three dimensional conformal radiotherapy (**3DCRT**) more accurate dose calculations with homogeneous fields are possible, leading to an increased normal tissue sparing. With the development of **IMRT** (intensity modulated radiotherapy) the normal tissue sparing could be further improved. In IMRT a varying number of beams from different beam directions are overlaid while modulating the intensity of radiation within each field. This intensity modulation is achieved by using multileaf collimators (MLC) (see figure 1.6). An exemplary IMRT treatment plan in comparison to carbon ion irradiation can be seen in figure 1.10.

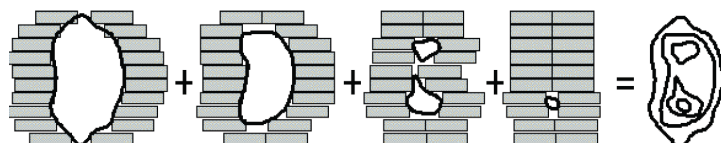


Figure 1.6.: Technical realization of IMRT by using multileaf collimators (MLC), enabling a photon dose deposition conformal to the target volume. Each lamellae can be moved individually, enabling an intensity modulation. Figure taken from [Schl01]

1.2.2 Carbon therapy

As already explained in section 1.1 ions display an inverse depth-dose profile and a higher biological effect compared to photons. This enables a high target conformity and a sparing of normal tissue, both of which are beneficial for radiotherapy. Since 1954, when the first ion beam therapy was carried out with protons at Berkeley Lab [Tob58] different projectile ions were used and their effect on target tissue studied.

Due to the their higher momentum and thus smaller lateral scattering (see section 1.1.2) the usage of heavy ions (heavier than protons) enables a better sparing of normal tissue and organs at risk (OAR), even if they are close to the target volume. In contrast to other ion types, the increased biological effectiveness of carbon ions coincides with the Bragg peak region (see section 1.1.3). Thus both the physical and biological properties of carbon ions offer the possibility of a beneficial treatment outcome.

Application technique

As in photon therapy, ion therapy application and thus target conformity improved over the decades after first treatments at Berkeley were performed by shooting the proton beam through the complete patient head [Tob58]. Depending on the provided accelerator as well as on the beam line properties passive and active techniques are distinguished both in beam delivery as well as beam shaping.

Concerning **beam delivery** particle acceleration to the therapeutic energies of several hundred MeV/u is carried out in cyclotrons and synchrotrons. **Cyclotrons**, which are used mainly in proton centers, offer the advantage of a more compact design compared to synchrotrons and allow a continuous beam extraction with stable intensities. On the other hand no active energy variation is possible, requiring the need for passive energy degraders. **Synchrotrons**, which are used in heavy ion centers, allow active energy variation.

Concerning **beam shaping** methods, which are used in order to deposit a homogeneous dose in the target volume, **passive methods** are used in some carbon ion centers as well as in the majority of proton centers. The devices rely on three different beam shaping steps [Chu93]. Firstly the beam is broadened by scattering and then further widened by using range modulators like e.g. a ridge filter. Thereby an extended and flat, but still homogeneous, field is formed which covers the tumor extent in longitudinal direction (Spread Out Bragg Peak: SOBP). Secondly, the range adjustment of the SOBP is achieved via flat degraders of variable thickness. Final conformity to the distal target border is achieved by patient individual compensators. Collimators

are used for a lateral conformity. A scheme of a passive beam shaping system can be seen in figure 1.7. Passive beam shaping devices offer the benefit that the historically unstable beam quality of research facilities - in which the first treatments were carried out - did not influence the homogeneity of the applied dose. Moreover, beam energy changes during treatment can be avoided, thus enabling a fast irradiation time. Nevertheless, passive beam application always requires the manufacture of patient individual compensators and an unavoidable limitation in volume conformity in the proximal tumor region as the SOBP width is fixed by the range modulator to the largest needed depth (see figure 1.7). Material in the beam path means furthermore intensity loss due to lateral scattering and an extra dose exposure due to fragmentation.

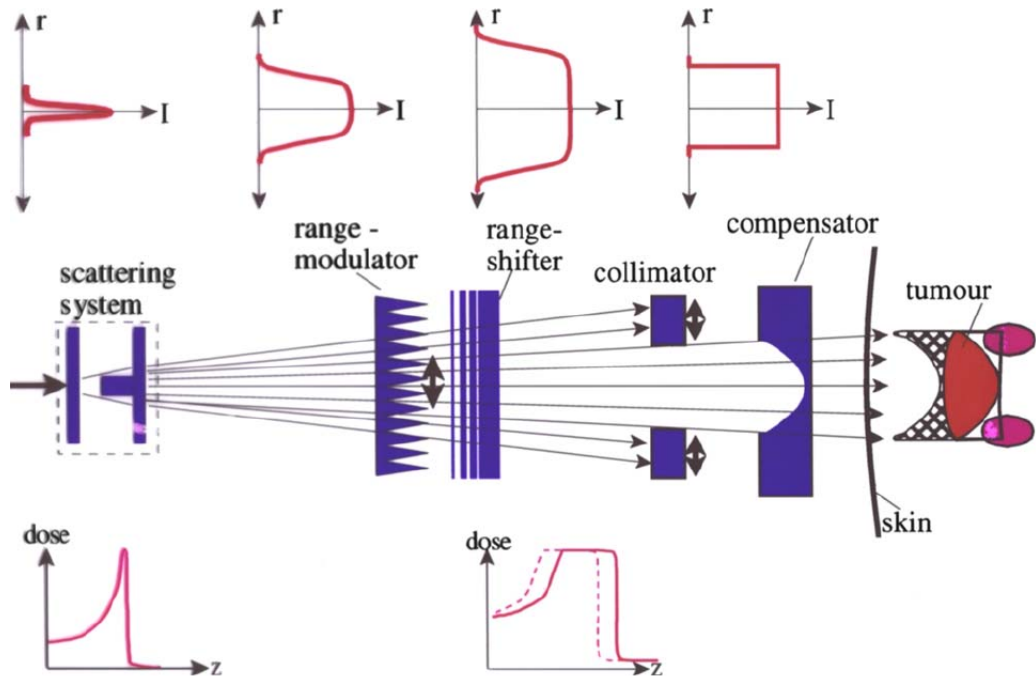


Figure 1.7.: Scheme of a passive beam shaping system. The beam is broadened by a scattering system and the width of the SOBP is determined by a range modulator. Via a range shifter the SOBP energy can be adjusted to a fixed range and thus depth. For lateral conformity collimators are used. The longitudinal conformity to the distal border of the target is achieved with a patient specific compensator. The proximal volume border can not be shaped, as is indicated in the hatched areas. Figure taken from [Sch10]

Active beam shaping is achieved with beam scanning, which offers a very good lateral target coverage as well as volume conformity also in the proximal field region. The target volume is thereby subdivided into slices of the same beam energy, so called iso-energy slices (IES). Each IES is again subdivided into a grid of target points which are irradiated sequentially. Hence many small pencil beams are used to generate a conformal dose deposition to any arbitrary target volume shape without the need of patient specific hardware. This drastically decreases the amount of material the beam has to traverse and hence reduces the unwanted neutron dose to the patient [Kad12]. Examples of beam scanning are spot scanning, which was developed for protons at the Paul Scherrer Institute (PSI, Swiss) [Ped95] or raster scanning, which was developed in parallel at GSI [Hab93].

At PSI a cyclotron is used and the energy variation is carried out with a degrader. The lateral deflection of the beam position is either achieved with magnets (Gantry 2 at PSI [Ped04]) or a combination of magnets and patient couch motion (Gantry 1). The beam is thereby switched off between different beam positions in the order of milli seconds.

Raster scanning on the other hand works in a continuous irradiation mode for one IES. A pencil beam is extracted from the synchrotron with a fixed energy and thus range, corresponding to a IES of the volume. By overlaying many different energies a SOBP is created to cover the longitudinal extension of the tumor (see figure 1.9b). The raster points within each IES are irradiated by deflecting the pencil beam via two orthogonal dipol magnets on an optimized path (see figure 1.8). When the pre-defined intensity of the raster point has been reached, the beam is moved to the next position. In order to establish a homogeneous dose coverage in the target volume the spacing, both in raster point position as well as IES distance, can be utilized. Robustness in longitudinal direction can be achieved with overlap of the individual IES slices. Nevertheless the number of IES slices should be kept small in order to guarantee a short treatment time. Hence a broadening of the Bragg Peak position is carried out with a so-called ripple filter (see figure 1.9b). It was found that a spacing of 3mm between IESs yields a robust result [Web99]. Furthermore the lateral overlap of the pencil beams needs to be chosen in such a way that the possibility of minor fluctuation in beam quality and position is compensated for. As the lateral beam profile is assumed to be Gaussian shaped and symmetric it was found that the full width half maximum (FWHM) of the beam is optimally chosen to be three times the raster spacing (see figure 1.9a) [Hab93].

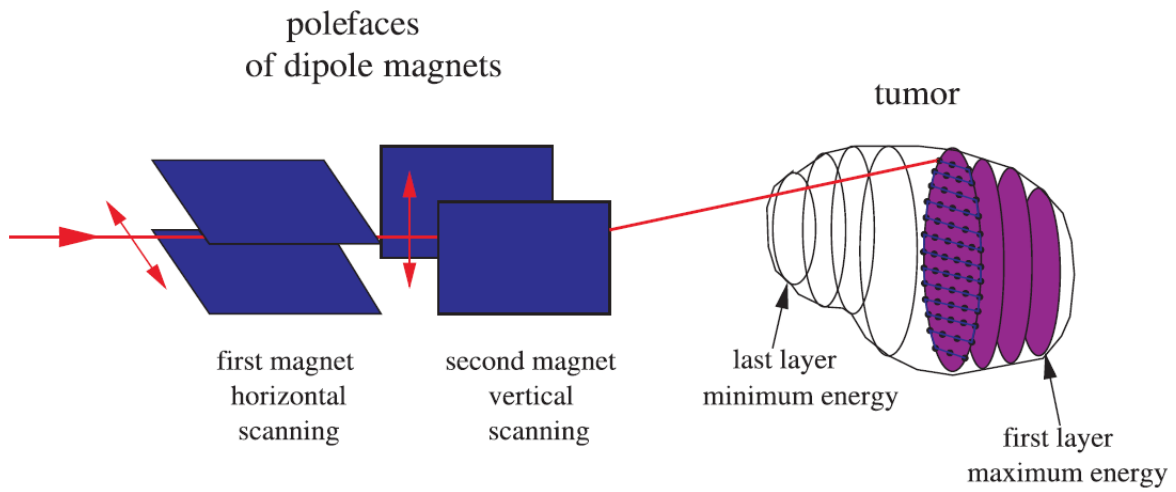


Figure 1.8.: Principle of the raster scanning technique at GSI. The target volume is divided into IES, which is again subdivided into a regular grid. By varying the particle energy from the accelerator and by deflecting the pencil beam via a magnetic scanning system the raster points are scanned. Figure taken from [Inf05]

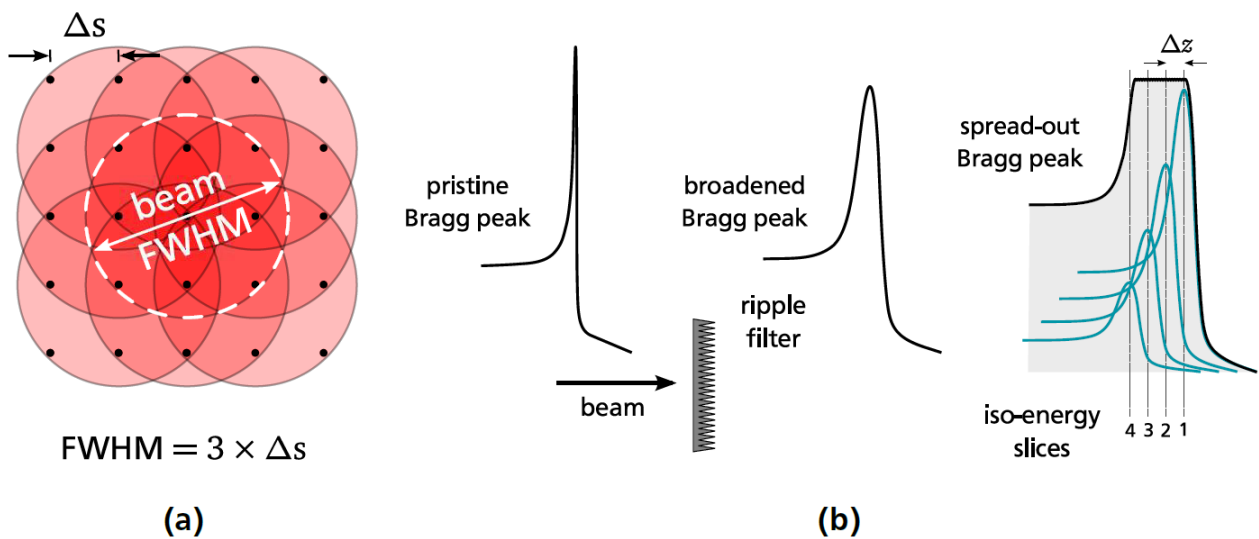


Figure 1.9.: Target dose homogeneity is achieved by sufficient overlap in lateral and longitudinal direction. a) In lateral direction the FWHM of the pencil beam is adjusted to three times the raster spacing Δs . b) In longitudinal direction the Bragg peaks are broadened in depth by using a ripple filter and then stacked in depth to a SOBP. An IES spacing Δz of typically 3mm is chosen. Figure taken from [Ric12]

GSI pilot project

Between 1997 and 2008 440 patients were treated with scanned carbon ions at GSI. Mostly head and neck tumors were irradiated. The typical fractionation scheme was 20 fractions within three weeks [Schu07]. An example of a resulting dose distribution with scanned carbon ions in comparison to IMRT can be seen in figure 1.10. The treatment outcome for skull-based chordomas can be seen in figure 1.11. In a later stage, also prostate and spinal cord tumors were treated.

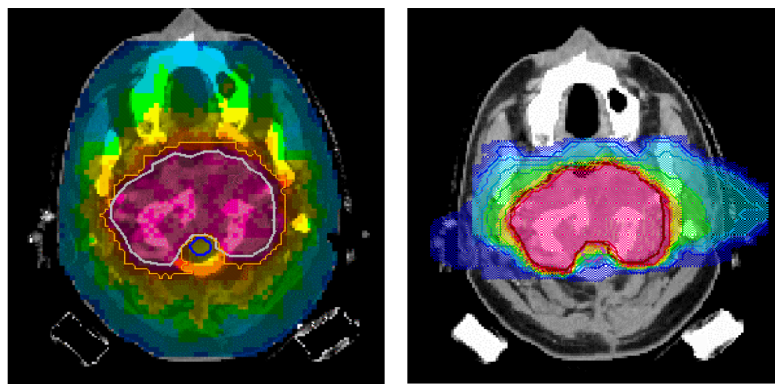


Figure 1.10.: Comparison of dose distributions results with IMRT (left side) and scanned carbon ions (right side). The dose to the normal tissue and especially organs at risk like the brainstem are drastically reduced for scanned carbon ions. Figure taken from [Gro04]

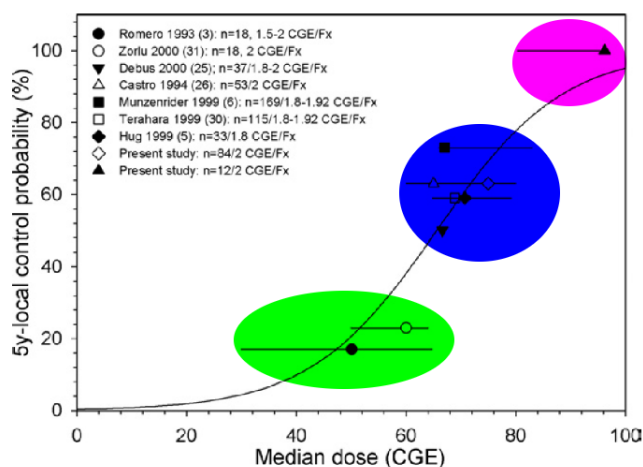


Figure 1.11.: Treatment outcome for the irradiation of skull-based chordomas for photons (green area), protons (blue area) and carbon ions (pink area). An improved effect after the irradiation of chordomas can be seen when doses exceeding 70 Cobalt Gray Equivalent (CGE) can be applied. For carbon ions a higher dose can be deposited in the target since the dose in the nearby OAR can be reduced. Figure taken from [Schu07]

The pilot project at GSI was carried out in a collaboration between GSI, the Heidelberg University hospital, the German cancer research center (DKFZ) and the research center Dresden-Rossendorf. Following the success in treatment outcome [Loe13] the Heidelberg Ion-Beam Therapy Center (HIT) was build, where patients are treated with scanned carbon ion beams and protons on a regular basis since 2009 [Com10]. Furthermore CNAO (centro nazionale di adroterapia oncologica, Pavia, Italy) [Ama04] started treating patients with scanned carbon ions beams in 2012 [PTCOG13]. In total roughly 10,000 patients have been treated with carbon ions up to the beginning of 2013 [Loe13], whereof about 2,000 patients were treated with scanned carbon ions [PTCOG13].

1.2.3 Treatment planning

Treatment planning is the optimization process in which the needed machine delivery parameters are determined for a chosen beam configuration in order to yield the prescribed dose to the target volume, while minimising the dose to the normal tissue, especially to the OARs [Ric12]. In modern radiotherapy treatment planning is based on CT scans, which represent photon attenuation through the different tissue types (Hounsfield units - HU) and can hence be converted to water-equivalent depths. On the patient image data the target and OARs are contoured and the needed dose and dose constraints, respectively, are determined. For cancer radiotherapy the delineation of the tumor includes certain safety margins, defined by the International Commission on Radiation units and Measurements (ICRU). As some of these margins will be also used in the context of cardiac targets, they will be shortly introduced here.

GTV (Gross Tumor Volume): "The GTV is the gross palpable or visible/demonstrable extent and location of the malignant growth." [ICRU93a]

CTV (Clinical Target Volume): "The CTV is a tissue volume that contains a GTV and/or subclinical microscopic malignant disease, which has to be eliminated. This volume thus has to be treated adequately in order to achieve the aim of therapy: cure or palliation." [ICRU93a]

PTV (Planning Target Volume): "The PTV is a geometrical concept, and it is defined to select and appropriate beam size and beam arrangements, taking into consideration the net effect of all the possible geometrical variations, in order to ensure that the prescribed dose is actually absorbed in the CTV." [ICRU93a]

IM (Internal Margin): "The IM, commonly asymmetric around the CTV, is intended to compensate for all movements and all variations in site, size and shape of the organs and tissues contained or adjacent to the CTV. They may result e.g. from respiration, different fillings of the bladder, different fillings of the rectum, swallowing, heart beat, movements of the bowel" [ICRU99]

Based on this definition, the **ITV** (**Internal Target Volume**) is commonly used for the volume in which the IM encompasses the CTV (see figure 1.12).

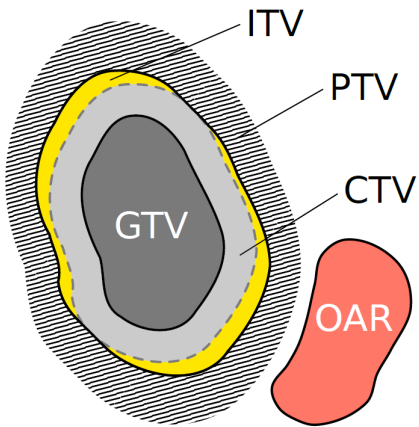


Figure 1.12.: Treatment planning volumes as defined by the ICRU. Figure taken from [Ric12]

As a result of treatment planning the ICRU recommends that 100% of the PTV should receive at least 95% and not more than 107% of the prescribed dose [ICRU93a]. In order to study if these recommendations are met, dose-volume-histograms (DVH) are computed in the treatment planning study process and the values V95 and V107 (the volume which receives 95% and 107% of the dose, respectively) determined. Furthermore D5 and D95, which denotes the dose covering 5% and 95% of the volume, are extracted. The difference between these two values (D5-D95) is a measure for the dose fall off and should be ideally close to zero. In general, the dose constraints of the OAR depends on the organ as well as fractionation scheme and radiation type and needs to be carefully examined in each individual case.

The treatment planning system and its result, the dose optimization, depends on the radiation type and on the used beam delivery technique. For scanned carbon ion beams the optimization task with the in-house treatment planning software TRiP98 [Krae00] [Krae00b] needs to determine the required energies of the IESs and the pencil beam positions as well as corresponding particle numbers for each raster point. This leads to an 'inverse' optimization process, in which the particle fluence to the target volume, which is given in the form of planar polygon originating from manual delineation on the axial CT slices [Ric13], is determined from the prescribed dose distribution [Krae00]. Furthermore, as the irradiation of the most distal IES deposits a certain dose in the more proximal slices only the distal slice receives a homogeneous fluence distribution while all other slices require irregular dose patterns (see figure 1.13). Using the physical and biological beam models (LEM, see RBE in section 1.1.3) the dose contributions from all raster points to each individual target voxel are calculated [Ric12].

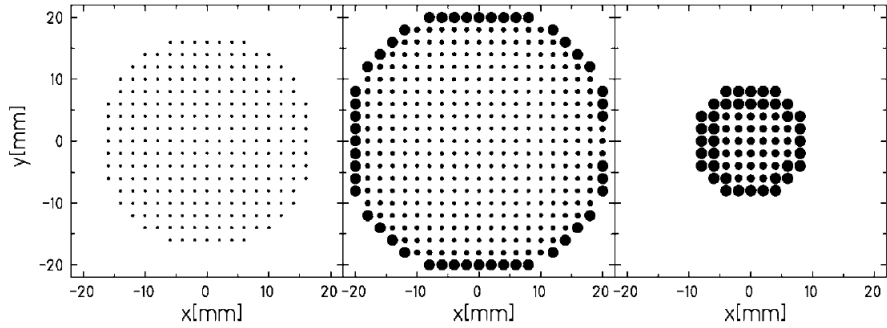


Figure 1.13.: Particle fluence distribution depending on the IES, starting with the most distal one (left) and moving to more proximal regions. Figure taken from [Krae00]

1.2.4 Organ motion in radiotherapy

Many target sites are influenced by temporal changes. Depending on the underlying mechanism, one distinguishes patient positioning related organ motion and organ motion in-between treatment fractions (interfractional motion) or during a treatment application (intrafractional motion). The different organ motion types will be specified in this section. Furthermore motion acquisition strategies as well as techniques to overcome the motion influence, so called motion mitigation techniques, will be presented. Finally an overview over the treatment planning workflow including motion (four dimensional - 4D) will be given.

Motion types

An overview of the different organ motion types is given by Langen and Jones [Lan01]. Three main categories can be determined: patient positioning related motion, interfractional motion and intrafractional motion. Examples of these different motion types can be seen in figure 2.2.1. It should be noted that all motion types can occur in a patient. Thus when dealing with intrafractional motion, interfractional motion as well as patient positioning needs to be accounted for.

Patient positioning can cause changes in tumor shape as well as uncertainties in the tumor position. A difference in positioning between image acquisition (e.g. CT) and treatment delivery may introduce systematic displacements and hence threaten the outcome of the treatment. Patient fixation systems and dedicated protocols are applied to overcome this motion influence. Stereotactic fixation with e.g. masks are used on a daily basis. The other two motion types however are purely internal and are distinguished according to the time scale they occur on.

Interfractional motion occurs within hours and days, hence between two treatment sessions (if multiple fractions are applied). Anatomical changes caused by interfractional motion are manifold. Prostate cancer patients are often subject to position changes due to varying gut and bladder fillings [Fok04]. For lung cancer patients, changes in the breathing pattern are troublesome. Sonke et al. [Son08] reported that even though the respiratory motion trajectory is often reproducible, the baseline of the tumor motion can vary significantly. Cancer patients in general are also subject to tumor shrinkage [Mor09] in the course of the treatment. In order to mitigate interfractional motion, repeated imaging needs to be carried out.

Intrafractional motion occurs on a time scale of seconds to minutes. The main reason for intrafractional motion are respiration and heart beat. Even though the exact motion patterns varies from patient to patient, it can be stated that breathing is a quite regular and slow process, with a rather big amplitude. Heart beat on the other hand has a smaller amplitude compared to respiration, but it is a high frequency motion with 60 to 80 heart beats per minute compared to 10 to 20 respiration cycles in the same time. These two motions superimpose and the influence of both will be studied in the framework of this work when targeting sites in the heart. Different motion mitigation techniques for intrafractional motion will be presented in a separate subsection.

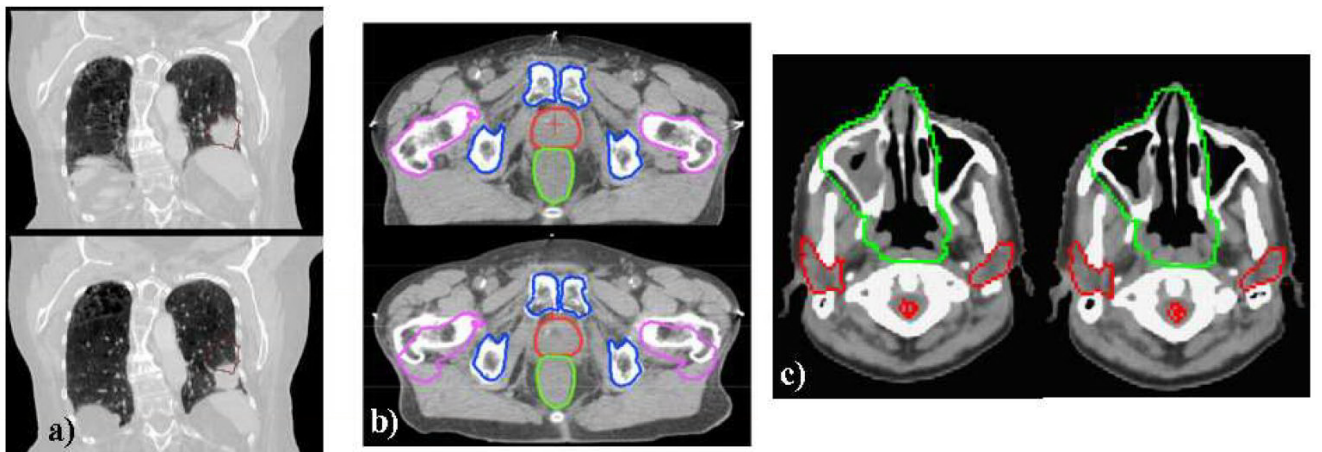


Figure 1.14.: Examples of the three major motion categories. On the left side (a) a lung tumor is displayed, which moves due to the respiration of the patient (intrafractional motion). Interfractional position changes are exemplarily shown in the middle (b), where two CT scans of a prostate patient are compared. Density variations between two CT scans are shown in (c). Figure taken from [Eng11]

Motion acquisition

For a successful irradiation of the moving target, the intrafractional motion of the target site must be known during the treatment process. This is for example achieved by time resolved computed tomography scans (4D-CTs) and the potential usage of online motion measurement.

For the acquisition of 4D-CT scans the motion signal is recorded during the imaging. The motion cycle is then divided into N quasi-stationary sections (so-called motion phases (MP)). In every MP a full regular CT scan is reconstructed. In order to achieve this data is recorded in every slice for a whole motion cycle. By correlating the data gained from the motion signal with the recorded CT information, the scans are afterwards rearranged according to their affiliation to a certain MP. For more information on 4D-CTs the reader is referred to e.g. [Rie05].

A review of the different motion detection techniques can be found at [Eva08]. One distinguishes between direct measurement techniques and surrogate signals. Examples for direct measurements are ultrasound and fluoroscopy. In fluoroscopy, the patient is irradiated with X-rays and the absorption pattern is displayed on a fluorescent screen, hence limiting the acquisition time of this method by the deposited dose. The monitoring time in ultrasound is not limited since no ionizing radiation is needed and hence a real time imaging is feasible [Pra12]. Nevertheless influence of air limits the resolution and thus raises difficulties when being applied in the thorax region of the patient. Surrogate signals detect variables which are directly related to the source of organ motion. Examples of these kind of techniques for respiration are methods which correlate the movement of the torso to the phase in the respiration cycle. One possibility is to monitor the height of the patient surface with camera systems or laser displacement sensors or additionally using infrared markers attached to the patient's body [Tad98, Ber05, Schw04, Ser13]. Alternatively the volume of the torso can be measured by using a belt-like strain gauge [Li06]. Other approaches measure e.g. the airflow of the patient [Kub96, Hanl99].

Combinations between direct measurement techniques and surrogate signal acquisition exist and are e.g. used in the Cyberknife system. Their Synchrony system (see also 1.3.4) combines fluoroscopy (direct) with an infrared camera system (surrogate). This offers the advantage of a drastically reduced fluoroscopy acquisition time as it is only used to check and update the surrogate system [Sha10, Lue12].

Motion mitigation techniques for intrafractional motion

In particle beam scanning the beam delivery interferes with the intrafractional target motion, causing local over- and underdosages in the target volume, an effect known as Interplay [Phi92, Ber08, Ber12, Loe13]. The exactly resulting interplay pattern is dependent on many different factors, like the beam direction, the scanning speed, the motion amplitude and starting phase etc. Thus techniques which mitigate the influence of the underlying target motion have to be applied. The three main techniques (rescanning, gating and tracking) will be explained in more detail.

Rescanning, also known as repainting, is a specific approach for beam scanning and based on statistical averaging of different interplay patterns [Phi92, Rie10]. Scanning the target N times with a reduced dose of $1/N$ results in a Gaussian distributed dose around the theoretically intended one (see figure 1.15). As the variance of the distribution is proportional to $1/\sqrt{N}$ the result will be better the more rescans are used. The technical realisation of rescanning is easier than for e.g. gating and beam tracking, especially as it does not require real-time motion monitoring, and results in a homogeneous dose to the inner region of the target when using enough rescans N . Anyhow it can lead to an increased dose deposition to the surrounding, normal tissue and to under dosages in the outer part of the target volume. So far rescanning has not been used in patient treatments, but certain centers (e.g. NIRS [Fur07]) and PSI [Zen10]) plan it for the future.

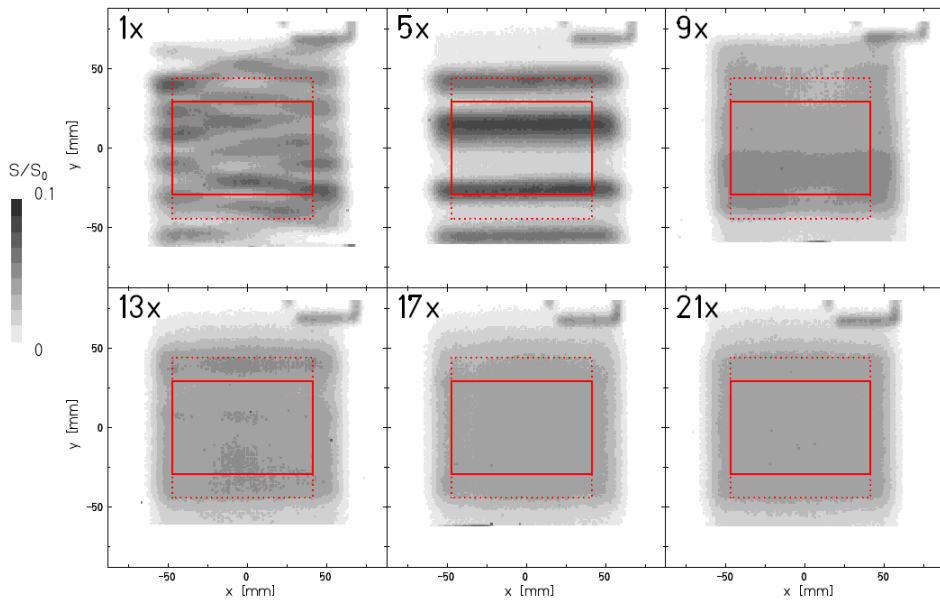


Figure 1.15.: Principle of rescanning in film irradiations. Averaging multiple interplay patterns leads to a homogeneous dose in the target area (solid red square). Figure taken from [Ber09b].

Gating is the interrupted irradiation of the target during a selected part of the motion cycle, the gating window [Kub96, Min00] [Li06] (see figure 1.16). Typically a gating window around the most reproducible motion states are chosen, which show a comparably small motion (e.g. end exhale in case of respiration). This technique is also used for passive beam delivery, as it reduces the size of ITV margins. In the gating window a small motion, the so-called residual motion, remains. In case of beam scanning this can result in small interplay effects. Different approaches are studied to overcome this drawback [Fur07, Zen10, Ber09]. Gating requires online motion monitoring and prolongs the treatment time. For centers with passive beam delivery gating has already been successfully used [Min00, Iwa10, Has06].

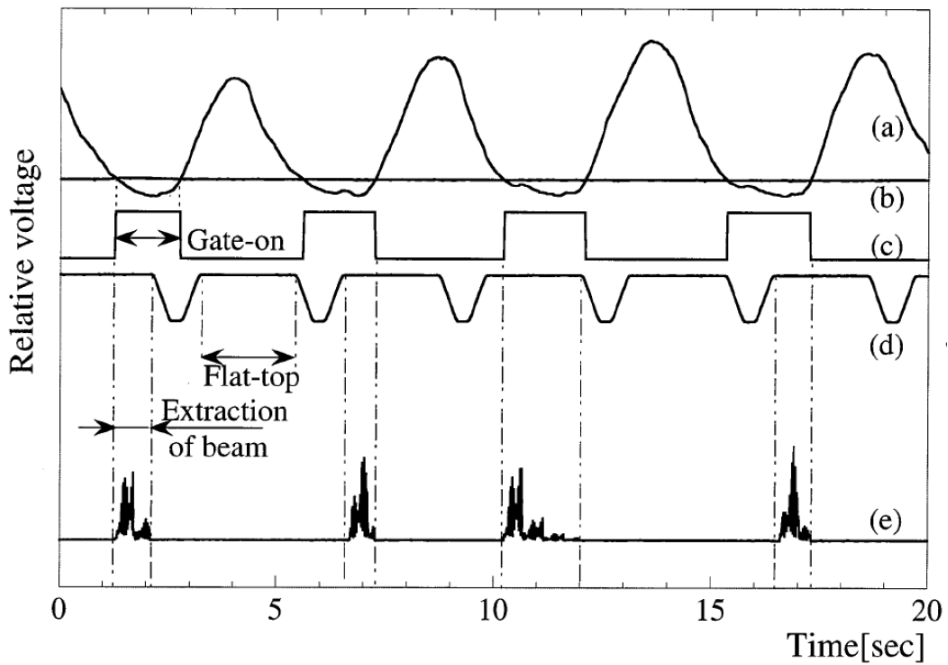


Figure 1.16.: Principle of gating. Line (a) is the respiratory signal. At end exhale the gradient of the respiration is flat, enabling an irradiation without large effects of the target motion. The beam (c) is thus only applied during this time. The gating window is activated as soon as the respiratory motion crosses line (b). Figure taken from [Min00]

Beam tracking of organ motion requires the adaptation of the beam position to the target motion in real time. It was originally proposed for IMPT [Kea01] and ideally requires no additional margins, nor prolongs the treatment time. Prerequisite of this method is a fast beam delivery system. Tracking is clinically used in the Cyberknife Synchrony system (see section 1.3.4). In comparison to photon irradiation, tracking with particles needs a careful consideration and adaptation of longitudinal changes due to the Bragg Peak structure of ions. The implemented tracking system at GSI [Gro04] uses fast deflecting dipole magnets, which are also used for beam scanning for the lateral adaptation of the beam. The longitudinal changes

are accounted for by two polymethyl methacrylate (PMMA) wedges, which are mounted on a fast, linear stepmotor close to the target (see figure 1.17) [Sai09]. By changing the relative distance between the wedges, the beam penetrates PMMA with different thicknesses, thereby changing its energy and hence range. Even though the high precision of the system has been proven [Ber07, Ber10, Sai09] a clinical use is not feasible yet due to the lack of fast and precise real-time internal motion monitoring that includes particle range information.

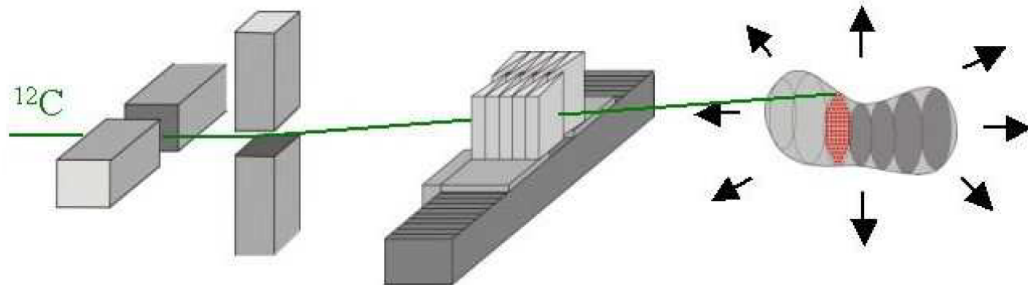


Figure 1.17.: Principle of tracking at GSI. The lateral deflection is achieved via dipole scanner magnets. For the longitudinal adaptation two PMMA wedges are mounted on step motors, enabling to change the depth the particle beam has to traverse. Figure taken from [Gro04]

Besides these major motion mitigation techniques, different combinations are currently studied. A combination between rescanning and gating is e.g. studied by Furukawa et al. [Fur07] or Seco et al. [Sec09] and a combination of rescanning at tracking by van de Water et al. [Wat09].

As breathing is the main reason for intrafractional motion in most radiotherapy applications, many different other techniques have been investigated to directly mitigate the influence of respiration. An example is abdominal pressure, which has been used in lung and liver cancer patients in treatments with photons [Neg01, Hof03] and recently also for scanned carbon ions at HIT (treatment of hepatocellular cancer [Com11]). Jet ventilation [Hof03] and apneic oxygenation [RPTC12] are also used to partially or completely suppress respiration of the patient.

4D Treatment planning at GSI

In order to account for intrafractional organ motion, time-resolved (4D) treatment planning is needed. The underlying data as well as the techniques for 4D treatment planning will be presented for the special case of scanned carbon ion beams at GSI.

As in the static case, treatment planning for ions is based on CT scans. In the special case of 4D treatment planning, these CT scans are time resolved (**4DCTs**, see section 1.2.4, Motion

acquisition). In order to use the information stored in the 4DCT, an **image registration** needs to be performed. With this a voxel-to-voxel mapping between the reference phase of the 4DCT and all other motion phases is gained, hence yielding a spatial correlation between the individual CT phases [Ric13]. Usually, rigid and deformable registration methods are distinguished. While rigid registration only contains linear transformation of the original object in all three room dimensions, deformable registration also accounts for compression. Brock et al. [Bro10] published a multi-institutional study where the accuracy of some of the available registration algorithms is presented. It can be stated that registration accuracy of most algorithms is in the order of millimeters, hence in the order of a CT voxel size, but is dependent on the image contrast (resulting in less accurate results when the contrast is diminished).

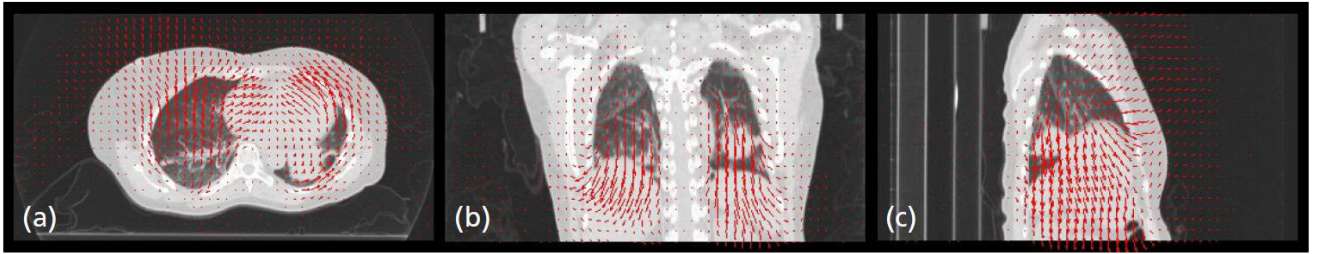


Figure 1.18.: End-exhale, 4D reference phase of a lung cancer patient with overlying deformation field to end-inhale in a) axial, b) coronal and c) sagittal view. Figure taken from [Ric12].

4D treatment planning at GSI is carried out with the in-house software **TRiP4D**. It was mainly developed by Daniel Richter [Ric13] and is based on TRiP98 as well as a predecessor program developed by Bert and Rietzel [Ber07b] together with the biological implementation under influence of target motion by Gemmel et al. [Gem11]. TRiP98 was developed for static target regions and was successfully applied in the GSI pilot project [Krae10, Krae00, Krae00b]. It is a command-line-based software without graphical interface which runs on an IBM AIX operating system and is written in C programming, using a pseudo object-oriented structure. For a detailed description of TRiP4D functionalities as well as of the software design and experimental verification the reader shall be referred to [Ric13]. However, a short overview of some of the most important functionalities will be given here.

The **4DCT structure** was implemented as a sequence of 3DCTs with a distinguished reference CT on which the dose optimization process is carried out. Thus the existing 3D functionalities, like the computation of water-equivalent path lengths, could be reused. Individual phases of the 4DCT are indexed by their position in the motion cycle. TRiP4D does not include native **image registration** functionalities but rather integrates and processes image registration output, obtained e.g. with the open source software package Plastimatch [Sharp07]. The resulting deformation maps need to be obtained in two directions (reference-moving and moving-reference)

as certain steps of the treatment planning like contour propagation require the inverse deformation maps. **Contours segmentation**, of target volumes as well as organs at risk, is stored as a volume dataset model, based on the 3D segmentation module of TRiP98 with planar polygons on axial CT slices. Based on this 4D segmentation functionality ITVs (see section 1.2.3) can be created, which are needed for certain motion mitigation techniques like e.g. rescanning. In general, the 4D treatment plan generation and **dose optimization** is very dependent on the employed motion mitigation technique. For the ITV concept [Gra12], and hence in motion mitigation techniques where the dosimetric effects caused by interplay are compensated but not the target motion itself, dose optimization is carried out on the 4DCT reference phase [Ric13]. For beam tracking on the other hand additional optimization is carried out, as motion compensation vectors have to be computed. Furthermore 4D optimization techniques (which include the target motion for optimization by using the full 4DCT dataset, the vectors from image registration as well as 4DVOIs for dose optimization [Gra13, Ele12]) can be developed and applied with TRiP4D. Based on the predecessor program of Bert and Rietzel the **treatment plan** is then split into quasi-static sub-plans where the raster points and the corresponding intensities are divided according to the motion phase they shall be irradiated in. For the overall **4D dose calculation** in TRiP4D, the sub-plans are then collected over all motion states for each dose voxel. Thereby the voxel position is transformed according to the deformation maps and by accounting for the radiological density distribution of the respective phase of the 4DCT. The total physical dose results as a summation of the dose distribution from all motion states in the reference state (see figure 1.19). For the biological dose calculation the particle and energy spectra are also accumulated over all motion states and used as input for the local effect model (LEM) to calculate the RBE [Scho94, Scho96, Gru12]. TRiP4D was extensively tested and verified in numerous experiments [Ric12, Ric13].

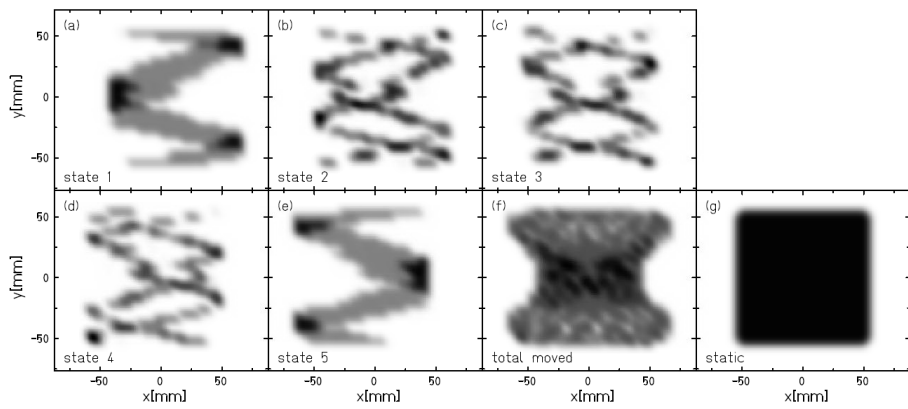


Figure 1.19.: Resulting film response in experimental validation of 4D dose calculation with TRiP4D. Images a)-e) show the individual dose deposition in each of the five motion states. In f) the total dose deposition in 4D is displayed. On the stationary film in g) a homogeneous dose is deposited in 3D. Figure taken from [Ric12]

1.3 Atrial fibrillation

Atrial fibrillation (AF) is the most common cardiac arrhythmia. It occurs in ~2% of the population older than eighty in Europe and the US, leading to over six million patients in Europe [ESC10] and over two million patients in the United States [CE09]. The lifetime risk of developing AF is ~25% for people over forty. Since age is an important risk factor for this cardiac arrhythmia the prevalence is estimated to double in the next fifty years due to ageing of society (see figure 1.20).

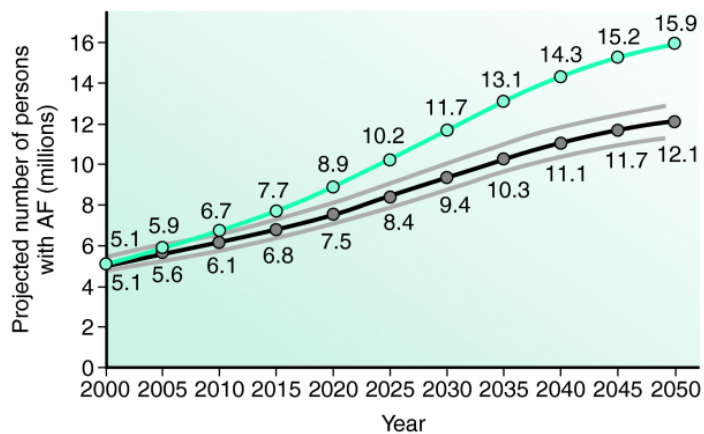


Figure 1.20.: Trend of AF incidences. The black curve indicates the projected number of patients assuming no further increase in age-adjusted AF incidences. The green curve represents the trend assuming a continuous increase in incident rates as evident in 1980 to 2000. Figure taken from [Miy06]

Even though in itself not life threatening, it alters the quality of life and increases the risk to suffer a stroke. It is estimated that the stroke risk in AF patients is 5-fold higher [Ben98, Wol91]. AF often remains undiagnosed (silent AF). It is stated that one out of five acute strokes is attributed to AF [ESC10]. Other late effects and related events include cognitive dysfunctions like vascular dementia and impairment of left ventricular function. In general death rates are stated to approximately double by AF [ESC10], leading to a ten year survival rate of 25% compared to 46% in patients with a normal sinus rhythm (age ranged from 14 to 73 years with a median of 42 years) [Oles62, ACC06].

In the following the normal signal propagation through the heart's conduction system will be explained in order to contrast the occurring differences in AF. Possible causes for AF and underlying risk factors as well as current treatment modalities will be presented.

1.3.1 Heart's conduction system

The conduction system of the heart controls the generation and propagation of electrical signals, so called action potentials, that cause the heart muscle to contract and hence to pump blood [Med]. The small electrical activity of the action potentials is measurable at the surface of the body, enabling a graphical record with an electronic recording instrument, the Electrocardiograph (ECG). In the following the events during a single heart beat and the corresponding detection in an ECG (see fig. 1.22) will be explained. The action potentials can originate spontaneously in any of the specialized cardiac muscle cells which form the conduction system. In a healthy heart each beat begins in the right atrium with an action potential from the sinoatrial (SA) node (see fig. 1.21), making it the natural pacemaker of the heart. The signal then spreads across both atrial chambers causing the muscle cells to contract (atrial systole) which is represented as the P-wave in an ECG. It is followed by a period of conduction (PR-segment in ECG) in which the signal enters the ventricles via the atrioventricular (AV) node. As the signal spreads the ventricles contract very rapidly (ventricular systole), which is displayed in the QRS-complex in an ECG. Atrial activity is hidden in the ECG by the QRS complex. As the signal passes out of the ventricles, the ventricular walls start to relax (ventricular diastole). The T-wave marks this ventricular repolarization. The sequence of these events and the corresponding ECG traces repeat with every single heartbeat.

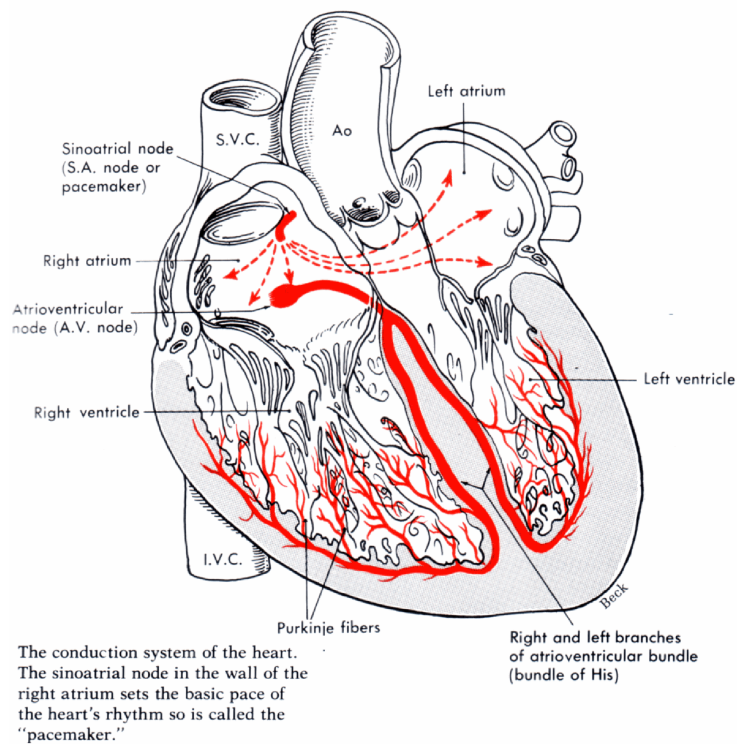


Figure 1.21.: Scheme of the conduction system of the heart. Figure taken from [amc]

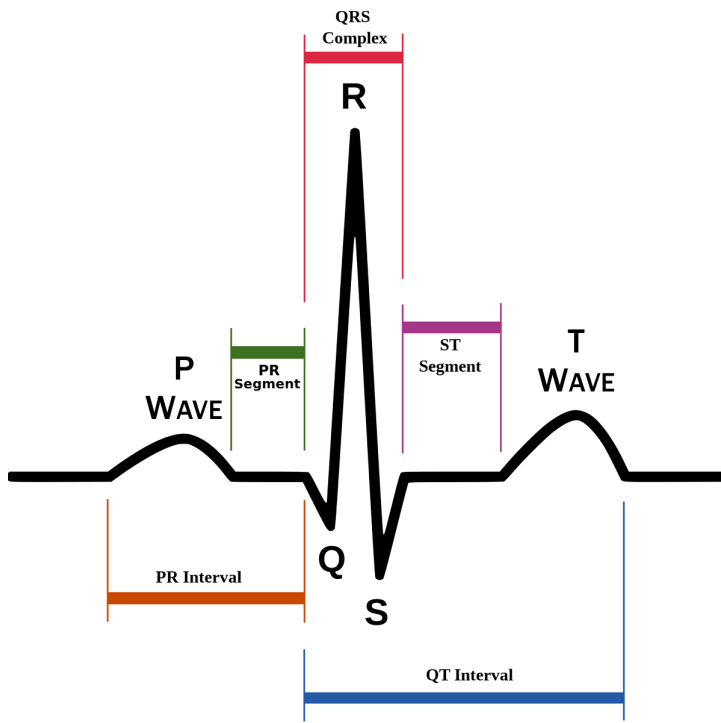


Figure 1.22.: ECG trace of a normal heart beat. Figure taken from [afib]

In AF there is unorganized atrial activity, leading to quivering motion and hence the atria are not able to sustain a healthy pumping rhythm. An exemplary ECG trace for AF can be seen in figure 1.23. Possible reasons and triggers for this abnormal action potential propagation are stated in the section 1.3.3.



(a) normal sinus rhythm



(b) AF patient

Figure 1.23.: ECG traces for a normal sinus rhythm (a) and for an AF patient (b). In AF, the tracing shows small, irregular fibrillation waves between heartbeats. The rhythm is irregular and erratic. Figure taken from [afib]

1.3.2 Types of atrial fibrillation

Based on the duration and presentation of the condition different types of AF are clinically distinguished [ESC10, CE09] (paroxysmal, persistent, long-standing and permanent) (see figure 1.24). Furthermore silent AF may present itself as any form of the stated AF types. As the name indicates, the condition is asymptomatic and hence undiagnosed. It usually manifests as an AF related complication like an ischemic stroke. About one third of people with AF are estimated to be unaware of their condition [ESC10].

Usually AF progresses over time. Starting as short and rare episodes the condition develops into longer and more frequent attacks [ESC10]. In figure 1.25 the typical time course of AF is indicated. In the lower part of the diagram different periods of AF are shown (dark blue boxes). Possible treatment possibilities at the different stages of AF are shown in the upper bars. Medication uptake which should prevent the formation of blood clots are represented by light blue boxes. These medications are recommended in the majority of AF patients. The red boxes indicate system relief therapies while the grey boxes represent rate control measures.

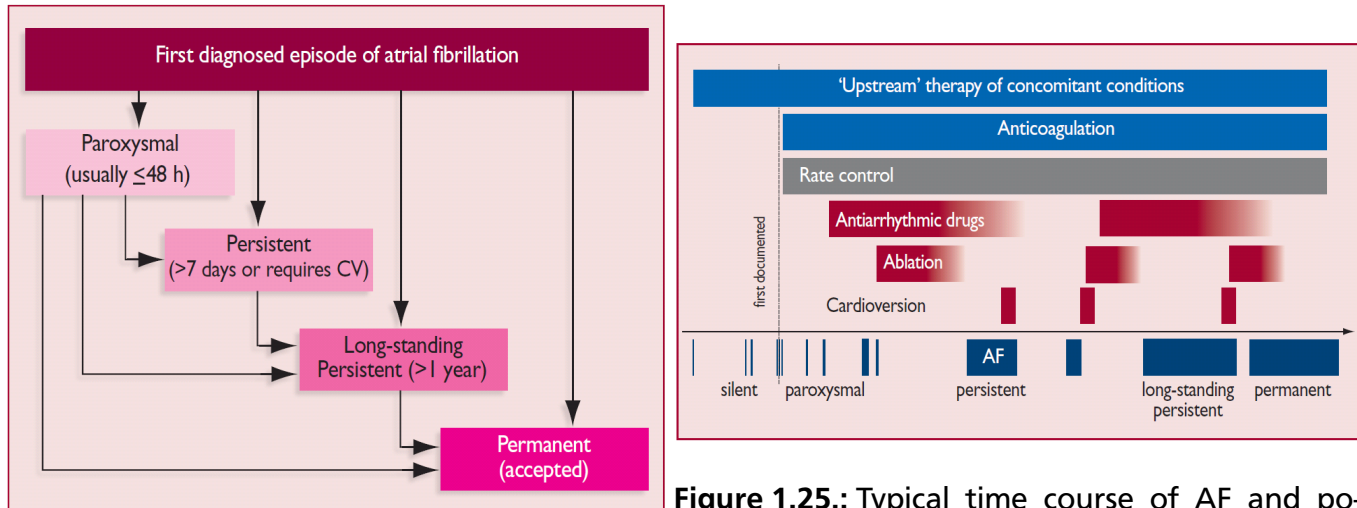


Figure 1.24.: Different types of AF. Figure taken from [ESC10]

Figure 1.25.: Typical time course of AF and potential treatment possibilities. Figure taken from [ESC10]

1.3.3 Possible causes for atrial fibrillation and risk factors

The mechanisms of AF are not yet fully understood. The multifactorial mechanisms may influence and sustain each other. Current research indicates that one can distinguish between focal mechanisms and multiple wavelets [CE09]. For most patients with paroxysmal AF a localized, focal trigger can be identified. This is not the case in patients with persistent or permanent AF, where the multiple wavelet hypothesis is believed to be more accurate.

An identified **focal trigger** site are the pulmonary veins (PVs). In the benchmark paper Haïssagurre et al. [Hai98] studied 45 patients with frequent episodes of AF ((344 ± 326) minutes episodes per 24 hours) finding ectopic beats¹ originating from the pulmonary veins in 94% of the cases. The underlying mechanism why PVs become arrhythmogenic in some patients while it remains dormant in others is still not clear [CE09]. The reason why PVs can become arrhythmogenic at all is based on stages during the embryonic development, in which the common PV is incorporated into the left atrium. Immunohistochemical studies have shown that the composition of the PV and the smooth-walled portion of the left atrium are identical (see figure 1.26) [CE09, Doug06].

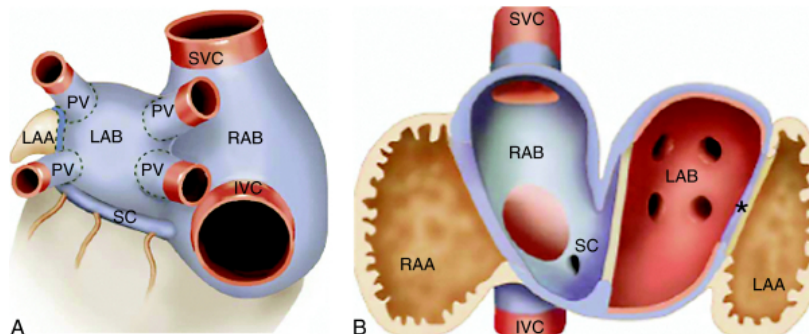


Figure 1.26.: Schematic depiction of outer side of atrial chambers with pulmonary veins (PV), left atrial appendage (LAA), left atrial body (LAB), right atrial body (RAB), superior vena cava (SCV) and inferior vena cava (IVC). LAB and RAB are covered by myocardium (heart muscle tissue) with smooth-walled inner aspect (blue), which stretches out over extra cardiac segments of PV (blue area above and below dotted line). In A the structures are illustrated from the outside, while B shows the tissue types from the inside of the atria. Figure taken from [Doug06]

Furthermore, according to the **multiple wavelet hypothesis** AF is sustained by the continuous propagation of several independent wavelets [CE09]. These wavelets are propagating through the muscles of the atria in a chaotic manner. Interference effects between various wavelets lead to amplification or cancellation. As long as the number of wave fronts does not decline a certain threshold level AF is sustained.

¹ beats which arise from cells outside the region in the heart muscle ordinarily responsible for impulse formation

Certain risk factors and indicators for AF can be found in the AF patient group [CE09]. Ageing generally increases the risk of developing AF. The reason might be due to age dependent loss of atrial myocardium and the associated conduction disturbances. Hypertension is also an age dependent factor which is a risk factor for the incidence of AF as well as AF-related complications such as stroke and systematic thromboembolism. Thyroid dysfunction can be the sole cause of AF and may induce AF related complications. 25% of AF patients are obese [Nab09] and 20% suffer of diabetes mellitus requiring medication. Chronic obstructive pulmonary disease (COPD) is found in (10 - 15)% of AF patients. Nevertheless it is possibly more a marker of general cardiovascular risk than an indicator for AF. Chronic renal disease is present in (10 - 15)% of AF patients and it is suggested that renal failure may increase the risk of AF related complications [CE09]. Independent of the stated risk factors AF has also a genetic component, especially considering an early onset of AF. In a study carried out by Fox et al. [Fox09] with 2243 offspring participants it was stated that the risk of developing AF compared to no parental AF was significantly increased (multivariable-adjusted odds ratio of 1.85, 95% confidence interval). The results were even stronger when age was limited to an age younger than 75 in parents as well as their offspring (multivariable-adjusted odds ratio of 3.23, 95% confidence interval).

1.3.4 Treatment modalities

The treatment modalities for AF have two main goals: to reset the rhythm or to control the ventricular rate and to prevent the formation of blood clots [Mayo, CE09]. The treatment strategy chosen for each individual patient depends on the type of AF and on careful consideration of patient individual factors, including the severity of symptoms and potential further heart problems.

Resetting the heart rhythm is the ideal treatment outcome and is carried out by cardioversion, either based on medication (anti-arrhythmic drugs) or electrically. In an electrical cardioversion an electrical shock is delivered to the heart, giving the conduction system of the heart the possibility to restore its normal activity. Commonly used anti-arrhythmic drugs are e.g. Amiodarone. These drugs have severe side effects and can act proarrhythmic, causing also life-threatening ventricular arrhythmias [Mayo].

If AF can not be converted to a normal heart rhythm through the above stated methods, the ventricular rate needs to be reduced instead. Heart rate control can be achieved either by the usage of different medication (e.g. Lanoxib) or by AV node ablation. This procedure requires simultaneously the implementation of a pacemaker to establish a heart beat. Hence the atria are still fibrillating, further medication with anti-arrhythmic medication as well as anticoagulants is required.

For paroxysmal or persistent AF further treatment modalities are needed. They include the **Maze procedure** or **radiofrequency catheter ablation**.

In the **Maze procedure** scar tissue in the atria is created, inhibiting the propagation of abnormal action potentials. Similar to a maze, only a single pathway from the SA node to the AV node remains accessible for electrical impulses [CTS13]. Besides an open chest surgery, the Maze procedure can also be carried out as minimal-invasive procedure or as cryotherapy. The success rates as well as complications of Maze versus catheter ablation will be described in the next section.

In **catheter ablation** the main strategy is anatomic based, which means that it is assumed that AF is triggered and sustained by the same anatomical sites (the PVs [Hai98]) in the majority of AF patients [CE09]. In radiofrequency ablation a flexible catheter is inserted into the patient through a vein close to the groin of the patient and threaded into the heart. An electrode on the tip of the catheter sends out radiofrequency waves, creating energy and thus heat. This is used to create a scar close to the junction between the pulmonary veins and the atria (see figure 1.27).

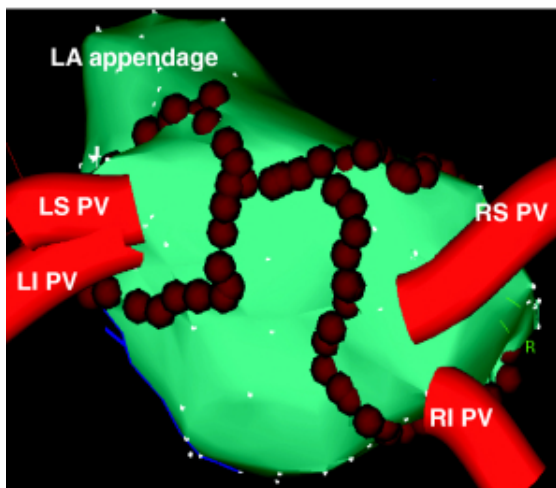


Figure 1.27.: Example of circumferential PV ablation. The ablation sites are indicated by the red dots. LI PV: Left inferior pulmonary veins, LS PV: left superior pulmonary veins, RI PV: right inferior pulmonary veins, RS PV: right superior pulmonary veins. Figure adapted from [Ora06]

Various ablation techniques exist, including the PV isolation by segmental ostial ablation, circumferential PV ablation (see fig. 1.27), wide-area circumferential ablation and antral PV isolation [Ora06, Ora03, Ouy04]. Antral PV isolation and wide-area circumferential ablation was shown to be effective for both patients with paroxysmal and persistent AF [CE09, Ora03]. In a randomized study circumferential PV ablation was found to result in a sinus rhythm in 74% of patients with chronic AF [Ora06].

The goal of PV ablation is to induce a complete electrical isolation of the PVs. This is verified by entrance and exit block during pacing at multiple sites within the PVs [CE09]. Freedom from recurrent AF can be predicted by termination and noninducibility of AF during catheter ablation [Ora02, Ora06, Hai05, Hai04, Ora04]. Termination of AF indicates elimination of all triggers and drivers of AF while noninducibility indicates the absence of residual triggers and drivers that may initiate and perpetuate AF [CE09]. Termination is hence not a reliable predictor in patients with paroxysmal AF while noninducibility is likely to predict that the patients are going to stay in sinus rhythm (see figure 1.28).

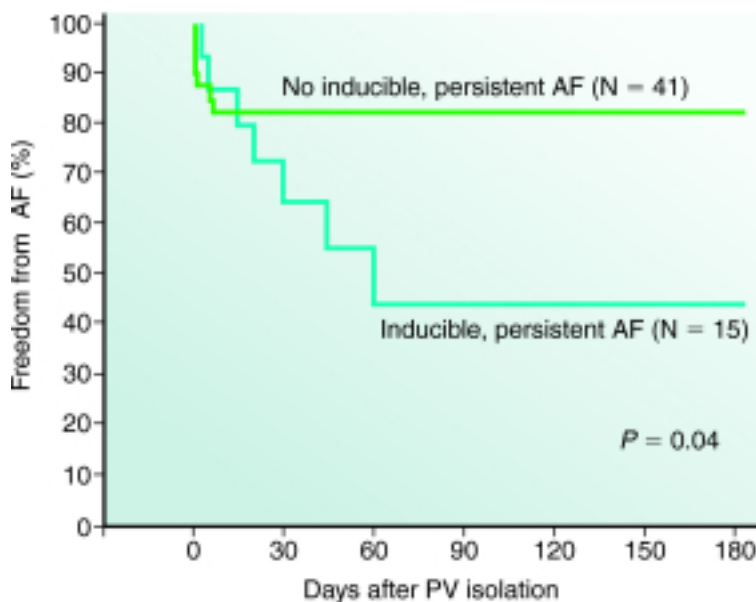


Figure 1.28.: Graph showing freedom from AF reoccurrence when patients had or had not inducible AF after circumferential PV isolation. Figure adapted from [Ora04]

Independent of the used procedure, anticoagulants like Warfarin are used in a diversity of patients. In order to establish international criteria for risk patients who should uptake anticoagulants, the CHADS₂-VASc score was defined [ESC12] (Congestive heart failure: 1 point, Hypertension: 1 point, Age (\geq 75): 2 points, Diabetes mellitus: 1 point, Stroke: 2 points, Vascular disease: 1 point, Age (65-74): 1 point, Sex (female): 1 point). Patients who obtain at least 2 point in the CHADS₂-VASc score are prescribed anticoagulants. Patients with 1 point might be prescribed anticoagulants, alternatively aspirin can be used. Patients with a score of 0 are supposed to only take aspirin [Fle]. The CHADS₂-VASc score has been validated in multiple cohorts [Lip11, Pot12, Ole12, Van11, Fri12, Ole11, Bor11].

Catheter ablation of AF: success rate and complications

The FAST trial compared the outcome of catheter ablation and surgical ablation in a randomized study with a small patient population of 127 patients. 63 patients were treated with catheter ablation, 64 with the invasive surgical ablation. The complication rate in catheter ablation was significantly lower (15.9% complication rate in catheter ablation versus 34.4% in surgical ablation) but at the same time the success rate in treatment outcome was reduced (36.5% for catheter ablation versus 65.6% for surgical ablation after 12 months) [Boe12].

In two nationwide surveys the success rates of catheter ablation as a treatment for AF and the resulting complications were studied [Cap05, Cap10]. The first worldwide multicenter survey was published in 2005 using data obtained from 181 centers in-between 1995 and 2002. From these centers 90 stated to have performed 12,830 catheter ablation procedures on 8,745 AF patients. It was stated that 52% of AF patients undergoing ablation were symptom free without the need of further antiarrhythmic medication and 23.9% of patients with the need of antiarrhythmic drugs. These success rates were achieved with the requirement of a second (in 24.3% of patients) or even third (in 3.1% of patients) procedure [Cap05]. Major complication rates were reported in 6% of patients. These complications included 4 early deaths (due to massive cerebral thromboembolism in two patients, extrapericardial PV perforation in one patient and unknown reasons in one patient), strokes (in 20 patients), transient ischemic attacks² (in 47 patients) and episodes of tamponade³ (in 107 patients). In a second survey which was performed in-between 2003 and 2006 [Cap10] and included 85 catheter ablation performing centers (16,309 patients), an improvement in treatment outcome was shown. The rate for a successful treatment outcome without the need of further antiarrhythmic medication increased to 70% while the rate with the need of further antiarrhythmic medication decreased to 10%, resulting in an overall success rate of 80% compared to 75.5% in the first survey. Concerning the number of needed procedures it was stated that 37.1% single treatments were performed, 59.8% dual treatments and 4.1% triple treatments.

Recent studies furthermore show that catheter ablation procedures in AF patients are associated with a substantial risk of developing silent cerebral embolism [Her13, Gai10, Marti13, Med13, Schr10, Lic06]. Silent cerebral embolism can cause cognitive impairment [Kne08]. A study by Medi et al. [Med13], which investigated the post-operative neurocognitive dysfunction in 150 patients undergoing ablation before and after the treatment, stated a 13% - 20% incidence at long-term follow up of 3 months compared to a control group.

² "mini-stroke"; stroke-like symptoms due to loss of blood flow, no permanent damage

³ fluid collects between the heart muscle and the pericardium, which is the sac containing the heart

Besides these major complications general disadvantages in the treatment modality of catheter ablation can be concluded. Procedures are tedious and can take up to five hours [Jong05]. As fluoroscopy is still the mainstay of catheter imaging in most laboratories the patients are furthermore exposed to relatively high X-ray dose [Ber10]. From an socio-economical point of view, catheter ablation causes high costs. A total of 13.5 billion Euro are spent on AF patients each year in the EU [Fus06].

It can be concluded that catheter ablation offers only a limited treatment success rate while major complications and even death due to the procedure may occur. Alternative treatment modalities are warranted. Catheter-free ablation using carbon ions could have the potential to accurately eliminate arrhythmogenic sources at any given cardiac location. So far conducted studies to irradiation of cardiac target sites will be presented in the next section.

Heart irradiation and cardiac radiosurgery

Target sites in the heart have been irradiated in different procedures. Re-stenosis⁴ after angioplasty⁵ for example has been treated with vascular brachytherapy [Nat99, Cot05]. Thereby a minimum dose of (8-16)Gy to a depth of 0.5mm into the vessel wall was required, while a maximum vessel dose did not exceed 32Gy. Cardiac angiosarcoma, a very rare tumor type in the heart with rare long-term survival of the patients, has been treated with carbon ions at the Japanese facility NIRS [Aok04]. A total dose of 64Gy was given in 16 fractions in a timeframe of 4 weeks. Follow-up of one and a half year did not show severe side effects.

Similar to the techniques used in vascular brachytherapy, Pérez-Castellano et al. [Per06] studied the possibility to use β -radiation as treatment modality for AF. They thereby used a phosphorus-32 source wire centered within a balloon catheter in a study with ten mini swine. The delivered dose was calculated to 60Gy at a depth of 1 mm from the contacting PV wall, resulting in observed PV fibrosis without PV stenosis or other side-effects.

In 2010 a study by Sharma et al. [Sha10] showed that they were able to successfully alter the electrical pathway of the heart noninvasively by using stereotactic robotic radiosurgery. In the CyberHeart system cardiac target sites in sixteen mini swine were irradiated under general anesthesia. The procedure was as follows. Cardiac CT scans of the anesthetized and intubated mini swine were acquired and an electroanatomic mapping⁶ was carried out before the irradiation. The voltage was mapped to enable a comparison with the later to be induced elec-

⁴ reoccurrence of blood vessel narrowing

⁵ mechanical widening of narrowed blood vessel e.g. with a balloon catheter

⁶ CARTO system; Biosense-Webster. Three known magnetic sources are used to calculate the orientation and position of the catheter tip in 3D, while at the same time the voltage values are determined [bw]

trophysiological effect. Different target sites in the heart were chosen. The respiratory motion was compensated by tracking with the CyberKnife Synchrony software, which correlates the outside motion of radiopaque markers on the chest wall with the internal motion [Ozh08]. For the cardiac motion an ITV approach was chosen. Target volumes were the cavotricuspid isthmus (CTI) (nine mini swine), the AV node (two mini swine), the pulmonary vein - left atrial junction (three mini swine) and the left atrial appendage (two mini swine). Dose ranges from 25Gy to 80Gy were applied (cavotricuspid isthmus: (25-80)Gy, AV node: (40-70) days, PV: (38-40)Gy and left atrial appendage: (32-80)Gy). Post irradiation the mini swine were stored at a farm. The follow-up time was dependent on the irradiated target in the mini swine (cavotricuspid isthmus: 25 to 89 days, AV node: 15 to 49 days, PV: 35 to 196 days and left atrial appendage: 16 to 33 days). In order to assess the irradiation outcome, the animals were again anesthetized and electroanatomically mapped. Afterwards the mini swine were euthanized and targets (heart) as well as organs at risk (lung, esophagus) were excised and fixed in formaldehyde. The results of the irradiation can be summarized as follows: The irradiation of the cavotricuspid isthmus evolved during the study, leading to changes in the method of targeting. While initially the respiratory and cardiac motion were not compensated for, synchrony and cardiac ITV concepts were later used. While all mini swine displayed a reduced conduction across the isthmus, only two animals showed bidirectional block and hence feasibility at 30 days and 40Gy. Targeting the AV node, one animal had to be sacrificed due to pacemaker pocket infection. The other one showed a complete AV block at 49 days, after being irradiated with 70Gy. For the left atrial appendage a decreased voltage was observed at 38Gy after 33 days. For the left pulmonary vein the feasibility was shown as the left atrium showed no local activation in all animals (present from day 35 for all doses) (see figure 1.29).

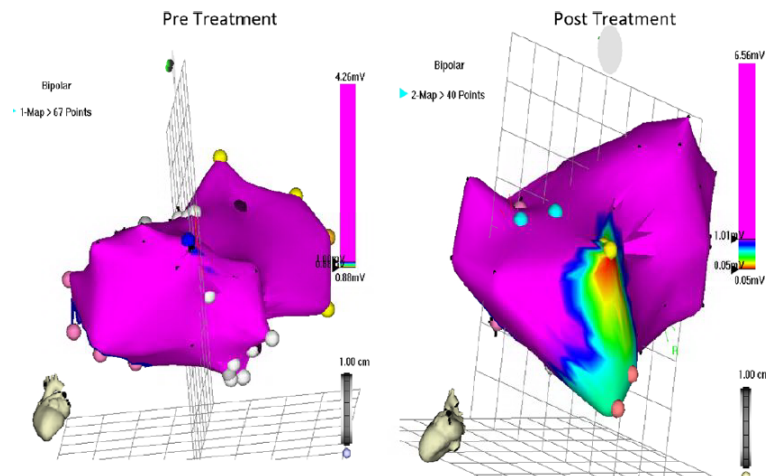


Figure 1.29.: Electroanatomic voltage map of left atrium before (left side) and after (right side) CyberHeart irradiation of PVs. Prior treatment no decreased voltage can be observed. Post treatment an area of low-amplitude action potential signals can be seen. Figure from [Sha10]

Sharma et al. stated that a dose of 25Gy or larger was needed to see a change in the electrophysiological properties in the animal model after 30 or more days. The dose needed for myocardial fibrosis is also known from other former studies. Fajardo et al. [Faj70, Faj73] for example studied radiation induced fibrosis in rabbit hearts. They observed myocardial fibrosis most often after 2 to 70 days when irradiating the rabbits with 20Gy. Overall Sharma et al. proved that stereotactic radiosurgery has the potential to become a noninvasive treatment modality for e.g. atrial fibrillation.

A subsequent study carried out with the CyberHeart system [Mag11] only targeted the pulmonary veins atrial junction. Two mini swine were irradiated with a single fraction treatment of 25Gy and 35Gy, respectively and followed for 6 months. It was stated that both animals showed circumferential fibrosis, leading to an electrical isolation of the PVs, which was detected with an electroanatomic mapping. The mini swine irradiated with 35Gy showed more extensive necrosis and vasculitis in intramyocardial vessels. It was hence implied that 25Gy are sufficient to induce a PV isolation with no major complications in the studied timespan.

In an animal study carried out by Blanck et al. [Bla13] 8 mini swine were irradiated with a single fraction of seven fields with doses between 17.5Gy and 35Gy. A 5D-ITV concept was applied, hence applying internal margins to the upper right PV accounting for the respiratory and heartbeat. Prior treatment electroanatomic mapping was carried out. The animals were followed for 6 months. In this study it was stated that a reduction of the electrical signal procession with correlating local transmural fibrosis in the target region was observed at doses above 30Gy. Nevertheless a complete block of the PVs could not be achieved. Stenosis in one branch of the PV was observed for the highest applied dose.

All these studies were carried out with photon irradiation. Due to the physical and biological properties of carbon ions (see section 1.1) an improved outcome is expected when treating these deep seated target volumes while sparing the critical organs close by and exposing less volume of myocardium to low dose of radiation [Ber12]. The feasibility of this treatment modalities with scanned carbon ions is the aim of the present work.



2 Irradiation of pulmonary veins under influence of respiration in human data

Contents

2.1. Material and methods	54
2.1.1. Treatment planning input data	54
2.1.2. Treatment planning parameters	55
2.1.3. Treatment planning studies	57
2.1.4. Analysis	57
2.2. Results	58
2.2.1. Motion assessment of respiration	58
2.2.2. Motion mitigation techniques for respiration	62
2.3. Discussion	73
2.4. Conclusion	75

PVs move due to the heartbeat and respiration of the patient. Both motion types are independent from each other and can hence be studied individually. While the influence of heartbeat is analyzed in chapter 3, the effect of respiratory motion will be discussed in this chapter. 4DCTs of nine lung cancer patients were recorded for cancer radiotherapy at MD Anderson Cancer Center in Houston (MDACC, Texas, USA) where patients were treated with proton therapy and IMRT. The same data has been used in previous studies on motion mitigation techniques using carbon ion beams (e.g. [Lue12, Woe11]). The PV were contoured and the resulting motion pattern, direction as well as motion amplitude of LPV and RPV due to respiration were studied for all cases. Respiration is also a problematic factor for catheter ablation as it can cause changes in catheter contact force and hence alter the result [Kum12]. For the proposed non-invasive treatment modality with a scanned carbon ion beam the respiratory motion will endanger the treatment outcome as it often leads to inhomogeneous dose coverage. Hence motion mitigation techniques are needed. The resulting interplay pattern for all patients as well as gating as a possible motion mitigation technique have been studied and the results will be presented in this chapter. Exemplary for two patient cases rescanning inside the gating window was analyzed.

2.1 Material and methods

Details on the input data as well as the used treatment planning parameters will be given. Afterwards an overview on all studies will be presented and the analysis procedure will be described.

2.1.1 Treatment planning input data

For treatment planning studies with the in-house treatment planning software TRiP4D [Ric13], 4DCT data sets, target and OAR contours as well as a deformable image registration for motion assessment in-between the different motion phases are needed. Details on the used input data as well as the used treatment planning parameters will be given.

In order to assess the motion of the PV due to respiration, lung cancer patient data was used. The 4DCTs of nine patients were recorded and anonymized at MDACC. Each of the 4DCT data consisted of ten motion phases, the reference phase was motion phase five at end exhale. The amplitude of the respiratory motion was assessed by measuring the difference between the (right) diaphragmatic dome in-between end exhale and end inhale on a frontal view of the 4DCT data. The amplitudes in the superior-inferior (SI) motion direction, the largest motion component in case of respiration, ranged from 2.5mm to 25mm (CT slice distance and hence resolution of 2.5mm). The varying motion amplitudes are displayed for all patients in table 2.1. Two of the nine patients (patient 6 and 7) displayed a very shallow breathing with an amplitude of less than 5mm. Five patients (patient 1 to 5) had a breathing amplitude between 10mm and 20mm in SI direction. Two patients (patient 8 and 9) were breathing deeply with an amplitude bigger than 20mm. This indicates different breathing patterns as well as varying lung volume expansion and hence heart displacement amongst the studied patients.

Table 2.1.: Respiratory motion in the direction of the largest motion component (SI) for all investigated patients. Furthermore the lung tumor location (left lung (L) or right lung (R)) is stated next to the tumor volume.

patient no	motion [mm]	tumor volume [cm ³]	tumor location (L/R)
1	17.5	236.5	L
2	20	572.2	R
3	10	160.2	R
4	17.5	676.1	L
5	15	372.1	R
6	2.5	706.1	R
7	5	123.8	L
8	25	44.7	L
9	22.5	125.3	L

Segmentation of the LPV and RPV was performed with an in-house display functionality for TRiP [Hil09]. Its graphical interface allows contouring on the axial slices of the reference phase of the 4DCT. The contours were checked and validated by a medical physicist who was involved in the animal studies of Sharma et al. [Sha10] as well as a cardiologist from Mayo Clinic. Only the motion influence and the motion mitigation possibilities will be studied here, hence contouring of other volumes or organs at risk was omitted. A detailed analysis of the dose to the organs at risk in human data is performed in chapter 3. The volumes of the contours for the ablation sites for LPV and RPV are presented for each patient in table 2.2.

Table 2.2.: Target volume for LPV and RPV for all investigated patients.

patient no	LPV [cm ³]	RPV [cm ³]
1	1.88	5.26
2	3.57	4.79
3	6.49	11.52
4	3.66	3.87
5	2.07	4.37
6	3.40	6.34
7	4.29	6.23
8	6.89	4.84
9	2.92	2.56

Non-rigid image registration of the nine motion phases on the reference phase have been performed with Plastimatch [Sharp07, Shack10]. A B-spline registration with the following parameters was chosen: The first step was carried out with 50 maximal iterations and an isotropic spacing of 35mm between the control points of the B-spline grid. In the second step, with 100 maximal iterations, the grid spacing was set to 11mm and the regularization to $\lambda=0.005$. The quality of registration was validated with visualization techniques: false color images [Bro07], checker board images [Bro07] as well as a qualitative check of the vector field regularization. These tests were carried out between the two most extreme motion phases: the reference phase at end exhale (motion phase five) and the phase at end inhale (motion phase zero).

2.1.2 Treatment planning parameters

Treatment plans without motion (3D, static) as well as with motion (4D) were generated. For the dose optimization process, 3D treatment plans were generated to homogeneously cover the CTVs in the reference phase while 4D treatment plans covered the ITV [Gra12], which was generated from all twenty motion phases. Besides the original volume of the CTV safety margins have been added to the volumes of the treatment planning study. These margins were applied in order to account for possible deviations in between treatment planning and delivery, like positioning errors, changes between CT acquisition and treatment delivery etc. Isotropic safety

margins of 3mm, 5mm and 7mm have been chosen. The ITV volumes used as the final PTV target were generated from the original CTV contour as well as the CTVs with margin, so that potential range variations were considered in the margins.

The grid spacing was chosen to be 1mm, both in x and y direction. The spacing between the IESs were chosen to be 3 mm_{H_2O} . A maximal contour extension¹ of 1.1 times the focal spot size of 4mm was chosen as well as a distal contour fall off of 4mm_{H_2O} . TRiP's 'all points divergent beam' algorithm was used to calculate the absorbed dose. All treatment plans were calculated as intensity modulated particle therapy (IMPT). Following Sharma et al. [Sha10] a physical dose of 25Gy was applied in one fraction in all simulations.

Three different beam entrance directions were used. For all beam directions the couch was rotated by 90° while the gantry angles were set to -45° , 135° and 0° , respectively. With these field number and directions a good sparing of normal tissue, especially of the coronary arteries as well as of the aorta and of the trachea could be obtained (see chapter 3). The field directions were validated by a cardiologist from Mayo Clinic.

The generation of treatment plans is furthermore also dependent on the theoretically possible beam application. Spill length, shape and particle intensity are thus important factors. For the here presented simulations HIT accelerator parameters have been used. Thereby a spill length of up to 5s is assumed. The pause in between spills has a mean value of 4.5s. The spill shape is rectangular. The particle intensities at HIT used for treatment planning vary between 5×10^6 and 8×10^7 particles per spill. Inbetween these two extreme intensity levels, eight different intensity levels can be used. In the resulting treatment plan, the intensity steps are automatically chosen [Krae00, Ric13]. The minimum particle number per beam spot was set to 11,000.

As the reconstruction of the 4DCTs was based on the time scale a phase-based motion state detection was employed. A Lujan motion type was chosen for the motion trajectories [Luj99]. In order to consider possible divergence in the respiratory motion pattern of patients, different periods (6s and 8s) as well as different starting phases (0° and 90°) were used. The motion periods were chosen according to the respiratory rate of 8 to 10 cycles per minute.

¹ determines the extent of rasterpoint positions outside the target contour

2.1.3 Treatment planning studies

3D treatment plans on the CTV volume were produced as reference values to the 4D cases, as it represents the ideal but not deliverable dose distribution. Different ITV margins (original and increased with 3mm, 5mm and 7mm margin) were studied for all patients in the 4D treatment plans. In order to prepare for these 4D simulations, the motion of the PVs due to respiration was assessed. 4D plans were distinguished between an underlying motion without any compensation, resulting in interplay patterns [Phi92, Ber08], and with the application of gating [Kub96] as motion mitigation technique. The gating window was set to 30% around end exhale (reference phase five), so that motion phases four, five and six were used. For two patient cases (patient 2 and 9) rescanning inside the gating window was furthermore studied. Thereby four different rescan numbers (five, ten, fifteen and twenty rescans) have been studied. Treatment plans for all patients were carried out with one beam channel combination (couch angle of 90° and gantry angles of -45°, 135° and 0°), all four safety margins, the stated treatment planning parameters and the four stated motion trajectories.

2.1.4 Analysis

For comparison of the resulting dose coverage dose-volume-histograms (DVHs) were studied. The V95 (measure of dose coverage) and V107 (measure of over dosage) of the CTVs were analyzed. As an indicator for the dose homogeneity, the width of the dose fall off was determined by analyzing the difference D5-D95. The stated values have been evaluated for all beam application techniques (static, interplay, gating, rescanning within gating window). Furthermore motion-volume-histograms (MVHs) were generated in order to assess the resulting motion of the PV due to respiration.

In order to study correlations between the diaphragm motion and the motion of the PVs the Pearson coefficient r was determined and is reported for limits of $p < 0.05$. Furthermore the relation of dose analysis parameters to different margin sizes and the studied irradiation technique was analyzed by a one-way analysis of variance (one-way ANOVA) and the proportion of variance explained (r^2 - which ranges from zero (fit has no predictive value) to one) and is reported with the corresponding p-value ($p < 0.0001$).

Boxplots of dose analysis parameters D5-D95 and V95 over all patient data sets, motion patterns and target volumes were moreover generated in order to study the influence of margin size and irradiation mode (static, interplay and gating). Thereby the median (50th percentile) as well as the 25th and 75th percentile are displayed next to the minimum and maximum.

2.2 Results

In the following the results of the motion assessment as well as of the treatment planning studies for all studied cases (static, interplay and gating as well as rescanning within the gating window) will be presented. The expected treatment time will be discussed.

2.2.1 Motion assessment of respiration

Using the resulting deformation maps from deformable image registration the motion of the ablation sites of LPV and RPV was assessed. Motion volume histograms (MVHs) [Ric13] displaying the relative displacement of every voxel of the investigated volume to the reference phase in all three motion directions (SI: superior-inferior, AP: anterior-posterior, LR: left-right) as well as the absolute displacement (ABS) were generated. The mean and standard deviation of these displacement values in each motion phase of LPV and RPV are plotted for all patients and motion directions in figure 2.1 and 2.2, respectively. The numerical values can be found in appendix A.1.

The mean and standard deviation of the displacement between the two extreme motion phases (end exhale and end inhale) are shown for all patients in tables 2.3 and 2.4 for the different motion directions and for the two target volumes, LPV and RPV, respectively. Depending on the patient the absolute displacement of the pulmonary veins were found to vary between three millimeters and more than one centimeter. From the nine studied patients patient 9 is displaying the highest absolute displacement, both in LPV and RPV. For all patients, the largest motion direction is SI, resulting in the largest contribution to the absolute displacement. The average in SI direction over the entire volume reaches up to 15.5mm (average over all patients of (6.8 ± 3.8) mm) for LPV and 10.9mm (average over all patients of (6.8 ± 2.5) mm) for RPV. The other two motion directions show a much smaller displacement. In AP direction the maximal motion is less than 2.5mm (standard deviation of less than 1mm) and in LR the PVs move less than 2.7mm (standard deviation of 1mm). Over all patients, the mean absolute displacement in-between end exhale and end inhale of the LPV is (6.8 ± 3.6) mm and (6.8 ± 2.5) mm for RPV. For the SI direction, the mean displacement over all patients is (-6.4 ± 3.8) mm for LPV and (-6.6 ± 2.4) mm for RPV.

It can furthermore be seen that the relative displacement of the target volumes around end exhale (motion phase five, reference phase) is small for all motion directions and patients. The difference between motion phase four and six was only 3mm in the absolute displacement of patient 9, which is the patient with the largest motion in the patient cohort. Hence gating around end exhale was expected to be an adequate motion mitigation technique for the irradiation of the PVs under influence of respiration.

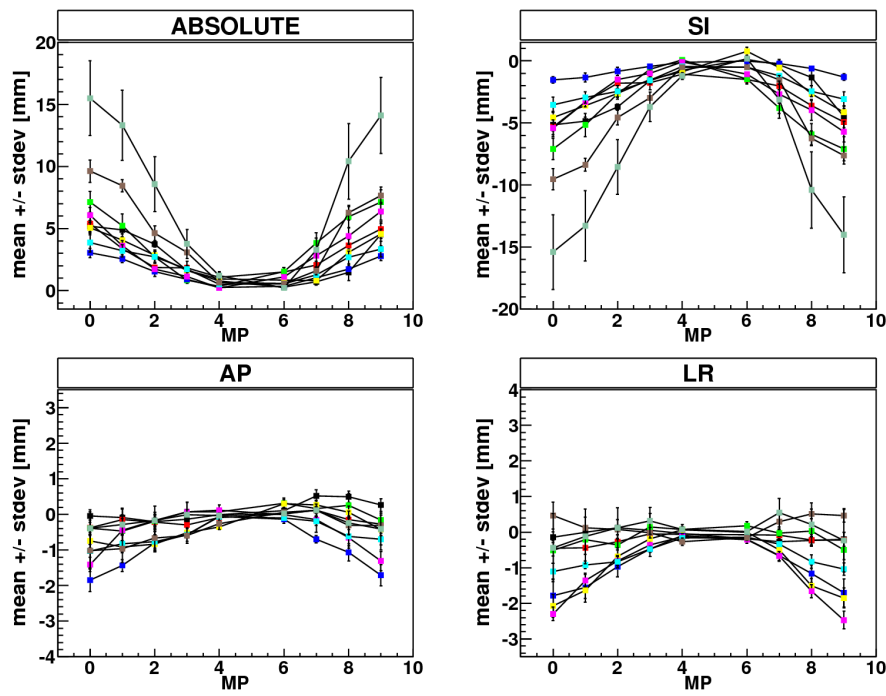


Figure 2.1.: LPV: Mean motion amplitude and standard deviation in each motion phase (MP) relative to the reference phase under influence of respiration for all patients (patient 1: black, patient 2: red, patient 3: green, patient 4: blue, patient 5: yellow, patient 6: pink, patient 7: turquoise, patient 8: brown, patient 9: olive).

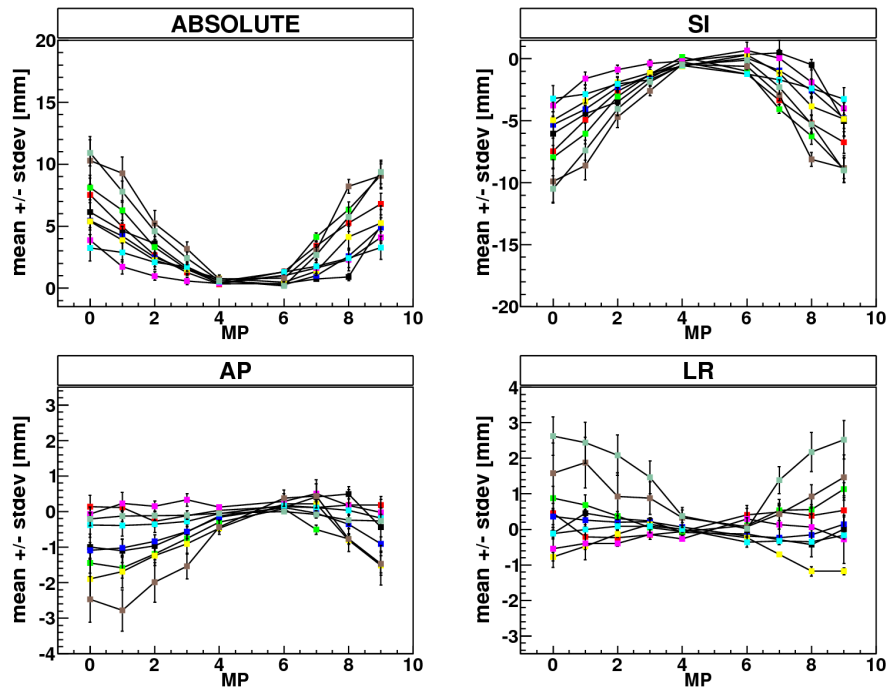


Figure 2.2.: RPV: Mean motion amplitude and standard deviation in each motion phase (MP) relative to the reference phase under influence of respiration for all patients (patient 1: black, patient 2: red, patient 3: green, patient 4: blue, patient 5: yellow, patient 6: pink, patient 7: turquoise, patient 8: brown, patient 9: olive).

Table 2.3.: LPV: Mean and standard deviation of target motion in-between end exhale (motion phase five) and inhale (motion phase zero) for all investigated patients.

patient no	ABS [mm]	SI [mm]	AP [mm]	LR [mm]
1	5.2 ± 0.5	-5.2 ± 0.5	-0.1 ± 0.2	-0.1 ± 0.2
2	5.3 ± 0.6	-5.3 ± 0.6	-0.4 ± 0.2	-0.5 ± 0.2
3	7.1 ± 0.9	-7.1 ± 0.9	-0.4 ± 0.4	-0.5 ± 0.4
4	3.0 ± 0.4	-1.5 ± 0.3	-1.9 ± 0.3	-1.8 ± 0.5
5	5.1 ± 0.6	-4.6 ± 0.5	-0.8 ± 0.2	-2.1 ± 0.3
6	6.1 ± 0.6	-5.4 ± 0.7	-1.4 ± 0.2	-2.3 ± 0.2
7	3.9 ± 0.8	-3.6 ± 0.6	-1.0 ± 0.4	-1.1 ± 0.2
8	9.6 ± 0.9	-9.5 ± 0.9	-1.0 ± 0.5	0.5 ± 0.4
9	15.5 ± 3.0	-15.4 ± 3.0	-0.4 ± 0.5	-0.4 ± 1.0

Table 2.4.: RPV: Mean and standard deviation of target motion in-between end exhale (motion phase five) and inhale (motion phase zero) for all investigated patients.

patient no	ABS [mm]	SI [mm]	AP [mm]	LR [mm]
1	6.1 ± 1.4	-6.0 ± 1.4	-1.00 ± 0.4	-0.1 ± 0.2
2	7.5 ± 1.4	-7.5 ± 1.4	0.1 ± 0.3	0.5 ± 0.4
3	8.1 ± 1.0	-7.9 ± 1.0	-1.5 ± 0.4	0.9 ± 0.3
4	5.5 ± 0.6	-5.3 ± 0.6	-1.1 ± 0.2	0.4 ± 0.2
5	5.4 ± 1.5	-5.0 ± 1.4	-1.9 ± 0.6	-0.8 ± 0.1
6	3.9 ± 0.5	-3.8 ± 0.5	-0.1 ± 0.2	-0.6 ± 0.5
7	3.3 ± 1.1	-3.2 ± 1.1	-0.4 ± 0.3	-0.1 ± 0.1
8	10.3 ± 1.9	-9.9 ± 1.7	-2.5 ± 0.6	1.6 ± 0.9
9	10.9 ± 1.1	-10.5 ± 1.1	-0.2 ± 0.2	2.6 ± 0.5

Possible correlations between the underlying respiration amplitude (see table 2.1) and the displacement of the ablation sites for the PVs have been studied. It can be stated that in AP and LR direction, no correlation was observed. In case of SI displacement the results varied depending on the target volume. While no correlation was observed between the diaphragma motion and the SI displacement of the LPV ablation, the site for RPV showed a strong linear relationship ($r=0.73$, $p<0.05$). This resulted in a strong correlation between diaphragm motion and the absolute displacement of the RPV ablation site ($r=0.79$, $p<0.05$). For the LPV again no correlation was observed in the absolute displacement.

It should be noted that these findings are based on a small number of lung cancer patients (see table 2.1), which can alter the breathing pattern and heart motion and hence the result. It is unclear whether atrial fibrillation patients would display the same motion dependence and correlation results, though the result was independent of the tumor position in the left or right lung.

The overall displacement field between the two extreme states, end exhale and end inhale, for two exemplary patients with a small motion amplitude (patient 7) and a large motion amplitude (patient 9) are shown in figure 2.3 and 2.4. In order to visualize the location of the displacement, an axial cut of the reference state CT is underlayed. The absolute values of the displacement vectors are shown as contour plots.

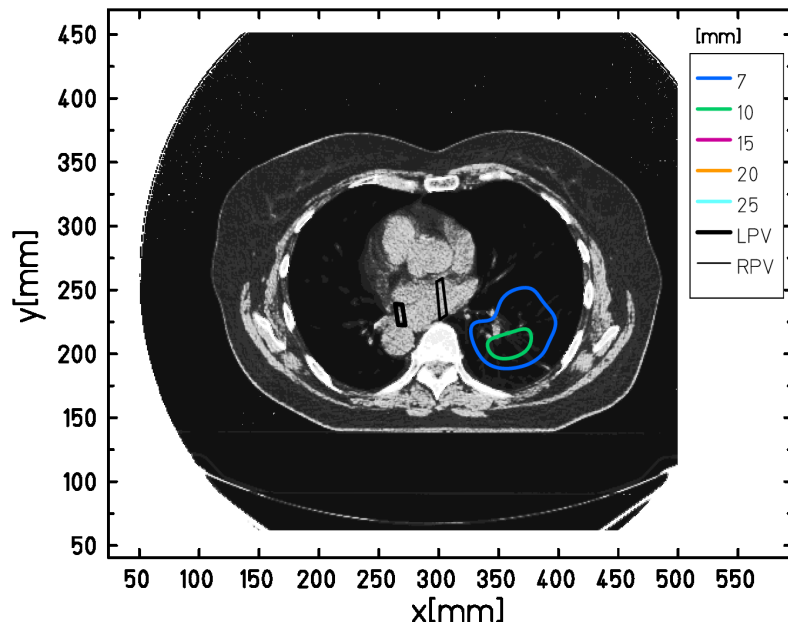


Figure 2.3.: Contour plot of Patient 7

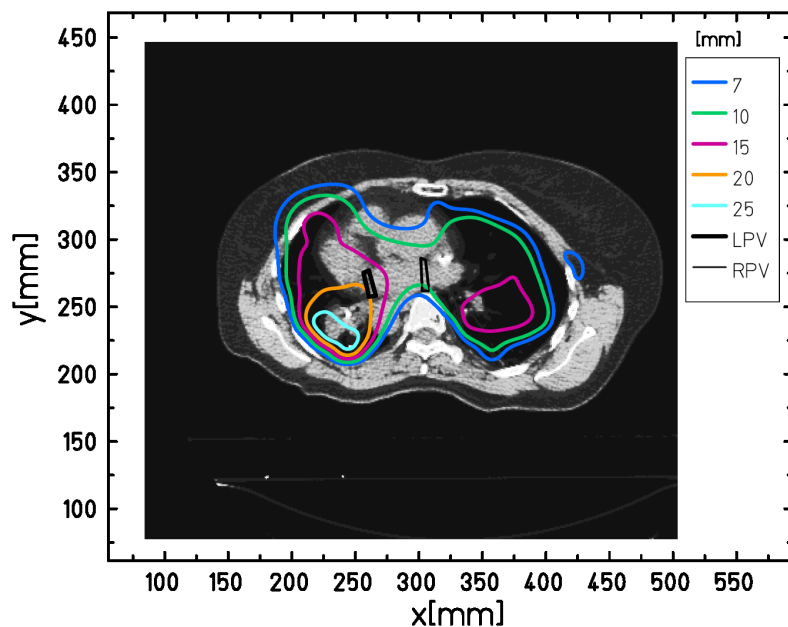


Figure 2.4.: Contour plot of Patient 9

2.2.2 Motion mitigation techniques for respiration

The absolute motion amplitudes of up to 1cm due to respiration are expected to yield dose inhomogeneity when not compensated for. The resulting interplay effect and dose deposition were studied for every patient for different motion patterns and different margins to the target volumes. The dose analysis values V95, V107 and D5-D95 were assessed and plotted. For comparison also the corresponding values for the 3D case (static) are shown. As shown in section 2.2.1 the motion displacement in the motion phases around end exhale (motion phase four to motion phase six) are rather small in all patient cases. Hence gating has the potential to be a well-suited motion mitigation technique to overcome the influence of target volume motion due to respiration. The results of the stated dose values in case of gating on the stated phases will be presented.

Dose deposition

A representative dose deposition for all studied techniques (static, interplay and gating) is shown exemplary for patient 9 (as this is the patient with the largest PV motion amplitude) in figure 2.5. Gating and interplay are shown for a motion period of 6s and a starting phase of 0°. The target volumes LPV and RPV were irradiated simultaneously and a margin of 3mm was added. It can already been seen from these dose cut figures that gating around end expiration drastically improves the outcome compared to interplay and yields a result which is comparable to the static case.

In order to assess the dose information for the whole volume the DVHs (see figure 2.6) of all patients were analyzed and compared for dose homogeneity, dose coverage as well as over dosage. The average results over all patients with the resulting standard deviation can be seen in figure 2.7. A more detailed analysis can be found in appendix A, where the corresponding numerical values are shown (tables A.19 - A.36) .

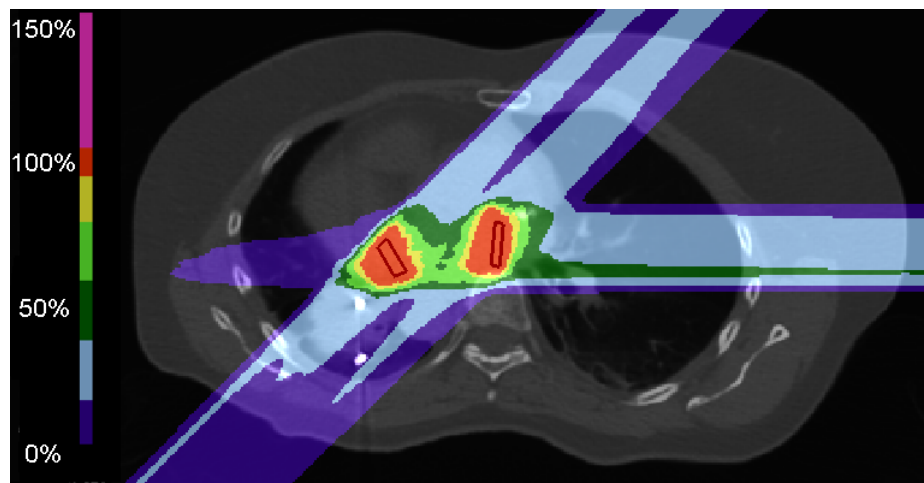
For interplay it can be seen that the results are dependent on the used motion period and starting phase. This can be seen in the mean values of the resulting dose parameter values for different underlying motion patterns. E.g. for LPV, the mean value of the dose coverage parameter over all patients is $V95 = (90.3 \pm 4.3)\%$ for a motion with 6s period and a starting phase of 90° and $(89.3 \pm 5.5)\%$ for a motion period of 8s and starting phase of 90°, while for a motion period of 8s and a starting phase of 0° the dose coverage is $(87.1 \pm 7.8)\%$. The safety margin influences the treatment outcome, as e.g. the dose coverage for a motion with 6s period and a starting phase of 90° has a mean value of $(94.2 \pm 4.8)\%$ with 3mm safety margin. All these dependencies are also valid for the other studied dose analysis parameters, dose homogeneity

and over dosage. The improvement of the dose coverage and dose homogeneity in relation to the size of the safety margin are also presented in figure 2.8 (a and b). The explained variance of the dose homogeneity versus the studied safety margins resulted in $r^2=0.30$ ($p<0.0001$).

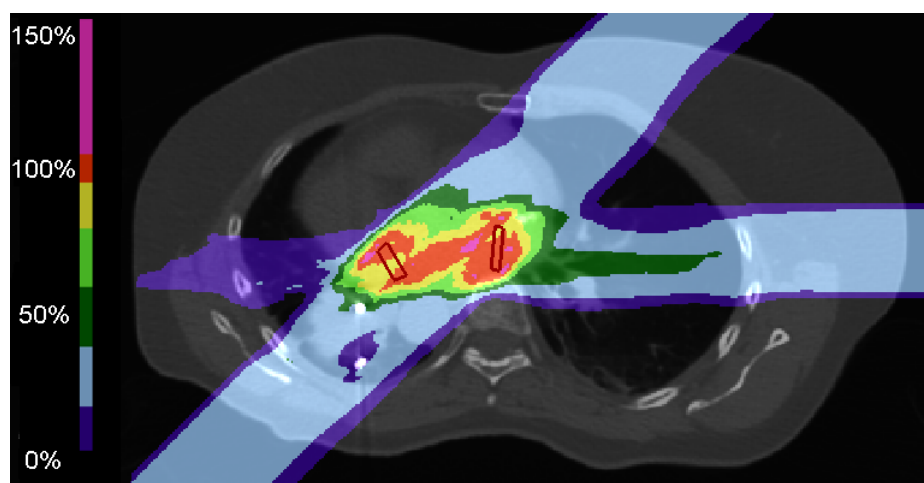
The underlying deformation map with its motion amplitude enables a prediction of the magnitude of the interplay effect. This was studied in more detail for the dose homogeneity, as these values were normally distributed. The explained variance of the maximal motion amplitude of the left and right PV (see table 2.3 and 2.4) and the resulting D5-D95 values for all studied margins was $r^2=0.25$ ($p<0.0001$).

Gating yielded improved results compared to interplay in all studied cases (see also figure 2.8). This is valid for dose homogeneity, dose coverage as well as over dosage. Especially dose coverage and over dosage are comparable to the static results for all patient and motion patterns (e.g. patient 1, V95 of 100% for all studied motion patterns and safety margins in RPV, see table A.20). In some patients the dose coverage is better with added safety margins (e.g. patient 9, V95 with no margin for motion period of 6s and starting phase of 0° is 94.1% for LPV, a V95 of 99.9% can be achieved for the same motion pattern with a margin of 3mm). Also in dose homogeneity a bigger safety margin tends to improve results (e.g. in LPV of patient 1 with motion period of 8s with starting phase of 0°: D5-D95 = 4.4% with margin of 3mm versus D5-D95 = 3.8% with margin of 5mm). These findings are also shown in figure 2.8. Here the dose coverage and dose homogeneity are shown for all patients, motion patterns and the two target sites (LPV and RPV) depending on the used safety margin. It can be seen that the dose coverage is already drastically improved with 3mm margin. Also the dose homogeneity is improved with increasing safety margin. The explained variance of D5-D95 versus all studied margins resulted in $r^2=0.40$ ($p<0.0001$). Keeping the safety margin constant, it was nevertheless found that in some cases the dose homogeneity is not drastically improved by gating compared to interplay. The LPV of patient 2 for example has a D5-D95 value of 6.8% for gating with a safety margin of 3mm (motion period of 6s and starting phase of 90°), which is only slightly under the interplay result of D5-D95=8.4% for the same safety margin and motion. However, the dose homogeneity value of interplay in this particular patient case is already lower than in other cases (e.g. D5-D95=10.6% in patient 1 or 20.93% in patient 9 for 3mm margin and a motion period of 6s, starting phase of 90°).

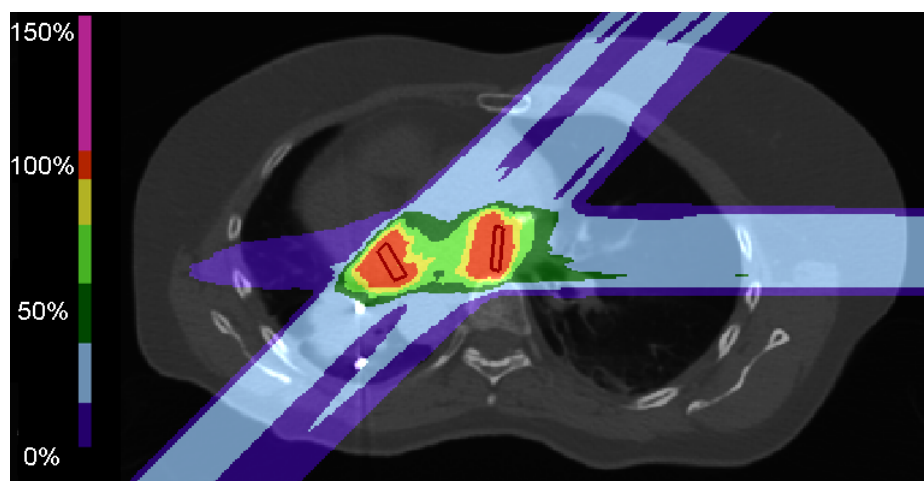
As a method to further improve the dose homogeneity rescanning inside the gating window was studied for two patient cases. The results are presented in the next section. It can nevertheless be concluded that gating of target volumes with safety margin yields results comparable to the static irradiation in case of under and overdosage and hence is an adequate motion mitigation technique for the irradiation of the PVs under influence of respiration.



(a) static

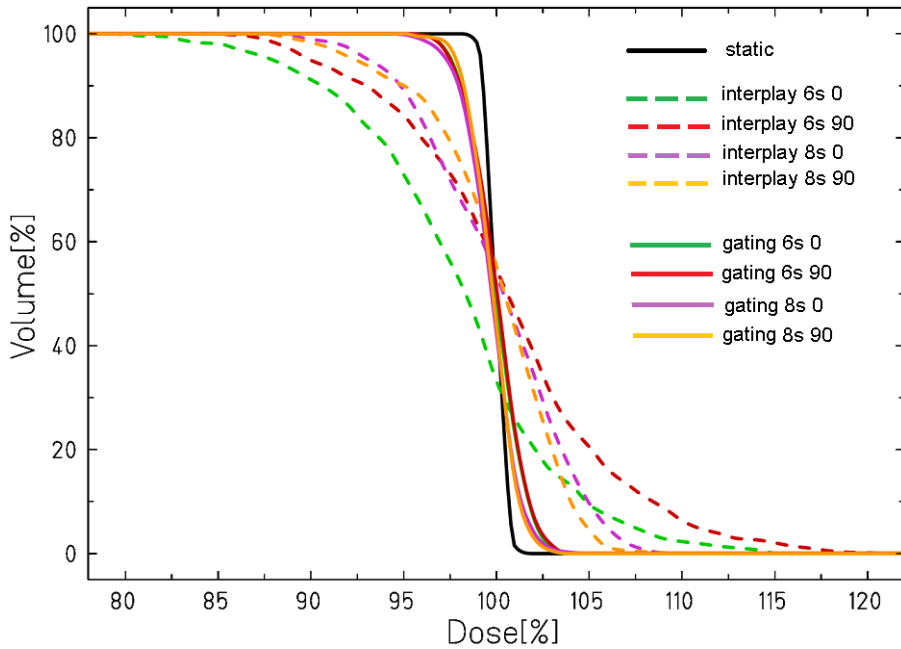


(b) interplay

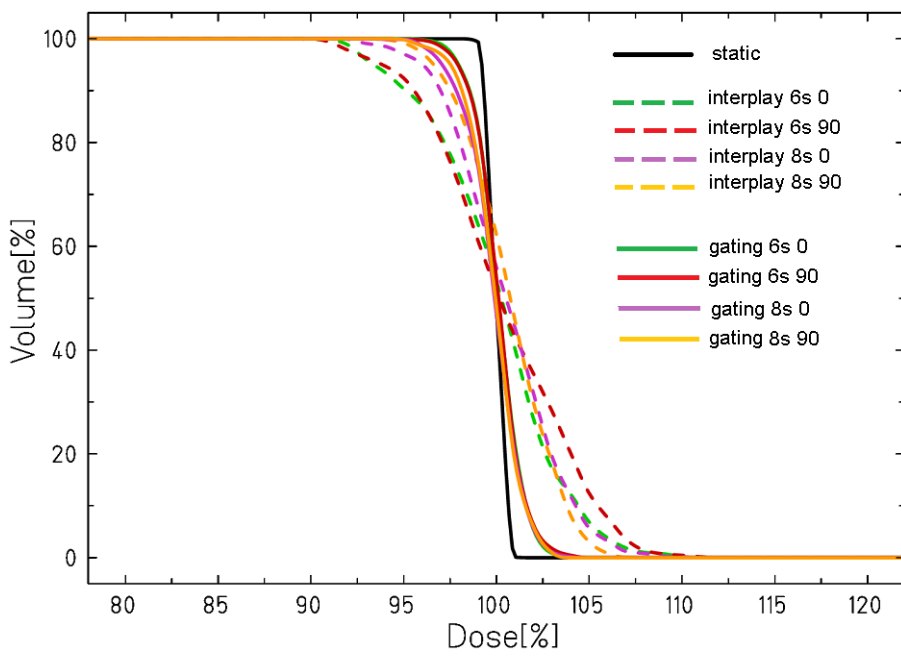


(c) gating

Figure 2.5.: Dose distribution of patient 9 for static (a) as well as interplay (b) and gating (c) at motion period of 6s and a motion starting phase of 0°. The target volume has an added margin of 3mm. The improved outcome of gating compared to interplay can already be seen in these dose cuts.



(a) LPV



(b) RPV

Figure 2.6.: Dose volume histograms for CTV of patient 9 for 3mm safety margin irradiation (LPV (a) as well as RPV (b)) in case of static irradiation (black), interplay (dashed) and gating (solid). The motion patterns are shown in colors (6s 0: Iujan motion with period of 6s and starting phase 0°, 6s 90: Iujan motion period of 6s and starting phase 90°, 8s 0: Iujan motion period of 8s and starting phase 0°, 8s 90: Iujan motion period of 8s and starting phase 90°).

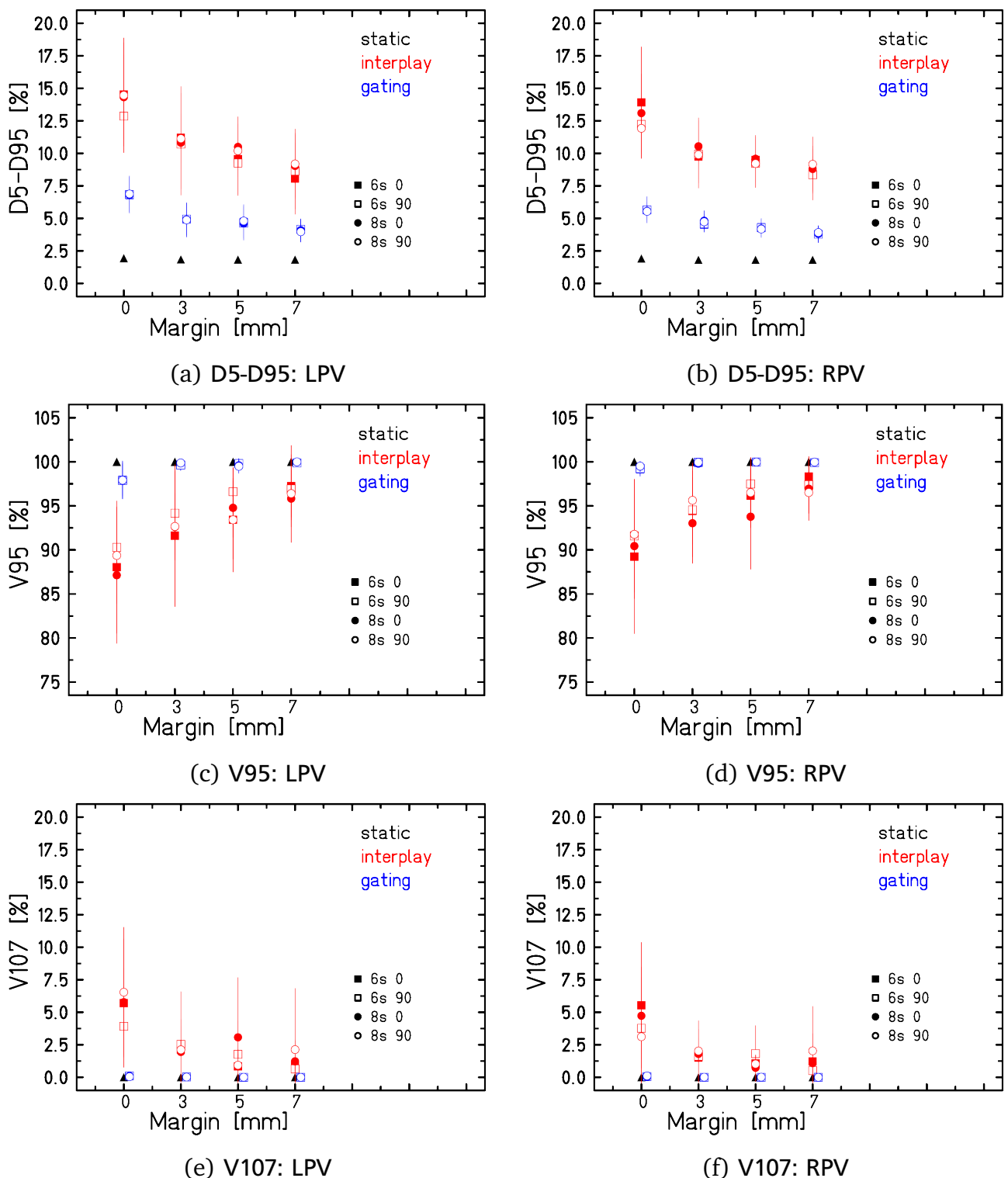
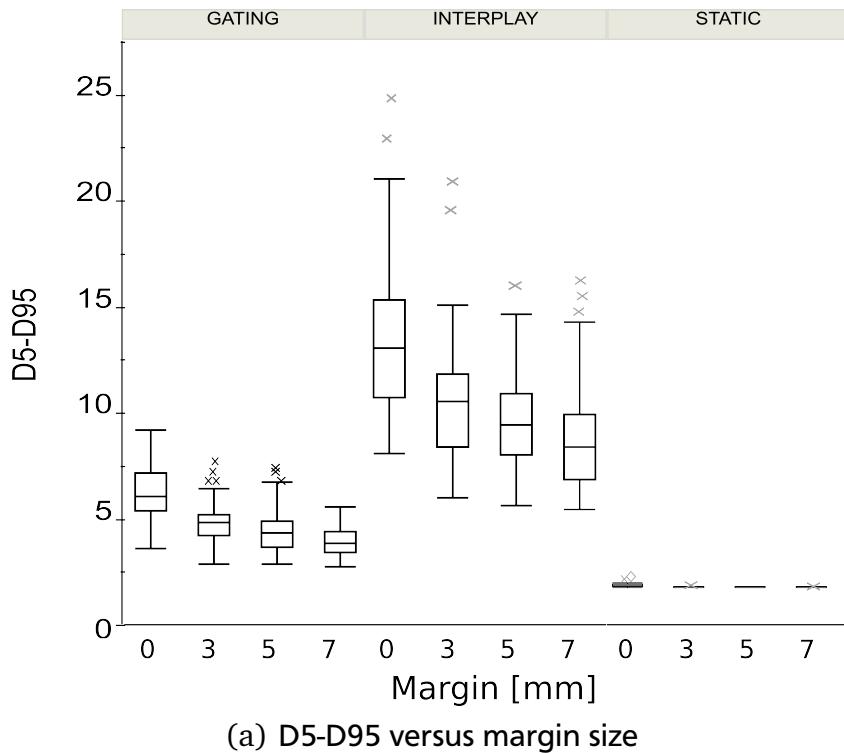
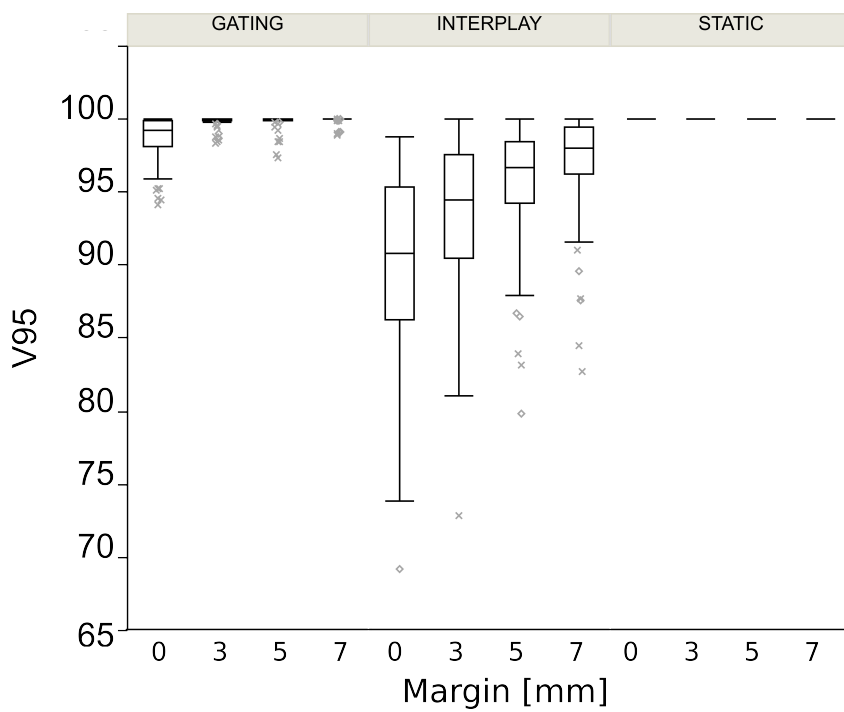


Figure 2.7.: Mean value and standard deviation of dose analysis parameters D5-D95 (first row), V95 (middle row) and V107 (last row) over all patients. The LPV (left column) and RPV (right column) were studied separately. Static (black) as well as interplay (red) and gating (blue) are compared for four different motions and different safety margins.



(a) D5-D95 versus margin size



(b) V95 versus margin size

Figure 2.8.: (a) and (b): Boxplot of dose analysis parameters D5-D95 and V95 over all patient data sets, motion patterns and target volumes (LPV: circle and RPV: cross) depending on the used margins size (0mm, 3mm, 5mm and 7mm) and irradiation mode (static, interplay and gating). Here, minimum and maximum of the data is plotted within 1.5 times the interquartile range, the other data points are stated as outliers. Figures are courtesy of Dr. Christian Graeff.

Rescanning of gated volume

The combination of two motion mitigation techniques, gating and rescanning, would directly apply when not only the respiratory motion but also the heartbeat would be compensated for (see chapter 3). In order to study the outcome of such a delivery, several number of rescans (5, 10, 15 and 20) were applied on the gated irradiation for patient 2 (as an example of a patient with a medium absolute displacement of the target volumes) and patient 9 (with the highest studied absolute displacement). The results can be seen in figure 2.11 and 2.9. For patient 9 the DVHs for static as well as the gating results for all motion patterns and the corresponding results for ten rescans within the gating window are shown in figure 2.10. All numerical results are shown in appendix A (tables A.37 to A.40).

It becomes obvious that rescanning does further improve the dose delivery regarding dose homogeneity. For patient 2 the dose homogeneity value of 6.8% of the prescribed physical dose of 25Gy achieved with gating in the LPV (3 mm margin, motion period of 6s and starting phase of 90°) can be slightly improved to 4.7% with five rescans or 3.8% with ten rescans. In RPV the dose homogeneity value of patient 2 of 5.0% for the same margin and motion can be improved to 4.8% with five rescans and 4.1% with ten rescans. For patient 9 the dose homogeneity value of 5.0% for LPV with 3mm margin and motion period of 6s, starting phase of 90° can be improved to 3.8% with five rescans. For the RPV dose homogeneity of 4.4% with the same margin and motion can be reduced to 3.9% with five rescans. Rescan numbers higher than ten only lead to a minor improvement. For example in Patient 9 the LPV irradiation with 3mm margin and the stated motion of 6s period and 90° starting phase results in 3.7%, both for fifteen and twenty rescans, respectively.

It can be concluded that the dose homogeneity can be slightly improved with rescanning within the gating window. A small number of rescans, e.g. five or ten, are already sufficient to yield acceptable results and the outcome can not be improved by using higher rescan numbers. As rescanning will be studied as motion mitigation technique for the heartbeat motion influence, the overlay of rescanning and gating will be carried out automatically in case of an application of the here studied non-invasive treatment modality for atrial fibrillation, as both, respiration and heartbeat, need to be accounted for.

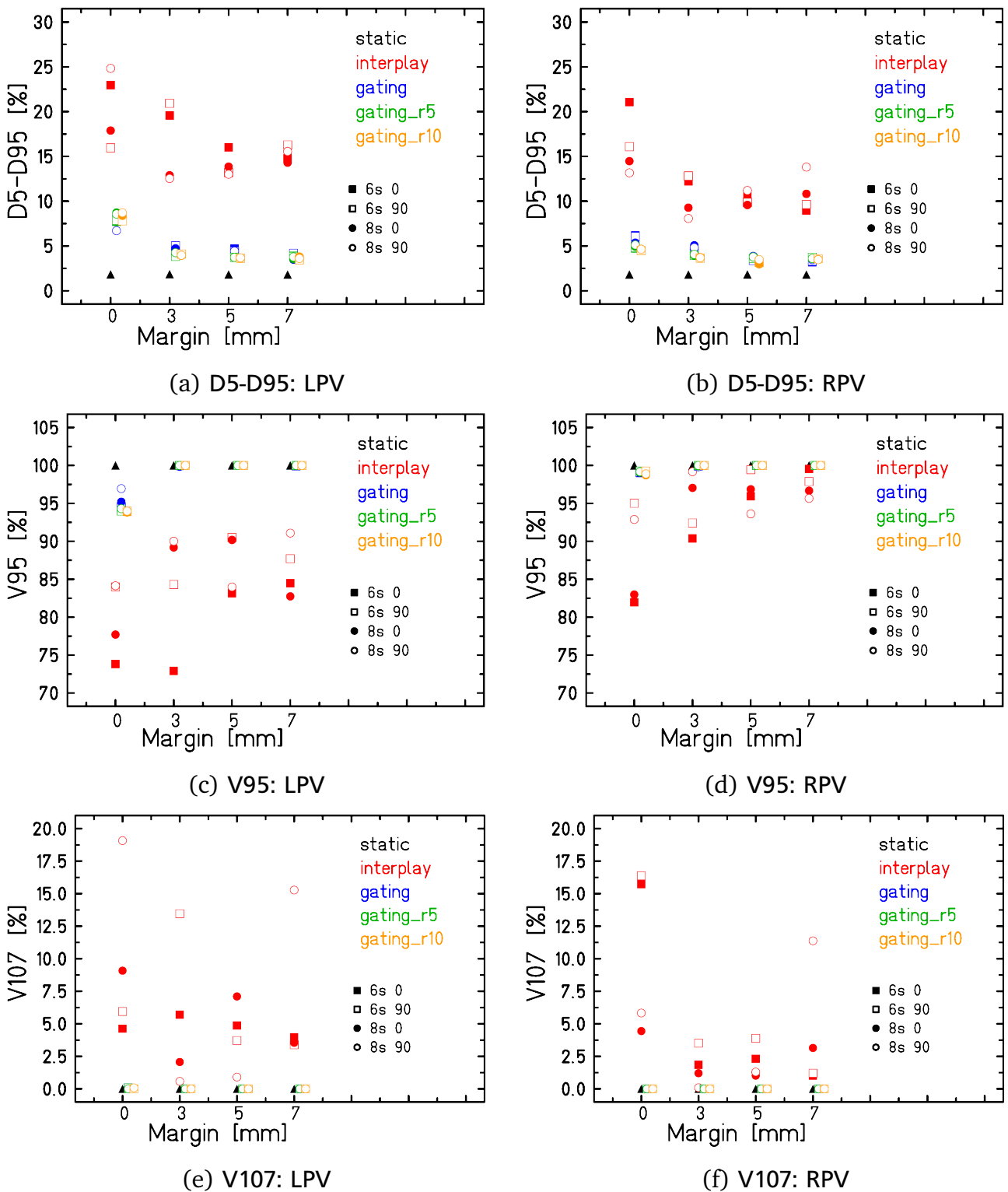


Figure 2.9.: Patient 9: Dose analysis parameters for LPV (left column) and RPV (right column). Besides static (black), interplay (red) and gating (blue) also different rescans numbers on the gated irradiation were applied (five (green) and ten rescans (orange)). The results are compared for four different motions and different safety margins. For a better visualization the rescanning data points for each motion pattern are shifted and the result for fifteen and twenty rescans are not displayed.

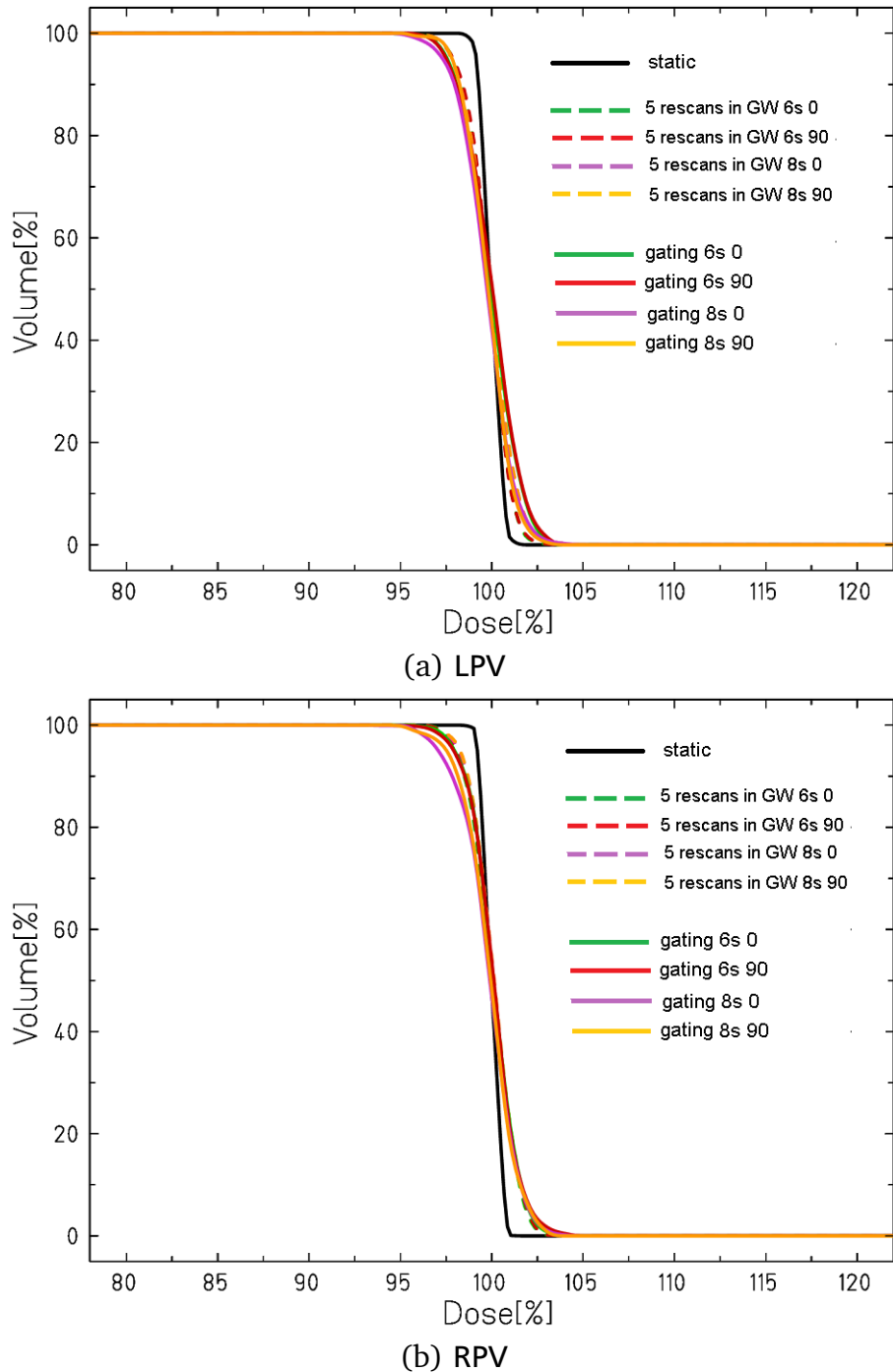


Figure 2.10.: Dose volume histograms for CTV of patient 9 for 3mm safety margin irradiation (LPV (a) as well as RPV (b)) in case of static irradiation (black), gating (solid) and five rescans inside the gating window (dashed). The motion patterns are shown in colors (6s 0: Iujan motion with period of 6s and starting phase 0°, 6s 90: Iujan motion period of 6s and starting phase 90°, 8s 0: Iujan motion period of 8s and starting phase 0°, 8s 90: Iujan motion period of 8s and starting phase 90°).

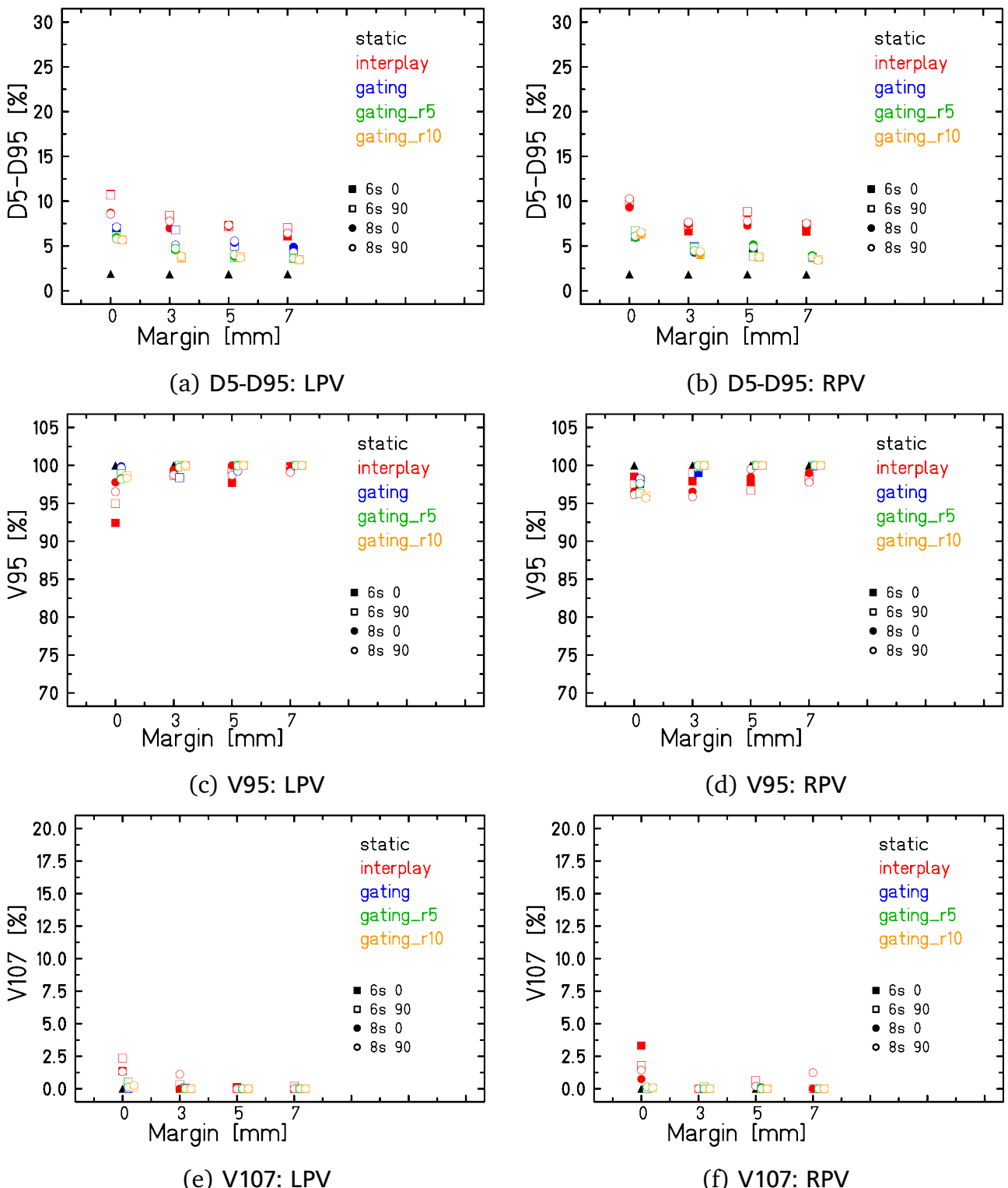
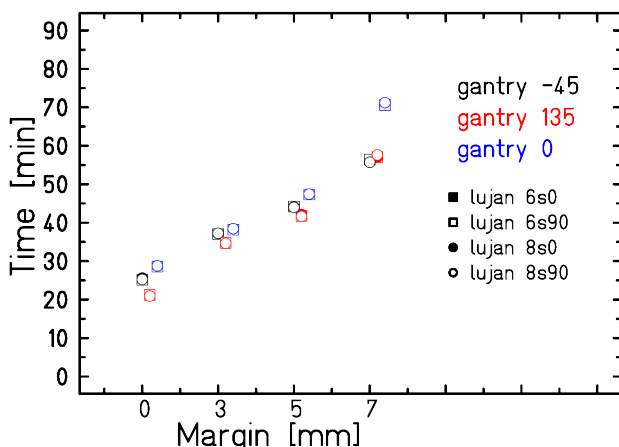


Figure 2.11.: Patient 2: Dose analysis parameters for LPV (left column) and RPV (right column). Besides static (black), interplay (red) and gating (blue) also different rescans numbers on the gated irradiation were applied (five (green) and ten rescans (orange)). The results are compared for four different motions and different safety margins. For a better visualization the rescanning data points for each motion pattern are shifted and the result for fifteen and twenty rescans are not displayed.

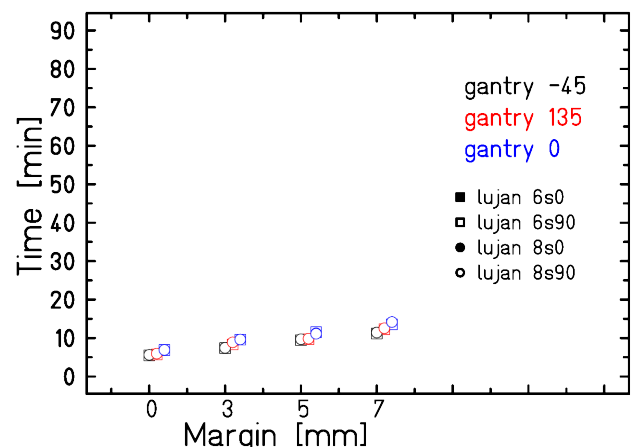
Irradiation time

One of the disadvantages of gating as motion mitigation technique is that the irradiation time is increased depending on the used gating window size. When a gating window of roughly 30% is used, like in this study, the irradiation is prolonged by a factor of three compared to the static irradiation. In figure 2.12 the needed irradiation time for the gated irradiation of LPV and RPV in patient 2 is shown for different safety margins and motion patterns. The duration for each beam entry channel (gantry angle of -45° , 135° and 0°) is plotted individually. On the left side the duration of an irradiation with a small minimal particle number (11,000 particles per beam spot) is shown, while on the right side an irradiation with a higher minimal particle number (55,000 particles per beam spot) is displayed. Even though a higher intensity is expected to result in a shorter treatment time and would hence be favorable for the efficiency of the treatment, it was shown that very high intensities endanger a homogenous dose coverage [Mue14]. The usage of lower intensities is hence motivated and needs to be studied in the individual cases.

As expected, the needed irradiation time increases with the used safety margin as the irradiated volume increases. Furthermore the irradiation time is independent of the motion pattern but varies depending on the used beam entry channel. While the low intensity irradiation can take up to 120 minutes (for a safety margin of 3mm), the overall duration can be reduced to only 30 minutes (for a safety margin of 3mm) for the irradiation with a higher intensity. It should be noted that this is the gating time for the respiratory motion alone and the overall treatment time will thus be prolonged, as cardiac motion is not yet compensated for.



(a) Patient 2: $N_{\min} = 11,000$



(b) Patient 2: $N_{\min} = 55,000$

Figure 2.12.: Irradiation time for gating for patient 2 for different intensities, different safety margins, underlying motion patterns and beam entry channels.

2.3 Discussion

In this chapter the influence of respiratory motion on the PVs was studied and treatment planning studies with gating as motion mitigation technique were carried out. Respiration was found to be an important motion component for the treatment of cardiac volumes. Recent studies in the cardiology community also indicate that real time compensation of breathing displacement would even be beneficial for catheter ablation [Kum12, Frie12].

Different studies on the influence of respiration on the PV motion exist as they are of interest for image guided ablation procedures. Thereby relative displacements (like deformation or splaying of the PVs) and absolute motion (translational and rotation) are distinguished. Noseworthy et al. [Nos05] studied the relative changes in the PV anatomy during the breathing cycle. They thereby investigated the changing branching angle between the inferior and superior LPV (LIPV, LSPV) and RPV (RIPV, RSPV), respectively. They stated that the PV splay increased during inspiration (branching angle of RPVs increased from $(40 \pm 10)^\circ$ to $(60 \pm 15)^\circ$ and for LPVs from $(50 \pm 11)^\circ$ to $(62 \pm 13)^\circ$). Furthermore they found a significant reduction in the diameter of the RIPV and RSPV during inspiration. Ector et al. [Ect08] on the other hand stated that they only found a slight, but significant diameter reduction in the RIPV. In their paper they furthermore studied the absolute translational motion. Their patient cohort had a mean diaphragmatic movement of $(35 \pm 16)\text{mm}$ for the right diaphragm, resulting in an absolute mean displacement for both LPV and RPV of $(19.1 \pm 8.6)\text{mm}$. The mean inferior motion was stated to $(14.6 \pm 7.7)\text{mm}$, in anterior direction to $(9.7 \pm 7.6)\text{mm}$ and the smallest motion direction was the leftward direction with $(0.4 \pm 3.8)\text{mm}$. Comparing motion patterns between veins the LPVs were found to move less in anterior direction than the RPVs, but did not differ significantly in other directions. They found a strong association between diaphragmatic motion and inferior PV motion.

In the here studied patient cohort of lung cancer patients a much smaller mean absolute displacement of the pulmonary veins was found over all patients with $(6.8 \pm 3.6)\text{mm}$ for LPV and (6.8 ± 2.5) for RPV. The SI motion had a mean value of $(-6.4 \pm 3.8)\text{mm}$ and $(-6.6 \pm 2.4)\text{mm}$ for RPV, respectively. In AP direction the mean amplitude for all patients was $(-0.8 \pm 0.5)\text{mm}$ for LPV and (-0.9 ± 0.8) for RPV, which corresponds to the finding by Ector et al. that the LPV move less in anterior direction than the RPV. For LR direction a mean displacement of (-0.9 ± 0.9) of LPV and $(0.5 \pm 1.0)\text{mm}$ of RPV was found over all patients. Contrary to Ector et al. a significant difference in the motion of the LPV compared to RPV was hence found in LR. A correlation between diaphragm motion and PV displacement was only found in the RPV ($r=0.79$, $p<0.05$). Even though a similar result was expected for the LPV, no correlation was observed here. It is unclear if this is due to location of the ablation site or due to the underlying lung

cancer patient data in comparison to AF patient data sets.

Recent studies in the cardiology community [Kum12] concluded that also for catheter ablation respiration plays an important role as it may reduce the catheter tip contact force. Consideration of respiratory motion is thus recommended. Besides ventilation and apnea, Friedmann [Frie12] also states that jet ventilation or breath-hold might be adequate strategies for catheter ablation. Even though these techniques may also be options for a non-invasive treatment of atrial fibrillation with a scanned carbon ion beam, gating was studied as a motion mitigation technique in the present work. In irradiation of cardiac volumes in the animal studies carried out at CyberHeart and at the Universitätsklinikum Schleswig-Holstein in Lübeck different approaches were used. While Blanck et al. [Bla13] used an ITV approach for the respiratory motion, Sharma et al. [Sha10] tracked the respiration with the underlying CyberKnife Synchrony software (see chapter 1, section 1.2.4). For particle therapy tracking is not feasible yet as no fast and precise real-time internal motion monitoring including particle range information exists. A simple enlargement of internal margins to produce an ITV for respiration was withdrawn due to expected high dose deposition in critical OAR close to the target sites (see chapter 3). Gating offers the advantage of a currently technical feasibility while keeping the dose to the normal tissue relatively small. Nevertheless it leads to a prolongation of the treatment time. However, with a high intensity of 55,000 minimum particles per spill a duration of only 30 minutes could be achieved (patient 2, safety margin of 3mm). This already offers a reduced treatment time compared to the results by Sharma et al. where a treatment time of one to two hours was estimated. While lower intensities lead to a longer treatment time, it is nevertheless known from previous studies [Mue14] that high intensities can result in inhomogeneous dose depositions. Other methods to reduce the treatment time might hence be needed in order to still guarantee a time efficient delivery. Tsunashima et al. [Tsu08] studied cyclotron settings that could lead to a reduced treatment time in particle gating. They thereby found that variable excitation cycles, in synchrony with the respiratory pattern of the patient, could reduce the treatment time prolongation to a factor two, instead of the usual factor three, for a 30% gating window. Iwata et al. [Iwa10b] furthermore proposed a method to reduce the needed time for energy changes inbetween IESs in synchrotrons. By using radiofrequency knockout excitors and multiple energy operation patterns, the beam would be accelerated to the maximum energy and than stepwise decelerated to lower energies, using an extension of the respective flattops to extract the particles with varying energies during a single operation cycle of the synchrotron.

Concerning the dose deposition with gating compared to interplay it can be concluded that gating yields good dose coverage. The V95 values were higher than 99% for all target sites with safety margin of 3mm or more and higher than 95% in all cases without safety margin (minimum of 95.21% in patient 9 for LPV, no safety margin and motion period of 8s, starting

phase of 0°). The V107 values were all smaller than 0.1% (maximum of 0.1% for patient 2, RPV, in case of 5mm margin and motion with period of 8s and starting phase of 90°). Hence an acceptable dose coverage could be achieved. The dose homogeneity did not exceed 9.18% without safety margin (patient 5, LPV, no safety margin and motion period of 8s, starting phase of 90°). With safety margin, the D5-D95 value did not exceed 8%. An additional safety margin is thus beneficial to guarantee a robust and successful treatment delivery. However, an extension of the target volume due to safety margins always results in more dose to the normal tissue and to potential critical OARs. A limited safety margin of 3mm or 5mm would offer the benefit of improved treatment outcome while keeping the irradiated volume low (see also chapter 3).

Rescanning within the gating window could slightly improve the results for dose homogeneity as it reduces the influence of residual motion inside the gating window. The dose homogeneity in the LPV of patient 9 for example (large motion amplitude) could be reduced from 5.01% (safety margin of 3mm, motion period 6s and 90° starting phase) to 3.83% with five rescans.

2.4 Conclusion

The PVs were found to move due to respiration with an amplitude of up to 2cm. This displacement creates interplay effects when irradiated with scanned carbon ions. Gating as motion mitigation technique was studied. It can be concluded that this method yields improved dose coverage (under and over dosage) and better dose homogeneity compared to interplay in all studied patient cases, for all motion patterns and safety margins and achieves results comparable to the static irradiations. It can thus be an adequate motion mitigation technique for the irradiation of PVs under influence of respiratory motion. As rescanning is a potential technique when compensating for displacements due to heartbeat (see chapter 3), the combination of these two motion mitigation technique could be feasible in a potential application. Hence rescanning inside the gating window was studied and it was shown that a small number of rescans (e.g. five or ten) are sufficient to improve the results of dose homogeneity.



3 Irradiation of pulmonary veins under influence of heartbeat in human data

Contents

3.1. Material and methods	78
3.1.1. Treatment planning input data	78
3.1.2. Treatment planning parameters	79
3.1.3. Treatment planning studies	81
3.1.4. Analysis	81
3.2. Results	83
3.2.1. Beam direction	83
3.2.2. Safety margin limitations	90
3.2.3. Motion assessment of heartbeat	96
3.2.4. Motion mitigation techniques for heartbeat	100
3.3. Discussion	107
3.3.1. Dose to critical structures	107
3.3.2. Beam channel directions and safety margins	109
3.3.3. Movement of PVs in cardiac cycle	110
3.3.4. Rescanning as motion mitigation technique	111
3.4. Conclusion	112

The PVs move on one hand due to the heartbeat and on the other hand due to respiration of the patient. Both motion types are independent from each other and can hence be studied individually. While the influence of respiration is analyzed in chapter 2, the effect of heartbeat motion will be discussed in this chapter. CTs of five AF patients, gated to the complete cardiac cycle in end-expiration, were acquired at Mayo Clinic (Rochester, Minnesota, USA). The motion direction as well as motion amplitude of LPV and RPV were studied for all cases. Motion influences on accuracy and homogeneity of the dose delivery in the PVs were studied using these data. The resulting interplay pattern for all patients as well as rescanning as possible motion mitigation technique have been analyzed and the results will be presented in this chapter.

3.1 Material and methods

The input data as well as the treatment planning parameters will be stated before all conducted studies will be specified. The analysis procedure will be explained.

3.1.1 Treatment planning input data

As was already stated in chapter 2 4DCT data sets, segmentation of the target volumes and OARs and deformable image registrations in-between the different motion phases are needed for the here presented treatment planning studies using the in-house software TRiP4D [Ric13].

In order to study the displacement of the PV due to heartbeat ECG gated 4DCTs in end exhale (breath hold) were studied. Five AF patient data sets (four male patients and one female) were recorded and anonymized at Mayo Clinic (Rochester, Minnesota, USA). The CT scans were acquired on a Sensation 64 CT scanner (Siemens). Each of the 4DCT data set consisted of twenty temporal equally distributed cardiac motion phases, the reference phase zero started at the R-peak of the QRS-complex (see chapter 1, section 1.3.1). In order to distinguish structures within the heart the CT scans were contrast enhanced. The radiopaque material was administered intravenously (150cc Omnipaque 350 at 4cc/sec). Segmentation of the target volumes (LPVs and RPVs) as well as the OAR (esophagus, trachea, aorta and cardiac structures) were carried out by a collaborating cardiologist at Mayo Clinic on the reference 4DCT phase with Eclipse™(Varian Medical Systems). The volumes of the contours for the ablation sites for LPV and RPV are presented for each patient in table 3.1.

Table 3.1.: Target volume for LPVs and RPVs for all investigated patients.

patient no	LPV [cm ³]	RPV [cm ³]
1	2.03	2.39
2	2.62	5.16
3	1.45	4.16
4	1.66	2.07
5	2.06	1.90

Non-rigid image registration of the nineteen motion phase on the reference phase have been performed with Plastimatch [Sharp07, Shack10]. Here the first step of the B-spline registration was carried out with 50 maximal iterations and an isotropic spacing of 20mm was chosen. The second step was carried out with 100 maximal iterations and the grid spacing was set to 3mm. The regularization was chosen to be $\lambda=0.0001$. The same visualization techniques as stated in chapter 2 were used for a quality assurance of the registration (false color images [Bro07], checker board images [Bro07] and a qualitative check of the vector field regularization). The

stated tests were carried out on the one hand between motion phase 3 (the motion phase of the maximal ventricular displacement) and the reference phase (motion phase zero) and on the other hand between motion phase 18 (maximal displacement of the atria) and the reference phase.

3.1.2 Treatment planning parameters

Also here 3D (static) and 4D treatment plans were generated. For informations on the dose optimization process, the ITV generation with the implementation of the studied safety margins (3mm, 5mm and 7mm), the used raster spacing and the dose algorithm the reader should be referred to 2.1.2.

All treatment plans were calculated as intensity modulated particle therapy (IMPT). Part of the study included the esophagus as critical structure in the optimization process (IMPT(OAR)). Thereby two different dose restrictions to this OAR were used. In one part of the calculations it was stated that the esophagus should not receive more than 70% of the physical dose. The strength of this restriction was determined by a weightfactor, which was set to 75%. In a second iteration the restrictions were stronger and the maximal physical dose to this structure was set to 30% with a weighting factor of 200%. Also here a physical dose of 25Gy was applied in one fraction in all simulations. Since potential biological effects were not included in the studies the applied dose is linear and the results, e.g. dose depositions to critical structures, can be scaled to other dose values ¹.

The generation of treatment plans is furthermore also dependent on the theoretically possible beam application. Spill length, shape and particle intensity are thus important factors. For the here presented simulations GSI accelerator parameters have been used. Thereby a spill length of 2.2s is assumed. The pause in between spills is either 2.2s, when no energy change is required afterwards, or 3.2s when an energy change is needed. The spill shape is approximated by a Gaussian function. The particle intensities feasible at GSI vary between 2×10^6 and 2×10^8 particles per spill. Inbetween these two extreme intensity levels, fifteen different intensity levels can be used. In the resulting treatment plan, the intensity steps are automatically chosen [Krae00, Ric13]. The minimum particle number per beam spot was set to 5,000.

As the reconstruction of the 4DCTs was based on the time scale a phase-based motion state detection was employed. In order to consider possible divergence in the heartbeat motion pattern of patients, different periods (1s and 0.7s) as well as different starting phases (0° and 90°) were used. The motion periods were chosen according to the heartbeat rate of 60 to 80 beats per minute.

¹ only limited by the minimal particle fluence per beam spot

Field number and beam directions

The field number and directions were systematically investigated and are listed in table 3.2. Four different field numbers (one to four) were studied. While for one field the gantry angle was kept constant to 0° and only the couch angle was changed, for higher field numbers different gantry angles were used. These angles are illustrated in figure 3.1.

Table 3.2.: Studied field number and beam channel directions

Field number	Couch angle [°]	Gantry angle [°]
1 field	-90	0
	-45	0
	-135	0
2 fields	90	-60/120
	90	-60/135
	90	-60/0
	90	-45/135
	90	-45/150
	90	-45/0
3 fields	90	-60/120/150
	90	-60/120/0
	90	-45/135/150
	90	-45/135/0
4 fields	90	-60/120/-45/135
	90	-60/120/0/180
	90	-45/135/0/180
	90	-160/90/-60/145

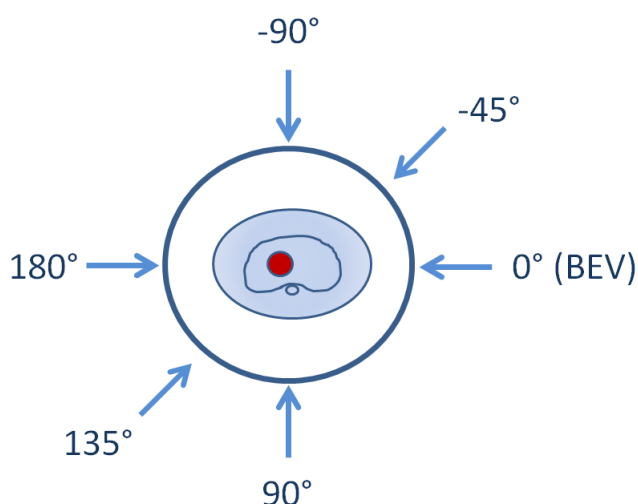


Figure 3.1.: Entry channels for different gantry directions for a couch angle of 90° . The beam's eye view (BEV) is marked.

3.1.3 Treatment planning studies

Besides representing a reference value for the 4D cases, 3D treatment plans were also generated here in order to find the best suited combinations of beam entry channels as well as to study possible safety margin limitations. In order to find a suitable field number and beam direction for the 4D treatment planning studies, static simulations on the original CTV volume (LPV together with RPV) with the above mentioned treatment planning parameters were carried out for all five patients. 17 different beam channel combinations were studied (see table 3.2). As a criteria for the best possible solution the dose to OAR was assessed. Furthermore, different ITV margins (original and increased with 3mm, 5mm and 7mm margin) were studied in 3D treatment plans for all patients. The resulting dose depositions were compared to dose deliveries with the same margins where the esophagus was included in the optimization process. Possible limitations were again analyzed according to the dose deposition in the OARs.

In order to prepare for the 4D simulations, the motion of the PVs due to heartbeat was assessed. 4D plans were distinguished between an underlying motion without any compensation, resulting in interplay patterns [Phi92, Ber08], and with the application of rescanning [Phi92] as motion mitigation technique. For rescanning different rescan numbers (5, 10, 15 and 20) were compared. Static, interplay as well as rescanning treatment plans for all patients were carried out with one beam channel combination (couch angle of 90° and gantry angles of -45°, 135° and 0°), all four safety margins, the stated treatment planning parameters and the four stated motion trajectories.

3.1.4 Analysis

Both the dose deposition in OAR as well as dose homogeneity in the target volume were studied. For the OAR dose-volume restrictions in esophagus, trachea, aorta and the whole heart were compared to values from RTOG study protocols (see next paragraph). As further OARs cardiac substructures (ventricles and coronary arteries) were studied. For comparison of the resulting dose coverage in the target region dose-volume-histograms (DVHs) were studied. Furthermore motion-volume-histograms (MVHs) [Ric13] were generated displaying the relative displacement of every voxel of the investigated volume to the reference phase in all three motion directions. With these values the resulting motion of the PVs due to heartbeat could be assessed.

Dose-volume constraints for organs at risk

The dose deposition in the OAR is an important limitation and selection criteria when studying the field number and beam channel direction as well as the possible safety margin limitations. Since a single fraction of 25Gy or higher is assumed to be used in this non-invasive treatment modality, dose tolerance limits used in stereotactic body radiotherapy (SBRT) are highly related [Ber12]. An extensive collection of dose-volume-limits for SBRT are presented in Grimm et al. [Gri11] and the AAPM Task Group Report [AAPM10]. Both are literature reviews of limits utilized and reported in existing publications. For the OAR in the here presented treatment planning study (esophagus, trachea, heart and aorta) the dose-volume-limits in both literature reviews were taken from the Radiation Therapy Oncology Group (RTOG). The RTOG is a national clinical cooperative group of over 360 institutions across the United States and Canada, which was funded by the National Cancer Institute (NCI) [RTOG]. In their study protocols RTOG 0631 (a phase II/III trial of SBRT for localized spine metastasis) [RTOG0631] and RTOG 0915 (a randomized phase II trial of SBRT for medically inoperable patients with stage I peripheral non-small cell lung cancer) [RTOG0915] the following dose-volume-limits were stated (see table 3.3).

Table 3.3.: Dose-volume limits for OAR.

OAR	Volume [cc]	Dose [Gy]	endpoint
Aorta / great vessels	10	31	Aneurysm
Esophagus	5	11.9	Stenosis / fistula
Heart	15	16	Pericarditis
Trachea	4	10.5	Stenosis / fistula

Since the heart is not only a critical organ but also the target site in this treatment modality, further differentiation of limits depending on the substructures of the heart are needed. Unfortunately, data on this topic is scarce. Literature on cardiac disease resulting from radiation exposure mostly relies on cancer patient data treated with radiotherapy (in particular breast cancer and Hodgkin's lymphoma) or atomic bomb survivors. Besides the stated dose-volume limitation, the mean dose and maximum point dose to the whole heart was studied. Furthermore the maximal irradiated heart volume ($V_{>0}$) was examined. Concerning substructures the left and right ventricle as well as the coronary arteries were analyzed for mean and maximum dose deposition and maximal irradiated volume contribution. Since the values were not normally distributed, boxplots were generated, where the median (50th percentile), the 25th and 75th percentile and the minimum and maximum values over all patient cases are displayed.

Dose deposition in target volume and motion of PVs

The V95, V107 as well as D5-D95 of the CTVs were analyzed. The stated values have been evaluated for all beam applications (static, interplay, rescanning). Furthermore the median and

percentile values of these parameters over all studied motion patterns and patient cases were generated. The relation of dose analysis parameters to different margin sizes and rescanning number was analyzed by a one-way ANOVA and the proportion of variance explained r^2 is reported with the corresponding p-value ($p < 0.0001$).

3.2 Results

In the following the results of the beam direction and safety margin study, of PV motion assessment as well as of the treatment planning studies will be discussed. As a criteria for an adequate field number and beam channel direction as well as safety margin limitation the dose to OAR will be presented. The motion due to heartbeat is shown. For the treatment planning study different dose analysis parameters will be presented and compared for different cases (static, interplay and rescanning).

3.2.1 Beam direction

In figures 3.2 and 3.3 the resulting dose to the pertinent OARs is shown for all studied beam directions and patients. Figure 3.2 displays the results as a boxplot over all patient cases for a respective field number (and hence different beam directions) while figure 3.3 shows the individual results for each patient and beam direction. The corresponding volumes result from the dose volume limits (see table 3.3, represented by a dashed line in the plots). In all studied cases, the difference between different beam directions for a certain patient is rather small, resulting in no obvious preferable beam direction for the five studied patients. For the four studied OAR it becomes furthermore obvious that while trachea and aorta are well spared for almost all beam directions in all patients, esophagus and in particular the heart are much more critical.

In the esophagus the median dose over all patients is 7.8Gy (75th percentile: 9.0Gy) for one field, 11.0Gy (14.1Gy) for two fields, 11.0Gy (13.9Gy) for three and 8.0Gy (11.9Gy) for four fields. The result is dependent on the underlying patient anatomy. While the majority of the beam directions for patient 1, 4 and 5 remain under the respective dose-volume limit, many plans for patient 2 and 3 exceed the dose-volume constraints. For these patients dose depositions of 11.9Gy or less are achieved in only about 98% and 65% of studied cases (patient 2 and 3, respectively). While a single field yields acceptable dose deposition in the esophagus, the beam channel results in higher dose depositions in the heart and cardiac substructures like the coronary arteries (see figure 3.5 and 3.4) and are thus inapplicable. For patient 2 higher field numbers and thus more beam directions result in dose limit exceeding depositions. Due to this result the esophagus was included in the optimization of the treatment delivery (IMPT(OAR)). This was studied in comparison to a simple IMPT irradiation (see section 3.2.2).

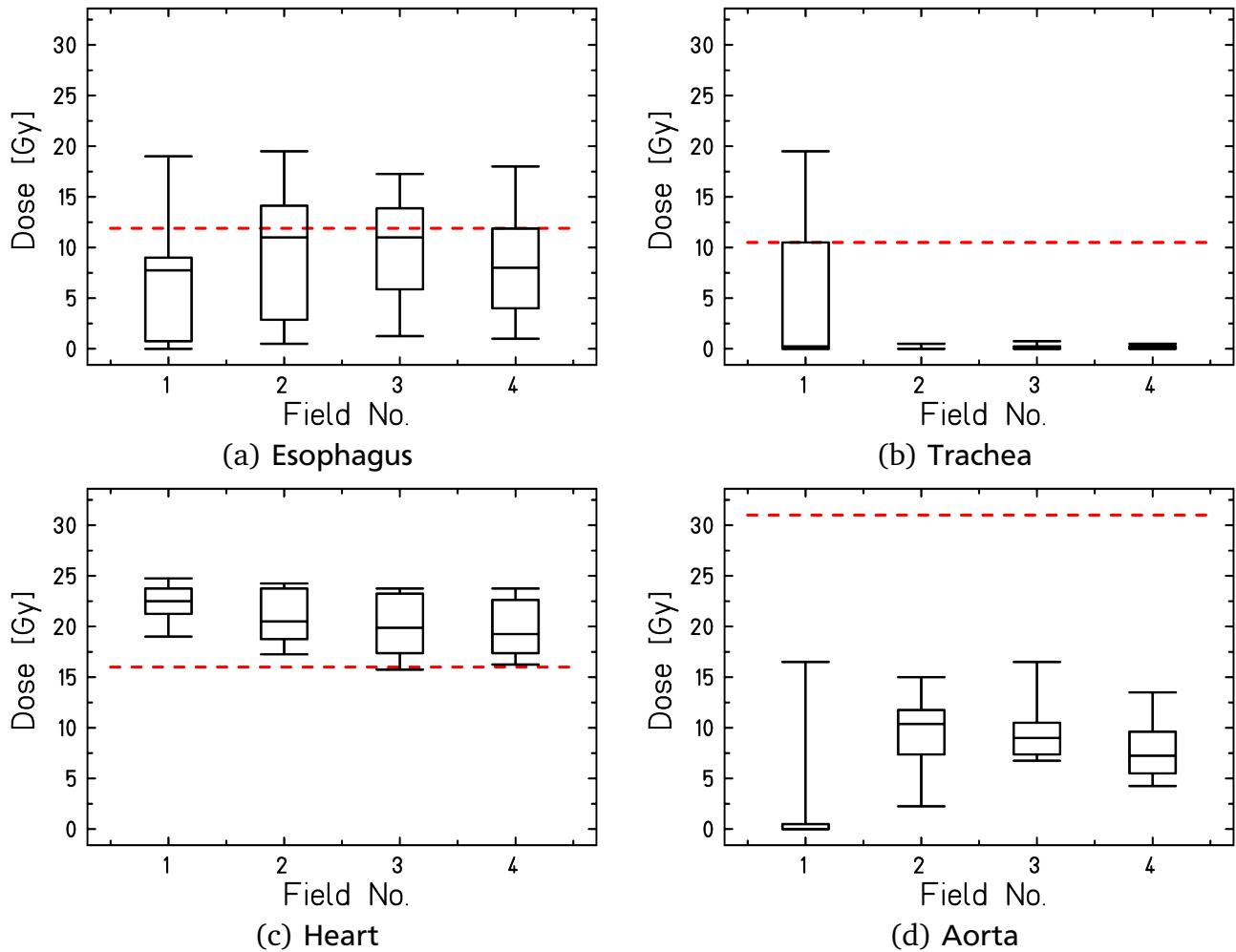


Figure 3.2.: Boxplots of dose-volume data for different field numbers (one to four fields) over all patients and over the respective beam directions. The data is plotted for different OARs when irradiating the LPV and RPV as IMPT in the five patient data sets. The dose-volume-limit for each critical organ is indicated with a dashed line in each plot, respectively.

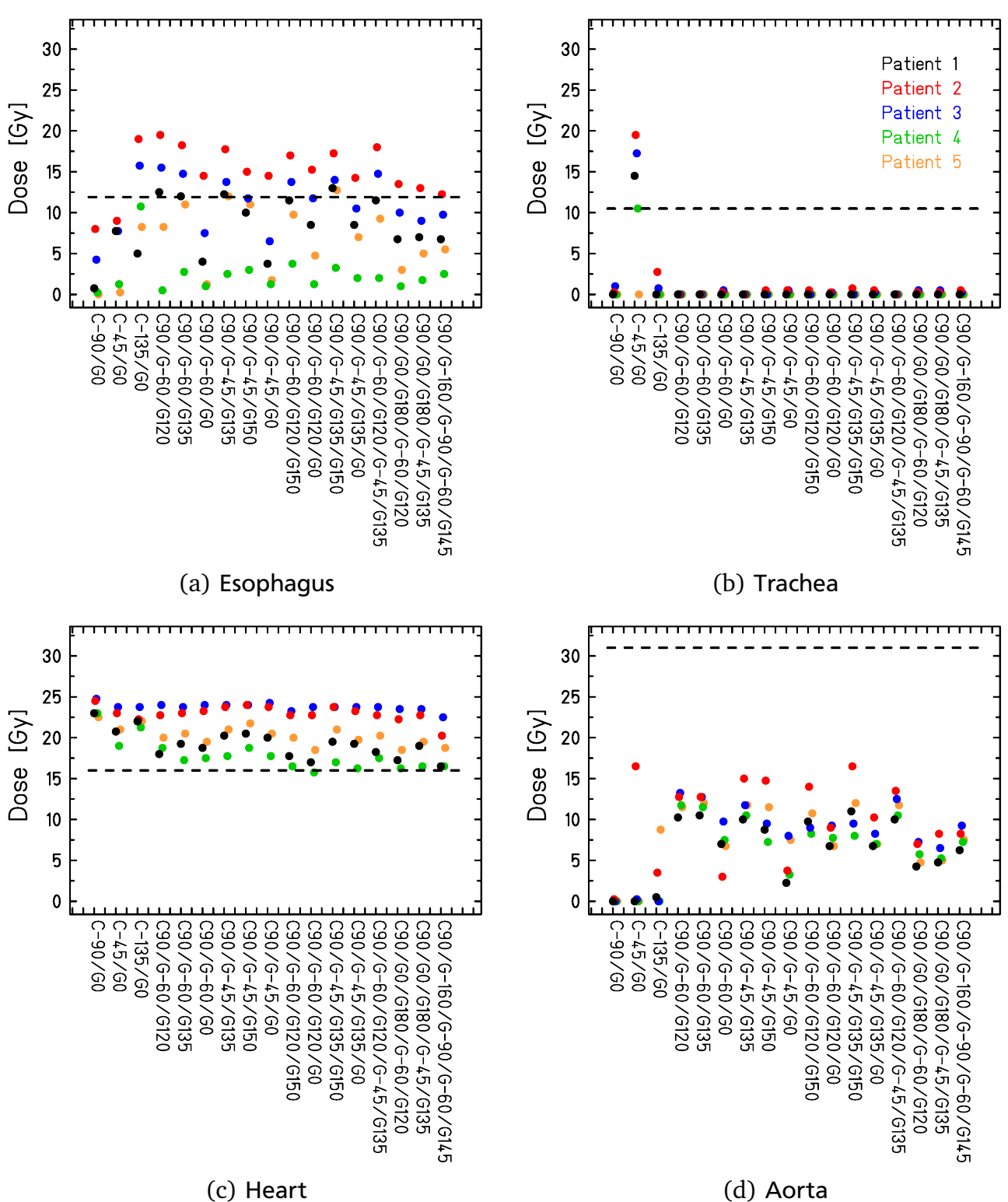


Figure 3.3.: Dose-volume data of different OAR when irradiating the LPV and RPV as IMPT in the five patient data sets (patient 1: black, 2: red, 3: blue, 4: green, 5: orange) with different field numbers (1 field, 2 fields, 3 fields, 4 fields) and different beam directions. The dose-volume-limit for each critical organ is indicated with a dashed line in each plot.

The dose volume limit for the heart is exceeded in all patients for all beam directions (see figure 3.2 and 3.3). As the heart is not only an OAR in this treatment modality, but some of its substructures are also the target itself, a closer analysis of the dose deposition in the heart is required. In the first row of figure 3.4 and figure 3.5 the mean and maximal dose deposition in the whole heart as well as the maximal irradiated volume are shown. The mean dose over all patients and beam directions is found to have a median of 1.3Gy (75th percentile: 1.5Gy). The median over the maximum point dose is 26.6Gy (27.1Gy). Concerning the maximal irradiated volume it can be seen that except for one result less than 30% of the heart is irradiated in all other cases. In the case of couch position 90° and gantry angles of -160°, -90°, -60° and 145° these maximal volume is drastically increased, and reaches up to 49.9% for patient 2. Hence this beam channel case (beam channel case 17) will be stated separately in the following analysis. The median of the maximal irradiated volume over all patients is 16.8% (20.5%), excluding beam channel case 17, and 17.4% (20.8%) including this case.

The results for the dose deposition in the cardiac substructures are presented in row two to five of figure 3.4 and figure 3.5. For the ventricles (LV: second row, RV: third row), the mean dose to both LV and RV is negligible. The maximal point dose on the other hand varies depending on beam direction and patient. Single beam directions yield a high maximal dose deposition in the LV as in the case of a couch angle of -90° or -135° the beam traverses the LV. Consequently for these beam directions the maximal dose to the RV is smaller. The overall maximal dose deposition has a median of 1.4Gy (75th percentile: 7.4Gy) for LV and 1.3Gy (5.0Gy) for RV. Besides some single beam directions no maximal point dose exceeds 11.2Gy and 10.1Gy for LV and RV, respectively. Concerning the maximal irradiated volume of the ventricles, it can be stated that the results differ depending on the studied patient. In case of the LV patient 2 has a higher irradiated volume compared to the other patients, while for this patient on the contrary the RV is better spared than in other patients. Over all patients the LV is irradiated to a higher extend than the RV. For LV the maximal irradiated volume over all beam directions and patients has a median of 1.2% (6.0%), when excluding the case of beam channel 17 and to 1.9% (6.4%) when including this case. For RV it is 0.2% (7.6%) excluding the beam channel case 17 and to 0.2% (8.3%) including it. For the coronary arteries the beam channel 17 also results in the highest irradiated volume. Even though the coronary arteries are found on the surface of the whole heart and hence also on the ventricles, the irradiated volume of these structures differ from the result of the ventricles. Here the RCA are irradiated to a higher extent than the LCA. The median maximal value for the LCA is 15.7% (28.0%) including the stated beam channel case 17 and 15.2% (27.4%) excluding it. For the RCA the median over the maximal value is much higher and found to be 27.9% (42.4%) including the beam channel case 17 and to 24.8% (42.1%) excluding it. For the mean dose deposited in the LCA one and four beam directions result in an increased dose deposition, while three fields yield in general a low

mean dose for all studied beam directions and patients. The same is true for the maximum point dose in the LCA. In the case of RCA, the results seem to be independent of field number and beam direction. Overall the median over the mean dose is 0.4Gy (1.0Gy) for LCA and 0.6Gy (1.6Gy) for RCA. For the maximal point dose the median dose deposition over all beam directions and patients is 6.8Gy (10.9Gy) for LCA. For the RCA it was found to be 5.4Gy (7.9Gy).

While it was not expected to find one beam direction feasible for all five patients, it is striking that no beam position results in a clear benefit for the OAR of the individual patients. This is due to the challenging position of the PV target site, which is in direct proximity to the esophagus and due to the fact that the heart is not only an OAR in this treatment modality, but also the target site itself. Nevertheless for the analyzed cardiac substructure, especially the radiosensitive LCA, it can be concluded that three beam channels seem to be beneficial for all patients. Regarding the mean dose deposition in the LCA as well as the maximal irradiated heart volume, combined with the requirement of a robust treatment and hence the benefit of large gantry angles in between different beam channels, a couch angle of 90° was chosen together with gantry angles of -45°, 135° and 0°. These beam channel directions were used for a closer analysis of safety margin limitation as well as for the treatment planning studies for all patients.

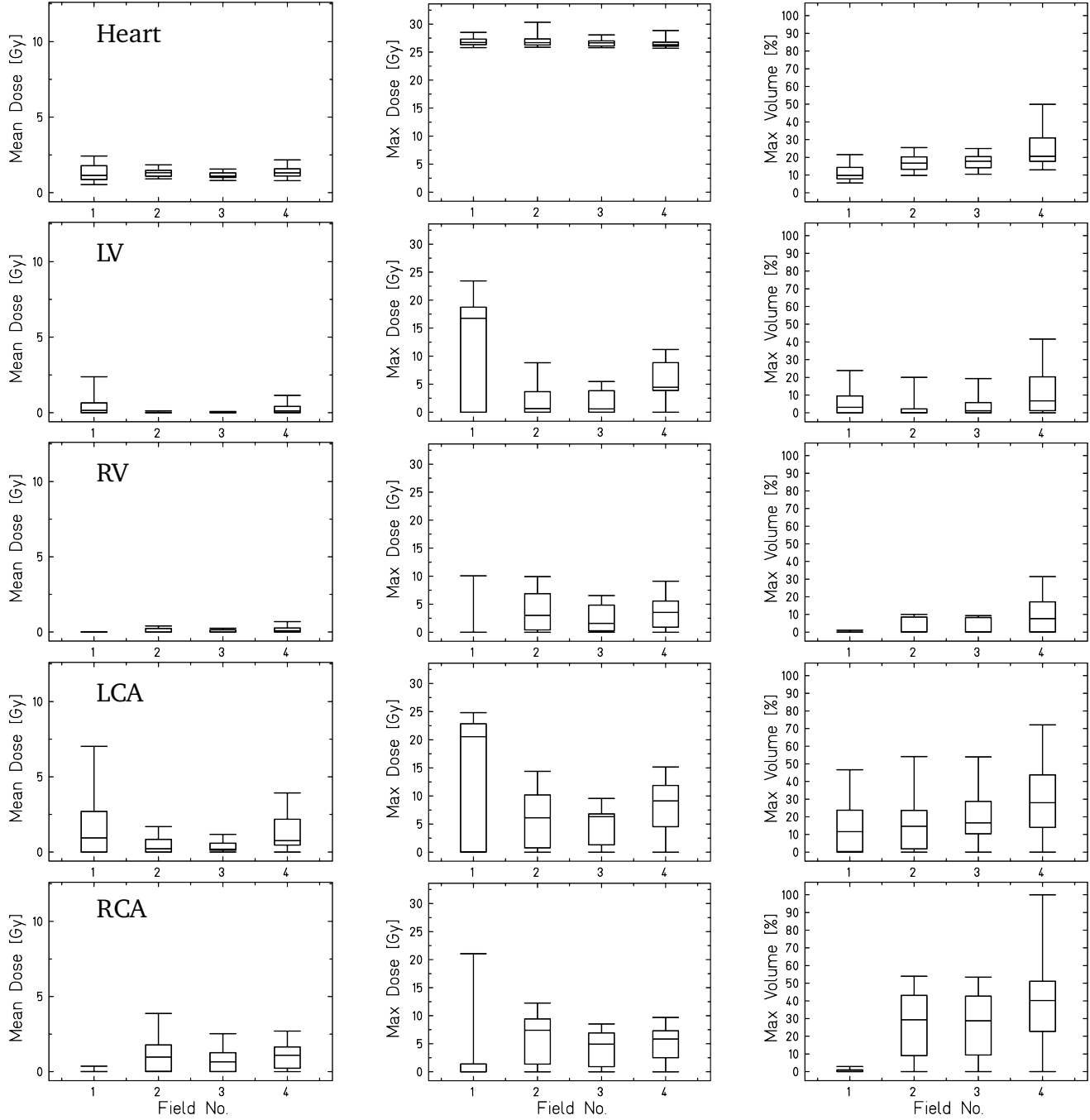


Figure 3.4.: Boxplots of mean and maximum dose as well as maximal irradiated volume for different field numbers (one to four fields) over all patients and over the respective beam directions. The data is plotted for different OARs (heart: first row, and cardiac substructures (LV: second row, RV: third row, LCA: fourth row, RCA: last row) when irradiating the LPVs and RPVs as IMPT treatment in the five patient data sets with different field numbers and thus beam directions.

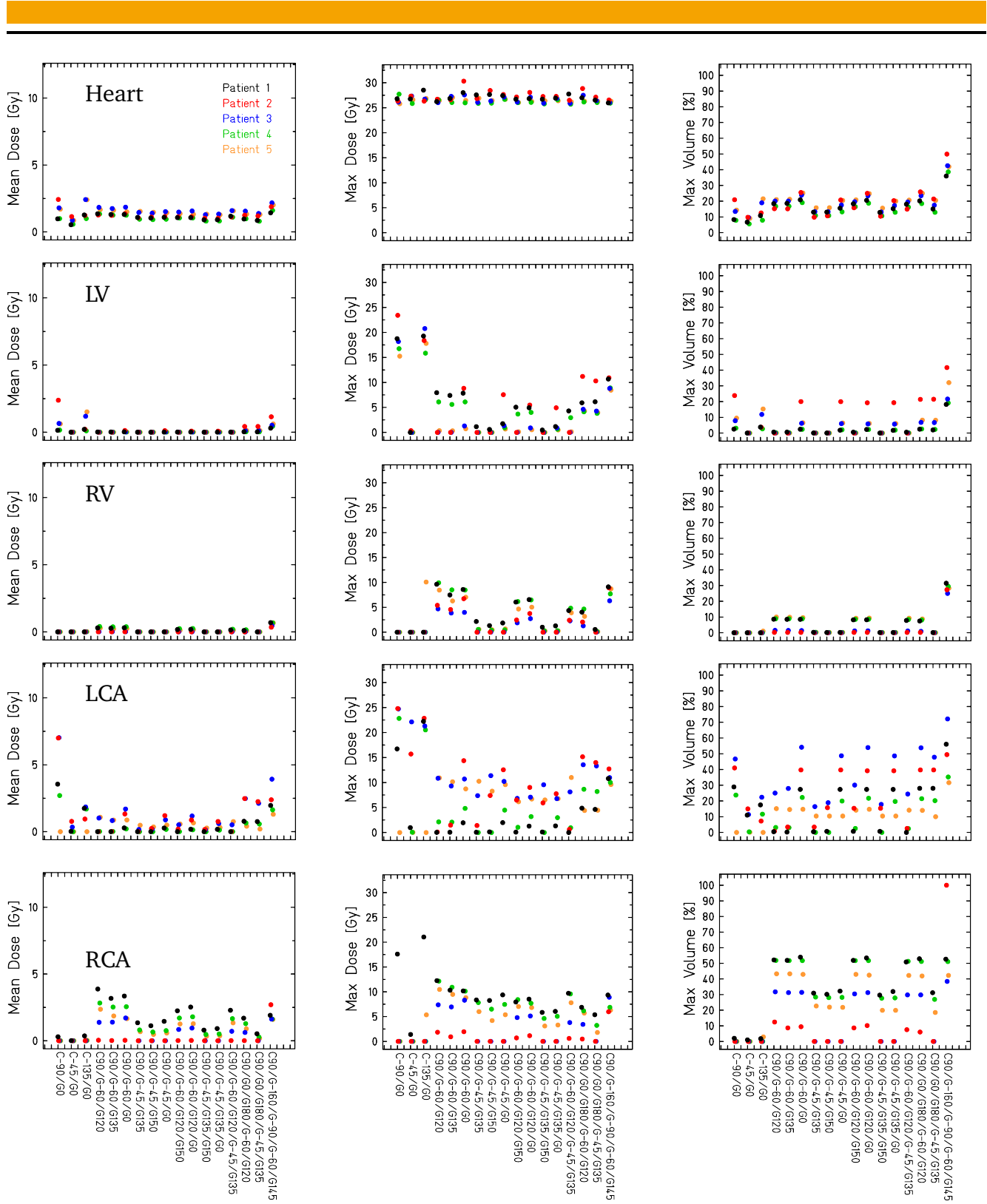


Figure 3.5.: Mean and maximum dose as well as maximal irradiated volume of the heart (first row) as well as cardiac substructures (second row: LV, third row: RV, fourth row: LCA, last row: RCA) when irradiating the LPV and RPV in the five patient data sets with different field numbers and beam directions. The different patients are displayed in different colors (patient 1: black, 2: red, 3: blue, 4: green, 5: orange). The different beam channel directions are stated in the the figures of the last row.

3.2.2 Safety margin limitations

Figure 3.6 shows the dose results for the main OARs when irradiating the PVs with no safety margin (0mm) and different additional, isotropic safety margins (3mm, 5mm or 7mm). The dose-volume-limits were studied according to the recommendation of RTOG (see table 3.3) and the limit for each organ is indicated by a dashed line in the boxplots. Besides an IMPT treatment IMPT(OAR) deliveries were also studied. Thereby the esophagus was implemented as a critical structure in the optimization process with two different restrictions (IMPT(OAR)_{R1}) and (IMPT(OAR)_{R2}). In IMPT(OAR)_{R1} it was stated that this structure should not receive more than 70% of the physical dose of 25Gy, while IMPT(OAR)_{R2} had stronger restrictions with the maximal dose deposition set to 30% of the physical dose. The results of these three treatment deliveries are shown in each column of the plot.

As expected, the dose to the enclosed OAR increases with increasing safety margin for all patients. This is the case for both IMPT and IMPT(OAR) deliveries. Nevertheless the IMPT(OAR) deliveries lead to a reduced dose deposition, especially in the esophagus. For no safety margin, the median dose to the esophagus over all patients is found to be 8.5Gy (75th percentile: 12.4Gy), which decreases to 7.0Gy (9.0Gy) with IMPT(OAR)_{R1} delivery and to 2.8Gy (4.4Gy) with IMPT(OAR)_{R2}. For 3mm safety margin and an IMPT irradiation the median dose resulted in 13.0Gy (18.6Gy) and reduces to 9.3Gy (12.1Gy) for IMPT(OAR)_{R1} and 3.5Gy (6.0Gy) for IMPT(OAR)_{R2}. With 5mm safety margin the RTOG limit of 11.9Gy starts to be exceeded for IMPT(OAR)_{R1} deliveries as it was found to be 11.8Gy (15.1Gy) (compared to 19.0Gy (22.8Gy) with IMPT). With the stronger restrictions on the other hand the dose to the esophagus remains under the stated limit with 4.3Gy(6.6Gy). Even for a margin of 7mm the stronger restrictions result in an appropriate dose deposition with a median of 6.0Gy (7.9Gy). For IMPT(OAR)_{R1} the 7mm margin result increased further to 14.3Gy (17.1Gy) (IMPT irradiation: 23.3Gy (24.6Gy)).

Even though only the esophagus is included in the IMPT optimization process, also other OAR profit from this irradiation mode. This can be understood as the beam stopping in front of the esophagus (gantry angle of -45°) is optimized into having less raster points in the IMPT(OAR) delivery compared to an IMPT irradiation and hence a reduced dose contribution to the total dose delivery. The other beam channels (gantry angles of 135° and 0°) are hence optimized into having more raster points compared to the IMPT delivery, contributing more to the dose deposition. Adjacent OAR to the esophagus, like trachea and aorta, are thus also receiving a smaller dose deposition from the beam channel stopping in proximity to them. As only an IMPT(OAR) treatment leads to acceptable dose depositions in the esophagus, the median dose to the other organs will only be stated for this delivery type.

Over all patients the trachea is receiving a median dose of 0Gy in all cases, since only patient 2 and 3 yield a dose in this critical structure. The 75th percentile is found to be 0.1Gy with no safety margin and 1.1Gy, 3.0Gy, 6.6Gy for 3mm, 5mm and 7mm, respectively for IMPT(OAR)_{R1}. For IMPT(OAR)_{R2} the 75th percentile results also to 0.1Gy for no safety margin and 0.5Gy, 3.0Gy, 7.4Gy for 3mm, 5mm and 7mm, respectively. All of these dose deposition are far below the recommended dose-volume-limit for the trachea (10.5Gy for 4cm³).

For the aorta an IMPT(OAR)_{R1} irradiation with no safety margin leads to a median dose deposition of 6.5Gy (8.5Gy), while 8.3Gy (10.6Gy), 9.8Gy (12.3Gy) and 11.3Gy (14.0Gy) are deposited with 3mm, 5mm and 7mm margin. In case of IMPT(OAR)_{R2} these results are further reduced to 3.5Gy (5.3Gy) with no safety margin and 5.0Gy (7.9Gy), 6.3Gy (12.0Gy) and 7.8Gy (13.6Gy) with 3mm, 5mm and 7mm margin, respectively. Also these results are far below the critical dose-volume limit of 31Gy for 10cm³. It can thus be concluded that trachea and aorta do not receive a critical dose deposition while treating the PVs with a dose of 25Gy.

For the heart the dose-volume limits are much more critical. A median of 18.3Gy (22.8Gy) was obtained for IMPT(OAR)_{R1} irradiations with no safety margin and 23.0Gy (24.9Gy), 24.3Gy (25.0Gy) and 24.8Gy (25.0Gy) for 3mm, 5mm and 7mm margin, respectively. These results are slightly decreased with IMPT(OAR)_{R2} where the median is found to be 16.5Gy (21.0Gy) for no margin and 20.0Gy (24.0Gy), 22.0Gy (25.3Gy) and 22.8Gy (17.8Gy) for 3mm, 5mm and 7mm margin, respectively. Hence all studied irradiations exceed by far the dose-volume limit of 16Gy for 15cm³. A close analysis of the radiosensitive cardiac substructures is presented on the next pages (in table 3.4 to table 3.11).

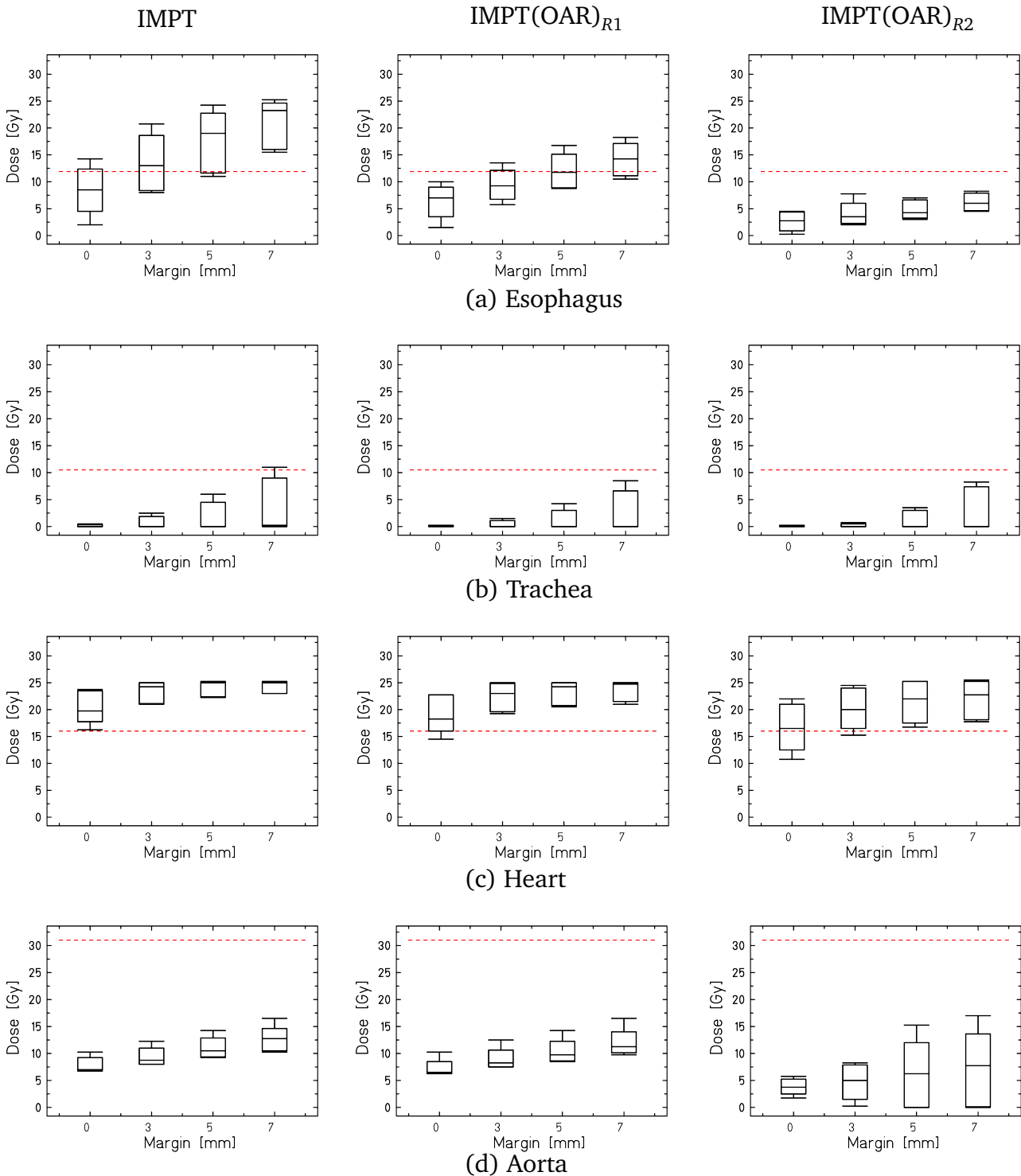


Figure 3.6.: Boxplots of dose-volume data for different safety margins (0mm, 3mm, 5mm and 7mm) over all patients. The data is plotted for different OARs when irradiating the LPV and RPV as IMPT (first column) or IMPT(OAR) in the five patient data sets. The results for the different IMPT(OAR) restrictions are plotted individually, so that IMPT(OAR)_{R1} (second column) are the treatment plans with a maximal dose of 70% of the physical dose and a weightfactor of 75% and IMPT(OAR)_{R2} (third column) are the results for the treatment plans with a maximal dose of 30% physical dose and a weightfactor of 200%. The dose-volume-limit for each critical organ is indicated with a dashed line in each plot, respectively.

Closer analysis of the dose deposition in the heart was carried out. The result of the median and 75th percentile over all patients is shown in table 3.4 for the mean dose and in table 3.5 for the maximal point dose. The mean deposited dose in the heart is negligible and does not increase with the size of the safety margins. Furthermore no difference in between IMPT and IMPT(OAR)_{R1} or IMPT(OAR)_{R2} irradiation can be observed. While also the maximum point dose does not increase with added safety margin, it can be seen that IMPT(OAR) treatment does lead to a higher point dose compared to an IMPT irradiation. This is higher for the irradiation with stronger restrictions on the maximal dose to the esophagus.

Table 3.4.: Mean dose to heart: median and 75th percentile.

Margin	IMPT [Gy]	IMPT(OAR) _{R1} [Gy]	IMPT(OAR) _{R2} [Gy]
0 mm	1.0 (1.3)	1.0 (1.1)	0.9 (0.9)
3 mm	1.3 (1.7)	1.3 (1.5)	1.1 (1.4)
5 mm	1.5 (1.9)	1.4 (1.7)	1.1 (1.4)
7 mm	1.6 (2.0)	1.5 (1.8)	1.1 (1.5)

Table 3.5.: Maximum point dose to heart: median and 75th percentile.

Margin	IMPT [Gy]	IMPT(OAR) _{R1} [Gy]	IMPT(OAR) _{R2} [Gy]
0 mm	26.9 (27.1)	27.6 (29.6)	34.1 (36.9)
3 mm	26.2 (27.3)	28.4 (29.7)	31.6 (36.4)
5 mm	26.5 (27.1)	28.0 (29.1)	30.7 (31.6)
7 mm	26.2 (28.0)	26.8 (27.9)	30.1 (31.0)

This can be understood as the esophagus and the other adjacent OAR (trachea, aorta) receive in general less dose with IMPT(OAR) due to the intensity reduction in one beam channel direction. Hence, the other beam channels have to deposit more particles. Especially gantry angle 0°, which traverses the heart, is leading to an increased dose deposition in the heart. Since this beam channel direction has to penetrate only a small volume of the heart, the maximal irradiated volume shows a slight improvement in IMPT(OAR) deliveries compared to an IMPT irradiation. The results are presented in table 3.6. Comparing the two IMPT(OAR) deliveries it can be seen that the results do not change, since the number of beam channels and hence penetrated volume does not change.

Table 3.6.: Maximal irradiated volume of heart: median and 75th percentile.

Margin	IMPT [Gy]	IMPT(OAR) _{R1} [Gy]	IMPT(OAR) _{R2} [Gy]
0 mm	17.2 (20.0)	15.7 (18.9)	15.7 (19.3)
3 mm	19.4 (22.6)	17.4 (21.2)	17.4 (21.8)
5 mm	20.7 (24.9)	18.5 (23.2)	18.5 (23.7)
7 mm	21.8 (26.4)	19.9 (24.4)	19.9 (25.2)

Concerning the ventricles the mean dose is negligible, with a median of less than 0.1Gy (75th percentile of less than 0.2Gy) for the LV and no dose exposure to the RV (median of 0.0Gy (75th percentile of 0.0Gy)). For the IMPT irradiations the median and 75th percentile of the maximal dose to the LV and RV over all patients and for all safety margin cases is shown in table 3.7. For both ventricles the dose is slightly increasing with the size of the safety margin. The left ventricle is receiving a higher maximum point dose than the right ventricle in case of an irradiation with the stronger dose restrictions. Concerning the maximal irradiated volume it can be stated that the LV is irradiated to a higher extend than the RV in all studied cases, and that also here the affected volume is increasing with the underlying safety margin size. Nevertheless it can be stated that the irradiated volume of both ventricles is negligible and that the maximum point dose is small.

Table 3.7.: Maximum point dose to ventricles: median and 75th percentile.

OAR	Margin	IMPT(OAR) _{R1} [Gy]	IMPT(OAR) _{R2} [Gy]
LV	0 mm	0.9 (2.8)	0.8 (3.3)
	3 mm	1.5 (3.9)	1.7 (7.9)
	5 mm	1.8 (5.0)	4.6 (6.5)
	7 mm	3.2 (6.1)	6.1 (9.0)
RV	0 mm	0.0 (0.5)	0.0 (0.0)
	3 mm	0.9 (2.1)	0.3 (0.9)
	5 mm	2.5 (3.7)	0.0 (1.5)
	7 mm	4.1 (5.0)	0.0 (3.7)

Table 3.8.: Maximal irradiated volume of ventricles: median and 75th percentile.

OAR	Margin	IMPT(OAR) _{R1} [%]	IMPT(OAR) _{R2} [%]
LV	0 mm	4.7 (12.0)	3.9 (11.2)
	3 mm	6.1 (14.7)	5.6 (14.5)
	5 mm	7.3 (16.7)	7.7 (15.8)
	7 mm	8.9 (18.7)	9.2 (17.9)
RV	0 mm	0.0 (0.1)	0.0 (0.0)
	3 mm	0.5 (0.6)	0.2 (0.2)
	5 mm	1.1 (1.7)	0.0 (1.1)
	7 mm	1.8 (3.0)	0.0 (2.3)

Concerning the coronary arteries, it can be seen that the LCA and RCA are receiving a comparable, small mean dose, which has a median of less than 1Gy in most studied cases. For both structures the maximum point dose increases with safety margin. The maximal deposited dose is higher in the LCA than in the RCA. In both cases the dose can be reduced with the stronger IMPT(OAR) restriction parameters, so that it can be concluded that also these structures benefit from the IMPT(OAR)_{R2} settings. Due to the small vessel size of the coronary arteries the dose deposition results in a relatively high maximal irradiated volume. In general, the maximum irradiated volume also increases with safety margin. While the maximal irradiated volume of the RCA can be drastically reduced for the stronger IMPT(OAR) settings, especially for large margins, the volume of the LPV does not change significantly. This is due to the proximity of the upper LCA branches to the LPV target site.

Table 3.9.: Mean dose to coronary arteries: median and 75th percentile.

OAR	Margin	IMPT(OAR) _{R1} [Gy]	IMPT(OAR) _{R2} [Gy]
LCA	0 mm	0.2 (0.7)	0.2 (0.7)
	3 mm	0.5 (0.9)	0.4 (1.7)
	5 mm	0.7 (1.2)	1.0 (2.0)
	7 mm	1.5 (2.0)	1.3 (2.8)
RCA	0 mm	0.3 (1.1)	0.1 (0.4)
	3 mm	0.5 (0.8)	0.3 (1.0)
	5 mm	0.7 (1.5)	0.1 (0.7)
	7 mm	1.0 (2.0)	0.2 (1.1)

Table 3.10.: Maximum point dose to coronary arteries: median and 75th percentile.

OAR	Margin	IMPT(OAR) _{R1} [Gy]	IMPT(OAR) _{R2} [Gy]
LCA	0 mm	6.0 (7.0)	5.2 (8.3)
	3 mm	7.4 (9.4)	8.0 (15.6)
	5 mm	8.7 (15.9)	12.3 (17.6)
	7 mm	20.1 (23.0)	16.2 (22.0)
RCA	0 mm	3.1 (5.2)	2.8 (5.7)
	3 mm	3.8 (6.5)	3.1 (7.8)
	5 mm	4.3 (8.8)	3.4 (9.8)
	7 mm	5.9 (15.3)	4.2 (11.9)

Table 3.11.: Maximal irradiated volume of coronary arteries: median and 75th percentile.

OAR	Margin	IMPT(OAR) _{R1} [Gy]	IMPT(OAR) _{R2} [Gy]
LCA	0 mm	26.7 (41.0)	25.3 (38.3)
	3 mm	28.5 (45.7)	28.0 (44.2)
	5 mm	29.6 (49.1)	30.3 (46.5)
	7 mm	31.4 (53.4)	31.2 (50.3)
RCA	0 mm	19.2 (28.6)	15.6 (23.6)
	3 mm	25.1 (32.2)	21.8 (30.2)
	5 mm	33.2 (37.6)	2.1 (29.6)
	7 mm	39.6 (43.4)	2.1 (36.1)

3.2.3 Motion assessment of heartbeat

Using the resulting deformation maps from deformable image registration the motion of the ablation sites of LPV and RPV was assessed. Motion volume histograms (MVHs) [Ric13] displaying the relative displacement of every voxel of the investigated volume to the reference phase in all three motion directions were generated. The mean and standard deviation of these displacement values in each motion phase of LPV and RPV are plotted for all patients and motion directions in figure 3.7 and 3.8, respectively. The numerical values can be found in appendix B.1.

The mean and standard deviation of each patient over all motion phases are stated in table 3.12. From the five studied patients patient 4 is displaying the highest absolute displacement, both in LPV and RPV. Furthermore it can be seen that none of the motion directions can be determined as the largest contribution to the absolute displacement, neither in LPV or RPV motion. In table 3.13 the maximal absolute displacement for each patient is presented together with the corresponding motion phase. While motion phase six is the motion phase with the biggest displacement in 30% of all cases, no evident maximal motion phase can be assessed. On average, the absolute amplitude over all motion phases and patients is found to be $(2.7 \pm 1.6)\text{mm}$ for LPV and $(2.6 \pm 1.4)\text{mm}$ for RPV. In SI direction, the mean amplitude is $(-0.6 \pm 1.4)\text{mm}$ for LPV and $(-0.2 \pm 1.6)\text{mm}$ for RPV. In AP direction it is $(0.8 \pm 1.0)\text{mm}$ for LPV and $(1.0 \pm 1.6)\text{mm}$ for RPV, while in LR direction it is found to be $(0.4 \pm 0.9)\text{mm}$ for LPV and $(-1.0 \pm 1.5)\text{mm}$ for RPV. Hence, averaged over all patients it can be stated that while the PVs are moving mostly in AP direction, the contribution of the other motion directions are in the same order of magnitude.

The motion phases of the heartbeat gated CT scan are based on the ECG trace and result in a division of a single heartbeat. The motion phases can hence be directly assigned to the contraction (systole) and dilatation (diastole) of both atria and ventricles. Contraction of the atria (atrial systole) is occurring in between motion phase four and nineteen, in the same time as the ventricular relaxation (ventricular diastole). The ventricular systole and at the same time atria diastole are hence much shorter, occurring in the remaining motion phases twenty to three. The maximal displacement of the atria should thus be observed in motion phase eighteen, while the maximal amplitude of the ventricle should be observed in motion phase three. The motion of the PVs on the other hand result in a chaotic displacement. No motion phase can be assessed to a maximal displacement in all patient cases and no dominant motion direction is observed. The underlying heartbeat motion which causes the PVs to move should hence be much more complex.

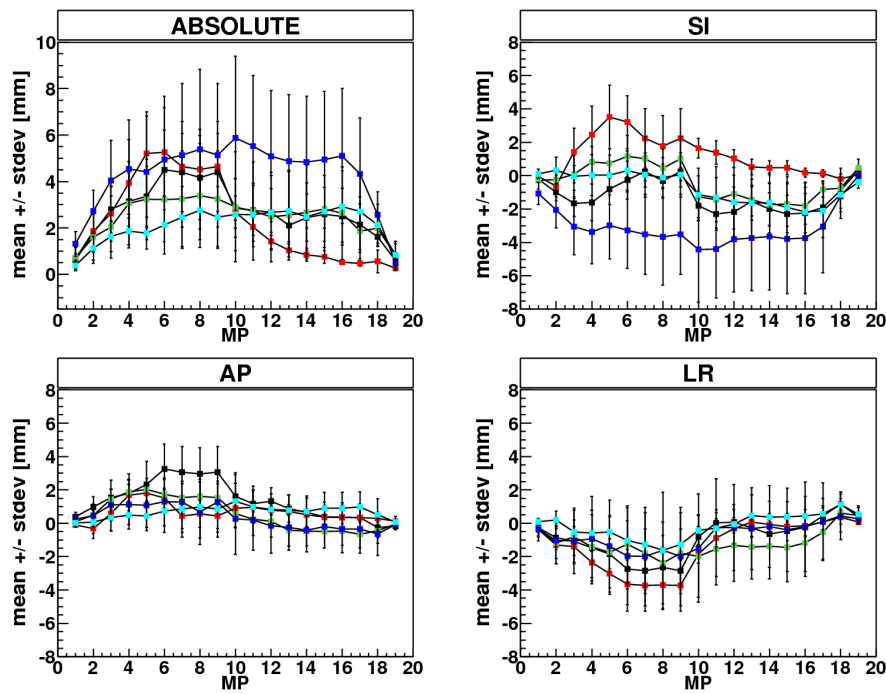


Figure 3.7.: Mean motion amplitude and standard deviation of LPV in each motion phase (MP) relative to the reference phase under influence of heartbeat for all patients (Patient 1: black, Patient 2: red, Patient 3: green, Patient 4: blue, Patient 5: turquoise). The motion is shown in the three studied motion directions (SI: superior-inferior, AP: anterior-posterior, LR: left-right) and the absolute (ABS) displacement.

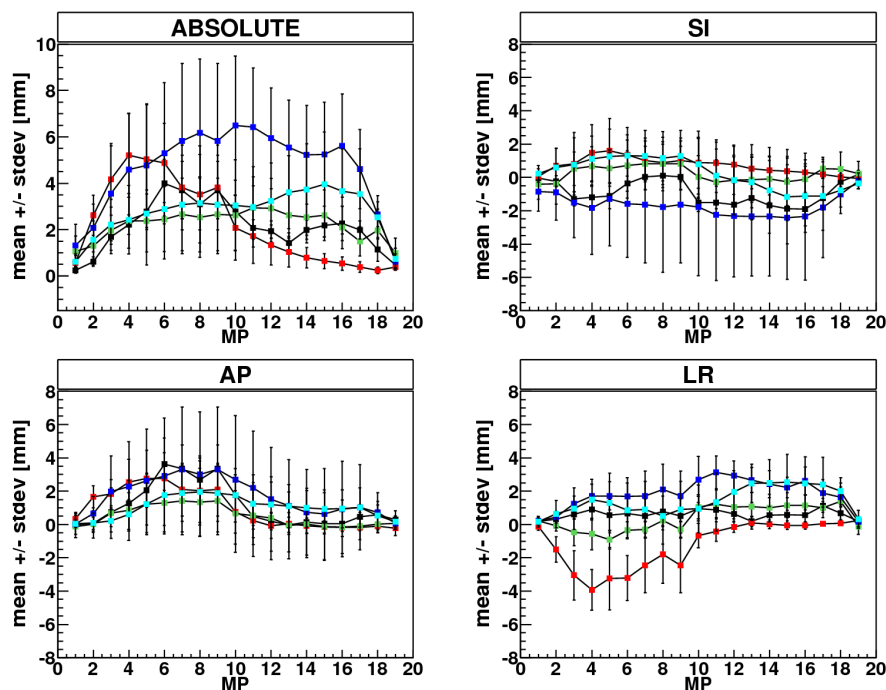


Figure 3.8.: Mean motion amplitude and standard deviation of RPV in each motion phase (MP) relative to the reference phase under influence of heartbeat for all patients (Patient 1: black, Patient 2: red, Patient 3: green, Patient 4: blue, Patient 5: turquoise).

Table 3.12.: Mean displacement of PVs over all motion phases (MP) in all patients and motion directions.

Patient	LPV: ABS [mm]	LPV: SI [mm]	LPV: AP [mm]	LPV: LR [mm]
1	2.7 ± 1.2	-1.2 ± 0.9	1.4 ± 1.1	-0.9 ± 0.8
2	2.3 ± 1.1	1.2 ± 1.1	0.6 ± 0.5	-1.4 ± 0.9
3	2.5 ± 1.8	-0.4 ± 1.1	0.5 ± 0.8	-1.2 ± 2.0
4	4.3 ± 2.5	-3.1 ± 2.5	0.3 ± 1.4	-0.8 ± 2.5
5	2.2 ± 1.2	-0.8 ± 1.4	0.7 ± 1.1	-0.2 ± 1.0

Patient	RPV: ABS [mm]	RPV: SI [mm]	RPV: AP [mm]	RPV: LR [mm]
1	2.1 ± 0.7	-0.9 ± 0.7	1.1 ± 0.9	0.6 ± 0.6
2	2.3 ± 1.3	0.7 ± 1.1	1.0 ± 1.1	-1.2 ± 1.0
3	2.2 ± 1.2	0.2 ± 1.3	0.5 ± 1.8	0.4 ± 0.7
4	4.6 ± 2.3	-1.7 ± 3.1	1.7 ± 2.8	1.8 ± 1.0
5	2.8 ± 1.7	0.2 ± 1.8	1.0 ± 1.3	1.4 ± 1.4

Table 3.13.: Biggest absolute displacement of PVs with corresponding motion phase (MP) in all patients.

Patient	LPV: max. ABS [mm]	MP
1	4.5 ± 1.7	06
2	5.3 ± 1.9	06
3	3.4 ± 2.2	08
4	5.5 ± 3.1	11
5	2.9 ± 1.5	16

Patient	RPV: max. ABS [mm]	MP
1	4.0 ± 1.4	06
2	5.2 ± 1.8	04
3	2.9 ± 1.4	11
4	6.5 ± 3.0	10
5	4.0 ± 4.0	15

The overall displacement field between the extreme states of the ventricular displacement (motion phase three) and atrial displacement (motion phase eighteen) for two exemplary patients with a small motion amplitude (patient 5) and a large motion amplitude (patient 4) are shown in figure 3.9. In order to visualize the location of the displacement, an axial cut of the reference state CT is underlaid. The absolute values of the displacement vectors are shown as contour plots.

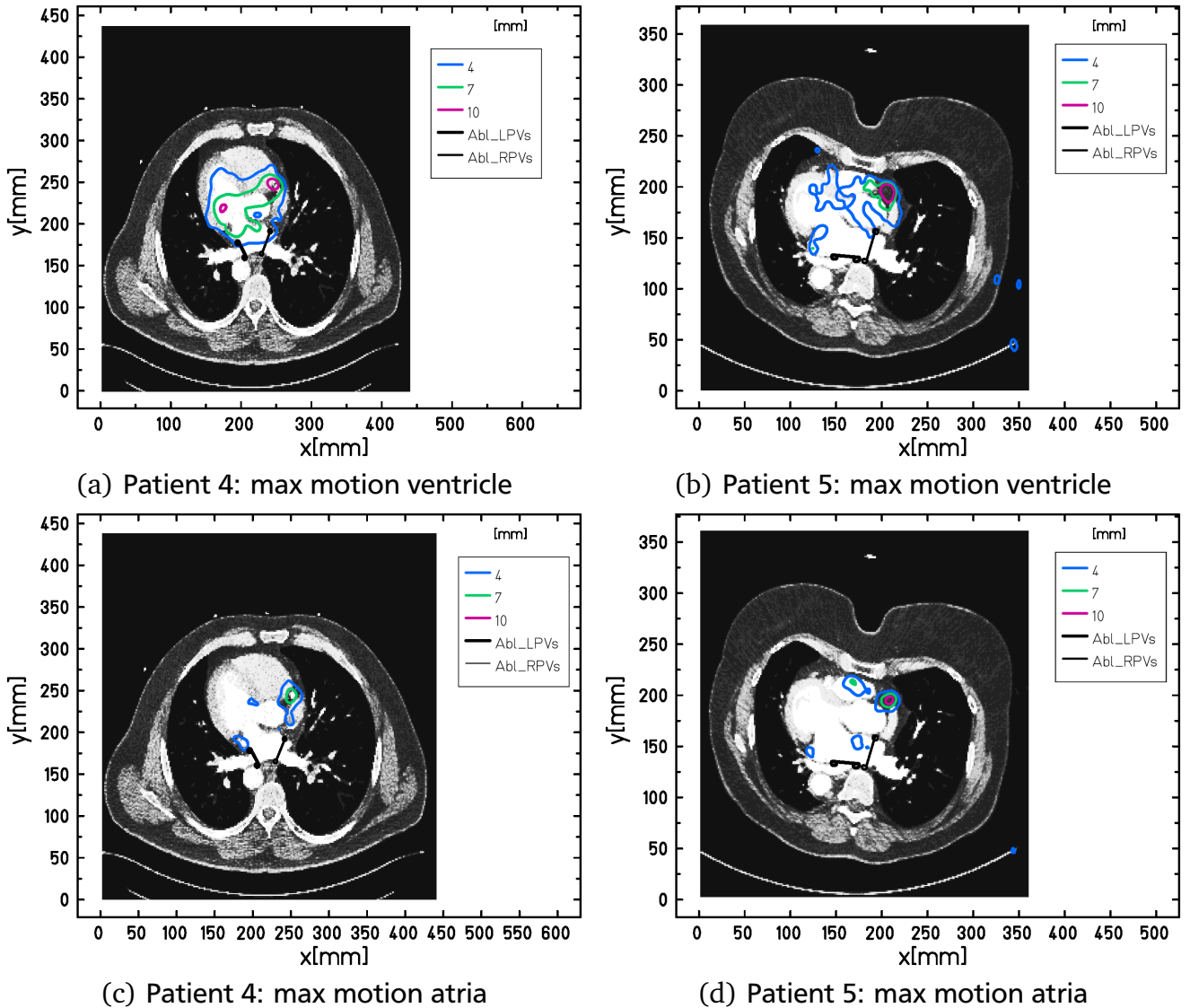


Figure 3.9.: Axial slices of the reference state of the CT overlaid with the absolute values of the displacement field (obtained from deformable image registration) in the corresponding slice for heartbeat motion. In the top row the displacement from the motion phase with the maximal ventricle motion to the reference phase is shown, in the lower row the displacement from the motion phase with the maximal atrial motion, for Patient 4 and Patient 5, respectively.

3.2.4 Motion mitigation techniques for heartbeat

The absolute motion amplitudes of up to 5mm due to heartbeat are expected to yield dose inhomogeneities when not compensated for. The resulting interplay effect and dose deposition were studied for every patient for different motion patterns and different margins to the target volumes. The dose analysis values V95, V107 and D5-D95 were assessed and plotted. For comparison also the corresponding values for the 3D case (static) are shown. Due to the small motion amplitude, rescanning was studied as motion mitigation technique. The results of the stated dose values in case of rescanning with different rescan numbers will also be presented.

Dose deposition

The dependencies of dose coverage and dose homogeneity on safety margin and rescan numbers are shown over all patients and motion patterns for the two target volumes, LPV and RPV, in figure 3.10. It can be shown that ten rescans yield a robust motion mitigation technique for the displacement of the PVs due to heartbeat motion. This will be studied in more detail in the following.

A representative dose deposition for all studied techniques (static, interplay and rescanning with ten rescans) is shown exemplary for patient 4 (as this is the patient with the largest PV motion amplitude both in LPV and RPV) in figure 3.11. Rescanning and interplay are shown for a motion period of 0.7s and a starting phase of 0°. The target volumes LPV and RPV were irradiated simultaneously and a margin of 3mm was added.

Exemplary for patient 4, DVHs of the CTV for a static irradiation as well as interplay and ten rescans for different motion patterns and a target volume with 3mm safety margin are displayed in figure 3.12. In order to assess the dose information of all patients the DVHs were analyzed and compared for dose steepness, dose coverage as well as over dosage. The average results over all patients with the resulting standard deviation can be seen in figure 3.13. A more detailed analysis can be found in appendix B, where the corresponding numerical values are shown (tables B.11 - B.20).

For interplay it can be seen that the results are slightly dependent on the used motion period and starting phase. This can be seen in the mean values of the resulting dose parameter values for different, underlying motion patterns. E.g. for LPV, the mean value of the dose coverage parameter over all patients is $V95 = (87.7 \pm 7.4)\%$ for a motion with 1s period and a starting phase of 90° and $(92.1 \pm 4.3)\%$ for a motion with 0.7s period and a starting phase of 90°, while for a motion with 0.7s period and a starting phase of 0° the dose coverage is found to be (90.4

$\pm 3.3\%$. Furthermore the result is also dependent on the studied safety margin, so that e.g. the dose coverage for a motion with 1s period and a starting phase of 90° is $(94.6 \pm 4.4)\%$ with 3mm safety margin. All these dependencies are also valid for the other studied dose analysis parameters, dose homogeneity and over dosage. The improvement of the dose coverage and dose homogeneity in relation to the size of the safety margin are also presented in figure 3.10 (a and b). The dose homogeneity resulting from interplay as well as all rescanning irradiations was studied in relation to the used margin size and the proportion of variance explained resulted in $r^2=0.35$ ($p<0.0001$), hence favoring the application of the necessary safety margins. It becomes obvious that a safety margin of 3mm is already sufficient to drastically improve the outcome.

The underlying deformation map with its motion amplitude does not enable a prediction of the magnitude of the interplay effect. This was studied in more detail for the dose homogeneity, as these values were normally distributed. The proportion of variance explained between the maximal motion amplitude of the left and right PV (see table 3.13) and the resulting D5-D95 values for all studied margins resulted in $r^2=0.02$ ($p<0.0001$).

As can be seen in figure 3.13 (as well as in more detail for all patients in appendix B.2) rescanning yields improved results compared to interplay in all studied cases. This is valid for dose steepness, dose coverage as well as over dosage. Especially dose coverage and over dosage are comparable to the static results for all patient and motion patterns. Exemplary, the dose coverage of patient 4 (with the largest absolute displacement) will be discussed. V95 for a static irradiation of the LPV of patient 4 with 3mm safety margin is found to be 99.8%. With a motion of 0.7s period length and a starting phase of 0° the value decreases to 90.0%. With rescanning, V95 can be improved to 99.8% with only five rescans. For RPV the static dose coverage with 3mm margin is found to be 100% for this patient. With the stated motion and safety margin the dose coverage decreases to 97.0% in case of interplay. Even though this is an acceptable value, the treatment gets more robust with rescanning and only five rescans are sufficient to increase the value to 100.0%. The improvement of dose coverage and over dosage compared to interplay is valid for all studied rescan numbers, starting from the smallest studied rescan number of five, as shown here. Nevertheless, in some studied cases five rescans is not enough to yield results comparable to the static irradiation. This was studied in more detail for the dose coverage parameter V95. For example for the LPV irradiation with five rescans in patient 1 with a motion period of 1s and 90° starting phase (3mm safety margin) V95 results in a smaller dose coverage (93.2%) than the static case (100%). Even though this result is improved compared to interplay (86.9%), a much better result can be gained with higher rescan numbers, starting with ten rescans (99.2%). Also the results for dose homogeneity improves with higher rescan numbers. For a motion pattern of 0.7s period and 0° starting phase (3mm safety margin) in

patient 4, the dose homogeneity in case of interplay is found to be 9.9%. With five rescans a dose homogeneity of 5.5% is yielded, which further decreases to 4.6% with ten rescans, 4.4% with fifteen rescans and 3.9% with twenty rescans (compared to 3.9% in the static irradiation). As the dose homogeneity was normally distributed, the relation between dose homogeneity and rescan number was analyzed. Thereby interplay was included as a rescan number of one. The explained variance was found to be $r^2=0.37$ ($p<0.0001$). It can thus be concluded that rescan numbers higher than five yield slightly better results, while ten rescans show results comparable to the static irradiation in all studied patient cases, for all studied safety margins and for all underlying motion patterns. This can also be seen in figure 3.10 (c) where the dose coverage over all patients and margins is studied in relation to the used rescan number. It can be seen that while interplay (one rescan) results into a median of 8.9% (75th percentile of 10.0%), five rescans can reduce it to 6.1% (8.1%). With ten rescans this can be further improved to 4.1% (5.9%). Fifteen and twenty rescans on the other hand do not lead to an improved result compared to ten rescans (fifteen: 4.1% (5.9%), twenty: 4.0% (5.7%)).

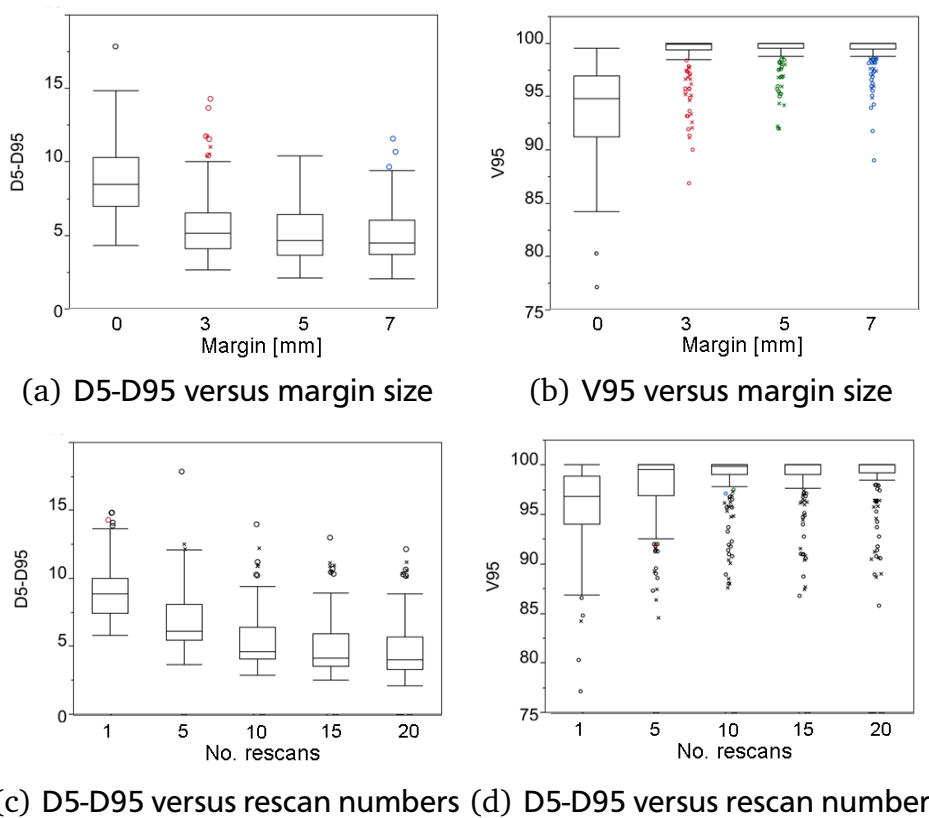
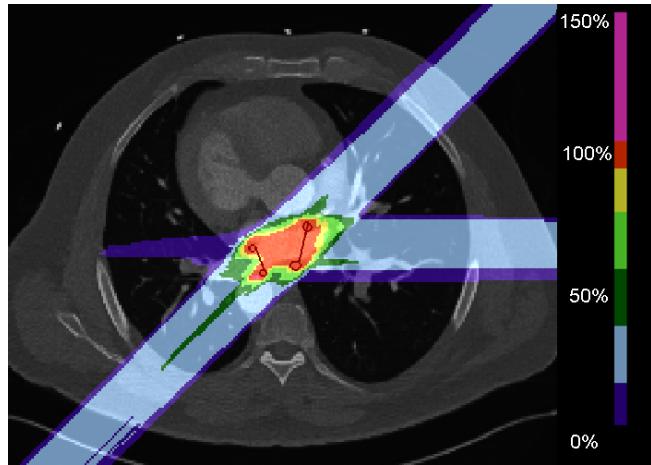
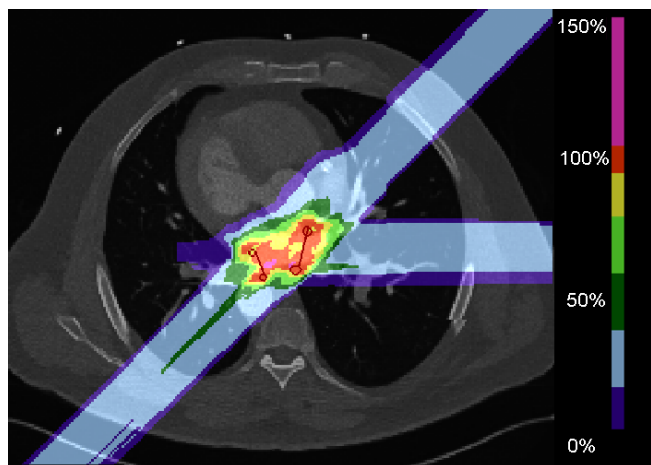


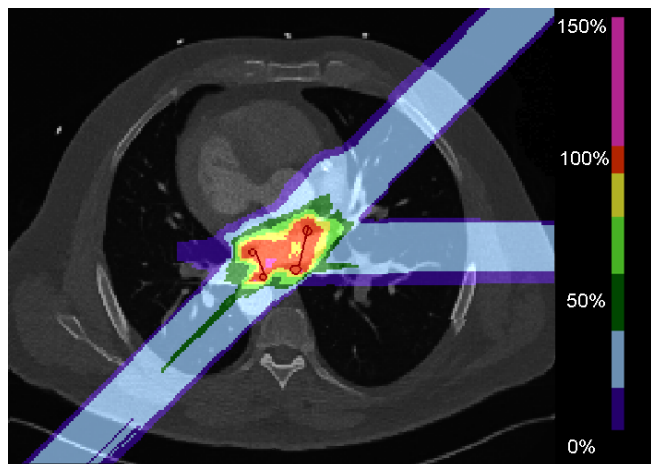
Figure 3.10.: Boxplots of dose analysis parameters D5-D95 and V95 over all patient data sets and target volumes (LPV: circle and RPV: cross) depending on the used margins size (0mm: black, 3mm:red, 5mm:green, 7mm:blue) or the used rescan number (one rescan equals interplay, rescanning with five, ten, fifteen and twenty rescans). Minimum and maximum of the data is plotted within 1.5 times the interquartile range, the other data points are stated as outliers. Figures are courtesy of Dr. Christian Graeff.



(a) static

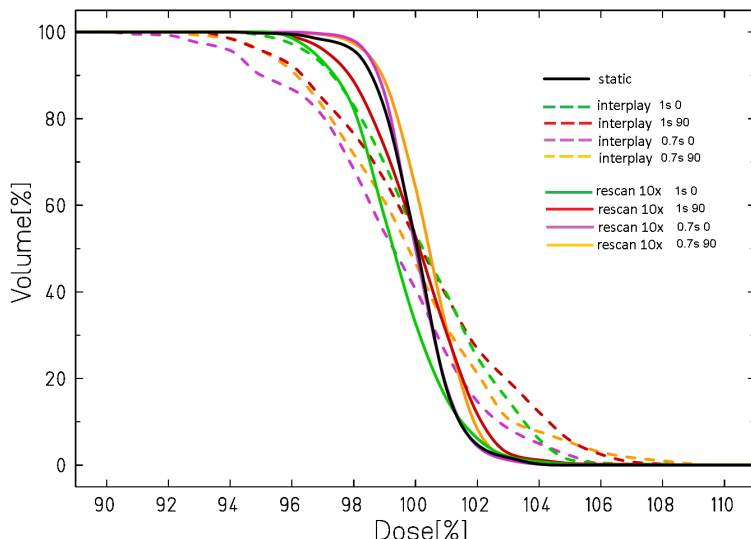


(b) interplay

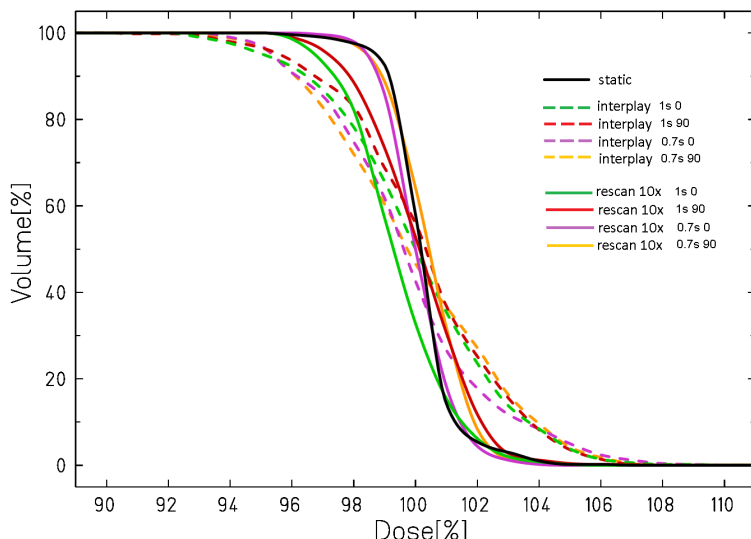


(c) rescanning (10x)

Figure 3.11.: Dose distribution of patient 4 for static (a) as well as interplay (b) and ten rescans (c) for a motion period of 0.7s and a motion starting phase of 0°. The target volume has an added margin of 3mm.



(a) LPV



(b) RPV

Figure 3.12.: Dose volume histograms for CTV of patient 4 for 3mm safety margin irradiation (LPV (a) as well as RPV (b)) in case of static irradiation (black), interplay (dashed) and rescanning with ten rescans (solid). The motion patterns are shown in colors (1s 0: motion period of 1s and starting phase 0°, 1s 90: motion period of 1s and starting phase 90°, 07s 0: motion period of 0.7s and starting phase 0°, 07s 90: motion period of 0.7s and starting phase 90°).

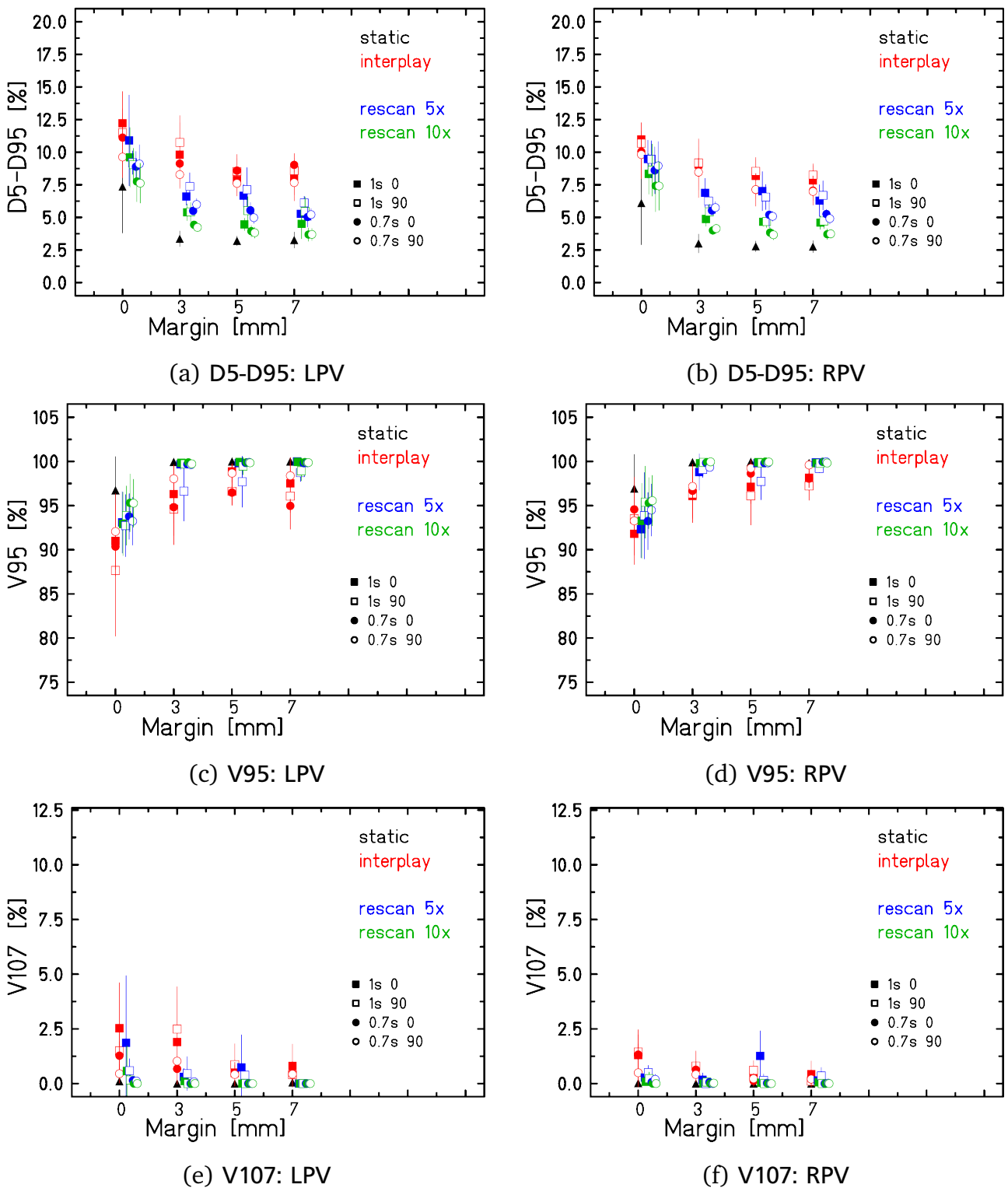


Figure 3.13.: Mean and standard deviation of dose analysis parameters D5-D95 (first row), V95 (middle row) and V107 (last row) over all patients. The LPV (left column) and RPV (right column) were studied separately. Static (black) as well as interplay (red) and different rescanning numbers (5 times: blue, 10 times: green) were compared for different motion patterns and safety margins. For a better visualization the rescanning data points for each motion pattern are shifted and the result for fifteen and twenty rescans are not displayed.

Irradiation time

In figure 3.14 the mean irradiation time over all patients for different rescanning irradiations of LPV and RPV are shown for different safety margins and motion patterns. The duration for each beam entry channel (gantry angle of -45° , 135° and 0°) is plotted individually. It can be seen that the needed irradiation time increases with the used safety margin as the irradiated volume increases. The irradiation time is independent of the motion pattern but varies depending on the used beam entry channel. The stated results were achieved with a low intensity irradiation (minimal particle number of 5,000). For an irradiation with 3mm margin around LPV and RPV the overall treatment time is calculated to $(13.7 \pm 0.9)\text{min}$ (see table 3.14) with rescanning as motion mitigation technique for heartbeat motion. This time could be increased if a higher minimum particle number per beam spot (e.g. 75,000) was used, which needs to be studied.

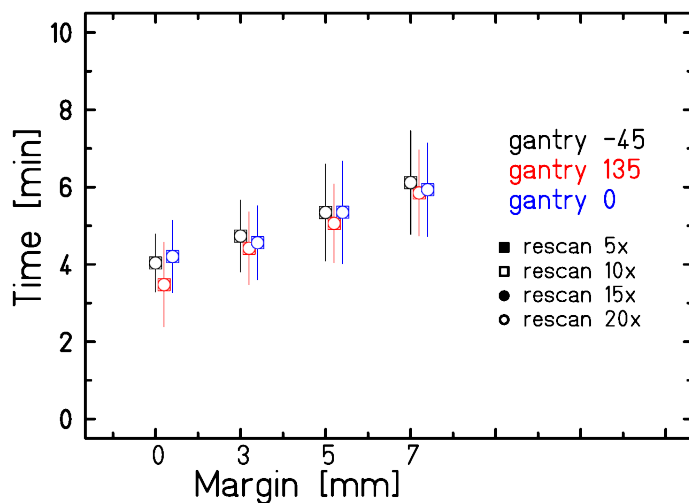


Figure 3.14.: Mean and standard deviation of the irradiation time over all patients for different underlying motion patterns and beam entry channels.

Table 3.14.: Mean irradiation time for LPV and RPV with a safety margin of 3mm over all patients.

Gantry angle [°]	time [min]	total [min]
-45	4.7 ± 0.9	
135	4.4 ± 0.9	
0	4.6 ± 1.0	13.7 ± 0.9

3.3 Discussion

In this chapter the influence of heartbeat motion on the PVs was studied and treatment planning studies with rescanning as motion mitigation technique were carried out. A detailed analysis of the dose depositions to the OAR was performed, with special emphasis on the irradiation of cardiac substructures. Beforehand, a study of the best suited field number and beam directions was conducted as well as an analysis of possible safety margin limitations.

3.3.1 Dose to critical structures

Concerning the dose deposition in OAR (esophagus, trachea, aorta and heart) dose-volume limits from SBRT were used. In SBRT treatment a high dose is applied in a single fraction and hence comparable to the here stated dose delivery of 25Gy physical dose in one treatment session. An extensive collection of dose-volume-limits for SBRT are presented in the study protocols of the Radiation Therapy Oncology Group (RTOG). The stated dose-volume limits for trachea (10.5Gy in 4cm^3) and aorta (31Gy in 10cm^3) were not exceeded for any of the studied field numbers and beam channel combinations. The same is valid while keeping the chosen three fields (couch angle of 90° and gantry angles of -45° , 135° and 0°) constant and changing the studied safety margins (0mm, 3mm, 5mm and 7mm). For the esophagus on the other hand, the dose-volume limits were much more critical. Most of the studied beam directions yielded a dose which exceeded the stated dose-volume limit (11.9Gy for 5cm^3). Hence IMPT(OAR) deliveries, including the esophagus in the optimization process, were necessary. With this delivery technique and the above stated beam direction, the dose to the esophagus could be drastically reduced. With restrictions to a maximum point dose of 70% to the esophagus (IMPT(OAR)_{R1} , weightfactor of 75%) only an irradiation of the PVs with 3mm safety margin resulted in a dose deposition into the esophagus which met the dose volume limit (median of 9.3Gy, 75th percentile: 12.1Gy). This result could be further improved with different IMPT parameters (IMPT(OAR)_{R2} , maximum dose of 30% and weightfactor of 200%), enabling a safe irradiation. Thus also safety margins higher than 3mm should result in an uncritical dose deposition to the esophagus. For the heart all beam channels, safety margins and delivery types (IMPT or IMPT(OAR)) exceeded the stated dose-volume limit (16Gy for 15cm^3). This is due to the fact that the heart is not only an OAR but part of the target itself. Hence a closer look on the affected cardiac substructures and the relevance of these dose depositions on cardiac toxicity and late effects were given.

QUANTEC (quantitative analysis of normal tissue effects in the clinic) [QUANTEC10] offers an comprehensive literature review on the available data of the last 20 years and is meant as an update of the extensively used dose-limits proposed by Emami et al. [Ema91]. In the QUANTEC publication by Gagliardi et al. [Gag10] radiation dose-volume effects in the heart are presented.

It is stated that radiation-induced cardiac diseases are distinguished between acute injuries like pericarditis², which can turn into a chronic disease, and late injuries which manifest months or even years after radiation exposure. Typical late injuries are congestive heart failure³, ischemia, coronary artery disease and myocardial infarction. It was summarized that it remains uncertain which region of the heart is most important for radiation induced tissue toxicities. But it is stated that the risk of cardiac events is probably related to both dose and irradiated volume. Pericarditis seems to be related to left ventricle (LV) irradiation, and it was found that LV shielding was able to drastically reduce the incidence rate [Car76]. It was stated that a mean cardiac dose of 27.1Gy and maximum dose of 47Gy seem to act as predictors for pericarditis [Mar98]. Wei et al. [Wei08] stated another discriminator for pericarditis which was found to be V30 < 46%, which translates in a mean pericardial dose of less than 26Gy. For coronary and ischemic events relevant substructures are assumed to be coronary arteries on the left ventricle (LCA) [Nie07, Tay07, Tay08]. Furthermore it is stated that excess deaths from heart disease are observed in patients receiving more than 42Gy [Han93] and that aortic and mitral stenosis incidences increased above a threshold dose of 30Gy [Tay07]. For long term cardiac mortality an increased rate was only observed at whole heart doses above 30Gy [Han93].

Hooning et al. [Hoo07] studied the cardiovascular disease incidence in more than 4000 breast cancer survivors after a follow-up period of more than 10 years as patients were treated from 1970 through 1986. It was the first study to examine the effects of cardiovascular risk factors in combination to radiotherapy. They found that the risk of congestive heart failure was significantly increased when the patients had received chemotherapy (95% confidence interval of 1.25 to 2.73) and that smoking drastically increased the risk of the patients to suffer a myocardial infarction (95% confidence interval of 2.03 to 4.55). Concerning radiotherapy they stated that a higher mean dose to the whole heart resulted in an increased risk of congestive heart failure and that an irradiation of the left vs right chest wall (thus more heart volume and in particular including the LV and apex) led to an increased risk of myocardial infarction.

A recent study by Darby et al. [Dar13] investigated more than 2000 breast cancer patients treated in between 1958 and 2001 for coronary events like myocardial infarction, coronary revascularization or death from ischemic heart disease. They found a mean heart dose of 4.9Gy (0.03Gy to 27.72Gy) and that the rates of major coronary events increased linearly with the mean heart dose. They stated an increase of incidences by 7.4% per Gy (95% confidence interval of 2.9 to 14.5) after five years post radiotherapy.

² inflammation of the sac containing the heart

³ heart is unable to maintain sufficient blood flow

For the here studied seventeen beam channel combinations, applying a physical dose of 25Gy, the mean dose to the heart of all five studied patients was found to have a median of 1.3Gy (75th percentile of 1.5Gy). The median over the maximal point dose was found to be up to 26.6Gy (75th percentile: 27.1Gy), while in general less than 30% of the heart was irradiated. With the chosen field number of three beam channels with a couch angle of 90° and gantry angles of -45°, 135° and 0°, the mean dose was found to be negligible (median of 1Gy, 75th percentile of up to 1.5Gy) in all studied patient cases. The median mean dose over all patients did not increase with increasing safety margin for both IMPT(OAR) deliveries. As the LV, and with it especially the LCA, are assumed to be radiosensitive structures within the heart the dose depositions to these structures were analyzed in more detail. It was found that three beam channel directions were best suited to yield a lower mean dose deposition in the LCA. Due to robustness criteria of the treatment delivery the above stated beam channel combination was chosen. With this delivery direction and an IMPT(OAR)_{R2} treatment it was found that the mean dose to the LCA was, dependent on the used safety margin, 0.2Gy(75th percentile: 0.7Gy) with no margin, 0.4Gy (75th percentile: 1.7Gy) for 3mm margin, 1.0Gy (75th percentile: 2.0Gy) for 5mm and 1.3Gy (75th percentile: 2.8Gy) for 7mm. The maximum point dose to the LCA with these beam channels nevertheless led to an increased dose in the left chamber compared to the right site. This is due to the proximity of the upper LCA branches to the LPV target site.

3.3.2 Beam channel directions and safety margins

In general, it can be stated that field number and beam direction always result in a trade-off between dose to the OAR, irradiation time and robustness. While less fields and hence beam directions shorten the treatment time, it does lead to a less robust treatment. In case OAR are displaced during the treatment (intrafractional motion, see Introduction) or move in between CT image acquisition and irradiation (interfractional motion) beam channels with a large angle in between them are more robust, as not all fields are affected by this displacement and hence only a small dose would be shifted. Furthermore, opposite fields (like -45° and 135°) (see figure 3.1) are more robust against potential range uncertainties and should hence be favored. Due to this reason, combined with the smaller LCA dose deposition in case of three field numbers, a couch angle of 90° and gantry angles of -45°, 135° and 0° were selected for the safety margin limitation studies as well as the motion mitigation treatment plans. Concerning safety margins, which need to be applied in order to account for possible deviations in between treatment planning and dose delivery, it can be stated that only a small margin tolerance was observed. This is due to the difficult position of the PVs close to radiosensitive structures like the esophagus and especially the heart. With IMPT treatment a delivery with 3mm safety margin was found to fulfill all the needed requirements. A more realistic safety margin of 5mm could be achieved with more restricted parameters in the IMPT optimization.

3.3.3 Movement of PVs in cardiac cycle

Lickfett et al. [Lic05] analyzed the volume changes and displacement of the PVs in 25 healthy volunteers with MRI images. They studied the posterior edge of the PV orifice and observed that the size and location changed considerably during the cardiac cycle. Displacements of up to 7.2mm were found and it could be concluded that the motion amplitudes were bigger in the coronal (left-right) than in the sagittal (anterior-posterior) direction. In more detail the largest coronal movement was found in the left superior PV, while the largest sagittal motion was observed in the right superior PV with 3.9mm. The smallest saggital displacement was 2.5mm in the left anterior PV. They suspected that the reason for movement is not resulting from a single influence, but is rather a mix of PV contraction, atrial contraction and ventricular force. The movement of PV due to heartbeat is also relevant for catheter ablation. Based on the stated finding Lickfett et al. recommended to keep a 5mm distance from the PV orifice during PV encircling ablation in order to reduce the risk for PV stenosis. Patel et al. [Pat08] studied the MRI images of 30 patients in sinus rhythm with paroxysmal atrial fibrillation. They stated that the mean displacement of the pulmonary veins was small. The left lower PV was found to move (2.7 ± 1.2) mm, the left upper PV (2.1 ± 1.1) mm, the right lower PV (1.9 ± 1.1) mm and the right upper PV (2.3 ± 1.0) mm.

In the here studied patient cohort of five AF patients no differentiation between the upper and lower PVs was carried out. The motion was assessed for the whole potential ablation site of LPV and RPV, respectively. Similar to the study by Patel et al. only a small mean displacement was found, resulting in an average absolute displacement of less than 3mm (LPV: (2.71 ± 1.57) mm, RPV: (2.62 ± 1.41) mm). Even though a tendency to a higher motion in AP direction could be observed, the contributions of the other motion directions were in the same order of magnitude (up to 1mm). Hence no dominant motion direction could be determined. The motion phases of the heartbeat gated CT scan were based on the ECG trace and resulted in a division of a single heartbeat. Thus the motion phases could be directly assigned to the contraction (systole) and dilatation (diastole) of both atria and ventricles. Nevertheless no motion phase could be assessed to yield the maximum displacement. This reinforces the hypothesis by Lickfett et al. that the underlying heartbeat motion, which causes the PVs to move, is much more complex.

3.3.4 Rescanning as motion mitigation technique

The small target volume displacement due to heartbeat led to small interplay effects, where the dose coverage was found to have V95 values smaller than 95% in only 31% of the studied cases. This result could be already improved by using safety margins, as 71% of these cases were irradiations with no safety margin and only 3% of the stated cases were irradiations with safety margins of 5mm or more. Nevertheless also irradiations with a safety margin of 7mm were found to have a V95 of 89% in some cases (e.g. in the irradiation of the LPV in patient 4 with a motion period of 1s and a starting phase of 90°). In order to guarantee a robust and conformal irradiation a motion mitigation technique was hence needed. Rescanning was studied and it can be concluded that this technique yields good results.

Regarding dose coverage V95 values were higher than 99% in 96.3% of all studied cases with a safety margin of 3mm or higher. The minimum dose coverage over all studied cases with safety margin was found in patient 1, in the irradiation of the LPV with a margin of 3mm and an underlying motion of 1s period and 90° starting phase (V95=93.2%). This result was obtained with five rescans. With higher rescans the dose coverage could be improved, so that only 1.5% of the studied cases with ten or more rescans had a dose coverage smaller than 99% (minimum: 97.1%; 10 rescans in patient 1, 7mm safety margin and motion of 1s period and 90° starting phase). The dose coverage for rescans without safety margin was worse, resulting in 93.1% cases under 99%. In comparison, the static irradiations without safety margin resulted in a V95<99% in only 17% of the cases. V107 values higher than 0% were obtained in 7.3% of all cases with safety margin (maximum of V107=3.7% in the LPV of patient 3 with safety margin of 5mm, 5 rescans and motion of 1s period and 0° starting phase) compared to 28.8% of cases without safety margin (maximum: V107=8.0% for the LPV of patient 2 with 5 rescans and motion of 1s period and 0° starting phase. This could be reduced to V107=2.9% with 10 rescans). With safety margin, the dose homogeneity D5-D95 did not exceed 8.9%. Without safety margin D5-D95 did not exceed 10.2%. Both of these values were achieved with 5 rescans and could be improved with 10 rescans (with safety margin to less than 7% and without to less than 9%). It can hence be concluded that additional safety margins enable a more robust and successful treatment delivery. However, if possible, these margins should be kept as small as technical feasible, as it increases the dose deposition in OARs. Regarding rescan numbers ten rescans yield improved results compared to five rescans. These results are not significantly improved with rescan numbers higher than ten.

All these results were found for slice-by-slice rescanning, which means that each IES is irradiated independently with the predefined number of rescans and the adapted particle numbers. In this case the treatment time is not prolonged. It needs to be studied if other rescanning tech-

niques like breath-sampled rescanning [Sec09] or phase-controlled rescanning [Fur07], where the rescanning of the individual IES are sampled according to the motion phase of the breathing period, are applicable to cardiac motion (ECG-sampled rescanning) and if this method would result in the need of fewer rescan numbers.

3.4 Conclusion

The PVs were found to move due to heartbeat with an amplitude of up to 6mm. This displacement creates interplay effects when irradiated with scanned carbon ions. Rescanning as motion mitigation technique was studied. It yields improved dose coverage and dose homogeneity compared to interplay in all studied patient cases, motion patterns and for all safety margins. It is thus an adequate motion mitigation technique for the irradiation of PVs under influence of heartbeat motion. A rescan number of ten is sufficient to obtain results comparable to the static irradiation. For the treatment delivery, IMPT dose optimization together with a rather small safety margin (of e.g. 3mm) results in dose depositions in the OARs (like esophagus as well as in the cardiac substructures) which are considered tolerable. In order to achieve this an ion gantry, such as the one at HIT, is needed, as it allows for ion beam entry channels which better spare the critical structures.

4 Irradiation of cardiac target volumes in porcine data

Contents

4.1. Material and methods	114
4.1.1. Treatment planning input data	114
4.1.2. Treatment planning parameters	115
4.1.3. Treatment planning studies	116
4.1.4. Analysis	116
4.2. Results	117
4.2.1. Motion directions and magnitude	117
4.2.2. Dose to organs at risk when irradiating the AV node	125
4.2.3. Motion mitigation techniques for AV node irradiation	126
4.3. Discussion	133
4.3.1. Movement of cardiac target volumes in cardiac cycle	134
4.3.2. Dose to organs at risk for the irradiation of AV node	135
4.3.3. Rescanning as motion mitigation technique for AV node irradiation	136
4.4. Conclusion	137

The presented results of planning studies for a non-invasive ablation of cardiac target sites in human data need to be experimentally validated. This will be carried out at GSI in 2014, in collaboration with HIT and University Hospital Heidelberg as well as Mayo Clinic (Rochester, Minnesota, USA). Porcine models will be used and the results will be compared to findings with photon irradiation, both from literature [Sha10, Bla13], as well as from studies currently performed at Mayo Clinic. For the feasibility study different cardiac target sites are conceivable: PV isolation, ablation of the CTI as well as the AV node. In a first iteration of the experiments, only the AV node of the pigs will be irradiated, both at Mayo Clinic with photons and at GSI with carbon ions. The experiments are planned to enable a direct comparison between particle therapy and photon irradiation, so that many of the treatment settings are kept constant inbetween the two centers. Also in pigs, cardiac target sites move due to respiration as well as heartbeat, causing potential interplay effects which threaten the treatment outcome. While the

breathing motion of the pigs is planned to be compensated with breath hold, controlled by a respirator, the influence of heartbeat motion needs to be studied in more detail. The resulting motion amplitude and direction will be studied and rescanning as motion mitigation technique will be presented.

4.1 Material and methods

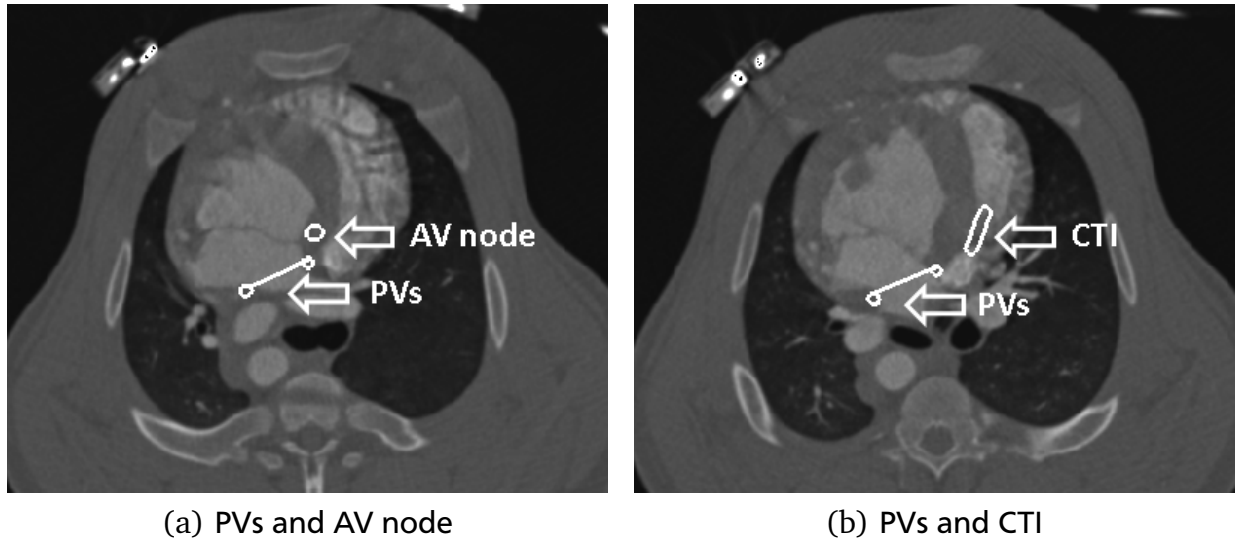
As in the previous chapter, the input data and treatment planning parameters will be given before stating all performed studies. Finally, the analysis procedure will be described.

4.1.1 Treatment planning input data

In order to assess the motion of the potential cardiac target sites (PV, CTI and AV node) in pigs under influence of heartbeat motion, ECG gated 4DCTs were studied. Four porcine data sets were recorded at Mayo Clinic (Rochester, Minnesota, USA) under anesthesia and respiration. The CT scans were acquired on a Definition Dual Source CT scanner (Siemens). The 4DCT data set consisted of twenty temporal equally distributed cardiac motion phases, the reference phase zero started at the R-peak of the QRS-complex (see chapter 1, section 1.3.1). Native CT scans were recorded. In order to distinguish structures within the heart, contrast enhanced CT scans were also acquired directly after the native scans. The radiopaque material was administered intravenously (100 mL contrast media at a rate of 4 mL/sec) and the CT scans were acquired 30 seconds after injection. Segmentation of the target volumes as well as the OARs (esophagus, trachea, aorta and cardiac structures) were carried out by a collaborating cardiologist at Mayo Clinic with Eclipse™ (Varian Medical Systems) on the reference phase. The volumes of the contours for the different ablation sites are presented for each pig in table 4.1. The location of these sites are visualized in figure 4.1 exemplarily for pig 1. Contrary to humans pigs have only one PV pair, distinguished inbetween inferior PV (IPV) and superior PV (SPV). The contour for the PV encircles both of these structures.

Table 4.1.: Target volume for the different cardiac target sites for all investigated pigs.

pig no	PVs [cm ³]	CTI [cm ³]	AV [cm ³]
1	0.72	0.20	0.08
2	1.01	0.13	0.05
3	1.09	0.24	0.06
4	1.03	0.31	0.02



(a) PVs and AV node

(b) PVs and CTI

Figure 4.1.: Cardiac target volumes (PV, CTI and AV node) in pig 1.

Also for these data sets, non-rigid image registration of the nineteen motion phase on the reference phase has been performed with Plastimatch [Sharp07, Shack10]. The first step of the B-Spline registration was carried out with 50 maximal iterations and an isotropic spacing of 4mm, while the second step had maximal 100 iterations with a grid spacing of 1mm. For the contrast enhanced CT scans the regularization was chosen to be $\lambda=0.005$, while for the native CT scans $\lambda=0.0001$ was chosen . The quality of registration was also here validated with visualization techniques (false color images [Bro07], checker board images [Bro07] and a qualitative check of the vector field regularization) between motion phase 3 and the reference phase 0 and motion phase 18 and the reference phase.

4.1.2 Treatment planning parameters

All treatment plans were generated on contrast-enhanced CT scans (see section 4.2.1) without motion (3D, static) as well as with motion (4D). For informations on the dose optimization process, the used raster spacing, dose algorithm and GSI beam applications the reader should be referred to 3.1.2.

Besides the original volume of the CTV, a safety margin has been added to the volumes of the treatment planning study. In agreement with the Mayo Clinic radiooncology an isotropic safety margins of 5mm has been chosen, which will also be applied in the irradiation with photons. The ITV volumes[Gra12], which were obtained from all twenty motion phases and were used as the final target, were generated from the original CTV contour as well as from the CTV with margin, so that potential range variations were considered in the margins.

All treatment plans were calculated as single field uniform dose (SFUD) deliveries, applying a physical dose of 25Gy in one fraction. The minimum particle number per beam spot was set to 75,000. The dose was applied from two different beam channel directions. With the fixed horizontal beam line available at GSI the beam positions were chosen as two lateral fields with couch angles of -90° and 90°. With these opposing fields the treatment should be more robust against potential uncertainties like range differences. Due to the GSI specific beam output, the particles are applied at an angle of -2.203°, which was integrated in the treatment plans as a gantry angle.

As the reconstruction of the 4DCTs was based on the time scale a phase-based motion state detection was employed. In order to consider possible divergence in the heartbeat motion pattern of the pigs, different motion periods (0.7s and 0.5s) as well as different starting phases (0° and 90°) were used. The fast motion periods were chosen according to the heartbeat rate of the pigs, between 110 and 120 beats per minute.

4.1.3 Treatment planning studies

On the basis of 3D treatment plans on the AV node the dose to nearby OARs were studied (see table 4.2). These were carried out on the CTV of all four pig data sets. Furthermore 3D (static) treatment plans were produced as reference values to the 4D cases. 4D plans were distinguished between an underlying motion without any compensation, resulting in interplay patterns [Phi92, Ber08], and with the application of rescanning [Phi92] as motion mitigation technique. For rescanning three different rescan numbers (5, 10 and 15) were compared. Static, interplay as well as rescanning treatment plans for all pigs where carried out with the two stated beam entry channels, a safety margin of 5mm, the stated treatment planning parameters and the four stated motion trajectories. All treatment planning studies were carried out on contrast enhanced CT scans due to the lack of contrast on native CT scans (see section 4.2.1).

4.1.4 Analysis

The dose deposition in the OAR as well as dose homogeneity in the target volume were studied. The dose deposition in the OARs (esophagus, trachea, aorta and the whole heart) were compared to dose-volume restriction stated in RTOG study protocols (see table 4.2) [RTOG0631, RTOG0915] (see chapter 3, section 3.1.4). As further OAR cardiac substructures (ventricles and coronary arteries) were studied. Here the mean dose into the structures as well as the maximum point dose and the maximal irradiated volume ($V_{>0}$) were analyzed. Since the values were not normally distributed, the median (50th percentile) as well as the 75th percentile were calculated over all pigs. Motion-volume-histograms (MVHs) [Ric13] were generated to display the relative displacement of every voxel of the investigated volume to the

reference phase in all three motion directions. With these values the resulting motion of the cardiac target sites due to heartbeat could be assessed. In particular, the motion assessable from the native CT scans were compared with the contrast enhanced motion information. For comparison the resulting DVHs from the different techniques were studied. The V95 (measure of dose coverage), V107 (over dosage) and D5-D95 (dose homogeneity) to the CTVs were assessed. Furthermore the median and percentile values (25th and 75th) of these parameters over all studied motion patterns and patient cases were generated. In one case a one-way ANOVA was carried out and the proportion of variance explained r^2 is reported with the corresponding p-value ($p < 0.0001$).

Table 4.2.: Dose-volume limits for OAR.

OAR	Volume [cc]	Dose [Gy]	endpoint
Aorta / great vessels	10	31	Aneurysm
Esophagus	5	11.9	Stenosis / fistula
Heart	15	16	Pericarditis
Trachea	4	10.5	Stenosis / fistula

4.2 Results

In the following the results of the motion assessment due to heartbeat will be shown. Afterwards the dose to OAR when irradiating the AV node will be presented in detail. For the treatment planning study different dose analysis parameters will be presented and compared for different cases (static, interplay and rescanning).

4.2.1 Motion directions and magnitude

Treatment planning for particle therapy is carried out on native CT scans, as the Hounsfield units (HU) give information on the electron density of the structures and hence enable a calculation of the needed particle range. In native CTs, however, the contrast between the cardiac muscle and blood is low. A comparison between motion assessments of the cardiac target volumes in native and contrast-enhanced CT scans will be presented for one porcine data set. Afterwards the motion of all target volumes (PVs, CTI and AV node) will be shown for all pigs.

Motion of cardiac target volumes in contrast enhanced versus native CT scans

Only one of the four porcine data sets (pig 3) offered identical depicted anatomy between native and contrast enhanced data sets. For all other data sets the pig was moved inbetween the CT acquisitions. For a fair comparison this data set was hence analyzed. Using the resulting

deformation maps from deformable image registration the motion of the ablation sites of PVs, CTI and AV node were assessed in both scans of pig 3. Motion volume histograms (MVHs) [Ric13] displaying the relative displacement of every voxel of the investigated volume to the reference phase in all three motion directions were generated. The mean and standard deviation of these displacement values in each motion phase are plotted for all motion directions in figures 4.2 - 4.4. It can be seen that the motion from the contrast enhanced CT is much larger than from the native CTs. While the mean absolute displacement in the native CT is smaller than 1mm in case of PVs and AV node and smaller than 1.5mm in case of CTI, the contrast CT enables a motion assessment which yields a mean absolute displacement of larger than 2mm in all studied target volumes (see table 4.3). The difference is especially large in the AV node. The maximal observable displacement for this structure in case of the native CT scan is (0.2 ± 0.1) mm (MP 12), while with the contrast enhanced CT an absolute displacement of (2.5 ± 0.4) mm is assessable in this motion phase and the maximal absolute displacement is found to be (4.4 ± 0.1) mm (MP 5) (see Appendix C.2). It can thus be concluded that contrast enhanced CTs are needed in order to fully assess the motion of cardiac target volumes in pigs. Since range deviations of contrast enhanced CT are in the order of 2.5% compared to native CTs [Wer04] and none of the treatment plans were applied in experiments, we decided to perform all subsequently presented calculations on contrast enhanced CTs. This allows to incorporate the larger motion amplitudes into the studies on influence of intrafractional motion.

Table 4.3.: Mean displacement of cardiac taget volumes in pig 3 over all motion phases.

	Target	ABS [mm]	SI [mm]	AP [mm]	LR [mm]
contrast CT	PVs	1.7 ± 0.8	-0.2 ± 0.6	0.7 ± 0.9	0.1 ± 0.8
	CTI	1.6 ± 0.6	0.4 ± 0.5	0.7 ± 0.7	0.2 ± 0.6
	AV	2.8 ± 0.4	0.0 ± 0.3	2.0 ± 0.3	-1.4 ± 0.6
native CT	PVs	0.9 ± 0.4	0.0 ± 0.4	0.1 ± 0.5	-0.1 ± 0.5
	CTI	1.1 ± 0.5	-0.1 ± 0.6	0.6 ± 0.5	-0.1 ± 0.5
	AV	0.1 ± 0.1	0.1 ± 0.1	0.0 ± 0.1	0.0 ± 0.1

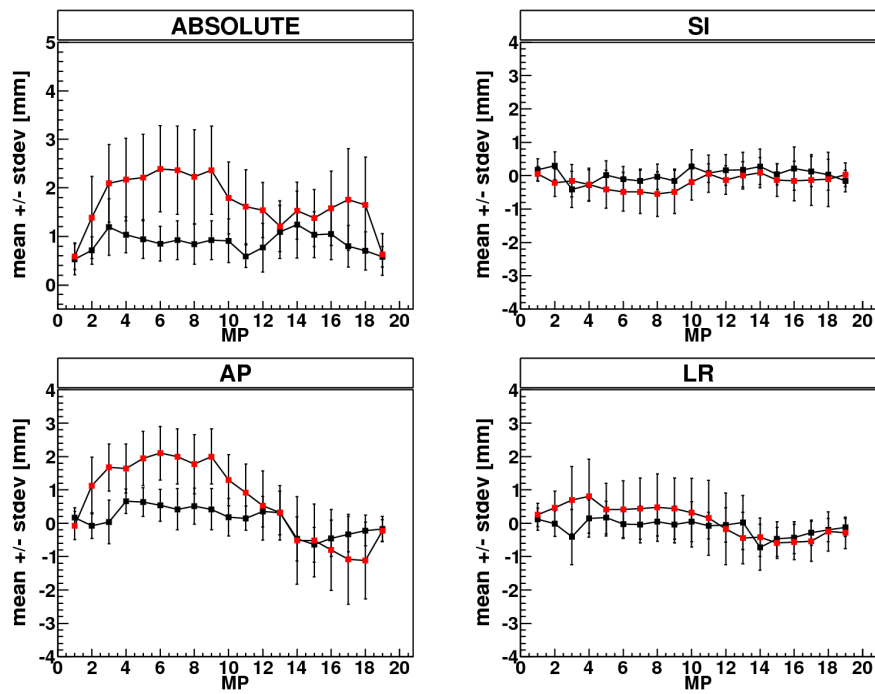


Figure 4.2.: PV: mean motion amplitude and standard deviation in each motion phase (MP) of the heartbeat relative to the reference phase. The displacement is shown for the three studied motion directions (SI: superior-inferior, AP: anterior-posterior, LR: left-right) and the absolute (ABS) displacement. Comparison between native CT data (black) and contrast CT (red) for Pig 3.

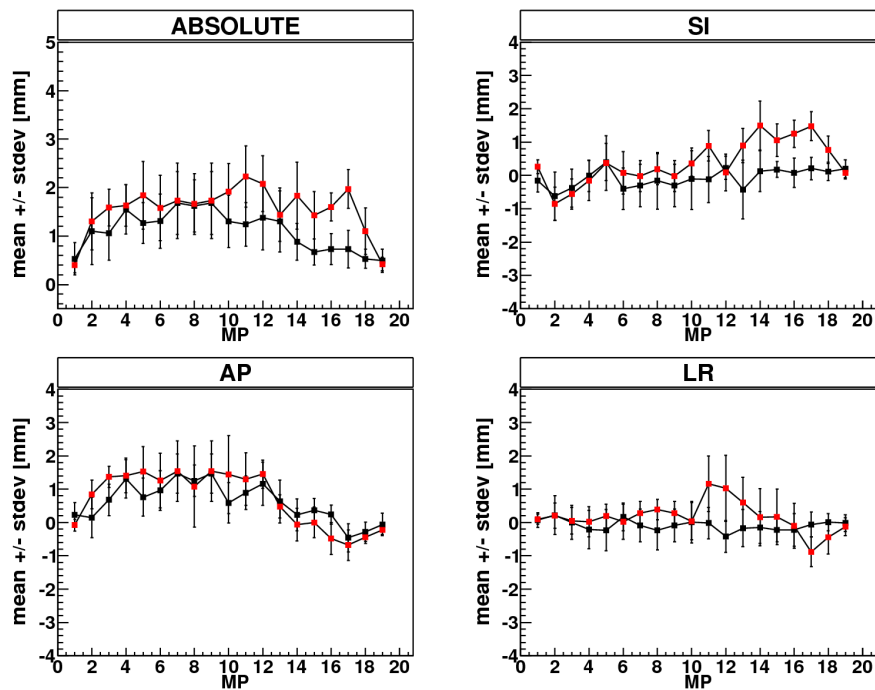


Figure 4.3.: CTI: mean motion amplitude and standard deviation in each motion phase (MP) of the heartbeat relative to the reference phase. Comparison between native CT data (black) and contrast CT (red) for Pig 3.

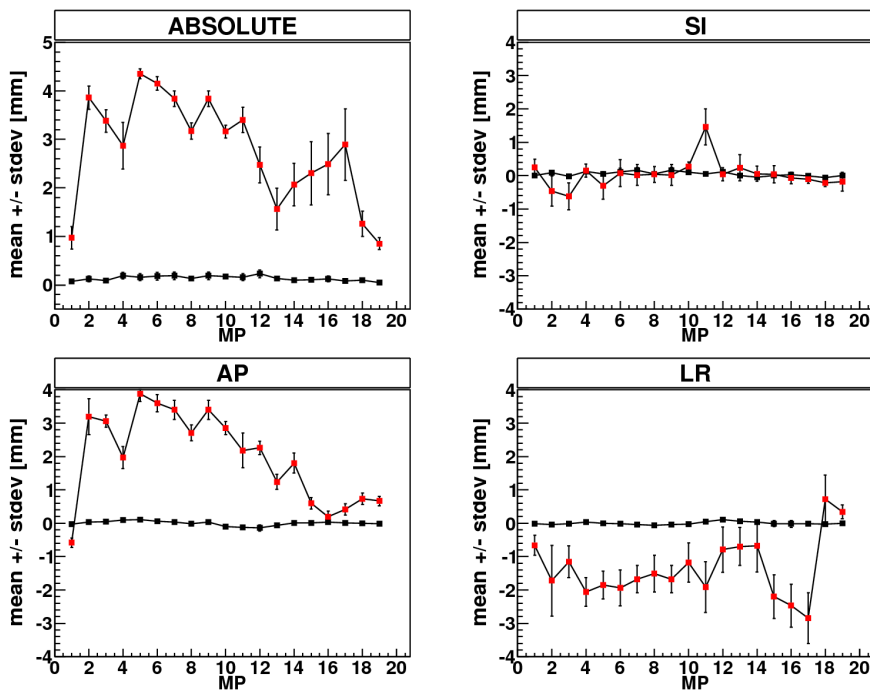


Figure 4.4.: AV: mean motion amplitude and standard deviation in each motion phase (MP) of the heartbeat relative to the reference phase. Comparison between native CT data (black) and contrast CT (red) for Pig 3.

Motion of cardiac target volumes due to heartbeat

The mean and standard deviation over all target volume voxels of the contrast enhanced CTs are plotted for each motion phase and for all pigs and motion directions in figure 4.5 to 4.7. The numerical values can be found in appendix C.2. It can be seen that the displacement within the cardiac target volume varies dependent on the studied pig and are hence dependent on the underlying anatomy. Furthermore the highest absolute displacement can be observed in different pigs, depending on the studied target volume. While the PVs move the most in pig 1 with a displacement of up to 5mm, pig 2 has the largest motion both in CTI and AV node (more than 6mm in both structures, respectively) (see also table 4.4). In this table it can be seen that the maximal absolute displacement varies depending on the studied volume. The CTI moves with a bigger amplitude than the other two target volumes in three of the four studied pigs (difference found in pig 3). The smallest displacement is found in the PVs, again in three of the four studied data sets (again the difference is found in pig 3). This can be interpreted in connection to the placement of the target volumes within the heart. While the PVs are found in the upper part of the atria, the CTI is located in the lower part of the atria and hence the influence of the ventricular motion should be bigger. The AV node is in between the atria and ventricles and was found to have an intermediate absolute displacement in most cases (exception in pig 3). Independent of the studied target volume the largest contribution

to the absolute displacement is found in AP direction for all pigs (see table 4.5). This can also be seen in the mean displacements over all pigs. For the PVs the mean amplitude in SI direction is (0.3 ± 0.8) mm, (1.5 ± 1.1) mm in AP direction and (-0.5 ± 1.0) mm in LR direction. In case of the CTI the mean amplitude in SI is (0.8 ± 0.7) mm, (1.8 ± 0.7) mm in AP and (0.5 ± 0.9) mm in LR. For the AV node it is (0.7 ± 0.3) mm in SI, (2.4 ± 0.4) mm in AP and (-0.7 ± 0.5) mm in LR. On average, the absolute amplitude over all motion phases and pigs is found to (2.3 ± 0.8) mm for the PVs, (2.8 ± 0.7) mm for CTI and (3.0 ± 0.4) mm for the AV node.

It can be seen in table 4.4 that no motion phase can be directly connected to the maximal absolute displacement of the target volumes. As stated in 3.2.3 the maximal displacement of the atria should thus be observed in motion phase eighteen, while the maximal amplitude of the ventricle should be observed in motion phase three. While this pattern is not directly connected to the motion of the cardiac volumes it can nevertheless be seen that for all pigs the displacement in the biggest motion direction (AP) results in a shallower motion in between MP 6 and 13 compared to the other MPs. For the PVs the motion in pig 1 (pig with the largest motion in this target volume) has a range of less than 0.5mm in the interval between MP 6 and 13, while the motion ranges more than 3mm in the other MPs (see appendix C.1). The same can be observed in case of the CTI, where pig 2 has a less shallow motion range of about 2mm within MP 6 and 13, but nevertheless a larger motion range of up to 4mm in the other MPs. Also for the AV node the motion within the MP interval (6-13) is lower (up to 2mm) compared to the the other MPs (range of about 4.5mm) in pig 2.

Table 4.4.: Biggest absolute displacement of target volumes for all pigs with corresponding motion phase.

Target	Pig 1 [mm] (MP)	Pig 2 [mm] (MP)	Pig 3 [mm] (MP)	Pig 4 [mm] (MP)
PVs	4.2 ± 1.1 (13)	3.7 ± 1.6 (12)	2.4 ± 0.9 (06)	3.1 ± 1.0 (11)
CTI	5.8 ± 1.0 (07)	6.3 ± 0.5 (08)	2.2 ± 0.6 (11)	4.0 ± 0.8 (13)
AV	4.9 ± 0.3 (13)	6.0 ± 0.2 (11)	4.4 ± 0.1 (05)	3.6 ± 0.7 (10)

Table 4.5.: Mean displacement of target volumes over all motion phases for all pigs and motion directions.

Target	Pig	ABS [mm]	SI [mm]	AP [mm]	LR [mm]
PVs	1	2.9 ± 0.7	0.2 ± 1.0	2.0 ± 1.3	-1.1 ± 1.1
	2	2.3 ± 0.9	0.9 ± 0.9	1.4 ± 1.7	-0.6 ± 1.0
	3	1.7 ± 0.8	-0.2 ± 0.6	0.7 ± 0.9	0.1 ± 0.8
	4	2.1 ± 0.6	0.3 ± 0.4	1.8 ± 0.7	-0.2 ± 0.7
CTI	Pig	ABS [mm]	SI [mm]	AP [mm]	LR [mm]
	1	3.5 ± 0.8	0.7 ± 0.8	2.3 ± 0.8	1.5 ± 0.9
	2	3.5 ± 0.8	1.0 ± 1.0	2.4 ± 0.5	0.3 ± 1.2
	3	1.6 ± 0.6	0.4 ± 0.5	0.7 ± 0.7	0.2 ± 0.6
AV	Pig	ABS [mm]	SI [mm]	AP [mm]	LR [mm]
	1	3.0 ± 0.4	0.4 ± 0.4	2.5 ± 0.5	-0.7 ± 0.4
	2	3.7 ± 0.4	1.9 ± 0.3	3.0 ± 0.3	0.1 ± 0.4
	3	2.8 ± 0.4	0.0 ± 0.3	2.0 ± 0.3	-1.4 ± 0.6
	4	2.1 ± 0.4	0.5 ± 0.2	1.7 ± 0.3	-0.7 ± 0.4

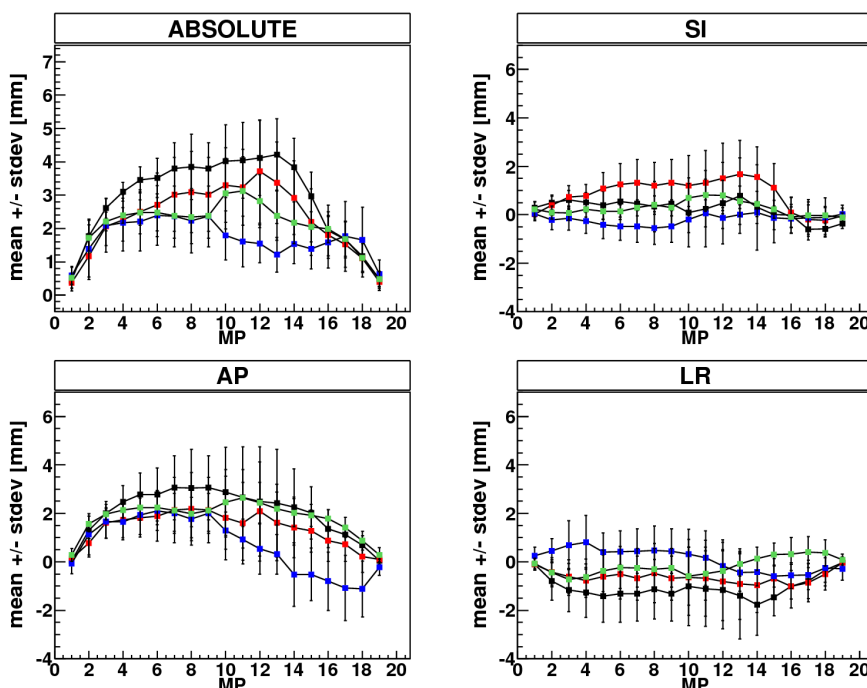


Figure 4.5.: PVs: Mean motion amplitude and standard deviation in each motion phase (MP) under influence of heartbeat for all porcine, obtained from contrast enhanced CT scans. (pig 1: black, pig 2: red, pig 3: blue, pig 4: green)

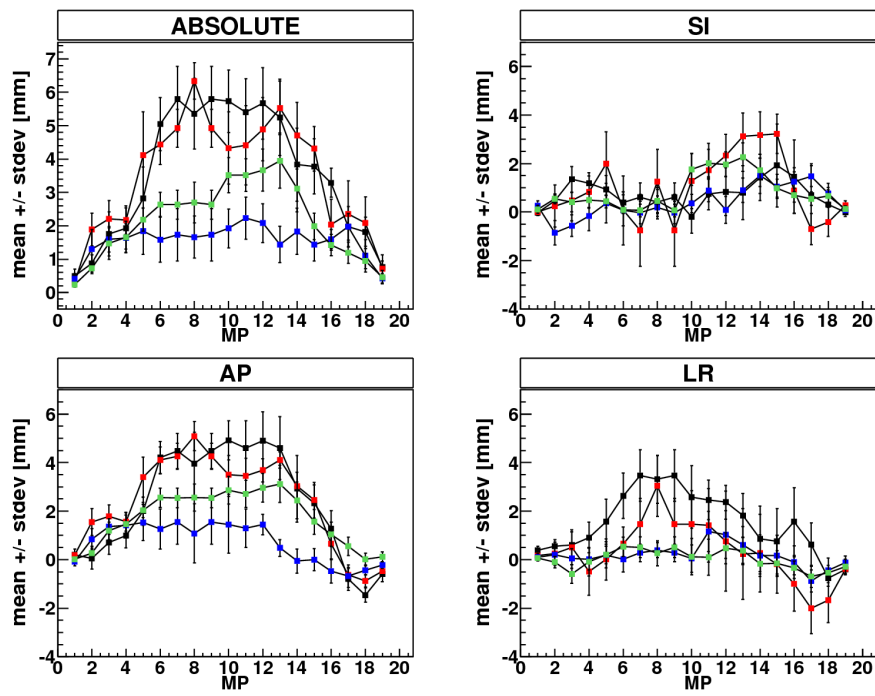


Figure 4.6.: CTI: Mean motion amplitude and standard deviation in each motion phase (MP) under influence of heartbeat for all porcine, obtained from contrast enhanced CT scans. (pig 1: black, pig 2: red, pig 3: blue, pig 4: green)

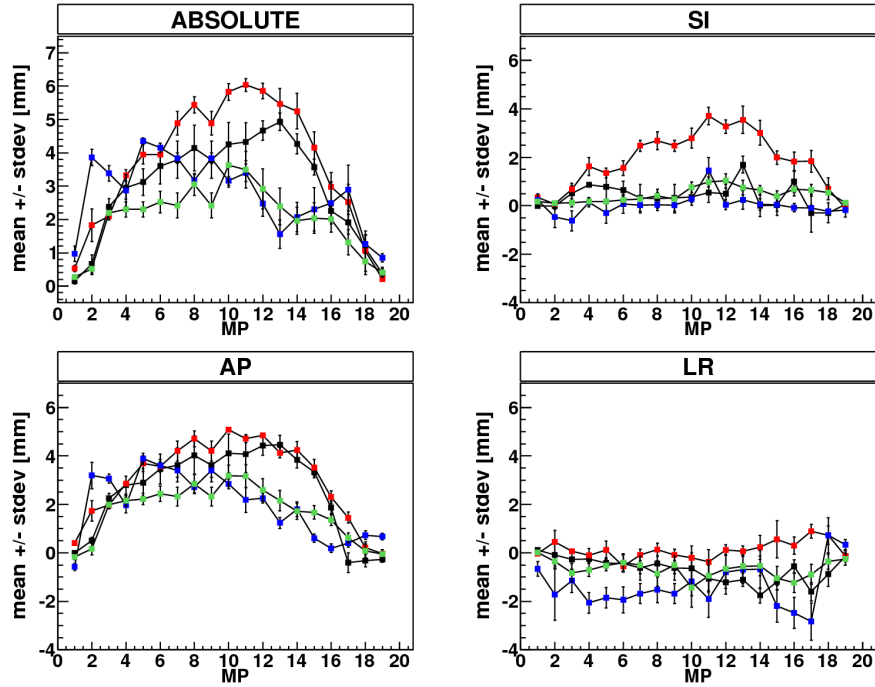


Figure 4.7.: AV node: Mean motion amplitude and standard deviation in each motion phase (MP) under influence of heartbeat for all porcine, obtained from contrast enhanced CT scans. (pig 1: black, pig 2: red, pig 3: blue, pig 4: green)

The overall displacement field for two exemplary pigs with a small motion amplitude (pig 4) and a large motion amplitude (pig 2) of the AV node are shown in figure 4.8. The field is shown for the maximal displacement motion phase of the respective pigs (motion phase 11 for pig 2 and motion phase 10 for pig 4, see table 4.4). In order to visualize the location of the displacement, an axial cut of the reference state CT is underlaid. The absolute values of the displacement vectors are shown as contour plots.

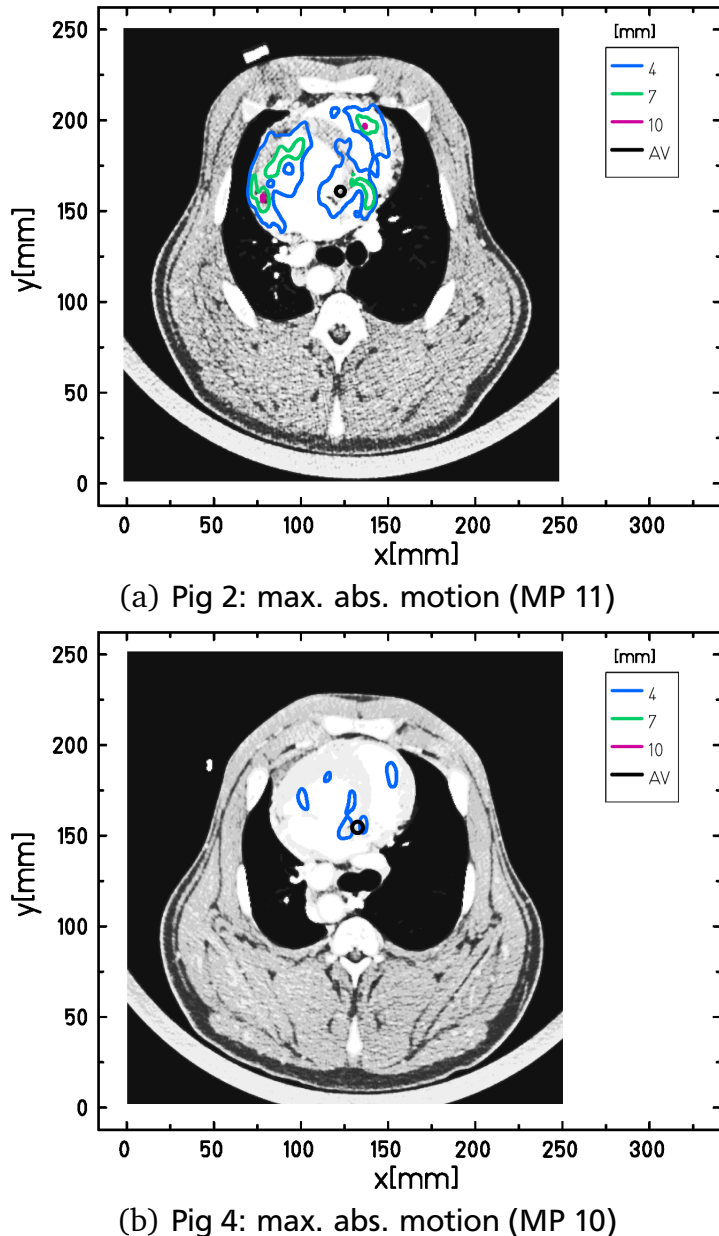


Figure 4.8.: Axial slices of the reference state of the CT overlaid with the absolute values of the displacement field (obtained from deformable image registration) in the corresponding slice for heartbeat motion. Above: the resulting displacement of pig 2 is shown in MP 11. Below: the results for pig 4 in MP 10.

4.2.2 Dose to organs at risk when irradiating the AV node

Due to the fact that the AV node is located in a large distance to the OARs (see figure 4.1), the dose deposition in the studied structures is not critical. Esophagus, trachea as well as the aorta are receiving no dose in all studied cases. Only the heart is receiving up to 7Gy for the studied volume of 15cm³. The respective dose-volume limit of 16Gy to 15cm³ is hence not exceeded. The dose deposited in the stated heart volume ranges from 4.8Gy (pig 3) to 7.3Gy (pig 4), which corresponds to 19% and 29% of the physical dose. Hence even higher doses of up to 40Gy would not exceed the dose volume limit. The results of a more detailed analysis of the affected cardiac substructures can be seen in table 4.6. Here the mean dose to the whole structure is stated next to the maximal point dose for all pigs and studied structures. Furthermore the maximal irradiated volume is shown.

Table 4.6.: Mean as well as maximum point dose to the whole heart and different cardiac substructures as well as maximal irradiated volume of the structures for all pigs.

OAR	Pig	Mean dose [Gy]	Max dose [Gy]	Max volume [%]
Heart	1	0.6	25.8	14.0
	2	0.5	25.4	12.7
	3	0.8	25.3	17.4
	4	0.8	25.7	16.6
LV	1	0.5	26.3	6.7
	2	0.5	26.3	6.1
	3	0.3	26.1	5.1
	4	0.4	26.0	4.5
RV	1	0.3	25.2	9.1
	2	0.2	25.2	8.0
	3	0.4	25.3	9.6
	4	0.5	25.8	14.3
LCA	1	0.8	7.4	19.9
	2	0.6	7.2	13.5
	3	0.2	6.4	8.9
	4	0.7	7.4	14.6
RCA	1	1.5	9.2	37.6
	2	1.1	8.4	24.0
	3	1.4	9.8	37.3
	4	1.4	9.6	34.1

Due to the physical dose deposition of 25Gy in the AV node the heart is receiving a relatively high maximum point dose with a median of 25.6Gy (75th percentile: 25.8Gy) over all pigs. The mean heart dose is found to have a median of 0.7Gy (0.8Gy) and the median of the maximal irradiated volume over all porcine data sets is 15.3% (17.7%). Comparing the dose deposition in the left and right ventricles it can be seen that the maximum point dose is higher in the LV than in the RV, with a median of 26.2Gy (26.3Gy) compared to 25.2Gy (25.5Gy). Nevertheless the mean dose is comparable with a median of 0.5Gy (0.5Gy) for the LV and 0.4Gy (0.5Gy) for the RV and the maximal irradiated volume is smaller for the LV compared to the RV with a median

of 5.6% (6.4%) compared to 9.3% (11.9 %). It should be noted that the total volume of the LV is much larger than the RV (e.g. about three times larger in pig 1), so that the absolute maximal irradiated volume results to be larger in case of the LV. Concerning the coronary arteries, it can be seen that the mean and maximal point dose to the LCA is smaller than to the RCA, resulting in a median mean dose of 0.6Gy (0.7Gy) in LCA compared to 1.4Gy (1.4Gy) in RCA and a median maximum point dose of 7.3Gy (7.4Gy) in LCA compared to 9.4Gy (9.7Gy) in LCA. Also the maximal irradiated volume is much smaller in the LCA compared to the RCA, resulting in a median maximum volume of 14.1% (17.2%) versus 35.7% (37.5%).

4.2.3 Motion mitigation techniques for AV node irradiation

The resulting interplay effect, caused by the displacement of the AV node of up to 6mm, and dose deposition were studied for every porcine data set for different motion patterns and 5mm margin to the target volume. The dose analysis values V95, V107 and D5-D95 were assessed and plotted. For comparison, also the corresponding values for the 3D case (static) are shown. Rescanning was studied as motion mitigation technique. The results of the stated dose values in case of rescanning with rescan numbers of five, ten and fifteen will be presented.

Dose deposition

Different motion pattern DVHs of fifteen rescans compared to the interplay results as well as a static irradiation are displayed for pig 2 (as this is the pig with the largest motion amplitude in the AV node) in figure 4.9 for 5mm safety margin. A representative dose deposition for all studied techniques (static, interplay and rescanning with fifteen rescans) is shown exemplary in figure 4.10. Rescanning and interplay are shown for a motion with a period of 0.5s and a starting phase of 90°. The target volume was irradiated with an added margin of 5mm. It can already be seen from this dose cut figures that rescanning with fifteen rescans improves the outcome compared to interplay and yields a result which is comparable to the static case. Due to the mechanism of rescanning, the field size is slightly increased compared to the static irradiation.

In order to assess the dose information of all pigs, the DVHs were analyzed and compared for dose steepness, dose coverage as well as over dosage. The results for all porcine data sets are shown in figure 4.11. The corresponding numerical values can be found in appendix C (tables C.14 - C.17).

The resulting interplay pattern is dependent on the underlying motion period and starting phase. This can also be seen in the mean values and standard deviations of the dose analysis parameters over all pigs for different motion patterns. The dose coverage for example is found to have a mean value of $V95=(84.3 \pm 17.5)\%$ for a motion with 0.7s period and a starting phase of 0° , while it is found to be $(91.0 \pm 10.3)\%$ for the same period and a starting phase of 90° . For a period of 0.5s the mean dose coverage over all pigs is found to be $(84.5 \pm 8.0)\%$ with a phase of 0° and to $(86.0 \pm 24.0)\%$ for a phase of 90° . The resulting high standard deviation shows that the result is also dependent on the studied porcine case. These dependencies are also valid for the other studied dose analysis parameters, dose homogeneity and over dosage.

It can furthermore be seen in figure 4.11 (as well as numerical values for all pigs in appendix C.1) that rescanning can improve the results for dose steepness, dose coverage as well as over dosage compared to the interplay case in all studied motion cases for three out of four pigs. Only pig 2, which was found to have the largest absolute displacement of the AV node out of the four studied porcine data sets, results in some rescanning cases where slightly inferior results compared to interplay are achieved. This is the case in dose steepness, where a motion with 0.7s and 90° starting phase is $D5-D95=8.2\%$ with five rescans and $D5-D95=7.9\%$ with ten rescans compared to $D5-D95=6.2\%$ without any compensation (interplay). For the same motion the dose coverage is found to be $V95=43.6\%$ with five rescans compared to $V95=99.0\%$ with interplay. This result can already be improved with ten rescans, where $V95$ is found to be 98.5%. In over dosage a motion pattern (period of 0.5s and starting phase of 0°) is found to have inferior results with ten rescans compared to interplay (9.3% versus 0%). The results for ten rescans could be slightly improved with fifteen rescans, so that, e.g., the dose coverage is found to be $V95=100\%$ for the stated motion pattern (0.7s period and 90° starting phase) (static: 100%). For pig 4, which has the smallest absolute displacement of the AV node in the studied porcine cohort, all rescanning results yield improved results compared to interplay. Moreover it can also be observed here that ten and fifteen rescans result in better dose analysis parameters and even tops the static outcome in some cases. E.g. the dose steepness is found to be $D5-D95=3.0\%$ with a motion period of 0.5s and starting phase of 0° for fifteen rescans and to be 5.1% with ten rescans, while in the static case it is found to be 5.5%. In this case also five rescans result in an improved dose steepness ($D5-D95=4.9\%$). Regarding the dose coverage, fifteen rescans yield results comparable to the static case (100%) for all motion patterns, while ten rescans yield comparable results (e.g. 97.8% for motion period of 0.7s and starting phase of 90° , interplay: 74.3%). Five rescans on the other hand show inferior results with, e.g., $D5-D95=86.3\%$ for a motion period of 0.5s and a starting phase of 0° .

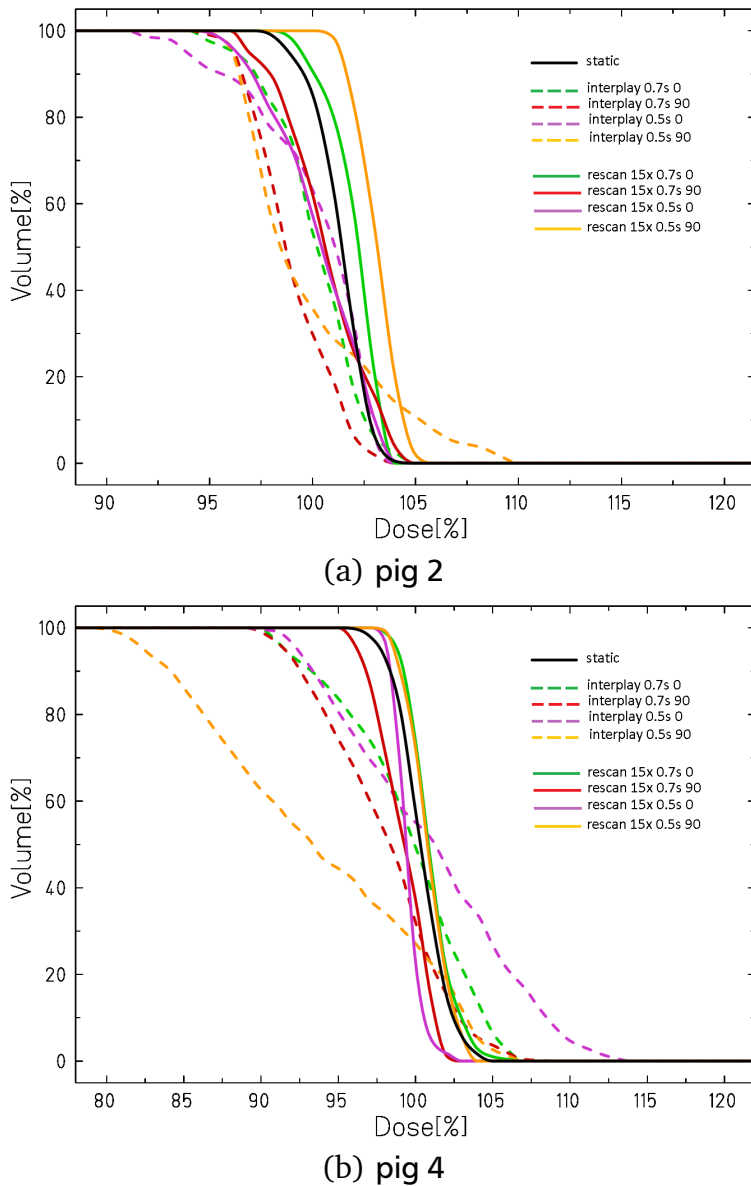


Figure 4.9.: Dose volume histograms for CTV of pig 2 (largest absolute displacement of AV node) and pig 4 (smallest absolute displacement of AV node) for 5mm safety margin irradiation of AV node in case of static irradiation (black), interplay (dashed) and rescanning with fifteen rescans (solid). The motion patterns are shown in colors (0.7s 0: motion period of 0.7s and starting phase 0°, 0.7s 90: motion period of 0.7s and starting phase 90°, 0.5s 0: motion period of 0.5s and starting phase 0°, 0.5s 90: motion period of 0.5s and starting phase 90°).

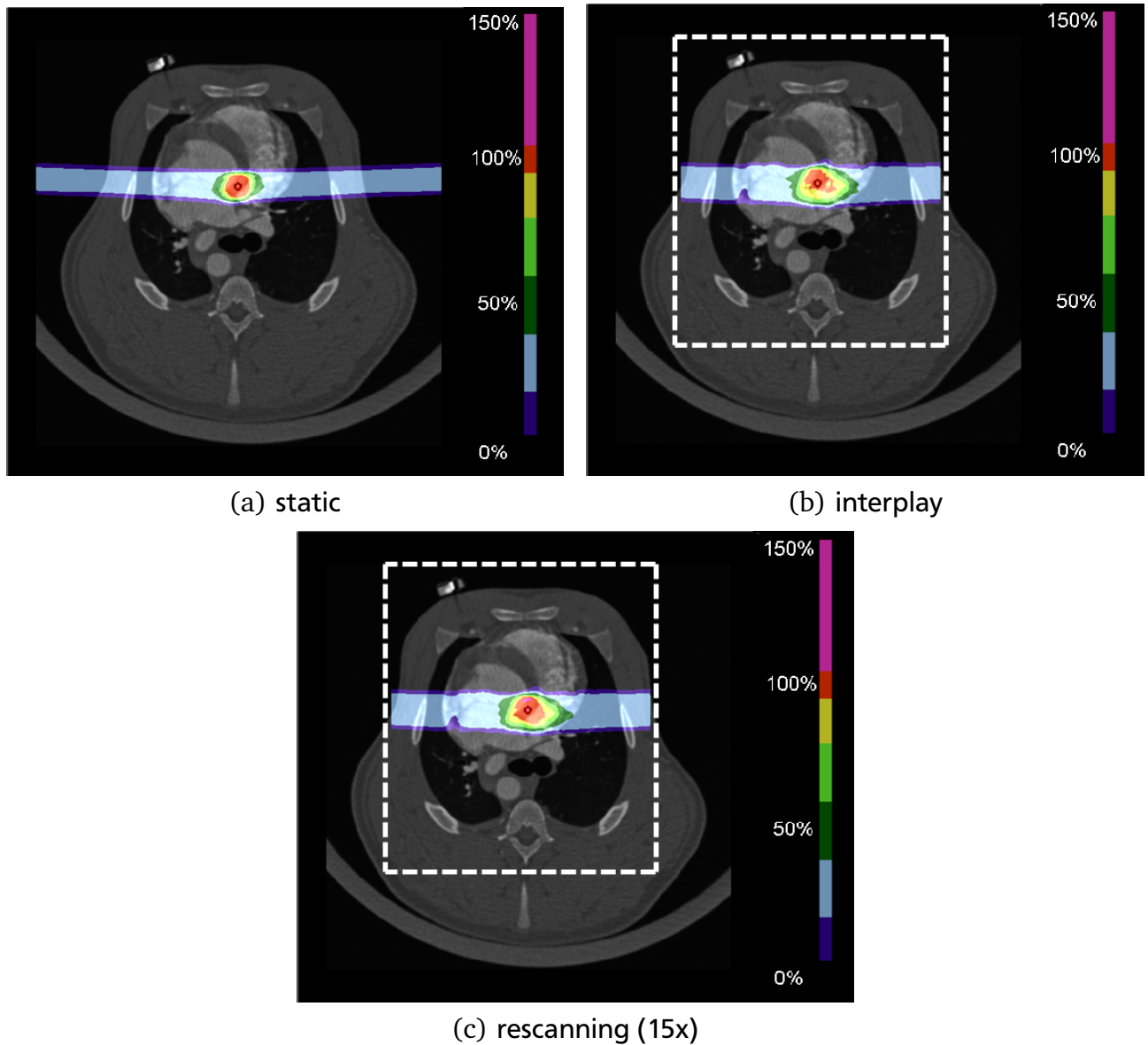
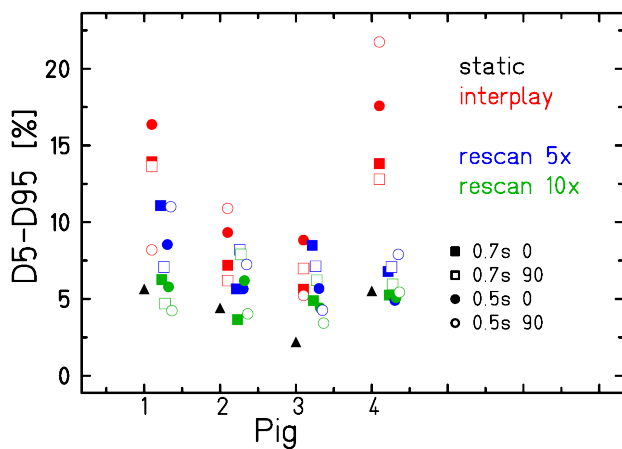
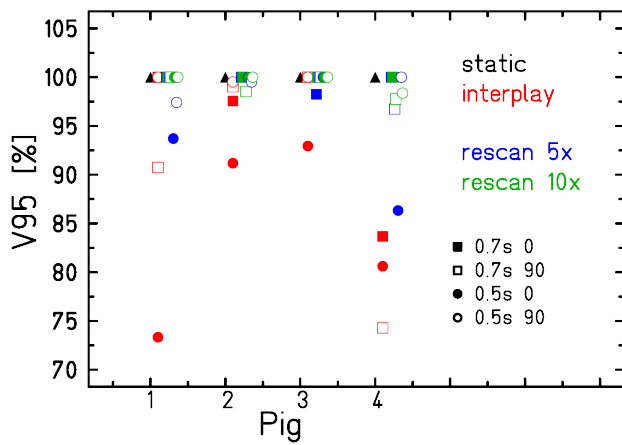


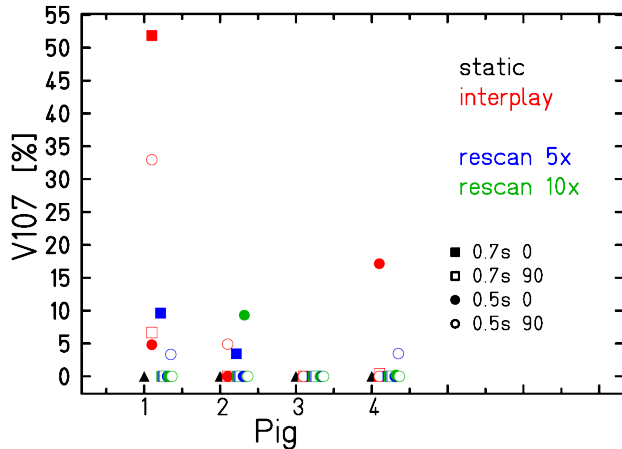
Figure 4.10.: Dose distribution of pig 2 for static (a) as well as interplay (b) and fifteen rescans (c) at motion period of 0.5s and a motion starting phase of 90°. The target volume has an added margin of 5mm. The improved outcome of rescanning compared to interplay can already be seen in these dose cuts. For interplay and rescanning the dose was calculated in a reduced volume as indicated by the white dashed line.



(a) D5-D95



(b) V95



(c) V107

Figure 4.11.: Dose analysis parameters D5-D95 (first row), V95 (middle row) and V107 (last row) for all porcine data sets when irradiating the AV node with 5mm safety margin. Static (black) as well as interplay (red) and different rescanning numbers (5 times: blue, 10 times: green,) were compared for different motion patterns and safety margins. For a better visualization the rescanning data points for each motion pattern are shifted and the results for fifteen rescans are not displayed.

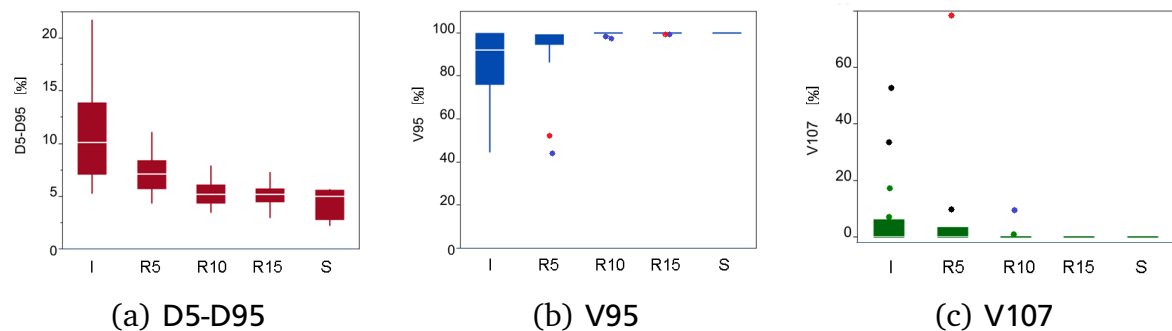


Figure 4.12.: Boxplot of dose analysis parameters D5-D95, V95 and V107 over all porcine data sets (pig 1: black, pig 2: blue, pig 3: red, pig 4: green) and motion patterns depending on the used technique (I: interplay, R5: five rescans, R10: ten rescans, R15: fifteen rescans, S: static). Figures are courtesy of Dr. Christian Graeff.

Figure 4.12 shows the results of the dose analysis parameters over all pigs and motion patterns depending on the studied technique. It can be seen that for all studied cases, rescanning yields improved dose depositions compared to the interplay case. For D5-D95 the median of the ideal, static case is 5.0% (75th percentile: 5.6%), which increases to 10.1% (13.9%) for the interplay distribution. With five rescans this can be already be improved to 7.1% (8.4%). A slightly better improvement is observed from ten rescans on, whereas no further benefit result from more than ten rescans (5.2% (6.1%) for ten rescans versus 5.2% (5.7%) for fifteen rescans). As this dose analysis parameter was normally distributed, the correlation between the dose homogeneity and rescan number was analyzed. Thereby interplay was included as a rescan number of one. The proportion of variance explained resulted in $r^2=0.46$ ($p<0.0001$). For V95 interplay resulted to have a median of 92.1% (25th percentile: 75.9%) versus 100% (100%) for the static case. The dose coverage could be improved to 99.8% (25th percentile: 94.5%) with five rescans and even to 100% (100%) for ten and fifteen rescans. For the over dosage the static case was found to have a median of 0% (75th percentile: 0%) which increased to 0% (6.3%) for interplay and could be reduced to 0% (0%) already with five rescans.

It can be concluded that five rescans are already sufficient to improve the interplay results, but ten or more rescans are needed in order to have treatment planning results comparable to the static irradiation. In order to enable a correct dose-escalation study ten rescans are hence favorable. For the here studied motion pattern and porcine data set cases this rescan number would lead to a dose deposition corresponding to the planned dose deposition.

Irradiation time

In figure 4.13 the irradiation time for rescanning of AV node are shown for all pigs and the two studied beam channel directions (couch angle 90° and -90°). The stated results were achieved with a low intensity irradiation (minimal particle number of 75,000 per beam spot)¹. For an irradiation with 5mm margin the treatment time over all pig data sets results to a mean value of about one minute per field (see table 4.7). Thus the overall treatment time would result to (1.9 ± 0.1) min with rescanning as motion mitigation technique for heartbeat motion in porcine data. Theoretically, this result could be further reduced with a higher minimum particle number and hence a higher irradiation intensity. Nevertheless these irradiation times are already very short due to the small target volume. It needs to be observed in the upcoming experiments if these short treatment times can be verified.

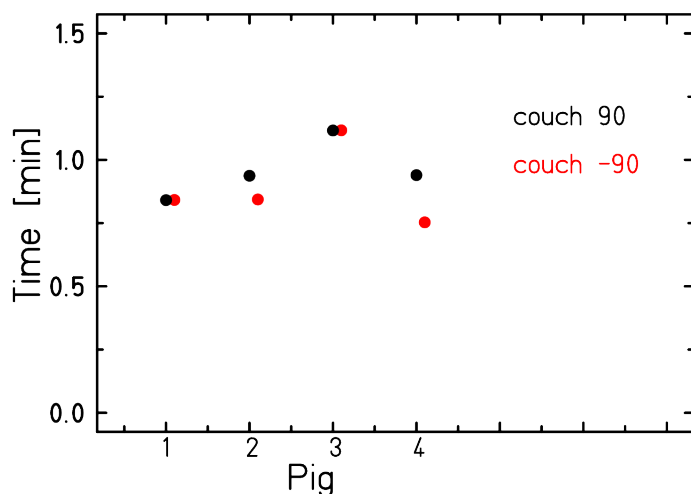


Figure 4.13.: Irradiation time of fifteen rescans for all pigs and beam entry channels.

Table 4.7.: Mean irradiation time for AV node with a safety margin of 5mm over all pigs.

Couch angle [°]	time [min]
-90	0.9 ± 0.1
90	1.0 ± 0.1
total	1.9 ± 0.1

¹ as this resulted in the maximal particle number still yielding a homogenous dose deposition in case of static irradiation. Further analysis is needed

4.3 Discussion

In this chapter the influence of heartbeat motion on different cardiac target volumes (PVs, CTI, AV node) in porcine data sets was studied and treatment planning studies with rescanning as motion mitigation technique were carried out. The dose deposition to OAR, including cardiac substructures, was analyzed. This analysis is motivated by the planned experiments on the feasibility of the non-invasive ablation of cardiac target sites with carbon ions in pigs. In experimental cardiology, dogs as well as pigs are most frequently used. As dogs are known to display certain differences in anatomy and physiology compared to man [Hug86, Cri98] it is planned to use pigs in the upcoming GSI experiments.

Even though it seems to be accepted in literature that the anatomy of pig hearts are very similar to that of humans [Lum66, Dou72, Hug86, Coo91, Whi93] Crick et al. [Cri98] carried out a detailed comparison between the anatomy of porcine and human hearts. They found several significant differences which they suspected to arise mainly from the different orientation of the bodies (unguligrade versus orthograde) and hence location of the heart in the thorax and from the differing form of the thorax itself. While the upper and lower borders of the hearts were found to have similar size and features, the general shape differs as the pig hearts are more 'Valentine' shaped and the human hearts more trapezoidal. This also leads to important differences in the internal anatomy. While in human hearts the right atrium is typically larger than the left, the atria of pigs have a similar size. Concerning the left atrium, only two orifices for the pulmonary veins exist, while humans have four pulmonary vein openings. The right atrium was furthermore stated to differ significantly from the human heart, especially in the atrial appendage. Regarding the ventricles Crick et al. stated that the right ventricle was observed to have a similar structure like human hearts, such as the tricuspid and pulmonary valvar arrangements. But also here differences were found (e.g. the orientation of the pulmonary valve). The left ventricles seem to have similar features to the human structure, but the ventricular wall was found to be much thicker in porcine. Furthermore it was stated that the left chambers of the pig hearts were significantly bigger compared to the right chambers, so that the apex was found to be composed entirely of left ventricular musculature. Also in human hearts the left ventricle is bigger than the right one. Concerning coronary circulation it was noted that most pigs displayed a blood supply to the sinus and atrioventricular node by branches of the right coronary artery, while in humans this is observed to a lesser extent.

Due to the different anatomy of pigs compared to humans it was expected to find different results in the motion of the cardiac target volumes as well as in the dose deposition to the OAR. The findings will be discussed in the next subsections.

4.3.1 Movement of cardiac target volumes in cardiac cycle

Due to the dense muscular structure of the heart contrast enhanced CT scans were acquired in comparison to native scans. Deformable image registrations were carried out on both data sets and the resulting motion displacement of the cardiac target volumes were assessed. It could be concluded that native CT scans do not enable an estimation of either the motion amplitude or direction. While e.g. the mean absolute displacement of the AV node was found to (0.1 ± 0.1)mm in the native scans of pig 3, the mean absolute displacement on contrast CT scans was found to be (2.0 ± 0.4)mm. This difference is sufficient to completely alter the results of the treatment planning study as an interplay pattern would be expected with the motion field from the contrast enhanced CT scans, while the motion of the native scans would be too small to yield an interplay effect. It is thus obvious that contrast enhanced CT scans are needed in order to correctly assess the motion of the cardiac target volumes. As contrast enhanced CT scans change the Hounsfield unit information, which are needed for range informations in particle therapy, it is not intended to deliver treatment plans created on these data sets. In the case of treatment planning studies for pure feasibility it can nevertheless be accepted as the range information does not need to be applied. In the planned experiments at GSI a strategy to use the motion displacement field of the contrast enhanced CT, while carrying out the treatment planning on native CT scans, is nevertheless needed. A first concept could be to enable a robust stabilization of the pigs during CT acquisition so that no position difference between the native CT scan and the injection of the contrast agent is induced. This would hence enable a direct application of the deformation field of the contrast enhanced CTs on the native CT scans.

Based on the contrast enhanced CT scans the motion of the cardiac target volumes - PV, CTI and AV node - in all four porcine data sets was assessed. It could be observed that the CTI moved the most in all four pigs, followed by the AV node. The PV moved to a lesser extend in all four pigs. It was assumed that these findings were connected to the location of the target volumes within the heart, where the PVs are found in the upper atria and the CTI in the lower atria, hence increasing the influence of the stronger ventricular motion. As the AV node is found in between ventricles and atria it can be hypothesized that the position is more stable and hence the influence of the ventricular motion on the displacement of the structure is slightly reduced. Furthermore it was found that in all four porcine data sets as well as for all three studied cardiac target volumes the displacement in AP direction was larger than in the other two motion directions (SI and LR). For the porcine data sets a shallower motion range of the target volumes was furthermore observed in-between MP 6 and 13, enabling a potential application of gating as another motion mitigation technique for the compensation of heartbeat motion in swines. Nevertheless a close analysis of the individual motion pattern of the respective pig is needed as the motion differed among the animals.

4.3.2 Dose to organs at risk for the irradiation of AV node

Due to a lack of corresponding data dose-volume limits for the studied OAR (esophagus, trachea, aorta and heart) were taken from the RTOG protocols for SBRT treatments of humans. These limits were not exceeded in the irradiation of AV node with 5mm safety margin. It can be argued that this is due to the large distance of the target volume from the analyzed critical structures. Nevertheless the resulting dose deposition with carbon ions is also smaller than the results for photon irradiation. A study by radiologists from the collaborating Mayo Clinic [Song14] stated that an IMRT irradiation of the AV node with 5-6mm margin and (32 ± 0.6) Gy in the same porcine data sets resulted in a mean dose to the esophagus of 1.6Gy. In case of carbon ions no dose deposition was found in this structure (mean: (0 ± 0) Gy). The mean dose to the trachea was found to be 2.2Gy with IMRT delivery, while also here no dose was deposited with carbon ions (mean: (0 ± 0) Gy). Concerning the mean overall cardiac dose it was stated that an IMRT delivery would result in (4.7 ± 1.3) Gy. For carbon ions a mean cardiac dose of $(0.03 \pm 0.00)\%$ of the physical dose was found, resulting in (0.7 ± 0.1) Gy for 25Gy or (1.0 ± 0.1) Gy for 32Gy, respectively. The better sparing of the critical structures with carbon ions compared to IMRT is on one hand due to the reduced beam channel number. On the other hand the physical advantages of carbon ions compared to photon delivery (e.g. Bragg peak) become obvious in these results. For a more detailed comparison of OAR dose depositions with photons compared to carbon ions, the reader shall be referred to chapter 5, section 5.1.3. The study by Song et al. also included an analysis of the dose deposition when irradiating the AV node with proton beams [Song14]. Here a single AP field was applied, resulting in (30.7 ± 0.2) Gy to the AV node. The mean overall cardiac dose was stated to result to (3.6 ± 1.5) Gy. The dose deposition to the surrounding heart is hence higher in case of proton irradiation compared to carbon ions. This is especially striking since only one field was used in proton treatment compared to the here presented two carbon ion beam channels, hence resulting in a bigger irradiated cardiac volume. Nevertheless it should be kept in mind that the beam channels can not be directly compared, since two lateral fields were used in carbon ion treatment planning, while a single AP field was applied in proton therapy.

The dose deposition in the cardiac substructures was also studied in the AV node irradiations with carbon ions. The LV resulted to receive a slightly higher maximum point dose compared to the RV, while the mean dose in the two structures were comparable and the maximal irradiated volume was smaller for the LV compared to the RV. In the study by Crick et. al it is stated that the LV is significantly bigger compared to the RV in swines and that sensitive structures like the apex are composed entirely of LV musculature [Cri98]. It can thus be understood why the maximal irradiated volume of the LV is significantly smaller than the RV even though the beam channels are symmetrical in lateral position. Concerning the coronary arteries it was found that

the mean and maximal point dose to the LCA is smaller than the RCA and also the maximal irradiated volume of the LCA is smaller compared to the RCA. Since no dose limit information exist it is unclear whether the larger exposure of the RCA compared to LCA is problematic, especially since pigs were found to supply the SA and AV node via branches of the RCA.

4.3.3 Rescanning as motion mitigation technique for AV node irradiation

In the irradiation of cardiac volumes in the animal study carried out at CyberHeart and at Universitätsklinikum Schleswig-Holstein in Lübeck, both with photons, only an ITV approach was used in order to compensate for heartbeat motion [Sha10, Bla13]. Due to the interference effects between the active carbon ion beam application and the assessed motion of up to 6mm of the AV node due to heartbeat, a different approach was needed for carbon ions. Rescanning was studied as potential motion mitigation technique for the non-invasive ablation of the AV node with an underlying heartbeat motion in swines.

By analyzing the dose coverage, dose homogeneity and over dosage for different underlying motion patterns it was found that rescanning results in an applicable dose deposition. The dose coverage was higher than 99% in 85% of all studied cases and even increased to 91% of the studied cases when more than ten rescans were analyzed (100% for only fifteen rescans). V107 values higher than 0% were obtained in 15% of all cases, which further reduced to 6% of the studied cases when only the DVHs for ten and fifteen rescans were evaluated. V107=0% was found in all studied cases for fifteen rescans. The dose homogeneity D5-D95 did not exceed 8% for ten rescans. This value could be slightly improved to 7% with fifteen rescans. For five rescans, the dose homogeneity reached up to 11%. It could be concluded that rescanning with ten rescans yields better results compared to only five rescans, while additional rescans do lead to a further improvement of the outcome.

All these results were found for slice-by-slice rescanning, which means that each IES is irradiated independently with the predefined number of rescans and the adapted particle numbers. In this case the treatment time is not prolonged. It needs to be studied if other rescanning techniques like breath-sampled rescanning [Sec09] or phase-controlled rescanning [Fur07], where the rescanning of the individual IES are sampled according to the motion phase of the breathing period, are applicable to cardiac motion (ECG-sampled rescanning). Due to the shallower displacement of the porcine cardiac target volumes between motion phase six and thirteen, gating [Kub96] on the cardiac cycle might be another feasible motion mitigation technique. In order to keep the treatment time as short as possible a fast beam extraction modality for synchrotrons with radiofrequency knock-out excitors is needed. This exist, e.g., at the National Institute of Radiological Science (NIRS) in Japan [Nod96, Fur05] and at the Heidelberg Ion Therapy Center (HIT) [Schoe11].

4.4 Conclusion

Contrast enhanced CT scans are needed in order to assess the motion of cardiac target volumes due to heartbeat motion. Potential cardiac target volumes in swine move due to heartbeat with an amplitude of up to a couple of millimeters and the dominant motion direction was found to be in AP direction. The displacement of the AV node creates interplay effects when irradiated with carbon ions. Rescanning as motion mitigation technique was studied. Rescanning with fifteen rescans yields improved dose analysis parameters compared to interplay in all studied pig cases and for all underlying motion patterns and achieved results comparable to the static irradiations. It is thus an adequate motion mitigation technique for the planned experimental validation in animal models where the AV node will be irradiated. Dose-volume limits to the surrounding OAR were not exceeded.



5 Discussion

Contents

5.1. Dose deposition	140
5.1.1. Dose to target area	140
5.1.2. Dose to OAR	141
5.1.3. Dose to OAR: Comparison to photons	143
5.2. Treatment planning of cardiac target volumes with scanned ions	150
5.2.1. Motion of cardiac volumes	150
5.2.2. Contrast enhanced CT scans	152
5.2.3. Motion mitigation techniques	152

The treatment planning results presented in the previous chapters are the first feasibility study to investigate the use of carbon ions for a non-invasive treatment of atrial fibrillation (AF). Currently existing treatment procedures for this cardiac arrhythmia have major drawbacks and due to the prevalence of this condition a new treatment modality would be beneficial [Cap05, Cap10]. It could be shown that scanned ion beams have the potential to become an accurate, fast and non-invasive treatment approach for AF.

Cardiac target volumes like the pulmonary veins (PVs) or the atrioventricular (AV) node move due to respiration of the patient as well as due to heartbeat. When treating moving targets with a scanned carbon ion beam interference effects between the particle delivery and the inter-fractional target motion are observed, leading to over and under dosages in the target volume and hence endangering the treatment outcome. Motion mitigation techniques are thus needed, which were studied independently for the respiratory and heartbeat motion influence. Cardiac target volumes are surrounded by critical structures and organs at risk (OAR) like esophagus, trachea and aorta. A detailed analysis of the OAR dose deposition was carried out, which will be discussed in section 5.1.2. In section 5.1.3 special emphasis will be given to the reduced OAR dose deposition with scanned carbon ions compared to a non-invasive treatment with photons. The target volume displacement will be discussed in section 5.2.1. Afterwards the findings of treatment planning studies with motion mitigation techniques will be discussed in section 5.2.3.

5.1 Dose deposition

In the here presented feasibility study of a non-invasive treatment of AF with carbon ions, a physical dose of 25Gy was applied in all treatment plans. This dose was chosen according to the publication by Sharma et al. [Sha10] in which it was stated as the minimal needed dose in order to see an electrophysiological effect induced by photon irradiation. Older studies with photon irradiations in animal models support the finding by Sharma et al. in which doses higher than 20Gy seem to be sufficient in order to induce fibrotic tissue [Faj70, Faj73]. A short overview will be given in section 5.1.1.

A close analysis of the dose deposition to the OARs was carried out in the here presented work. Human data was studied for PVs ablation (chapters 2 and 3). In preparation for animal studies, which will be carried out at GSI in 2014, the irradiation of the AV node in pigs was analyzed (chapter 4). The findings will be discussed in section 5.1.2 and a comparison with photon irradiation will be given in 5.1.3. For critical structures like the aorta, esophagus, trachea and the heart itself dose-volume limits from SBRT were used [RTOG0631, RTOG0915]. As the heart is not only an OAR in this studied treatment, but the target site itself, the dose-volume limits for this organ were often exceeded. Closer analysis of the irradiated cardiac substructures was hence performed.

5.1.1 Dose to target area

Sharma et al. stated that a dose of at least 25Gy is needed in order to induce a change in the conduction system of the heart with photon beams [Sha10]. Nevertheless also higher doses have been applied in the animal model study, reaching up to 80Gy. Part of the planned animal experiments at GSI will be a dose escalation study, in which the needed carbon ion dose for the generation of the desired fibrosis in the target area will be examined more closely. It is already known from former studies on the effect of radiation on the heart which dose depositions as single fraction doses are sufficient in order to induce fibrotic tissue [Faj70, Faj73, Phil64, Bis65, Ste68, Efs56].

Fajardo et al. [Faj70, Faj73] investigated the evolution of radiation induced myocardial damage after a single dose of 20Gy in rabbits as well as a fractionated treatment, both with 6MV photons. They stated that their findings were independent of the time course of the irradiation, hence if the dose was applied as a single fraction or in different fractions. They found that there are three distinct stages in the evolution of radiation induced cardiac damage and divided it into an acute phase (an inflammation within the first 48hours), a latent stage (which can last up to seventy days) and the late stage where fibrotic lesions occur. Their explanation

for the formation of fibrotic tissue is a failure of microcirculation, resulting from a failure of the complete reconstruction of capillaries in the endothelial cells after irradiation. They state that the occurring ischemia leads to myocardium fibrosis, which becomes maximal beyond 120 days. Other studies by Phillips et al. [Phil64] and Bishop et al. [Bis65] irradiated hearts of dogs and rodents with single photon doses of 60Gy to 96Gy. Both authors stated that they found severe functional abnormalities as well as myocardial fibrosis or even necrosis [Ste68]. Efskind et al. [Efs56] found fatal myocardial damage after 80Gy photon irradiation to the heart of rabbits.

It can thus be assumed that the required dose for the desired generation of fibrotic tissue in the cardiac target volumes will require at least 20Gy, while high single fraction doses of up to 60Gy might induce necrosis, which needs to be avoided. Preliminary studies using the LEM for the calculation of biological doses in single fraction deliveries with the stated 25Gy resulted to have a RBE of 1.1. This needs to be verified. Nevertheless studies exist, where the RBE was found to become smaller with high single fraction doses and reaching a plateau [Cara07]. In this case the physical dose could be considered proportional to the biological dose. Hence the dose to the target volume, as well as the dose to the critical structures, could be directly scaled to the desired value.

5.1.2 Dose to OAR

In the studied human data it was found that the dose deposition in the aorta and trachea were uncritical and did not exceed the stated dose-volume limits. This was valid for all the studied safety margins (3mm, 5mm and 7mm) of the target volume, independent of the fact that the OAR dose deposition correlates with margin size. The esophagus on the other hand is an endangered organ due to its proximity to the studied irradiation site of the PVs. Different beam directions and field channel numbers were studied in IMRT setting, none of which resulted in a satisfactory sparing of this structure. Dose-volume exceeding results were already obtained for a small safety margin of 3mm in some patient cases, or even without the usage of any margin in other cases. An IMPT(OAR) treatment was hence necessary, where the maximal dose to the esophagus was implemented in the dose optimization process. Two different IMPT(OAR) settings were used. One which was planned to deposit no more than a maximal dose of 17.5Gy (70% of 25Gy) in this organ and another with a maximal dose of 7.5Gy (30% of 25Gy) to the structure. While the weaker restriction already led to an improved result, the dose depositions were still too high, for one patient case even with only 3mm margin. The stronger restriction on the other hand resulted in dose depositions that did not exceed the dose-volume limit in all studied patient cases and for all studied safety margins. The dose restrictions for the esophagus even led to a further reduced dose deposition in the trachea of the studied patients due to the direct proximity of these two organs with respect to the used beam channel directions.

In order to guarantee a safe delivery in a potential patient application a dedicated protocol to ensure adequate esophagus sparing is nevertheless needed. Possible solutions to detect range uncertainties before the delivery of the high single fraction dose are pre-irradiations with small doses in the order of mGy [Bent12] and the usage of in-beam PET monitoring with a probing beam [Fie10, Lin12], which are presented in more detail in section 5.2.2. Analog to studies by Rucinski et al. [Ruc13], Christodouleas et al. [Chr13] and van Gysen et al. [Gys14] for prostate cancer or studies by Viswanathan et al. [Vis13] for gynecologic cancers it was furthermore considered if the injection of a spacer like hydrogel would be beneficial in order to increase the distance between the esophagus and the ablation sites. Due to an increased risk for infections in the cervical region this approach is considered unfeasible in this case (Prof. Christoph Bert, personal communication, April 10, 2014).

Even though the dose-volume limits for the heart were exceeded, it should be noted that the heart is also the target volume in this feasibility studied. Further analysis of the maximal point dose, the maximal irradiated volume as well as the median dose were in good agreement to limitations stated in literature [Gag10, Mar98, Wei08, Han93] and hence no pericarditis should be expected. Concerning the irradiated cardiac substructures it was found that three beam directions yielded a lower mean dose to the LCA. A mean dose over all patient cases of up to 1.5Gy for 7mm safety margin was found. According to a study by Darby et al. [Dar13] major coronary events increase by 7.4% per Gy photon irradiation after five years post radiotherapy. Due to the advanced age of the atrial fibrillation patient cohort the irradiation of the coronary arteries might hence play a less significant role. Moreover, recent studies indicate that an irradiation of the heart with carbon ions might even lead to beneficial effects in the intercellular communication. Studies by Amino et al. indicate that single fraction carbon ion irradiations of more than 10Gy lead to an increased expression of Connexin 43 (Cx43) [Ami06, Ami10]. This protein is involved in the construction of gap junctions in mammalian hearts, which are intercellular channels enabling current flow and hence the propagation of action potentials (see chapter 1, section 1.3.1). It has been shown that remodelling of connexin expression and gap junction organization are featured in pathological conditions of the heart, including ischemia and heart failure [Sev04, Sev08]. Recent studies indicate that connexin expression is also implied in the induction and sustaining of AF [Kan04, Pol01, Yeh01, Bik11]. Amino et al. could show in animal models that a cardiac irradiation with carbon ions led to a dose-dependent up-regulation of Cx43 expression [Ami06], lasting for at least one year [Ami10]. It was found that this result improved the conductivity and repolarization of the animal hearts, hence having the potential for an additional antiarrhythmic effect. The clinical relevance of these findings needs to be investigated.

Due to the anatomical differences of pigs compared to humans and due to the larger distance of the AV node to critical structures (esophagus, trachea and aorta) dose depositions to OAR for the irradiation of the AV node in the planned animal model were found to be negligible. Dose-volume limits were not exceeded and the stated OARs as well as the radiosensitive cardiac substructures were well spared. The dose-volume limits for the heart were also not exceeded. Maximal point dose to the heart as well as maximal irradiated volume and mean dose were also in very good agreement to the literature findings for human data. Late effects due to e.g. coronary events would also not be expected from the obtained dose deposition in these structures. It should be noted that a potential detection of these events would not be feasible due to the short lifespan of the animals used in the planned animal model feasibility study planned at GSI.

5.1.3 Dose to OAR: Comparison to photons

A non-invasive treatment with carbon ions is expected to result in a better sparing of the surrounding tissue and OARs compared to an irradiation with photons. In order to study this assumption results of treatment planning studies based on the same patient data sets and the resultant dose deposition to the OAR were studied. This was carried out both for human data sets as well as porcine data sets. The photon treatment plans are courtesy of Dr. Limin Song and Dr. Amanda Deisher (Mayo Clinic, Rochester, Minnesota, USA).

Human data

Photon treatment plans were carried out on the reference CT phase of patient 2 and patient 4 (see chapter 3) with a 6MV photon beam. These two data sets were chosen as the carbon ion treatment plans resulted in the highest studied dose deposition to the esophagus in patient 2, while patient 4 resulted in the lowest dose deposition to this structure in the studied patient cohort. The photon plans were carried out as a seven field IMRT(OAR) treatment (see figure 5.1). The delivery was also planned as a single fraction irradiation of 25Gy. For the ITV generation the PVs target volumes were isotropically expended by 3mm. The final PTV was generated by applying an additional isotropic expansion of 5mm margin to the ITV. For the carbon ion treatment, which were carried out as IMPT plans, an isotropic safety margin of 5mm was added to the CTV. Afterwards additional ITV margins were generated from the 4DCTs, accounting also for range variations [Gra12]. The IMPT plans were computed with three beam channel directions (see chapter 3, section 3.2.1). The CTV target volume as well as the contours of the OAR were kept identical in both photon and carbon study, enabling a direct comparison of the treatment planning outcome.

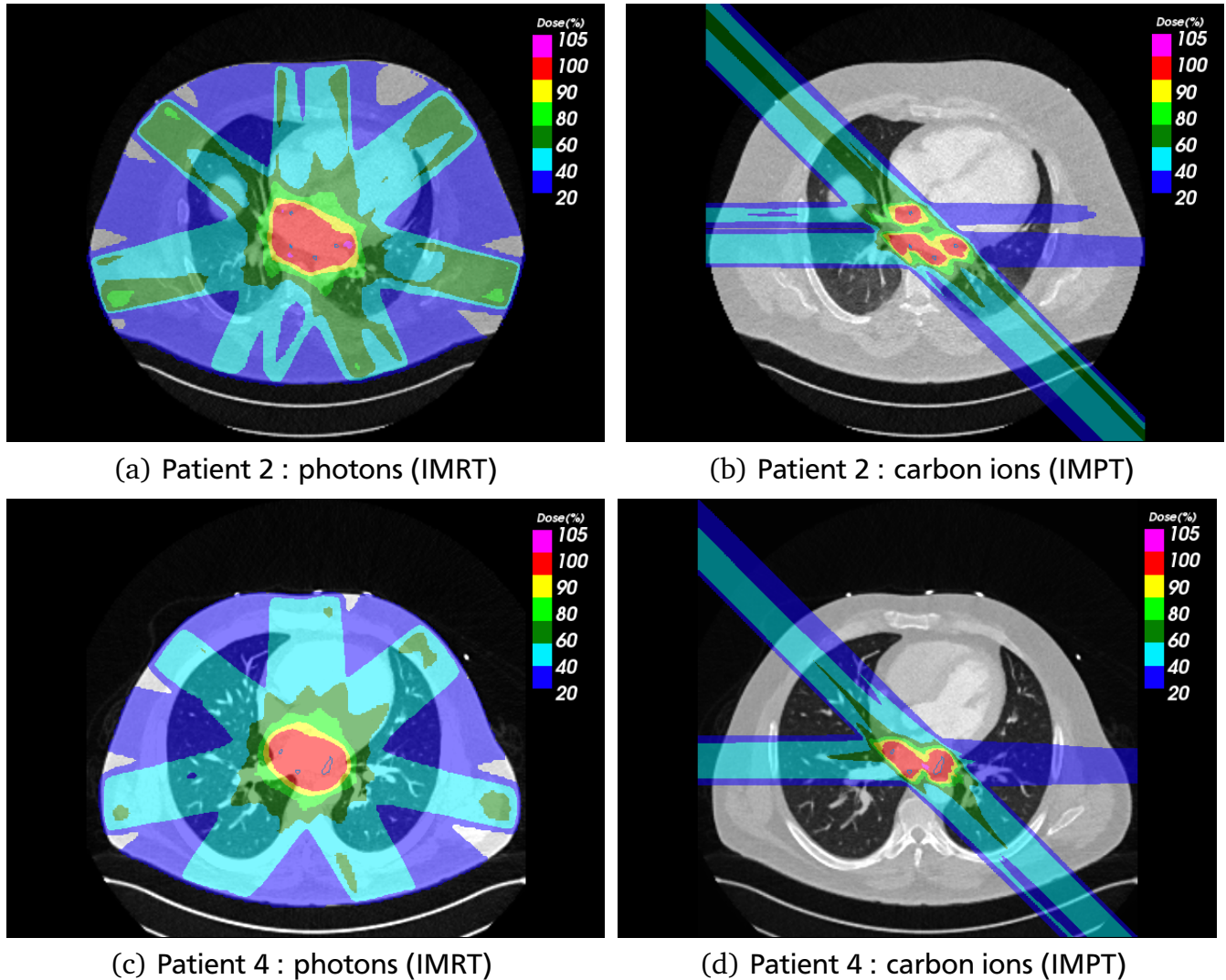


Figure 5.1.: Comparison of dose cuts with photons (IMRT) and carbon ions (IMPT) treatment are shown for Patient 2 and Patient 4, respectively. As target volumes for the LPV and RPV the CTV is displayed. Photon treatment plans are courtesy of Dr. Amanda Deisher, Mayo Clinic, USA. The results of both treatment plans are displayed in the software Slicer.

Table 5.1.: Dose-volume limits for OARs. The volumes are stated in cc, dose values in Gy. The photon irradiation (IMRT) is compared with two different IMPT setting for carbon ions (weak: maximal 70% of the physical dose to the esophagus, strong: maximal 30%). The maximal applicable physical dose to the target region for the dose-volume limits of the critical structures is stated in the last column for the strong IMPT setting.

Patient	OAR	Volume	Dose	endpoint	IMRT	IMPT (weak)	IMPT (strong)	max.D (strong IMPT)
2	Aorta / great vessels	10	31	Aneurysm	22.0	14.3	15.3	50.6
	Esophagus	5	11.9	Stenosis / fistula	24.6	22.5	7	42.5
	Heart	15	16	Pericarditis	27.1	25.3	30.0	(13.3)
	Trachea	4	10.5	Stenosis / fistula	7.6	4.3	3	87.5
4	Aorta / great vessels	10	31	Aneurysm	21.3	8.5	6.3	123.0
	Esophagus	5	11.9	Stenosis / fistula	20.2	18.5	3.5	85.0
	Heart	15	16	Pericarditis	26.1	24.5	22.3	(18.0)
	Trachea	4	10.5	Stenosis / fistula	0	0	0	∞

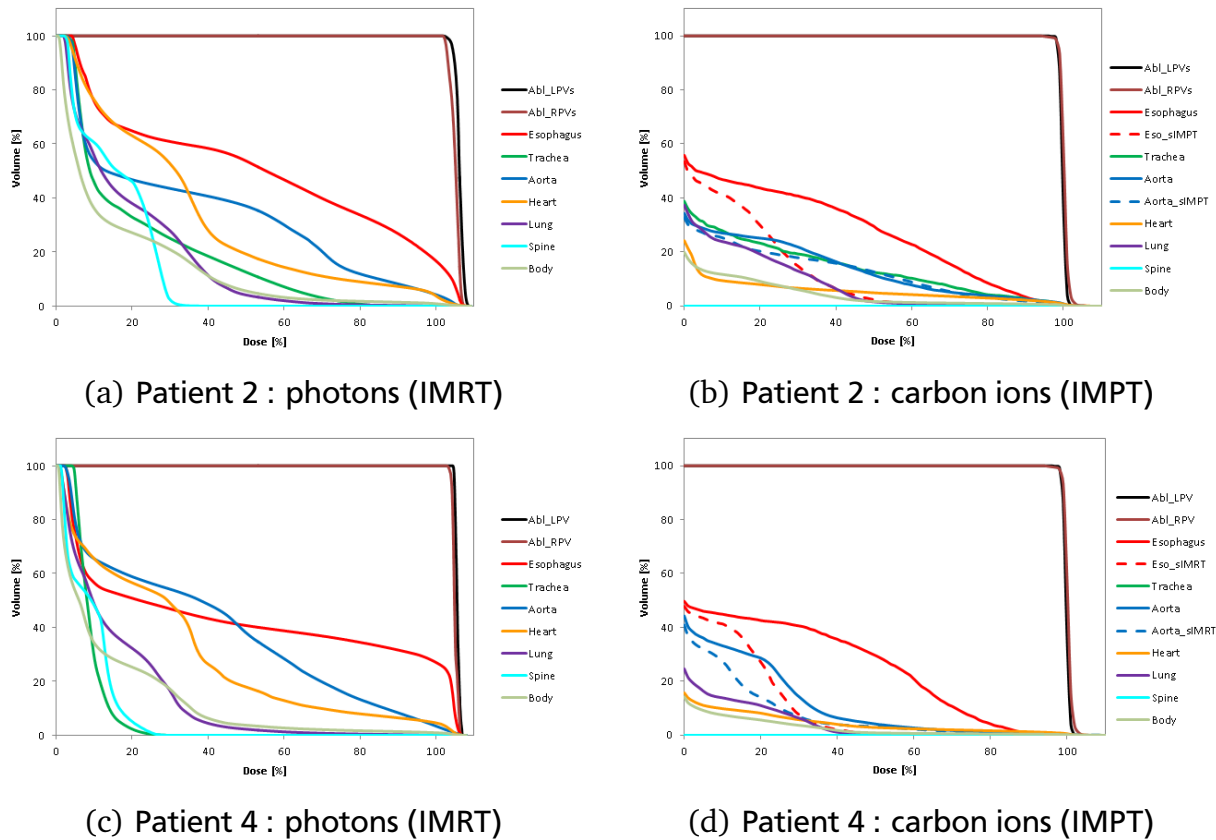


Figure 5.2.: Comparison of DVHs are displayed for a treatment with photons (IMRT) versus carbon ions (IMPT). Target dose deposition are shown in black for the LPVs and brown for the RPVs, the dose to the esophagus is displayed in red, the trachea dose in green, the aorta dose in blue, the heart dose in orange, the lung dose in purple and the spinal cord dose in light blue. Photon treatment plans are courtesy of Dr. Amanda Deisher, Mayo Clinic, USA. For the carbon ion treatment plans different IMPT parameters are shown, where a better sparing of the esophagus is achieved with stronger limitation parameters, shown in dashed lines.

Table 5.2.: Integral dose in $[Gy \times cm^3]$ for photon treatment (IMRT) and the two studied IMPT(OAR) deliveries for carbon ion irradiation (weak: maximal 70% of the physical dose to the esophagus, strong: maximal 30%).

Patient	OAR	IMRT	IMPT(OAR) (weak)	IMPT(OAR) (strong)
2	Esophagus	359	184	80
	Trachea	81	57	48
	Aorta	983	388	356
	Heart	13,863	2,762	2,544
	Lung	10,932	4,761	4,326
5	Esophagus	166	81	32
	Trachea	20	0	0
	Aorta	912	264	180
	Heart	6,992	1,250	1091
	Lung	11,274	3,126	2,730

Due to the different interaction mechanism of photons and ions with matter (see chapter 1, section 1.1.2), and the resulting inverse depth dose profile of ions the surrounding tissue - including the OARs - can be better spared with carbon ions. Hence smaller field channel numbers can be chosen (see figure 5.1). The sparing of the OAR are shown both in the resulting dose-volume deposition to OARs in table 5.1 as well as in the comparison of the resulting DVHs for photons and carbon ions (see figure 5.2). For the carbon ion study two different IMPT parameter settings were used and both results are shown: An IMPT delivery with a weak dose restriction to the esophagus of maximal 70% of the physical dose of 25Gy and an IMPT setting with a stronger restriction of maximal 30% physical dose to the esophagus. As can be seen in table 5.1 the IMPT delivery with the weaker restriction to the esophagus results in dose-volume depositions comparable to the studied photon treatment, while the irradiation with the stronger dose restrictions results in a much better sparing of the studied OARs. An exception is the heart, as it is also the target volume itself. This structure requires a closer analysis on the irradiated substructures. Nevertheless it can already be seen from the DVH information of both patients, that the irradiated heart volume is drastically reduced with carbon ions compared to photons, due to the reduced number of beam channels feasible with carbon ions. The dose cut images (figure 5.1) also display that the left ventricles are better spared with a non-invasive irradiation of the PVs with carbon ions due to the chosen beam channel directions. It can thus be expected that this leads to a better sparing of the radiosensitive left coronary arteries.

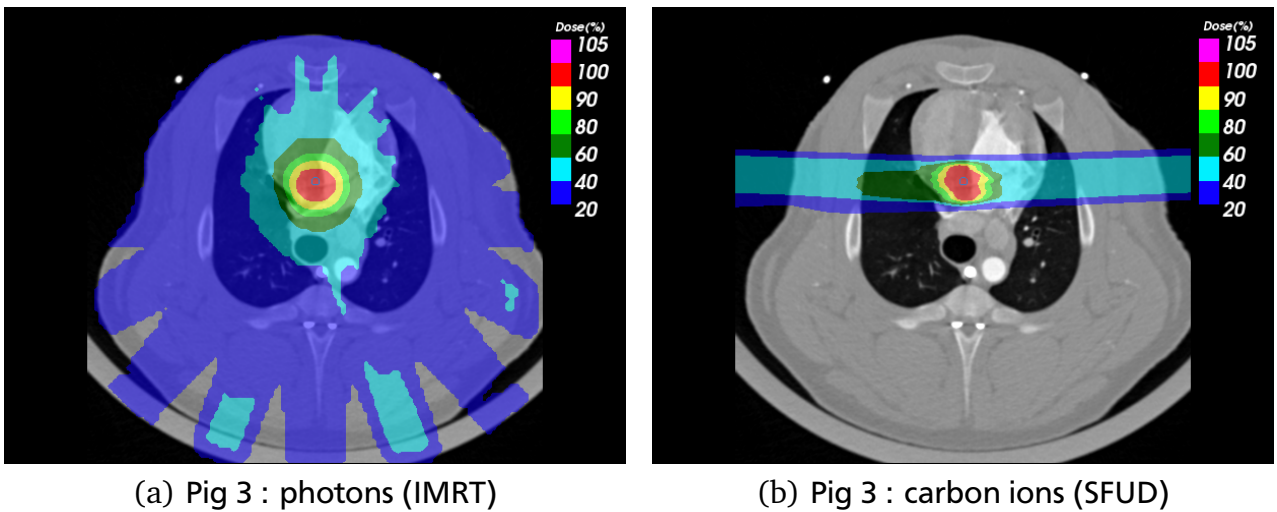
Another method to compare the dose distribution for two different delivery techniques and quality beams is to calculate the integral dose, a measure of the total energy absorbed in the treated volume [Kha10]. It is calculated as the product of the mass of the irradiated tissue and the absorbed dose. Here, no organ specific density was assumed, but the integral dose was calculated as the dose volume product. The results for different critical structures (esophagus, trachea, heart, aorta and lung) are shown in table 5.2 and it can be seen that the absorbed energy of these organs can be drastically reduced with carbon ions compared to photons.

Porcine data

Photon treatment plans for the irradiation of the AV node were carried out on different CT phases for all four porcine data sets (see chapter 4) as a five field IMRT treatment (see figure 5.3) with 6MV photons. In order to keep the ITV margin small the center phase of the motion was chosen as planning phase. This resulted in a treatment planning on 70% of the cardiac phase for Pig 1, on 20% for Pig 2, 0% (reference phase) for Pig 3 and 70% for Pig 4. The delivery was also planned as a single fraction irradiation of 25Gy. For the ITV additional 3mm isotropic expansions were used, resulting in the final PTV. For a fair comparison the shown carbon ion results were calculated on the same CT scan phases. The plans are SFUD irradiations with an isotropic safety margin of 5mm to the CTV. The SFUD carbon ion plans were generated with two opposing beam channel directions (see chapter 4). The target volume as well as the contours of the OAR were kept identical in both deliveries, enabling a direct comparison of the treatment planning outcome.

The sparing of the OARs are shown both in the resulting dose-volume deposition in table 5.3 as well as in the comparison of the resulting DVHs for photons and carbon ions (see figure 5.4). Due to the inverse depth-dose profile of carbon ions a reduced number of beam channel entry directions is feasible, resulting in a better sparing of the OARs compared to an irradiation of the AV node with photons. Due to the used beam channel directions it can be seen that the esophagus as well as the trachea do not receive any dose deposition. The dose deposition in the aorta is negligible, resulting in an irradiated volume of less than 10cc. Also the heart itself (which is here shown with subtracted PTV volume) is much better spared with carbon ions, resulting in no dose-volume-limit exceeding irradiation for this structure. For photons on the other hand the limit is exceeded in three out of the four studied data sets. It should be noted that the analyzed heart volume excludes the irradiated AV node volume and hence also the highest dose deposition, the target dose of 25Gy physical dose.

Also in the porcine data sets the body was only partially displayed on the CT scans and hence no density information could be derived for the calculation of the integral dose. The specific integral dose for both treatment delivery techniques were determined also for these cases. Thereby the sum over all dose volume products was calculated for the body contour volume. The results are shown in table 5.4 and it can be seen that the absorbed energy to the body volume can be drastically reduced with carbon ions compared to photons.



(a) Pig 3 : photons (IMRT)

(b) Pig 3 : carbon ions (SFUD)

Figure 5.3.: Comparison of dose cuts with photons and carbon ions treatment are shown for Pig 3. The photon delivery was planned as IMRT treatment and the carbon irradiation as SFUD irradiation, respectively. As the AV target volume the CTV is displayed. Photon treatment plans are courtesy of Dr.Limin Song, Mayo Clinic, USA. The results of both treatment plans are displayed in the software Slicer.

Table 5.3.: Dose-volume limits for OARs. The volumes are stated in cc, dose values in Gy. The photon irradiation (IMRT) is compared with SFUD carbon ion irradiation

Pig	OAR	Volume	Dose	endpoint	IMRT	SFUD
1	Aorta / great vessels	10	31	Aneurysm	1.1	0.0
	Esophagus	5	11.9	Stenosis / fistula	0.2	0.0
	Heart-PTV	15	16	Pericarditis	18	6.3
	Trachea	4	10.5	Stenosis / fistula	6.5	0.0
2	Aorta / great vessels	10	31	Aneurysm	2.1	0.0
	Esophagus	5	11.9	Stenosis / fistula	0.4	0.0
	Heart-PTV	15	16	Pericarditis	16.1	6.5
	Trachea	4	10.5	Stenosis / fistula	2.6	0.0
3	Aorta / great vessels	10	31	Aneurysm	0.9	0.0
	Esophagus	5	11.9	Stenosis / fistula	0.3	0.0
	Heart-PTV	15	16	Pericarditis	23	4.8
	Trachea	4	10.5	Stenosis / fistula	0.2	0.0
4	Aorta / great vessels	10	31	Aneurysm	0.7	0.0
	Esophagus	5	11.9	Stenosis / fistula	0.3	0.0
	Heart-PTV	15	16	Pericarditis	14.3	7.3
	Trachea	4	10.5	Stenosis / fistula	4.6	0.0

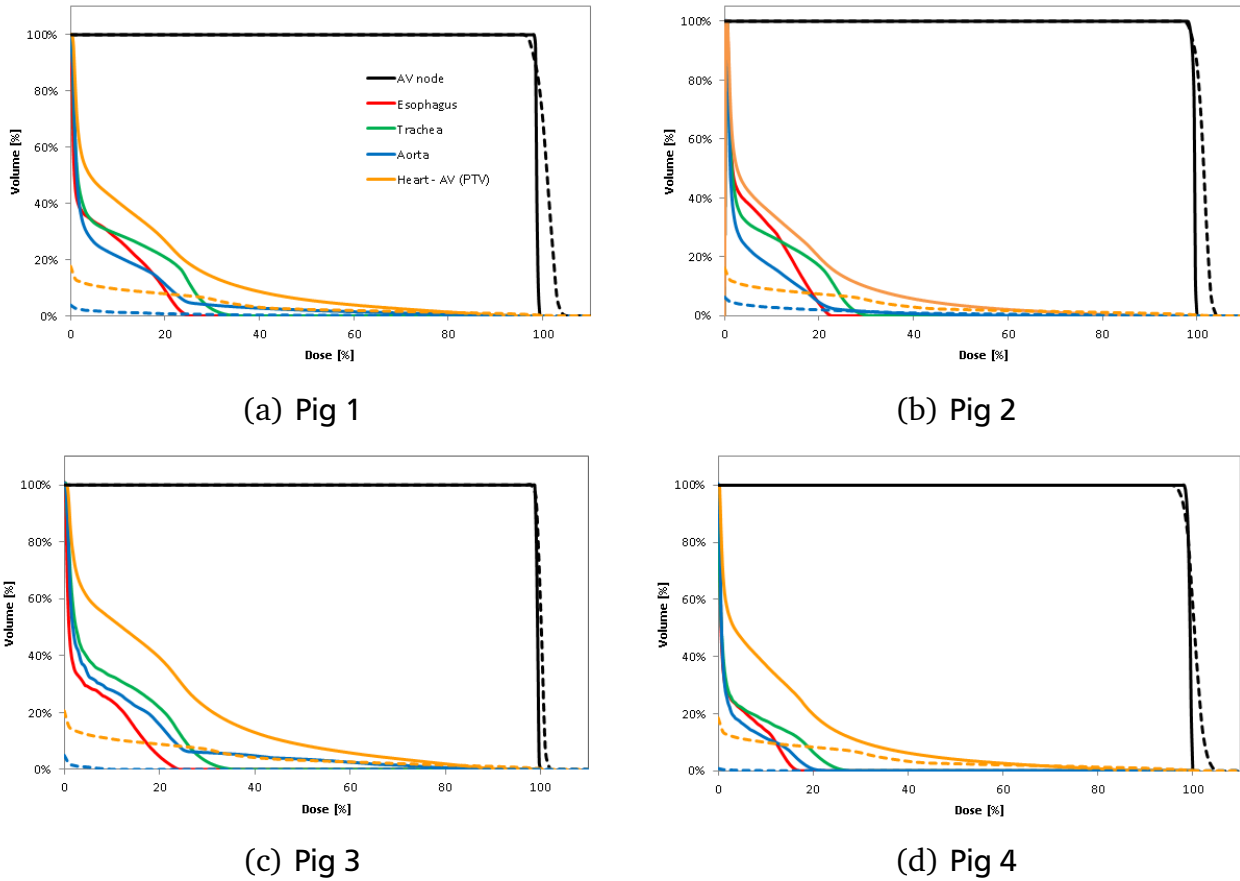


Figure 5.4.: Comparison of DVH results with photons (solid) and carbon ions (dashed). The photon delivery was planned as IMRT treatment and the carbon irradiation as SFUD irradiation, respectively. The target dose to the AV node is displayed in black, the dose to the esophagus in red, to the trachea in green, the aorta in blue and the irradiated heart (with the subtracted PTV volume) is shown in orange. In case of carbon SFUD deliveries, the esophagus and trachea do not receive any dose. Photon treatment plans are courtesy of Dr. Limin Song, Mayo Clinic, USA.

Table 5.4.: Integral dose in [Gy×cm³], exemplarily for pig 3, for photon irradiation (IMRT) and carbon ion treatment (SFUD).

Pig	OAR	IMRT	SFUD
3	Esophagus	14	0
	Trachea	62	0
	Aorta	66	1
	Heart-PTV	1,374	289
	Lung	1,195	187

5.2 Treatment planning of cardiac target volumes with scanned ions

In order to assess the displacement of the cardiac volumes due to respiration and heartbeat, 4DCTs gated on respiration or heartbeat were analyzed and the findings will be discussed in section 5.2.1. Afterwards the usage of contrast enhanced CT scans due to the poor contrast between the heart muscle and the contained blood will be discussed in section 5.2.2 and possible experimental solutions for resulting range uncertainties will be proposed. In section 5.2.3 the result of the used motion mitigation techniques for the irradiation of cardiac target volumes with a scanned carbon ion beam will be deliberated.

5.2.1 Motion of cardiac volumes

Target volumes in the heart move on one hand due to the respiration of the patient, a motion with a large amplitude and a slow cycle time of ten to fifteen respiratory cycles per minute, and on the other hand due to heartbeat, a motion with a small amplitude and cycle time of sixty to eighty beats per minutes. Even though both motions occur simultaneously in patients, they were studied independently in the here presented treatment planning studies. This can be justified as a CT gated to both motion types would require long CT acquisitions and hence unnecessary dose exposures to the patient.

PVs motion in humans

The motion of PVs ablation sites in humans due to respiration were studied based on respiratory gated time resolved computed tomographies (4DCTs) of nine lung cancer patients, recorded for radiotherapy at MD Anderson Cancer Center (MDACC), USA. The heartbeat influence was studied on cardiac gated 4DCTs of five AF patients, recorded at Mayo Clinic, USA.

The movement of the ablation sites of the PVs were studied in the three motion directions (superior-inferior (SI), anterior-posterior (AP) and left-right (LR)) as well as for the absolute displacement. Different studies concerning the PVs displacement due to respiration can also be found in literature [Ect08, Nos05], as breathing is also relevant for catheter ablation due to the reduction in catheter tip contact force [Kum12]. While Ector et al. stated an absolute mean displacement of $(19.1 \pm 8.6)\text{mm}$ for both LPV and RPV, a much smaller absolute mean displacement of $(6.8 \pm 3.6)\text{mm}$ and $(6.8 \pm 2.5)\text{mm}$ was found in the here studied patient cohort for LPV and RPV, respectively. The SI motion was the biggest motion direction with a mean displacement of $(-6.4 \pm 3.8)\text{mm}$ for LPV and $(-6.6 \pm 2.4)\text{mm}$ for RPV. AP and LR directions were almost negligible with a mean motion of less than 2mm. The difference between the two cardiac sites is more pronounced in AP and LR, so that, e.g., the LPV move more in anterior direction. In

LR direction a difference between LPV and RPV motion resulted, where the mean displacement of the LPV is almost double compared to the RPV. Ector et al. on the other hand found a mean displacement of (14.6 ± 7.7) mm in inferior direction, (9.7 ± 7.6) mm in anterior direction and (0.4 ± 3.8) mm in the left direction, hence concluding a much bigger displacement in SI and AP directions. It remains to be analyzed if this discrepancy is due to the here studied lung tumor patient cohort in comparison to the AF patients studied by Ector et al.. Nevertheless it should be noted that both analyses are based on a small patient number (nine patients and sixteen patients, respectively).

The motion of the ablation sites for the PVs due to heartbeat was studied for the left and right structures, respectively, in the three above stated motion directions. Only a small mean absolute displacement over all patients of less than 3mm was observed. The biggest absolute displacement reached a mean value of up to (6.5 ± 3.0) mm in one patient case for the RPV and (5.5 ± 3.1) mm for the LPV. No dominant motion direction was found, even though a tendency to a bigger motion in AP direction could be assumed. Furthermore, no motion pattern could be derived from the five studied patient data sets, indicating that the underlying motion causing the PV ablation sites to move is much more complex and the result of different motion influences. For further studies concerning the PV displacement due to heartbeat, the reader should be referred to Lickfett et al. [Lic05] and Patel et al. [Pat08]. Lickfett et al. found comparable maximal displacements of up to 7.2mm in some of the healthy volunteers. Patel et al., who studied the displacement in thirty AF patients, stated mean values in the order of 3mm. The here presented results are hence in good agreement with the literature values.

Motion in porcine due to heartbeat

The motion of different potential cardiac ablation sites (AV node, CTI and PVs) were studied in pigs based on cardiac gated 4DCTs of four swines, recorded at Mayo Clinic, USA. The acquired CT scans were both native and contrast enhanced. It was found that native CT scans do not enable an assessment of the cardiac target volume displacement due the low contrast between the cardiac muscle and the contained blood. Analysis was hence carried out on the contrast enhanced CT scans. Concerning the motion of the three studied potential target sites it could be stated that the PVs moved to the smallest extent (maximal displacement of up to 5mm), followed by the AV node (maximal displacement of up to 6mm) and that the CTI moved the most (maximal displacement of 7mm). It was speculated that this is due to the location of the volumes, where a proximal location on or near the ventricles lead to a larger movement. Even though also in the porcine data sets no maximal motion phase or motion pattern could be observed due to heartbeat it was found that the displacement was shallower between certain motion phases (motion phase 6 to 13) and hence, contrary to the studied human data, gating

could be an optional motion mitigation technique. Moreover, in comparison to the human data, the displacement in AP direction in the porcine data was clearly larger than in the other two studied directions.

5.2.2 Contrast enhanced CT scans

Particle treatment planning needs to be carried out on native CT scans in order to obtain the correct range information [Wer04]. In case of the intended irradiation of cardiac target volumes it was found that native CT scans do not provide sufficient contrast between the heart muscle and the contained blood. As stated, the motion information can thus only be assessed from contrast-enhanced CT scans. It needs to be studied if the displacement vector field obtained from registration on the contrast enhanced CT scans yield a good enough agreement when directly used on the native data sets for the actual treatment planning. The resulting range uncertainties need to be carefully considered, especially regarding the dose to critical structures like the esophagus. Analog to studies by e.g. el Bentefour et al. [Bent12], where in vivo range verifications were successfully achieved with a small dose deposition ($<0.5\text{cGy}$) in silicone diodes, a possible solution could be to predeposit the resulting treatment plan with a small dose in the order of mGy. By placing such a detector with a catheter inside the patient, either in front of or inside the esophagus, it would allow to test for range of the planned energies and hence for potential miscalculation or interfractional changes of the organs. Range uncertainties to the target area could furthermore be corrected before irradiation with the total single fraction dose. By using in-beam PET monitoring with ^{11}C and ^{10}C fragments (see chapter 1, section 1.1.2) it would be possible to irradiate a low dose in order to detect the range and position uncertainties. This was already carried out at GSI, where ^{10}C resulted to be best suited as a probing beam for range verifications [Lin12]. The accuracy of PET monitoring for ion range determination was studied by Fiedler et al. [Fie10] for more than 80 of the 400 patients irradiated in the GSI pilot project. It was stated that in-beam PET method demonstrated a high sensitivity for the detection of range deviations and would thus be beneficial for the here presented treatment modality.

5.2.3 Motion mitigation techniques

Due to the large motion of the PV ablation sites induced by the respiratory motion in the studied patient cohort, interplay was observed to lead to strong underdosage, so that in some cases only V95=70% was achieved with no safety margin and V95=80% with safety margins of 5mm. Due to the large motion amplitude of more than 1cm gating was studied as potential motion mitigation technique (see next paragraph). For the displacements induced by heartbeat a smaller motion of less than 1cm was observed in all studied human data, so that rescanning was studied

as an adequate motion mitigation technique for this case. As expected, the interplay effect in this case was smaller than for respiration, with minimal underdosages of V95=85% for no safety margin and a minimal V95 of 92% for 5mm and 7mm margin, respectively. Even though this underdosage with safety margin already yields a clinically acceptable dose coverage the usage of an additional motion mitigation technique leads to a more robust treatment delivery. For the porcine data, where the motion influence of the heartbeat on the AV node target volume was studied and only a single margin of 5mm was used, the interplay effect led to larger minimal underdosages of 56% in some of the studied pig data sets. Hence the usage of rescanning as motion mitigation technique was needed in this case as well.

Respiratory motion

In the animal model studies by Sharma et al. [Sha10] the target displacement due to respiration was tracked with the CyberKnife system. In the study by Blanck et al. [Bla13] an ITV approach was used for the respiratory motion. Here, gating was used as a potential motion mitigation technique. It is suited for larger target displacements, since only a fraction of the motion cycle is used. The gating window is positioned at end exhale, enabling a more robust delivery with only a small amount of residual motion. To this date, gating is already used in ion beam centers with passive particle delivery [Min00] as well as in IMRT treatments in photon centers [Kea06]. A pilot study with scanned carbon ions was recently conducted on liver patients at HIT by using gating and abdominal compression [Ric12]. In the here studied case, gating was found to be an adequate motion mitigation technique so that underdosages could be increased up to a minimum of 98% for all studied safety margins and patient cases. Even in cases with no safety margin underdosage could be increased to a minimum of 94%. It can nevertheless be stated that safety margins, which are needed in order to account for e.g. position inaccuracies, improved the outcome and made the delivery more robust. It was furthermore studied in two patient data sets if the treatment outcome improved when rescanning was applied for the residual motion inside the gating window. This is proposed as phase-controlled rescanning [Fur07] or breath-sampled rescanning [Sec09]. It resulted in a marginal improvement compared to only gating, whereas no improvement was observed when using more than ten rescans. Since the irradiation of the PV ablation sites were also studied to include rescanning as mitigation for heartbeat motion, the combination of these two techniques will be automatically achieved. Concerning the treatment time it was expected that gating would increase the treatment time dependence on the used gating window. Since only 30% of the motion cycle was used for irradiation, the treatment resulted into a delivery time of about 30min with a high intensity of 55,000 minimum particles per beam spot and for a safety margin of 3mm. Compared to the radiofrequency ablation procedure which takes up to a couple of hours, and to the photon irradiation of up to two hours [Sha10], the treatment time is drastically reduced. This was found

for the HIT beam parameters, where a relatively long time for an energy change is needed. The particle intensity could be further increased, leading to an even further reduced treatment time. Nevertheless it was shown that very high intensities can endanger a homogenous dose coverage [Mue14]. New accelerator concepts with variable excitation cycles [Tsu08] or faster energy changes [Iwa10] might hence be needed. An alternative to gating could be the usage of apneic oxygenation, which is currently used at the Rinecker Proton Therapy Center in Munich [Ber11, RPTC12] for the treatment of tumors in the upper abdomen and thorax. This approach will also be used in the planned animal experiments with pigs which will be carried out at GSI in the summer of 2014.

Heartbeat motion

In the animal model studies by Sharma et al. [Sha10] and by Blanck et al. [Bla13] an ITV approach was used for the heartbeat motion. In the here presented study rescanning was used as a motion mitigation technique for heartbeat motion, both in human as well as for the porcine data sets. Especially in human data only rescanning seemed to be an adequate technique due to the lack of a motion pattern or a region of shallower motion. For the porcine data on the contrary, cardiac gating might be another option, which needs to be investigated. In the human data it was found that the dose coverage was higher than 99% in about 96% of the studied cases with safety margins over 3mm. This result could be even further improved if ten or more rescans were applied. Nevertheless it can be argued that five rescans already yield a very good dose deposition in the target volume. For the porcine data and the studied AV node ablation it was found that the dose coverage was higher than 99% in 85% of the studied cases with a safety margin of 5mm. This finding could be slightly improved to 91% of the studied cases for ten rescans. A higher rescan number of fifteen rescans did not lead to a significant improvement. The finding indicates that ten rescans are already sufficient to enable a robust and stable irradiation of the cardiac target volume in the presence of heartbeat. Due to the high single dose the resulting intensity per rescan is expected to be large and hence the application should be feasible without further prolonging the treatment time. All the studied rescanning results were obtained for slice-by-slice rescanning. This means that each IES is rescanned independently with the predefined numbers of rescans. In other studies it has nevertheless been found that other rescan methods, like e.g. breath-sampled rescanning [Sec09] or phase-controlled rescanning [Fur07], result in an increased robustness while requiring fewer rescan numbers compared to slice-by-slice rescanning as it breaks up possible synchronicities between beam application and target motion [Mue14]. In breath-sampled rescanning the IES are rescanned individually, but the rescans are sampled according the motion phase of the breathing period, so that every motion phase receives dose applications. An analog delivery according to the heartbeat and hence an ECG-sampled rescanning might be feasible and could lead to improved results.

6 Conclusion and outlook

This is the first work to study the irradiation of intrafractionally moving, non-cancerous target volumes with carbon ions. Its aim was to investigate the feasibility of a non-invasive treatment for cardiac arrhythmias like atrial fibrillation by particle radiosurgery.

The search for a new treatment modality for this condition is motivated by the currently existing possibility of catheter ablation, which has varying success rates and can lead to severe side effects [Cap05, Cap10, Jong05, Her13, Gai10, Med13]. Studies for the potential of a non-invasive treatment with photon irradiation already exist [Sha10]. Due to differing interaction mechanisms of photons with matter in comparison to ions, a better sparing of the surrounding tissue was expected for the here studied radiosurgery with ions [Ber12]. This could be demonstrated in this thesis, where carbon ion and photon delivery were compared on the same data sets. The difference in dose deposition to the organs at risk (OAR) was significant and made a strong case to use ions in cardiac radiosurgery.

Due to successful treatment outcomes in cancer radiotherapy an increasing number of therapy centers treat patients with scanned particle therapy [PTCOG13]. Up to now clinical applications of these centers have been mostly conducted on tumors which showed no intrafractional displacements [Loe13]. This is due to the otherwise occurring interference effects between the existing target motion and the actively applied particle beam, leading to local over and under dosages (interplay effect) and hence to the need of motion mitigation techniques [Phi92, Ber08].

The here relevant intrafractional motion of the pulmonary veins atria junction was studied separately in human data for the underlying respiratory and heartbeat motion. These intrafractional motion types differ in motion period and amplitude. While the respiration is a rather slow motion which causes the pulmonary vein junction to move in particular in the superior-inferior direction up to more than 2cm, the heartbeat displays a fast motion period causing a fairly irregular motion of the ablation site with an amplitude of up to 1cm. The interplay effect caused by respiration was hence found to be more pronounced than in case of heartbeat motion. In order to guarantee a robust treatment delivery, motion mitigation techniques have also been studied in case of heartbeat displacements. For the influence of the respiratory motion, the interrupted irradiation during a selected part of the motion cycle (gating) [Kub96] was studied and was found to be an adequate technique for a 30% gating window around end exhale. Nevertheless, gating always results in a prolonged treatment time. Alternative methods could be jet ventila-

tion [Hof03] or apneic oxygenation [RPTC12], where the patient is kept in a steady respiratory phase and which would result in a shorter treatment time. In order to mitigate the influence of the heartbeat motion, an averaging effect of different interplay patterns by scanning the same slice multiple times (rescanning) [Phi92] was applied. Also this motion mitigation technique resulted in a good dose coverage, already for small rescan numbers. This delivery would not prolong the treatment time. Other rescanning techniques are nevertheless known to result in an increased robustness while requiring fewer rescan numbers, like e.g. breath-sampled rescanning [Sec09] or phase-controlled rescanning [Fur07], where the rescans are equally distributed over the motion cycle. Thus a similar technique should be investigated in the future for the cardiac motion (ECG-sampled rescanning). In case of the studied porcine data, where the cardiac target volumes also displayed an irregular motion but had a more shallow motion region in common, cardiac gating could furthermore be a potential application. This would require the application of a fast beam extraction modality for synchrotrons with radiofrequency knock-out excitors, which exist, e.g., at NIRS [Nod96, Fur05] and HIT [Schoe11] and are tested in first studies at GSI [Ber09]. In preparation for the planned animal experiments with pigs at GSI, which will be an experimental validation of the here found treatment planning results, rescanning was found to be a well suited technique to overcome the heartbeat motion influence in the atrioventricular node of swine. For the breathing motion of the animals a respirator will be used.

In all presented treatment planning results a physical dose of 25Gy was used. Biological effects leading to a relative biological effectiveness higher than one might occur, even though preliminary studies did not support this assumption and a RBE of 1.1 was found. It is expected that the RBE reaches a plateau for high single fraction doses [Cara07], in which case the physical dose could be considered proportional to the biological dose and the deposition in the organs at risk could be directly scaled to the desired value. Older photon studies suggested that 20Gy are sufficient to induce fibrotic tissue in the heart [Faj70, Faj73]. Nevertheless higher doses than the here stated might be needed to create a complete electrophysiological block in the desired target area. The planned dose escalation studies in the animal models will offer valuable data in respect to this question. The treatment planning results were obtained on contrast-enhanced CT scans, since the contrast between cardiac muscle and blood was not sufficient in native CT scans. A closer analysis on the resulting range uncertainties is needed. Potential experimental validations like small dose depositions in silicon diodes [Bent12] or PET probing beams [Lin12] were suggested in order to test for potential range differences which might endanger critical structures. These need to be investigated and tested for suitability.

In general it became obvious that a non-invasive treatment is challenging due to the amount of OAR which are in direct proximity of the desired target area. Intensity modulated particle therapy was hence needed in order to adhere to dose-volume limits stated for these structures

[RTOG0631, RTOG0915]. Furthermore a delivery with an ion beam gantry would be beneficial as this allows to choose suitable beam entry channels, enabling a sparing of the critical structures.

Besides the here studied potential ablation sites of the pulmonary veins junction and the atrioventricular node, other applications are also conceivable in the future. Catheter ablation started to be also used for isolation of low-voltage areas in the ventricles of patients who suffered a myocardial infarction in order to prevent the formation of life-threatening ventricular tachycardias [Til14, Mad14]. It has furthermore been shown that the underlying myocardial scar and border zones can be visualized in contrast-enhanced CT scans [Tia14]. Treatment planning for this condition is hence potentially feasible. Due to the larger distance of the ventricles to many critical structures this delivery might even be easier achievable. Nevertheless the displacements of ventricular target sites are expected to be larger than the here studied motion, so that further research on suitable motion mitigation techniques might be needed.



A Appendix of chapter 2

A.1 Motion of PV due to respiration

The mean relative displacement and standard deviation of the target volumes (LPV and RPV) to the reference phase five will be shown for the three studied motion directions (SI: superior-inferior, AP: anterior-posterior, LR: left-right) and the absolute (ABS) displacement.

Table A.1.: Patient 1, LPV: Mean and standard deviation of target motion in all phases of the respiration, relative to the reference phase.

motion phase	ABS [mm]	SI [mm]	AP [mm]	LR [mm]
00	5.17 ± 0.48	-5.16 ± 0.48	-0.05 ± 0.18	-0.14 ± 0.15
01	4.88 ± 0.33	-4.87 ± 0.34	-0.09 ± 0.26	-0.01 ± 0.09
02	3.73 ± 0.24	-3.72 ± 0.24	-0.21 ± 0.13	0.12 ± 0.08
03	1.62 ± 0.14	-1.61 ± 0.15	-0.14 ± 0.13	0.05 ± 0.08
04	0.76 ± 0.13	-0.75 ± 0.13	-0.01 ± 0.07	-0.04 ± 0.05
06	0.28 ± 0.09	0.12 ± 0.04	0.10 ± 0.15	-0.19 ± 0.05
07	0.69 ± 0.26	-0.30 ± 0.27	0.52 ± 0.17	-0.27 ± 0.11
08	1.46 ± 0.67	-1.35 ± 0.66	0.49 ± 0.16	-0.24 ± 0.12
09	4.51 ± 0.91	-4.49 ± 0.89	0.26 ± 0.18	-0.20 ± 0.20

Table A.2.: Patient 1, RPV: Mean and standard deviation of target motion in all phases of the respiration, relative to the reference phase.

motion phase	ABS [mm]	SI [mm]	AP [mm]	LR [mm]
00	6.12 ± 1.43	-6.03 ± 1.41	-1.00 ± 0.37	-0.11 ± 0.16
01	4.61 ± 0.63	-4.44 ± 0.61	-1.10 ± 0.33	0.45 ± 0.11
02	3.61 ± 0.28	-3.46 ± 0.28	-0.96 ± 0.16	0.31 ± 0.10
03	1.70 ± 0.41	-1.58 ± 0.38	-0.57 ± 0.16	0.24 ± 0.09
04	0.34 ± 0.23	-0.20 ± 0.30	-0.13 ± 0.05	-0.09 ± 0.09
06	0.39 ± 0.12	0.33 ± 0.15	0.11 ± 0.04	-0.13 ± 0.04
07	0.73 ± 0.18	0.47 ± 0.28	0.41 ± 0.09	-0.29 ± 0.05
08	0.89 ± 0.27	-0.48 ± 0.42	0.49 ± 0.13	-0.43 ± 0.08
09	5.06 ± 1.27	-5.03 ± 1.24	-0.44 ± 0.42	0.01 ± 0.13

Table A.3.: Patient 2, LPV: Mean and standard deviation of target motion in all phases of the respiration, relative to the reference phase.

motion phase	ABS [mm]	SI [mm]	AP [mm]	LR [mm]
00	5.37 ± 0.62	-5.33 ± 0.62	-0.38 ± 0.22	-0.45 ± 0.22
01	3.36 ± 0.30	-3.32 ± 0.29	-0.15 ± 0.14	-0.44 ± 0.18
02	1.86 ± 0.20	-1.81 ± 0.21	-0.22 ± 0.22	-0.27 ± 0.09
03	1.82 ± 0.53	-1.78 ± 0.54	-0.30 ± 0.05	-0.05 ± 0.07
04	1.08 ± 0.44	-1.07 ± 0.44	-0.09 ± 0.06	-0.06 ± 0.07
06	1.50 ± 0.36	-1.50 ± 0.36	0.01 ± 0.04	-0.07 ± 0.10
07	2.05 ± 0.29	-2.03 ± 0.29	0.12 ± 0.20	-0.08 ± 0.12
08	3.63 ± 0.50	-3.61 ± 0.49	-0.15 ± 0.11	-0.22 ± 0.16
09	4.94 ± 0.62	-4.92 ± 0.62	-0.27 ± 0.08	-0.22 ± 0.22

Table A.4.: Patient 2, RPV: Mean and standard deviation of target motion in all phases of the respiration, relative to the reference phase.

motion phase	ABS [mm]	SI [mm]	AP [mm]	LR [mm]
00	7.51 ± 1.35	-7.47 ± 1.35	0.14 ± 0.32	0.46 ± 0.41
01	4.96 ± 1.06	-4.94 ± 1.06	0.11 ± 0.11	-0.21 ± 0.24
02	2.65 ± 0.59	-2.61 ± 0.59	-0.27 ± 0.16	-0.24 ± 0.24
03	1.28 ± 0.23	-1.26 ± 0.23	-0.11 ± 0.06	-0.15 ± 0.08
04	0.31 ± 0.20	-0.25 ± 0.23	0.04 ± 0.06	-0.06 ± 0.09
06	1.34 ± 0.22	-1.25 ± 0.17	0.14 ± 0.17	0.41 ± 0.18
07	3.39 ± 0.34	-3.34 ± 0.32	0.11 ± 0.23	0.49 ± 0.24
08	5.25 ± 0.70	-5.22 ± 0.69	0.18 ± 0.26	0.38 ± 0.26
09	6.78 ± 0.88	-6.75 ± 0.87	0.18 ± 0.25	0.54 ± 0.35

Table A.5.: Patient 3, LPV: Mean and standard deviation of target motion in all phases of the respiration, relative to the reference phase.

motion phase	ABS [mm]	SI [mm]	AP [mm]	LR [mm]
00	7.14 ± 0.85	-7.09 ± 0.85	-0.39 ± 0.40	-0.51 ± 0.37
01	5.22 ± 0.94	-5.17 ± 0.93	-0.47 ± 0.35	-0.21 ± 0.27
02	2.71 ± 0.43	-2.65 ± 0.42	-0.19 ± 0.25	-0.36 ± 0.29
03	0.85 ± 0.29	-0.68 ± 0.33	0.07 ± 0.27	0.15 ± 0.37
04	0.33 ± 0.12	0.08 ± 0.23	0.07 ± 0.19	0.07 ± 0.14
06	1.52 ± 0.33	-1.47 ± 0.33	0.31 ± 0.15	0.18 ± 0.11
07	3.82 ± 0.41	-3.81 ± 0.41	0.16 ± 0.23	-0.03 ± 0.09
08	5.93 ± 0.84	-5.92 ± 0.85	0.25 ± 0.34	0.03 ± 0.16
09	7.13 ± 0.97	-7.09 ± 0.97	-0.16 ± 0.37	-0.50 ± 0.28

Table A.6.: Patient 3, RPV: Mean and standard deviation of target motion in all phases of the respiration, relative to the reference phase.

motion phase	ABS [mm]	SI [mm]	AP [mm]	LR [mm]
00	8.12 ± 0.98	-7.94 ± 0.95	-1.45 ± 0.28	0.88 ± 0.33
01	6.28 ± 0.79	-6.03 ± 0.83	-1.58 ± 0.29	0.68 ± 0.29
02	3.32 ± 0.45	-3.06 ± 0.51	-1.19 ± 0.16	0.37 ± 0.13
03	1.52 ± 0.49	-1.25 ± 0.59	-0.76 ± 0.17	0.05 ± 0.15
04	0.41 ± 0.15	0.14 ± 0.21	-0.30 ± 0.15	-0.06 ± 0.09
06	1.04 ± 0.23	-1.02 ± 0.25	0.08 ± 0.07	0.11 ± 0.10
07	4.13 ± 0.34	-4.06 ± 0.35	-0.51 ± 0.13	0.54 ± 0.12
08	6.32 ± 0.65	-6.25 ± 0.65	-0.77 ± 0.12	0.56 ± 0.14
09	9.10 ± 1.09	-8.90 ± 1.10	-1.48 ± 0.24	1.13 ± 0.18

Table A.7.: Patient 4, LPV: Mean and standard deviation of target motion in all phases of the respiration, relative to the reference phase.

motion phase	ABS [mm]	SI [mm]	AP [mm]	LR [mm]
00	3.03 ± 0.39	-1.53 ± 0.26	-1.85 ± 0.32	-1.78 ± 0.47
01	2.56 ± 0.32	-1.34 ± 0.35	-1.44 ± 0.17	-1.56 ± 0.41
02	1.53 ± 0.40	-0.83 ± 0.33	-0.80 ± 0.23	-0.97 ± 0.29
03	0.89 ± 0.20	-0.46 ± 0.15	-0.57 ± 0.09	-0.47 ± 0.21
04	0.24 ± 0.10	-0.13 ± 0.12	-0.06 ± 0.13	-0.10 ± 0.09
06	0.35 ± 0.15	-0.02 ± 0.24	-0.14 ± 0.11	-0.20 ± 0.12
07	1.04 ± 0.16	-0.21 ± 0.31	-0.70 ± 0.10	-0.66 ± 0.16
08	1.73 ± 0.25	-0.62 ± 0.17	-1.07 ± 0.24	-1.17 ± 0.25
09	2.78 ± 0.35	-1.30 ± 0.25	-1.71 ± 0.30	-1.71 ± 0.40

Table A.8.: Patient 4, RPV: Mean and standard deviation of target motion in all phases of the respiration, relative to the reference phase.

motion phase	ABS [mm]	SI [mm]	AP [mm]	LR [mm]
00	5.46 ± 0.57	-5.33 ± 0.59	-1.09 ± 0.22	0.36 ± 0.23
01	4.21 ± 0.32	-4.06 ± 0.33	-1.02 ± 0.24	0.26 ± 0.27
02	2.47 ± 0.40	-2.30 ± 0.38	-0.84 ± 0.19	0.20 ± 0.19
03	1.51 ± 0.35	-1.38 ± 0.30	-0.56 ± 0.20	0.21 ± 0.11
04	0.59 ± 0.20	-0.56 ± 0.20	-0.16 ± 0.08	0.06 ± 0.07
06	0.26 ± 0.04	0.04 ± 0.12	0.12 ± 0.05	-0.19 ± 0.04
07	0.99 ± 0.17	-0.95 ± 0.19	-0.04 ± 0.11	-0.24 ± 0.06
08	2.57 ± 0.49	-2.54 ± 0.50	-0.35 ± 0.13	-0.15 ± 0.15
09	4.89 ± 0.79	-4.79 ± 0.82	-0.91 ± 0.20	0.15 ± 0.20

Table A.9.: Patient 5, LPV: Mean and standard deviation of target motion in all phases of the respiration, relative to the reference phase.

motion phase	ABS [mm]	SI [mm]	AP [mm]	LR [mm]
00	5.06 ± 0.57	-4.55 ± 0.48	-0.75 ± 0.19	-2.07 ± 0.32
01	4.07 ± 0.27	-3.61 ± 0.23	-0.92 ± 0.13	-1.63 ± 0.23
02	2.84 ± 0.32	-2.62 ± 0.29	-0.84 ± 0.16	-0.68 ± 0.18
03	1.62 ± 0.37	-1.51 ± 0.34	-0.52 ± 0.12	-0.19 ± 0.19
04	0.94 ± 0.23	-0.86 ± 0.23	-0.36 ± 0.05	0.06 ± 0.10
06	0.83 ± 0.33	0.77 ± 0.32	0.30 ± 0.11	0.00 ± 0.07
07	0.79 ± 0.10	-0.53 ± 0.15	0.26 ± 0.06	-0.50 ± 0.07
08	3.06 ± 0.29	-2.66 ± 0.23	0.06 ± 0.17	-1.51 ± 0.21
09	4.56 ± 0.38	-4.14 ± 0.29	-0.43 ± 0.19	-1.85 ± 0.28

Table A.10.: Patient 5, RPV: Mean and standard deviation of target motion in all phases of the respiration, relative to the reference phase.

motion phase	ABS [mm]	SI [mm]	AP [mm]	LR [mm]
00	5.37 ± 1.51	-4.96 ± 1.44	-1.89 ± 0.56	-0.77 ± 0.12
01	3.88 ± 1.12	-3.45 ± 1.05	-1.69 ± 0.46	-0.48 ± 0.09
02	2.26 ± 0.52	-1.88 ± 0.45	-1.24 ± 0.27	-0.13 ± 0.09
03	1.48 ± 0.37	-1.15 ± 0.28	-0.91 ± 0.26	0.15 ± 0.06
04	0.77 ± 0.15	-0.60 ± 0.15	-0.47 ± 0.09	-0.01 ± 0.07
06	0.47 ± 0.12	0.31 ± 0.15	0.22 ± 0.09	-0.24 ± 0.02
07	1.37 ± 0.11	-1.14 ± 0.13	0.22 ± 0.14	-0.71 ± 0.04
08	4.12 ± 1.06	-3.85 ± 1.06	-0.80 ± 0.33	-1.18 ± 0.13
09	5.24 ± 1.40	-4.85 ± 1.35	-1.51 ± 0.56	-1.18 ± 0.10

Table A.11.: Patient 6, LPV: Mean and standard deviation of target motion in all phases of the respiration, relative to the reference phase.

motion phase	ABS [mm]	SI [mm]	AP [mm]	LR [mm]
00	6.08 ± 0.61	-5.43 ± 0.68	-1.41 ± 0.20	-2.30 ± 0.19
01	3.60 ± 0.42	-3.30 ± 0.42	-0.45 ± 0.11	-1.36 ± 0.17
02	1.72 ± 0.16	-1.50 ± 0.15	-0.17 ± 0.15	-0.81 ± 0.13
03	1.13 ± 0.20	-1.02 ± 0.24	0.07 ± 0.26	-0.36 ± 0.06
04	0.22 ± 0.06	-0.07 ± 0.10	0.12 ± 0.07	-0.13 ± 0.05
06	1.11 ± 0.12	-1.08 ± 0.12	-0.01 ± 0.13	-0.21 ± 0.08
07	2.81 ± 0.20	-2.70 ± 0.22	-0.15 ± 0.35	-0.67 ± 0.13
08	4.39 ± 0.66	-3.98 ± 0.80	-0.65 ± 0.23	-1.66 ± 0.18
09	6.38 ± 0.71	-5.70 ± 0.84	-1.31 ± 0.27	-2.47 ± 0.25

Table A.12.: Patient 6, RPV: Mean and standard deviation of target motion in all phases of the respiration, relative to the reference phase.

motion phase	ABS [mm]	SI [mm]	AP [mm]	LR [mm]
00	3.85 ± 0.46	-3.77 ± 0.48	-0.07 ± 0.20	-0.55 ± 0.52
01	1.72 ± 0.58	-1.59 ± 0.51	0.23 ± 0.31	-0.39 ± 0.46
02	0.98 ± 0.34	-0.87 ± 0.35	0.15 ± 0.15	-0.39 ± 0.08
03	0.57 ± 0.30	-0.38 ± 0.31	0.33 ± 0.18	-0.14 ± 0.14
04	0.36 ± 0.05	-0.19 ± 0.06	0.13 ± 0.04	-0.27 ± 0.05
06	0.99 ± 0.53	0.68 ± 0.66	0.29 ± 0.21	0.29 ± 0.38
07	1.64 ± 0.61	0.05 ± 1.52	0.51 ± 0.39	0.13 ± 0.56
08	2.29 ± 0.90	-1.91 ± 1.18	0.17 ± 0.53	0.06 ± 0.83
09	4.09 ± 0.45	-4.01 ± 0.47	-0.02 ± 0.37	-0.28 ± 0.68

Table A.13.: Patient 7, LPV: Mean and standard deviation of target motion in all phases of the respiration, relative to the reference phase.

motion phase	ABS [mm]	SI [mm]	AP [mm]	LR [mm]
00	3.87 ± 0.75	-3.55 ± 0.63	-1.03 ± 0.47	-1.11 ± 0.23
01	3.21 ± 0.49	-2.96 ± 0.46	-0.83 ± 0.25	-0.92 ± 0.11
02	2.72 ± 0.55	-2.46 ± 0.47	-0.77 ± 0.29	-0.83 ± 0.17
03	1.74 ± 0.29	-1.56 ± 0.24	-0.57 ± 0.19	-0.48 ± 0.09
04	0.52 ± 0.10	-0.46 ± 0.13	-0.07 ± 0.11	-0.17 ± 0.09
06	0.54 ± 0.18	-0.51 ± 0.17	-0.10 ± 0.06	-0.14 ± 0.09
07	1.28 ± 0.17	-1.21 ± 0.16	-0.19 ± 0.12	-0.34 ± 0.04
08	2.67 ± 0.51	-2.44 ± 0.43	-0.62 ± 0.33	-0.83 ± 0.19
09	3.34 ± 0.63	-3.08 ± 0.58	-0.70 ± 0.30	-1.04 ± 0.17

Table A.14.: Patient 7, RPV: Mean and standard deviation of target motion in all phases of the respiration, relative to the reference phase.

motion phase	ABS [mm]	SI [mm]	AP [mm]	LR [mm]
00	3.25 ± 1.08	-3.21 ± 1.06	-0.38 ± 0.34	-0.12 ± 0.10
01	2.88 ± 0.76	-2.84 ± 0.73	-0.39 ± 0.30	-0.01 ± 0.14
02	2.08 ± 0.57	-2.04 ± 0.54	-0.36 ± 0.23	0.09 ± 0.09
03	1.74 ± 0.37	-1.70 ± 0.35	-0.27 ± 0.16	0.09 ± 0.19
04	0.54 ± 0.11	-0.53 ± 0.11	-0.06 ± 0.07	0.01 ± 0.09
06	1.30 ± 0.23	-1.23 ± 0.21	0.17 ± 0.08	-0.36 ± 0.14
07	1.76 ± 0.57	-1.71 ± 0.58	0.12 ± 0.16	-0.33 ± 0.08
08	2.43 ± 0.77	-2.40 ± 0.77	0.03 ± 0.21	-0.35 ± 0.08
09	3.26 ± 0.94	-3.24 ± 0.93	-0.18 ± 0.28	-0.17 ± 0.10

Table A.15.: Patient 8, LPV: Mean and standard deviation of target motion in all phases of the respiration, relative to the reference phase.

motion phase	ABS [mm]	SI [mm]	AP [mm]	LR [mm]
00	9.61 ± 0.90	-9.53 ± 0.86	-1.02 ± 0.52	0.47 ± 0.38
01	8.45 ± 0.50	-8.37 ± 0.51	-0.96 ± 0.39	0.12 ± 0.30
02	4.62 ± 0.59	-4.56 ± 0.58	-0.67 ± 0.28	0.08 ± 0.27
03	3.06 ± 0.18	-2.99 ± 0.17	-0.60 ± 0.21	-0.02 ± 0.15
04	0.65 ± 0.21	-0.50 ± 0.20	-0.26 ± 0.17	-0.27 ± 0.10
06	0.56 ± 0.21	-0.52 ± 0.21	0.06 ± 0.08	-0.15 ± 0.07
07	1.58 ± 0.32	-1.53 ± 0.35	0.12 ± 0.10	0.29 ± 0.20
08	6.28 ± 0.59	-6.24 ± 0.60	-0.31 ± 0.25	0.51 ± 0.14
09	7.66 ± 0.68	-7.63 ± 0.69	-0.31 ± 0.29	0.47 ± 0.19

Table A.16.: Patient 8, RPV: Mean and standard deviation of target motion in all phases of the respiration, relative to the reference phase.

motion phase	ABS [mm]	SI [mm]	AP [mm]	LR [mm]
00	10.30 ± 1.91	-9.89 ± 1.74	-2.47 ± 0.64	1.58 ± 0.85
01	9.25 ± 1.34	-8.60 ± 1.16	-2.78 ± 0.58	1.88 ± 0.71
02	5.21 ± 1.06	-4.69 ± 0.86	-1.99 ± 0.56	0.93 ± 0.66
03	3.17 ± 0.56	-2.59 ± 0.39	-1.54 ± 0.35	0.88 ± 0.46
04	0.75 ± 0.30	-0.44 ± 0.18	-0.44 ± 0.20	0.33 ± 0.28
06	0.80 ± 0.27	-0.60 ± 0.27	0.38 ± 0.23	0.07 ± 0.26
07	3.04 ± 0.46	-2.93 ± 0.46	0.44 ± 0.34	0.43 ± 0.42
08	8.21 ± 0.57	-8.11 ± 0.56	-0.77 ± 0.15	0.93 ± 0.33
09	9.06 ± 0.95	-8.80 ± 0.86	-1.47 ± 0.32	1.46 ± 0.64

Table A.17.: Patient 9, LPV: Mean and standard deviation of target motion in all phases of the respiration, relative to the reference phase.

motion phase	ABS [mm]	SI [mm]	AP [mm]	LR [mm]
00	15.50 ± 3.02	-15.40 ± 3.01	-0.39 ± 0.46	-0.44 ± 0.96
01	13.30 ± 2.83	-13.30 ± 2.83	-0.29 ± 0.44	-0.12 ± 0.77
02	8.57 ± 2.21	-8.54 ± 2.21	-0.17 ± 0.40	0.12 ± 0.56
03	3.75 ± 1.17	-3.71 ± 1.19	-0.01 ± 0.15	0.32 ± 0.38
04	1.19 ± 0.24	-1.19 ± 0.25	-0.03 ± 0.04	0.07 ± 0.05
06	0.22 ± 0.08	0.19 ± 0.12	0.02 ± 0.03	0.02 ± 0.05
07	3.26 ± 1.38	-3.12 ± 1.50	0.12 ± 0.17	0.55 ± 0.40
08	10.40 ± 3.05	-10.40 ± 3.07	-0.24 ± 0.33	0.21 ± 0.61
09	14.10 ± 3.07	-14.00 ± 3.06	-0.41 ± 0.45	-0.24 ± 0.88

Table A.18.: Patient 9, RPV: Mean and standard deviation of target motion in all phases of the respiration, relative to the reference phase.

motion phase	ABS [mm]	SI [mm]	AP [mm]	LR [mm]
00	10.90 ± 1.06	-10.50 ± 1.06	-0.21 ± 0.19	2.62 ± 0.54
01	7.79 ± 0.86	-7.38 ± 0.81	-0.13 ± 0.15	2.44 ± 0.58
02	4.58 ± 0.64	-4.04 ± 0.55	-0.12 ± 0.13	2.09 ± 0.57
03	2.40 ± 0.50	-1.87 ± 0.32	-0.10 ± 0.12	1.47 ± 0.46
04	0.61 ± 0.17	-0.47 ± 0.11	-0.04 ± 0.05	0.37 ± 0.18
06	0.17 ± 0.11	-0.11 ± 0.14	0.00 ± 0.03	0.02 ± 0.08
07	2.69 ± 0.62	-2.28 ± 0.58	-0.08 ± 0.10	1.38 ± 0.38
08	5.75 ± 0.78	-5.30 ± 0.74	-0.24 ± 0.14	2.18 ± 0.55
09	9.36 ± 0.96	-8.99 ± 0.97	-0.26 ± 0.18	2.52 ± 0.54

A.2 Values of dose analysis parameters for all patients

In the following the D5-D95, V95 and V107 values will be presented for all patient data sets (patient 1 to 9) and target volumes (LPV and RPV). All studied techniques (static, interplay and gating inbetween motion phase four and six) will be shown for four different motion patterns and all studied safety margins (0mm, 3mm, 5mm, 7mm). Moreover rescanning within the gating window was studied for the target volumes of patient 2 (medium absolute displacement of the PVs due to respiration) and patient 9 (largest studied absolute displacement of the PVs due to respiration).

Table A.19.: Patient 1, LPV

Case	motion period	motion starting phase	Margin	D5-D95	V95	V107
STATIC	-	-	0mm	2.00	100.00	0.00
STATIC	-	-	3mm	1.83	100.00	0.00
STATIC	-	-	5mm	1.86	100.00	0.00
STATIC	-	-	7mm	1.82	100.00	0.00
INTERPLAY	6s	0	0mm	16.23	75.30	5.01
INTERPLAY	6s	90	0mm	11.37	98.81	8.47
INTERPLAY	8s	0	0mm	14.51	89.74	7.28
INTERPLAY	8s	90	0mm	15.31	85.32	7.88
INTERPLAY	6s	0	3mm	11.73	86.52	1.31
INTERPLAY	6s	90	3mm	10.60	97.37	4.30
INTERPLAY	8s	0	3mm	8.75	92.24	0.24
INTERPLAY	8s	90	3mm	9.98	96.90	3.10
INTERPLAY	6s	0	5mm	8.91	94.15	0.24
INTERPLAY	6s	90	5mm	7.98	97.97	0.36
INTERPLAY	8s	0	5mm	8.69	98.57	0.36
INTERPLAY	8s	90	5mm	10.02	97.49	0.60
INTERPLAY	6s	0	7mm	5.79	100.00	0.00
INTERPLAY	6s	90	7mm	6.86	99.88	0.00
INTERPLAY	8s	0	7mm	7.74	98.09	0.00
INTERPLAY	8s	90	7mm	8.09	96.78	0.12
GATING	6s	0	0mm	5.37	99.40	0.00
GATING	6s	90	0mm	5.53	99.28	0.00
GATING	8s	0	0mm	5.65	99.40	0.00
GATING	8s	90	0mm	5.57	99.28	0.00
GATING	6s	0	3mm	4.41	99.88	0.00
GATING	6s	90	3mm	4.41	99.88	0.00
GATING	8s	0	3mm	4.39	99.52	0.00
GATING	8s	90	3mm	4.43	99.64	0.00
GATING	6s	0	5mm	3.88	100.00	0.00
GATING	6s	90	5mm	3.76	100.00	0.00
GATING	8s	0	5mm	3.77	99.76	0.00
GATING	8s	90	5mm	4.36	99.88	0.00
GATING	6s	0	7mm	3.50	100.00	0.00
GATING	6s	90	7mm	3.47	100.00	0.00
GATING	8s	0	7mm	3.29	100.00	0.00
GATING	8s	90	7mm	3.17	100.00	0.00

Table A.20.: Patient 1, RPV

Case	motion period	motion starting phase	Margin	D5-D95	V95	V107
STATIC	-	-	0mm	2.36	100.00	0.00
STATIC	-	-	3mm	1.81	100.00	0.00
STATIC	-	-	5mm	1.85	100.00	0.00
STATIC	-	-	7mm	1.84	100.00	0.00
INTERPLAY	6s	0	0mm	20.62	69.21	6.22
INTERPLAY	6s	90	0mm	16.39	75.47	1.08
INTERPLAY	8s	0	0mm	18.83	80.30	8.57
INTERPLAY	8s	90	0mm	15.38	76.42	3.47
INTERPLAY	6s	0	3mm	10.54	91.03	0.54
INTERPLAY	6s	90	3mm	11.63	92.38	1.49
INTERPLAY	8s	0	3mm	11.86	88.68	1.71
INTERPLAY	8s	90	3mm	10.59	96.48	2.39
INTERPLAY	6s	0	5mm	9.46	96.71	1.13
INTERPLAY	6s	90	5mm	9.72	94.54	0.32
INTERPLAY	8s	0	5mm	12.43	79.80	0.72
INTERPLAY	8s	90	5mm	9.11	99.10	1.40
INTERPLAY	6s	0	7mm	9.29	97.88	1.22
INTERPLAY	6s	90	7mm	10.18	89.59	0.00
INTERPLAY	8s	0	7mm	11.44	87.65	0.50
INTERPLAY	8s	90	7mm	9.92	91.61	0.45
GATING	6s	0	0mm	3.62	99.95	0.00
GATING	6s	90	0mm	3.63	99.95	0.00
GATING	8s	0	0mm	4.02	99.95	0.00
GATING	8s	90	0mm	4.03	99.91	0.00
GATING	6s	0	3mm	3.40	100.00	0.00
GATING	6s	90	3mm	3.40	100.00	0.00
GATING	8s	0	3mm	3.51	100.00	0.00
GATING	8s	90	3mm	3.45	100.00	0.00
GATING	6s	0	5mm	3.40	100.00	0.00
GATING	6s	90	5mm	3.37	100.00	0.00
GATING	8s	0	5mm	3.04	100.00	0.00
GATING	8s	90	5mm	2.98	100.00	0.00
GATING	6s	0	7mm	3.00	100.00	0.00
GATING	6s	90	7mm	3.08	100.00	0.00
GATING	8s	0	7mm	3.09	100.00	0.00
GATING	8s	90	7mm	3.22	100.00	0.00

Table A.21.: Patient 2, LPV

Case	motion period	motion starting phase	Margin	D5-D95	V95	V107
STATIC	-	-	0mm	1.89	100.00	0.00
STATIC	-	-	3mm	1.85	100.00	0.00
STATIC	-	-	5mm	1.85	100.00	0.00
STATIC	-	-	7mm	1.86	100.00	0.00
INTERPLAY	6s	0	0mm	10.82	92.42	1.37
INTERPLAY	6s	90	0mm	10.68	94.97	2.35
INTERPLAY	8s	0	0mm	8.70	97.78	1.31
INTERPLAY	8s	90	0mm	8.56	96.54	1.31
INTERPLAY	6s	0	3mm	8.38	98.82	0.07
INTERPLAY	6s	90	3mm	8.41	98.63	0.33
INTERPLAY	8s	0	3mm	6.98	99.41	0.00
INTERPLAY	8s	90	3mm	7.77	98.76	1.11
INTERPLAY	6s	0	5mm	7.34	97.71	0.13
INTERPLAY	6s	90	5mm	7.15	99.28	0.00
INTERPLAY	8s	0	5mm	7.20	100.00	0.13
INTERPLAY	8s	90	5mm	7.32	98.69	0.00
INTERPLAY	6s	0	7mm	6.07	99.87	0.00
INTERPLAY	6s	90	7mm	7.01	99.48	0.20
INTERPLAY	8s	0	7mm	6.40	99.48	0.00
INTERPLAY	8s	90	7mm	6.44	99.08	0.00
GATING	6s	0	0mm	6.96	99.41	0.13
GATING	6s	90	0mm	6.93	99.28	0.00
GATING	8s	0	0mm	6.71	99.87	0.00
GATING	8s	90	0mm	7.12	99.67	0.00
GATING	6s	0	3mm	6.81	98.43	0.07
GATING	6s	90	3mm	6.79	98.37	0.07
GATING	8s	0	3mm	4.94	99.93	0.00
GATING	8s	90	3mm	5.10	99.93	0.00
GATING	6s	0	5mm	5.27	100.00	0.00
GATING	6s	90	5mm	4.98	99.93	0.00
GATING	8s	0	5mm	5.39	99.41	0.00
GATING	8s	90	5mm	5.54	99.22	0.00
GATING	6s	0	7mm	4.60	100.00	0.00
GATING	6s	90	7mm	4.53	100.00	0.00
GATING	8s	0	7mm	4.89	100.00	0.00
GATING	8s	90	7mm	4.30	100.00	0.00

Table A.22.: Patient 2, RPV

Case	motion period	motion starting phase	Margin	D5-D95	V95	V107
STATIC	-	-	0mm	1.85	100.00	0.00
STATIC	-	-	3mm	1.82	100.00	0.00
STATIC	-	-	5mm	1.84	100.00	0.00
STATIC	-	-	7mm	1.81	100.00	0.00
INTERPLAY	6s	0	0mm	10.03	98.51	3.32
INTERPLAY	6s	90	0mm	9.87	97.52	1.78
INTERPLAY	8s	0	0mm	9.31	96.53	0.74
INTERPLAY	8s	90	0mm	10.27	96.14	1.44
INTERPLAY	6s	0	3mm	6.64	97.92	0.00
INTERPLAY	6s	90	3mm	7.38	99.01	0.00
INTERPLAY	8s	0	3mm	7.43	96.53	0.00
INTERPLAY	8s	90	3mm	7.67	95.84	0.00
INTERPLAY	6s	0	5mm	8.73	97.77	0.64
INTERPLAY	6s	90	5mm	8.84	96.73	0.64
INTERPLAY	8s	0	5mm	7.29	98.47	0.20
INTERPLAY	8s	90	5mm	7.80	99.50	0.20
INTERPLAY	6s	0	7mm	6.61	98.61	0.00
INTERPLAY	6s	90	7mm	7.38	98.07	0.00
INTERPLAY	8s	0	7mm	7.01	99.01	0.00
INTERPLAY	8s	90	7mm	7.53	97.77	1.24
GATING	6s	0	0mm	6.04	97.57	0.00
GATING	6s	90	0mm	6.02	98.07	0.00
GATING	8s	0	0mm	6.32	98.17	0.00
GATING	8s	90	0mm	6.19	98.27	0.00
GATING	6s	0	3mm	4.87	99.01	0.00
GATING	6s	90	3mm	4.95	99.70	0.00
GATING	8s	0	3mm	4.27	99.90	0.00
GATING	8s	90	3mm	4.37	99.75	0.00
GATING	6s	0	5mm	4.26	100.00	0.00
GATING	6s	90	5mm	4.05	100.00	0.00
GATING	8s	0	5mm	4.28	99.95	0.00
GATING	8s	90	5mm	3.92	99.95	0.10
GATING	6s	0	7mm	3.70	100.00	0.00
GATING	6s	90	7mm	3.73	100.00	0.00
GATING	8s	0	7mm	3.81	99.95	0.00
GATING	8s	90	7mm	3.81	99.85	0.00

Table A.23.: Patient 3, LPV

Case	motion period	motion starting phase	Margin	D5-D95	V95	V107
STATIC	-	-	0mm	2.24	100.00	0.00
STATIC	-	-	3mm	1.84	100.00	0.00
STATIC	-	-	5mm	1.82	100.00	0.00
STATIC	-	-	7mm	1.82	100.00	0.00
INTERPLAY	6s	0	0mm	15.27	89.72	8.00
INTERPLAY	6s	90	0mm	13.25	89.24	4.35
INTERPLAY	8s	0	0mm	15.22	88.98	7.56
INTERPLAY	8s	90	0mm	13.31	88.72	3.80
INTERPLAY	6s	0	3mm	10.89	93.14	1.51
INTERPLAY	6s	90	3mm	11.06	90.93	1.36
INTERPLAY	8s	0	3mm	10.35	96.06	1.22
INTERPLAY	8s	90	3mm	11.36	93.25	1.58
INTERPLAY	6s	0	5mm	11.44	89.50	1.14
INTERPLAY	6s	90	5mm	10.98	96.83	3.83
INTERPLAY	8s	0	5mm	10.54	92.41	0.63
INTERPLAY	8s	90	5mm	10.86	94.36	2.73
INTERPLAY	6s	0	7mm	9.75	97.09	1.58
INTERPLAY	6s	90	7mm	8.92	96.31	0.55
INTERPLAY	8s	0	7mm	10.81	98.45	4.50
INTERPLAY	8s	90	7mm	11.06	94.25	2.43
GATING	6s	0	0mm	7.09	99.04	0.22
GATING	6s	90	0mm	7.45	98.93	0.18
GATING	8s	0	0mm	7.53	98.16	0.44
GATING	8s	90	0mm	8.06	96.98	0.22
GATING	6s	0	3mm	6.43	99.93	0.00
GATING	6s	90	3mm	6.43	100.00	0.04
GATING	8s	0	3mm	6.27	99.93	0.15
GATING	8s	90	3mm	6.27	99.85	0.15
GATING	6s	0	5mm	6.44	99.89	0.04
GATING	6s	90	5mm	6.35	99.85	0.04
GATING	8s	0	5mm	5.82	99.71	0.00
GATING	8s	90	5mm	6.40	98.71	0.07
GATING	6s	0	7mm	5.22	99.96	0.04
GATING	6s	90	7mm	5.16	100.00	0.00
GATING	8s	0	7mm	5.02	100.00	0.00
GATING	8s	90	7mm	5.00	100.00	0.00

Table A.24.: Patient 3, RPV

Case	motion period	motion starting phase	Margin	D5-D95	V95	V107
STATIC	-	-	0mm	1.89	100.00	0.00
STATIC	-	-	3mm	1.82	100.00	0.00
STATIC	-	-	5mm	1.81	100.00	0.00
STATIC	-	-	7mm	1.86	100.00	0.00
INTERPLAY	6s	0	0mm	12.34	88.95	1.01
INTERPLAY	6s	90	0mm	12.23	91.57	3.84
INTERPLAY	8s	0	0mm	12.39	91.63	3.69
INTERPLAY	8s	90	0mm	11.66	93.24	3.05
INTERPLAY	6s	0	3mm	9.29	95.81	0.56
INTERPLAY	6s	90	3mm	9.46	97.11	1.26
INTERPLAY	8s	0	3mm	12.20	92.64	3.05
INTERPLAY	8s	90	3mm	12.80	92.04	5.07
INTERPLAY	6s	0	5mm	8.79	98.39	1.42
INTERPLAY	6s	90	5mm	9.26	97.42	0.91
INTERPLAY	8s	0	5mm	10.30	97.01	1.88
INTERPLAY	8s	90	5mm	9.88	96.19	1.15
INTERPLAY	6s	0	7mm	9.31	97.32	1.09
INTERPLAY	6s	90	7mm	8.63	98.78	0.49
INTERPLAY	8s	0	7mm	10.44	94.89	1.79
INTERPLAY	8s	90	7mm	9.97	95.98	0.72
GATING	6s	0	0mm	5.00	99.86	0.00
GATING	6s	90	0mm	5.02	99.86	0.00
GATING	8s	0	0mm	5.31	99.86	0.00
GATING	8s	90	0mm	5.57	99.77	0.06
GATING	6s	0	3mm	4.49	100.00	0.00
GATING	6s	90	3mm	4.58	100.00	0.00
GATING	8s	0	3mm	4.49	100.00	0.06
GATING	8s	90	3mm	4.88	100.00	0.02
GATING	6s	0	5mm	4.94	100.00	0.00
GATING	6s	90	5mm	4.89	100.00	0.00
GATING	8s	0	5mm	4.45	100.00	0.00
GATING	8s	90	5mm	4.29	100.00	0.00
GATING	6s	0	7mm	4.08	100.00	0.00
GATING	6s	90	7mm	3.89	100.00	0.00
GATING	8s	0	7mm	3.85	99.98	0.00
GATING	8s	90	7mm	3.84	100.00	0.00

Table A.25.: Patient 4, LPV

Case	motion period	motion starting phase	Margin	D5-D95	V95	V107
STATIC	-	-	0mm	1.90	100.00	0.00
STATIC	-	-	3mm	1.83	100.00	0.00
STATIC	-	-	5mm	1.87	100.00	0.00
STATIC	-	-	7mm	1.82	100.00	0.00
INTERPLAY	6s	0	0mm	11.02	93.01	1.20
INTERPLAY	6s	90	0mm	10.34	93.08	1.13
INTERPLAY	8s	0	0mm	16.87	84.43	7.32
INTERPLAY	8s	90	0mm	14.22	85.89	4.92
INTERPLAY	6s	0	3mm	6.43	99.40	0.00
INTERPLAY	6s	90	3mm	7.46	98.74	0.07
INTERPLAY	8s	0	3mm	11.73	90.69	2.53
INTERPLAY	8s	90	3mm	12.31	85.43	0.86
INTERPLAY	6s	0	5mm	6.66	98.20	0.00
INTERPLAY	6s	90	5mm	7.47	98.94	0.00
INTERPLAY	8s	0	5mm	9.12	96.67	0.73
INTERPLAY	8s	90	5mm	9.91	94.48	0.47
INTERPLAY	6s	0	7mm	6.21	97.94	0.00
INTERPLAY	6s	90	7mm	7.09	98.60	0.00
INTERPLAY	8s	0	7mm	7.18	98.14	0.00
INTERPLAY	8s	90	7mm	6.74	99.53	0.60
GATING	6s	0	0mm	3.89	99.93	0.00
GATING	6s	90	0mm	3.81	99.93	0.00
GATING	8s	0	0mm	3.94	99.93	0.00
GATING	8s	90	0mm	4.48	99.87	0.00
GATING	6s	0	3mm	2.87	100.00	0.00
GATING	6s	90	3mm	2.88	100.00	0.00
GATING	8s	0	3mm	3.20	100.00	0.00
GATING	8s	90	3mm	3.10	100.00	0.00
GATING	6s	0	5mm	2.90	100.00	0.00
GATING	6s	90	5mm	3.03	100.00	0.00
GATING	8s	0	5mm	2.94	100.00	0.00
GATING	8s	90	5mm	3.13	100.00	0.00
GATING	6s	0	7mm	2.99	100.00	0.00
GATING	6s	90	7mm	3.01	100.00	0.00
GATING	8s	0	7mm	2.88	100.00	0.00
GATING	8s	90	7mm	2.83	100.00	0.00

Table A.26.: Patient 4, RPV

Case	motion period	motion starting phase	Margin	D5-D95	V95	V107
STATIC	-	-	0mm	1.83	100.00	0.00
STATIC	-	-	3mm	1.80	100.00	0.00
STATIC	-	-	5mm	1.80	100.00	0.00
STATIC	-	-	7mm	1.80	100.00	0.00
INTERPLAY	6s	0	0mm	12.60	89.91	1.94
INTERPLAY	6s	90	0mm	11.01	90.89	1.82
INTERPLAY	8s	0	0mm	13.99	87.18	5.29
INTERPLAY	8s	90	0mm	13.89	86.21	3.71
INTERPLAY	6s	0	3mm	9.72	93.13	0.30
INTERPLAY	6s	90	3mm	9.21	96.60	0.61
INTERPLAY	8s	0	3mm	10.68	91.92	1.46
INTERPLAY	8s	90	3mm	11.23	91.07	1.52
INTERPLAY	6s	0	5mm	9.77	95.57	0.18
INTERPLAY	6s	90	5mm	8.60	98.12	0.24
INTERPLAY	8s	0	5mm	9.75	94.47	0.43
INTERPLAY	8s	90	5mm	9.55	97.21	1.28
INTERPLAY	6s	0	7mm	6.84	96.17	0.00
INTERPLAY	6s	90	7mm	6.25	99.70	0.00
INTERPLAY	8s	0	7mm	8.04	98.66	0.00
INTERPLAY	8s	90	7mm	8.81	93.92	0.00
GATING	6s	0	0mm	4.81	100.00	0.00
GATING	6s	90	0mm	4.86	100.00	0.00
GATING	8s	0	0mm	5.46	100.00	0.06
GATING	8s	90	0mm	5.21	99.94	0.12
GATING	6s	0	3mm	4.04	100.00	0.00
GATING	6s	90	3mm	4.03	100.00	0.00
GATING	8s	0	3mm	4.10	100.00	0.00
GATING	8s	90	3mm	4.26	100.00	0.00
GATING	6s	0	5mm	3.61	100.00	0.00
GATING	6s	90	5mm	3.64	100.00	0.00
GATING	8s	0	5mm	3.59	100.00	0.00
GATING	8s	90	5mm	3.62	100.00	0.00
GATING	6s	0	7mm	2.79	100.00	0.00
GATING	6s	90	7mm	2.81	100.00	0.00
GATING	8s	0	7mm	3.29	100.00	0.00
GATING	8s	90	7mm	3.24	100.00	0.00

Table A.27.: Patient 5, LPV

Case	motion period	motion starting phase	Margin	D5-D95	V95	V107
STATIC	-	-	0mm	1.94	100.00	0.00
STATIC	-	-	3mm	1.84	100.00	0.00
STATIC	-	-	5mm	1.83	100.00	0.00
STATIC	-	-	7mm	1.82	100.00	0.00
INTERPLAY	6s	0	0mm	18.21	89.36	18.18
INTERPLAY	6s	90	0mm	14.34	88.25	5.10
INTERPLAY	8s	0	0mm	16.67	81.26	7.87
INTERPLAY	8s	90	0mm	14.40	92.13	8.98
INTERPLAY	6s	0	3mm	14.58	89.14	6.32
INTERPLAY	6s	90	3mm	12.31	88.58	1.66
INTERPLAY	8s	0	3mm	14.69	85.92	6.98
INTERPLAY	8s	90	3mm	14.49	90.02	6.76
INTERPLAY	6s	0	5mm	10.64	83.92	0.11
INTERPLAY	6s	90	5mm	13.25	95.57	7.76
INTERPLAY	8s	0	5mm	14.70	92.35	14.74
INTERPLAY	8s	90	5mm	11.10	87.92	0.44
INTERPLAY	6s	0	7mm	8.34	99.89	1.44
INTERPLAY	6s	90	7mm	7.34	96.01	0.00
INTERPLAY	8s	0	7mm	10.66	96.34	1.77
INTERPLAY	8s	90	7mm	10.14	95.57	0.22
GATING	6s	0	0mm	7.22	99.45	0.67
GATING	6s	90	0mm	7.21	99.45	0.67
GATING	8s	0	0mm	8.88	95.23	0.33
GATING	8s	90	0mm	9.18	95.23	0.11
GATING	6s	0	3mm	6.10	98.78	0.00
GATING	6s	90	3mm	6.16	98.56	0.11
GATING	8s	0	3mm	7.27	99.78	0.00
GATING	8s	90	3mm	7.71	99.45	0.00
GATING	6s	0	5mm	6.81	98.45	0.00
GATING	6s	90	5mm	6.76	98.45	0.00
GATING	8s	0	5mm	7.44	97.34	0.00
GATING	8s	90	5mm	7.25	97.56	0.00
GATING	6s	0	7mm	5.28	98.89	0.00
GATING	6s	90	7mm	5.43	99.00	0.00
GATING	8s	0	7mm	5.60	100.00	0.00
GATING	8s	90	7mm	5.36	100.00	0.00

Table A.28.: Patient 5, RPV

Case	motion period	motion starting phase	Margin	D5-D95	V95	V107
STATIC	-	-	0mm	1.85	100.00	0.00
STATIC	-	-	3mm	1.85	100.00	0.00
STATIC	-	-	5mm	1.81	100.00	0.00
STATIC	-	-	7mm	1.81	100.00	0.00
INTERPLAY	6s	0	0mm	12.27	95.36	6.05
INTERPLAY	6s	90	0mm	11.59	93.63	2.38
INTERPLAY	8s	0	0mm	16.30	86.88	8.91
INTERPLAY	8s	90	0mm	12.29	94.87	5.35
INTERPLAY	6s	0	3mm	11.61	95.52	4.16
INTERPLAY	6s	90	3mm	9.22	94.98	0.92
INTERPLAY	8s	0	3mm	12.87	87.53	2.86
INTERPLAY	8s	90	3mm	12.27	97.68	7.02
INTERPLAY	6s	0	5mm	11.58	92.98	1.46
INTERPLAY	6s	90	5mm	11.04	95.25	2.70
INTERPLAY	8s	0	5mm	12.42	86.77	1.84
INTERPLAY	8s	90	5mm	12.55	86.45	2.05
INTERPLAY	6s	0	7mm	9.05	99.08	0.59
INTERPLAY	6s	90	7mm	8.15	98.92	0.11
INTERPLAY	8s	0	7mm	8.60	98.11	0.65
INTERPLAY	8s	90	7mm	8.96	98.87	1.46
GATING	6s	0	0mm	5.79	99.89	0.00
GATING	6s	90	0mm	5.78	99.89	0.00
GATING	8s	0	0mm	5.44	99.62	0.00
GATING	8s	90	0mm	5.38	99.68	0.00
GATING	6s	0	3mm	5.19	100.00	0.00
GATING	6s	90	3mm	5.10	100.00	0.00
GATING	8s	0	3mm	5.99	100.00	0.00
GATING	8s	90	3mm	5.67	100.00	0.00
GATING	6s	0	5mm	4.54	99.89	0.00
GATING	6s	90	5mm	4.57	99.95	0.00
GATING	8s	0	5mm	4.62	100.00	0.00
GATING	8s	90	5mm	4.92	100.00	0.00
GATING	6s	0	7mm	3.86	100.00	0.00
GATING	6s	90	7mm	3.83	100.00	0.00
GATING	8s	0	7mm	4.27	100.00	0.00
GATING	8s	90	7mm	4.68	100.00	0.00

Table A.29.: Patient 6, LPV

Case	motion period	motion starting phase	Margin	D5-D95	V95	V107
STATIC	-	-	0mm	1.86	100.00	0.00
STATIC	-	-	3mm	1.84	100.00	0.00
STATIC	-	-	5mm	1.81	100.00	0.00
STATIC	-	-	7mm	1.83	100.00	0.00
INTERPLAY	6s	0	0mm	12.07	91.36	4.04
INTERPLAY	6s	90	0mm	12.94	86.83	1.13
INTERPLAY	8s	0	0mm	17.12	75.14	5.17
INTERPLAY	8s	90	0mm	16.66	81.02	4.32
INTERPLAY	6s	0	3mm	11.39	95.25	3.54
INTERPLAY	6s	90	3mm	8.61	96.60	0.35
INTERPLAY	8s	0	3mm	10.19	93.41	0.42
INTERPLAY	8s	90	3mm	11.22	94.41	2.62
INTERPLAY	6s	0	5mm	8.22	97.80	0.57
INTERPLAY	6s	90	5mm	8.17	96.32	0.00
INTERPLAY	8s	0	5mm	11.32	90.37	1.20
INTERPLAY	8s	90	5mm	10.66	92.42	1.20
INTERPLAY	6s	0	7mm	7.62	97.52	0.00
INTERPLAY	6s	90	7mm	8.20	96.88	0.14
INTERPLAY	8s	0	7mm	9.18	92.78	0.71
INTERPLAY	8s	90	7mm	8.25	94.83	0.00
GATING	6s	0	0mm	7.75	96.32	0.00
GATING	6s	90	0mm	7.83	95.96	0.00
GATING	8s	0	0mm	7.48	97.95	0.00
GATING	8s	90	0mm	7.49	98.37	0.00
GATING	6s	0	3mm	4.92	100.00	0.00
GATING	6s	90	3mm	4.92	100.00	0.00
GATING	8s	0	3mm	5.04	100.00	0.00
GATING	8s	90	3mm	4.63	100.00	0.00
GATING	6s	0	5mm	4.21	100.00	0.00
GATING	6s	90	5mm	4.17	100.00	0.00
GATING	8s	0	5mm	4.34	100.00	0.00
GATING	8s	90	5mm	4.21	100.00	0.00
GATING	6s	0	7mm	4.13	100.00	0.00
GATING	6s	90	7mm	4.12	100.00	0.00
GATING	8s	0	7mm	4.45	100.00	0.00
GATING	8s	90	7mm	4.26	100.00	0.00

Table A.30.: Patient 6, RPV

Case	motion period	motion starting phase	Margin	D5-D95	V95	V107
STATIC	-	-	0mm	1.84	100.00	0.00
STATIC	-	-	3mm	1.81	100.00	0.00
STATIC	-	-	5mm	1.81	100.00	0.00
STATIC	-	-	7mm	1.82	100.00	0.00
INTERPLAY	6s	0	0mm	10.31	96.14	3.00
INTERPLAY	6s	90	0mm	10.75	91.82	0.60
INTERPLAY	8s	0	0mm	10.86	95.68	2.93
INTERPLAY	8s	90	0mm	8.92	98.27	1.31
INTERPLAY	6s	0	3mm	10.26	98.05	3.75
INTERPLAY	6s	90	3mm	7.78	98.05	0.08
INTERPLAY	8s	0	3mm	9.51	97.07	1.73
INTERPLAY	8s	90	3mm	8.26	98.80	0.64
INTERPLAY	6s	0	5mm	7.57	99.10	1.05
INTERPLAY	6s	90	5mm	7.80	99.44	0.83
INTERPLAY	8s	0	5mm	8.46	95.68	0.26
INTERPLAY	8s	90	5mm	7.17	98.16	0.15
INTERPLAY	6s	0	7mm	6.83	99.77	0.00
INTERPLAY	6s	90	7mm	8.54	99.70	2.03
INTERPLAY	8s	0	7mm	7.30	97.82	0.08
INTERPLAY	8s	90	7mm	7.45	97.07	0.08
GATING	6s	0	0mm	6.72	98.20	0.08
GATING	6s	90	0mm	6.85	98.20	0.00
GATING	8s	0	0mm	6.47	99.59	0.04
GATING	8s	90	0mm	6.06	99.74	0.26
GATING	6s	0	3mm	5.09	100.00	0.00
GATING	6s	90	3mm	5.23	99.96	0.00
GATING	8s	0	3mm	5.84	98.69	0.00
GATING	8s	90	3mm	5.04	99.96	0.08
GATING	6s	0	5mm	4.57	100.00	0.00
GATING	6s	90	5mm	4.60	100.00	0.00
GATING	8s	0	5mm	4.91	100.00	0.00
GATING	8s	90	5mm	4.87	100.00	0.04
GATING	6s	0	7mm	4.79	99.14	0.00
GATING	6s	90	7mm	4.89	99.14	0.00
GATING	8s	0	7mm	4.03	100.00	0.00
GATING	8s	90	7mm	4.10	99.96	0.00

Table A.31.: Patient 7, LPV

Case	motion period	motion starting phase	Margin	D5-D95	V95	V107
STATIC	-	-	0mm	1.94	100.00	0.00
STATIC	-	-	3mm	1.91	100.00	0.00
STATIC	-	-	5mm	1.82	100.00	0.00
STATIC	-	-	7mm	1.83	100.00	0.00
INTERPLAY	6s	0	0mm	9.82	96.78	2.00
INTERPLAY	6s	90	0mm	13.32	89.78	4.16
INTERPLAY	8s	0	0mm	9.07	98.61	1.78
INTERPLAY	8s	90	0mm	9.51	97.89	2.44
INTERPLAY	6s	0	3mm	6.04	99.94	0.06
INTERPLAY	6s	90	3mm	7.69	95.78	0.00
INTERPLAY	8s	0	3mm	10.55	94.45	2.61
INTERPLAY	8s	90	3mm	8.83	94.45	0.50
INTERPLAY	6s	0	5mm	7.87	98.45	0.00
INTERPLAY	6s	90	5mm	5.85	99.50	0.00
INTERPLAY	8s	0	5mm	8.96	96.67	0.78
INTERPLAY	8s	90	5mm	8.23	96.72	0.11
INTERPLAY	6s	0	7mm	5.48	99.83	0.00
INTERPLAY	6s	90	7mm	6.16	99.44	0.00
INTERPLAY	8s	0	7mm	6.63	98.94	0.00
INTERPLAY	8s	90	7mm	7.18	99.78	0.06
GATING	6s	0	0mm	6.55	99.28	0.00
GATING	6s	90	0mm	6.60	99.11	0.00
GATING	8s	0	0mm	5.70	99.78	0.06
GATING	8s	90	0mm	5.55	99.72	0.00
GATING	6s	0	3mm	3.46	100.00	0.00
GATING	6s	90	3mm	3.51	100.00	0.00
GATING	8s	0	3mm	3.66	100.00	0.00
GATING	8s	90	3mm	3.71	100.00	0.00
GATING	6s	0	5mm	3.66	100.00	0.00
GATING	6s	90	5mm	3.63	100.00	0.00
GATING	8s	0	5mm	3.65	100.00	0.00
GATING	8s	90	5mm	3.56	100.00	0.00
GATING	6s	0	7mm	3.70	99.94	0.00
GATING	6s	90	7mm	3.69	99.94	0.00
GATING	8s	0	7mm	3.40	99.94	0.00
GATING	8s	90	7mm	3.41	100.00	0.00

Table A.32.: Patient 7, RPV

Case	motion period	motion starting phase	Margin	D5-D95	V95	V107
STATIC	-	-	0mm	1.98	100.00	0.00
STATIC	-	-	3mm	1.80	100.00	0.00
STATIC	-	-	5mm	1.81	100.00	0.00
STATIC	-	-	7mm	1.80	100.00	0.00
INTERPLAY	6s	0	0mm	9.07	96.63	0.81
INTERPLAY	6s	90	0mm	8.12	98.80	0.46
INTERPLAY	8s	0	0mm	9.16	97.10	0.39
INTERPLAY	8s	90	0mm	9.57	95.28	0.31
INTERPLAY	6s	0	3mm	6.02	100.00	0.00
INTERPLAY	6s	90	3mm	6.76	99.23	0.00
INTERPLAY	8s	0	3mm	7.28	99.69	0.39
INTERPLAY	8s	90	3mm	7.52	99.23	0.04
INTERPLAY	6s	0	5mm	6.53	99.26	0.00
INTERPLAY	6s	90	5mm	5.62	99.77	0.00
INTERPLAY	8s	0	5mm	7.31	98.68	0.00
INTERPLAY	8s	90	5mm	6.23	99.81	0.00
INTERPLAY	6s	0	7mm	5.87	99.73	0.00
INTERPLAY	6s	90	7mm	6.25	99.81	0.00
INTERPLAY	8s	0	7mm	6.06	99.73	0.00
INTERPLAY	8s	90	7mm	5.99	99.34	0.04
GATING	6s	0	0mm	7.19	98.95	0.58
GATING	6s	90	0mm	7.05	98.99	0.50
GATING	8s	0	0mm	6.05	100.00	0.08
GATING	8s	90	0mm	6.14	100.00	0.35
GATING	6s	0	3mm	5.23	100.00	0.00
GATING	6s	90	3mm	5.23	100.00	0.00
GATING	8s	0	3mm	5.29	99.77	0.00
GATING	8s	90	3mm	5.25	99.92	0.00
GATING	6s	0	5mm	5.34	99.96	0.00
GATING	6s	90	5mm	5.29	100.00	0.00
GATING	8s	0	5mm	3.92	99.92	0.00
GATING	8s	90	5mm	4.03	99.85	0.00
GATING	6s	0	7mm	4.06	100.00	0.00
GATING	6s	90	7mm	4.06	100.00	0.00
GATING	8s	0	7mm	3.76	100.00	0.00
GATING	8s	90	7mm	4.27	100.00	0.00

Table A.33.: Patient 8, LPV

Case	motion period	motion starting phase	Margin	D5-D95	V95	V107
STATIC	-	-	0mm	1.87	100.00	0.00
STATIC	-	-	3mm	1.83	100.00	0.00
STATIC	-	-	5mm	1.82	100.00	0.00
STATIC	-	-	7mm	1.87	100.00	0.00
INTERPLAY	6s	0	0mm	14.40	90.64	6.93
INTERPLAY	6s	90	0mm	13.52	87.62	2.64
INTERPLAY	8s	0	0mm	12.77	90.54	4.64
INTERPLAY	8s	90	0mm	13.36	92.68	6.16
INTERPLAY	6s	0	3mm	11.81	89.48	0.70
INTERPLAY	6s	90	3mm	9.36	96.55	1.23
INTERPLAY	8s	0	3mm	11.30	92.16	1.48
INTERPLAY	8s	90	3mm	11.67	90.78	1.93
INTERPLAY	6s	0	5mm	9.04	97.96	0.46
INTERPLAY	6s	90	5mm	9.32	94.58	0.25
INTERPLAY	8s	0	5mm	10.09	95.81	2.00
INTERPLAY	8s	90	5mm	10.69	94.69	1.93
INTERPLAY	6s	0	7mm	8.53	98.49	1.06
INTERPLAY	6s	90	7mm	9.93	98.03	1.51
INTERPLAY	8s	0	7mm	8.46	97.50	0.56
INTERPLAY	8s	90	7mm	9.27	96.62	0.49
GATING	6s	0	0mm	8.30	94.55	0.00
GATING	6s	90	0mm	8.43	94.44	0.00
GATING	8s	0	0mm	7.57	95.29	0.04
GATING	8s	90	0mm	7.77	95.15	0.07
GATING	6s	0	3mm	4.51	99.93	0.00
GATING	6s	90	3mm	4.51	99.93	0.00
GATING	8s	0	3mm	4.72	99.96	0.04
GATING	8s	90	3mm	4.86	100.00	0.04
GATING	6s	0	5mm	4.70	100.00	0.00
GATING	6s	90	5mm	4.66	100.00	0.00
GATING	8s	0	5mm	4.34	100.00	0.00
GATING	8s	90	5mm	4.36	100.00	0.00
GATING	6s	0	7mm	3.86	100.00	0.00
GATING	6s	90	7mm	3.86	100.00	0.00
GATING	8s	0	7mm	3.80	100.00	0.00
GATING	8s	90	7mm	3.79	100.00	0.00

Table A.34.: Patient 8, RPV

Case	motion period	motion starting phase	Margin	D5-D95	V95	V107
STATIC	-	-	0mm	1.85	100.00	0.00
STATIC	-	-	3mm	1.82	100.00	0.00
STATIC	-	-	5mm	1.81	100.00	0.00
STATIC	-	-	7mm	1.81	100.00	0.00
INTERPLAY	6s	0	0mm	16.96	86.51	11.76
INTERPLAY	6s	90	0mm	14.01	89.57	5.64
INTERPLAY	8s	0	0mm	12.52	95.65	7.61
INTERPLAY	8s	90	0mm	12.15	92.63	3.61
INTERPLAY	6s	0	3mm	11.49	87.99	2.47
INTERPLAY	6s	90	3mm	15.13	81.07	6.72
INTERPLAY	8s	0	3mm	13.77	86.16	3.86
INTERPLAY	8s	90	3mm	10.66	90.36	1.48
INTERPLAY	6s	0	5mm	12.35	89.72	1.43
INTERPLAY	6s	90	5mm	12.44	96.69	6.87
INTERPLAY	8s	0	5mm	8.72	96.19	0.30
INTERPLAY	8s	90	5mm	9.45	98.52	1.68
INTERPLAY	6s	0	7mm	12.64	96.89	7.12
INTERPLAY	6s	90	7mm	10.21	94.02	0.84
INTERPLAY	8s	0	7mm	9.53	99.90	3.71
INTERPLAY	8s	90	7mm	10.06	98.37	2.97
GATING	6s	0	0mm	5.64	99.06	0.00
GATING	6s	90	0mm	5.63	99.11	0.00
GATING	8s	0	0mm	5.67	99.21	0.15
GATING	8s	90	0mm	6.06	99.11	0.20
GATING	6s	0	3mm	4.29	100.00	0.00
GATING	6s	90	3mm	4.29	100.00	0.00
GATING	8s	0	3mm	4.83	100.00	0.00
GATING	8s	90	3mm	4.87	100.00	0.00
GATING	6s	0	5mm	4.85	99.85	0.00
GATING	6s	90	5mm	4.79	99.80	0.00
GATING	8s	0	5mm	5.23	99.85	0.00
GATING	8s	90	5mm	5.09	100.00	0.00
GATING	6s	0	7mm	4.62	99.95	0.00
GATING	6s	90	7mm	4.38	100.00	0.00
GATING	8s	0	7mm	4.72	99.90	0.00
GATING	8s	90	7mm	4.60	99.95	0.00

Table A.35.: Patient 9, LPV

Case	motion period	motion starting phase	Margin	D5-D95	V95	V107
STATIC	-	-	0mm	1.83	100.00	0.00
STATIC	-	-	3mm	1.86	100.00	0.00
STATIC	-	-	5mm	1.82	100.00	0.00
STATIC	-	-	7mm	1.81	100.00	0.00
INTERPLAY	6s	0	0mm	22.96	73.82	4.62
INTERPLAY	6s	90	0mm	15.96	83.98	5.95
INTERPLAY	8s	0	0mm	17.89	77.70	9.08
INTERPLAY	8s	90	0mm	24.83	84.15	19.08
INTERPLAY	6s	0	3mm	19.57	72.91	5.70
INTERPLAY	6s	90	3mm	20.93	84.31	13.46
INTERPLAY	8s	0	3mm	12.89	89.18	2.06
INTERPLAY	8s	90	3mm	12.54	90.01	0.58
INTERPLAY	6s	0	5mm	16.02	83.15	4.87
INTERPLAY	6s	90	5mm	13.18	90.50	3.72
INTERPLAY	8s	0	5mm	13.85	90.17	7.10
INTERPLAY	8s	90	5mm	13.01	83.98	0.91
INTERPLAY	6s	0	7mm	14.77	84.48	3.96
INTERPLAY	6s	90	7mm	16.28	87.70	3.39
INTERPLAY	8s	0	7mm	14.30	82.74	3.55
INTERPLAY	8s	90	7mm	15.55	91.08	15.28
GATING	6s	0	0mm	8.03	94.14	0.08
GATING	6s	90	0mm	7.77	94.55	0.08
GATING	8s	0	0mm	7.79	95.21	0.00
GATING	8s	90	0mm	6.71	96.94	0.00
GATING	6s	0	3mm	4.90	99.92	0.00
GATING	6s	90	3mm	5.01	100.00	0.00
GATING	8s	0	3mm	4.72	99.83	0.00
GATING	8s	90	3mm	4.12	100.00	0.00
GATING	6s	0	5mm	4.70	100.00	0.00
GATING	6s	90	5mm	4.42	100.00	0.00
GATING	8s	0	5mm	3.92	100.00	0.00
GATING	8s	90	5mm	4.42	100.00	0.00
GATING	6s	0	7mm	3.96	100.00	0.00
GATING	6s	90	7mm	4.18	99.92	0.00
GATING	8s	0	7mm	3.47	100.00	0.00
GATING	8s	90	7mm	3.59	100.00	0.00

Table A.36.: Patient 9, RPV

Case	motion period	motion starting phase	Margin	D5-D95	V95	V107
STATIC	-	-	0mm	1.81	100.00	0.00
STATIC	-	-	3mm	1.81	100.00	0.00
STATIC	-	-	5mm	1.82	100.00	0.00
STATIC	-	-	7mm	1.80	100.00	0.00
INTERPLAY	6s	0	0mm	21.06	81.96	15.73
INTERPLAY	6s	90	0mm	16.08	95.00	16.37
INTERPLAY	8s	0	0mm	14.47	82.98	4.44
INTERPLAY	8s	90	0mm	13.16	92.88	5.83
INTERPLAY	6s	0	3mm	12.22	90.38	1.85
INTERPLAY	6s	90	3mm	12.82	92.41	3.52
INTERPLAY	8s	0	3mm	9.28	97.04	1.20
INTERPLAY	8s	90	3mm	8.07	99.17	0.09
INTERPLAY	6s	0	5mm	10.72	95.93	2.31
INTERPLAY	6s	90	5mm	9.86	99.44	3.89
INTERPLAY	8s	0	5mm	9.57	96.85	1.02
INTERPLAY	8s	90	5mm	11.19	93.62	1.30
INTERPLAY	6s	0	7mm	8.96	99.54	1.02
INTERPLAY	6s	90	7mm	9.63	97.87	1.20
INTERPLAY	8s	0	7mm	10.82	96.67	3.15
INTERPLAY	8s	90	7mm	13.80	95.65	11.38
GATING	6s	0	0mm	6.18	98.98	0.00
GATING	6s	90	0mm	6.05	99.07	0.00
GATING	8s	0	0mm	5.35	98.98	0.00
GATING	8s	90	0mm	5.19	99.17	0.00
GATING	6s	0	3mm	4.14	100.00	0.00
GATING	6s	90	3mm	4.42	99.91	0.00
GATING	8s	0	3mm	5.07	99.91	0.00
GATING	8s	90	3mm	4.82	99.82	0.00
GATING	6s	0	5mm	3.43	100.00	0.00
GATING	6s	90	5mm	3.38	100.00	0.00
GATING	8s	0	5mm	3.87	100.00	0.00
GATING	8s	90	5mm	3.85	100.00	0.00
GATING	6s	0	7mm	3.18	100.00	0.00
GATING	6s	90	7mm	3.33	100.00	0.00
GATING	8s	0	7mm	3.59	100.00	0.00
GATING	8s	90	7mm	3.48	100.00	0.00

Table A.37.: Patient 2, LPV

Case	Rescan no.	motion period	motion starting phase	Margin	D5-D95	V95	V107
RESCANNING	5	6s	0	0mm	6.08	98.89	0.52
RESCANNING	10	6s	0	0mm	5.69	98.63	0.13
RESCANNING	15	6s	0	0mm	5.56	98.76	0.13
RESCANNING	20	6s	0	0mm	5.63	98.63	0.07
RESCANNING	5	6s	90	0mm	6.08	98.89	0.52
RESCANNING	10	6s	90	0mm	5.69	98.63	0.13
RESCANNING	15	6s	90	0mm	5.56	98.76	0.13
RESCANNING	20	6s	90	0mm	5.63	98.63	0.07
RESCANNING	5	8s	0	0mm	5.97	98.30	0.13
RESCANNING	10	8s	0	0mm	5.69	98.30	0.26
RESCANNING	15	8s	0	0mm	5.91	97.97	0.26
RESCANNING	20	8s	0	0mm	6.14	98.82	0.20
RESCANNING	5	8s	90	0mm	5.78	98.17	0.13
RESCANNING	10	8s	90	0mm	5.65	98.30	0.26
RESCANNING	15	8s	90	0mm	5.82	98.50	0.13
RESCANNING	20	8s	90	0mm	5.95	98.95	0.13
RESCANNING	5	6s	0	3mm	4.72	100.00	0.00
RESCANNING	10	6s	0	3mm	3.64	100.00	0.00
RESCANNING	15	6s	0	3mm	3.78	99.93	0.00
RESCANNING	20	6s	0	3mm	3.74	99.80	0.00
RESCANNING	5	6s	90	3mm	4.69	100.00	0.00
RESCANNING	10	6s	90	3mm	3.75	99.87	0.00
RESCANNING	15	6s	90	3mm	3.95	100.00	0.00
RESCANNING	20	6s	90	3mm	3.71	99.87	0.00
RESCANNING	5	8s	0	3mm	4.54	99.80	0.00
RESCANNING	10	8s	0	3mm	3.89	100.00	0.00
RESCANNING	15	8s	0	3mm	3.80	100.00	0.00
RESCANNING	20	8s	0	3mm	3.88	100.00	0.00
RESCANNING	5	8s	90	3mm	4.71	99.74	0.00
RESCANNING	10	8s	90	3mm	3.85	100.00	0.00
RESCANNING	15	8s	90	3mm	3.85	100.00	0.00
RESCANNING	20	8s	90	3mm	4.24	100.00	0.00
RESCANNING	5	6s	0	5mm	3.70	100.00	0.00
RESCANNING	10	6s	0	5mm	3.83	100.00	0.00
RESCANNING	15	6s	0	5mm	3.74	100.00	0.00
RESCANNING	20	6s	0	5mm	3.63	100.00	0.00
RESCANNING	5	6s	90	5mm	3.70	100.00	0.00
RESCANNING	10	6s	90	5mm	3.83	100.00	0.00
RESCANNING	15	6s	90	5mm	3.74	100.00	0.00
RESCANNING	20	6s	90	5mm	3.63	100.00	0.00
RESCANNING	5	8s	0	5mm	3.81	100.00	0.00
RESCANNING	10	8s	0	5mm	3.64	100.00	0.00
RESCANNING	15	8s	0	5mm	3.58	100.00	0.00
RESCANNING	20	8s	0	5mm	3.70	100.00	0.00
RESCANNING	5	8s	90	5mm	4.02	99.93	0.00
RESCANNING	10	8s	90	5mm	3.66	100.00	0.00
RESCANNING	15	8s	90	5mm	3.54	100.00	0.00
RESCANNING	20	8s	90	5mm	3.66	100.00	0.00
RESCANNING	5	6s	0	7mm	3.63	100.00	0.00
RESCANNING	10	6s	0	7mm	3.46	100.00	0.00
RESCANNING	15	6s	0	7mm	3.43	100.00	0.00
RESCANNING	20	6s	0	7mm	3.43	100.00	0.00
RESCANNING	5	6s	90	7mm	3.63	100.00	0.00
RESCANNING	10	6s	90	7mm	3.48	100.00	0.00
RESCANNING	15	6s	90	7mm	3.44	100.00	0.00
RESCANNING	20	6s	90	7mm	3.46	100.00	0.00
RESCANNING	5	8s	0	7mm	3.56	100.00	0.00
RESCANNING	10	8s	0	7mm	3.46	100.00	0.00
RESCANNING	15	8s	0	7mm	3.70	100.00	0.00
RESCANNING	20	8s	0	7mm	3.55	100.00	0.00
RESCANNING	5	8s	90	7mm	3.62	100.00	0.00
RESCANNING	10	8s	90	7mm	3.46	100.00	0.00
RESCANNING	15	8s	90	7mm	3.67	100.00	0.00
RESCANNING	20	8s	90	7mm	3.52	100.00	0.00

Table A.38.: Patient 2, RPV

Case	Rescan no.	motion period	motion starting phase	Margin	D5-D95	V95	V107
RESCANNING	5	6s	0	0mm	6.68	96.29	0.00
RESCANNING	10	6s	0	0mm	6.29	95.89	0.05
RESCANNING	15	6s	0	0mm	6.01	96.24	0.05
RESCANNING	20	6s	0	0mm	5.62	96.14	0.05
RESCANNING	5	6s	90	0mm	6.70	96.29	0.00
RESCANNING	10	6s	90	0mm	6.33	95.94	0.05
RESCANNING	15	6s	90	0mm	5.84	96.34	0.05
RESCANNING	20	6s	90	0mm	5.62	96.09	0.05
RESCANNING	5	8s	0	0mm	5.92	97.52	0.15
RESCANNING	10	8s	0	0mm	6.37	95.74	0.10
RESCANNING	15	8s	0	0mm	5.75	95.99	0.10
RESCANNING	20	8s	0	0mm	6.13	95.89	0.10
RESCANNING	5	8s	90	0mm	6.11	97.62	0.15
RESCANNING	10	8s	90	0mm	6.54	95.69	0.10
RESCANNING	15	8s	90	0mm	5.85	95.94	0.05
RESCANNING	20	8s	90	0mm	6.10	96.14	0.05
RESCANNING	5	6s	0	3mm	4.84	99.85	0.10
RESCANNING	10	6s	0	3mm	4.02	100.00	0.00
RESCANNING	15	6s	0	3mm	3.85	99.95	0.00
RESCANNING	20	6s	0	3mm	4.09	99.90	0.00
RESCANNING	5	6s	90	3mm	4.78	99.85	0.15
RESCANNING	10	6s	90	3mm	4.11	100.00	0.00
RESCANNING	15	6s	90	3mm	3.82	99.95	0.00
RESCANNING	20	6s	90	3mm	4.01	99.90	0.00
RESCANNING	5	8s	0	3mm	4.41	100.00	0.00
RESCANNING	10	8s	0	3mm	4.11	100.00	0.00
RESCANNING	15	8s	0	3mm	4.30	100.00	0.00
RESCANNING	20	8s	0	3mm	4.05	99.90	0.00
RESCANNING	5	8s	90	3mm	4.47	100.00	0.00
RESCANNING	10	8s	90	3mm	4.38	100.00	0.00
RESCANNING	15	8s	90	3mm	4.26	100.00	0.00
RESCANNING	20	8s	90	3mm	4.10	99.90	0.00
RESCANNING	5	6s	0	5mm	3.82	100.00	0.00
RESCANNING	10	6s	0	5mm	3.77	100.00	0.00
RESCANNING	15	6s	0	5mm	3.63	100.00	0.00
RESCANNING	20	6s	0	5mm	3.57	100.00	0.00
RESCANNING	5	6s	90	5mm	3.82	100.00	0.00
RESCANNING	10	6s	90	5mm	3.77	100.00	0.00
RESCANNING	15	6s	90	5mm	3.64	100.00	0.00
RESCANNING	20	6s	90	5mm	3.57	100.00	0.00
RESCANNING	5	8s	0	5mm	5.16	100.00	0.10
RESCANNING	10	8s	0	5mm	3.71	100.00	0.00
RESCANNING	15	8s	0	5mm	3.61	100.00	0.00
RESCANNING	20	8s	0	5mm	3.87	100.00	0.05
RESCANNING	5	8s	90	5mm	4.87	100.00	0.00
RESCANNING	10	8s	90	5mm	3.77	100.00	0.00
RESCANNING	15	8s	90	5mm	3.60	100.00	0.00
RESCANNING	20	8s	90	5mm	3.83	99.95	0.05
RESCANNING	5	6s	0	7mm	3.75	100.00	0.00
RESCANNING	10	6s	0	7mm	3.48	100.00	0.00
RESCANNING	15	6s	0	7mm	3.26	100.00	0.00
RESCANNING	20	6s	0	7mm	3.48	100.00	0.00
RESCANNING	5	6s	90	7mm	3.75	100.00	0.00
RESCANNING	10	6s	90	7mm	3.48	100.00	0.00
RESCANNING	15	6s	90	7mm	3.32	100.00	0.00
RESCANNING	20	6s	90	7mm	3.50	100.00	0.00
RESCANNING	5	8s	0	7mm	3.94	100.00	0.00
RESCANNING	10	8s	0	7mm	3.39	100.00	0.00
RESCANNING	15	8s	0	7mm	3.43	100.00	0.00
RESCANNING	20	8s	0	7mm	3.46	100.00	0.00
RESCANNING	5	8s	90	7mm	3.78	100.00	0.00
RESCANNING	10	8s	90	7mm	3.39	100.00	0.00
RESCANNING	15	8s	90	7mm	3.43	100.00	0.00
RESCANNING	20	8s	90	7mm	3.46	100.00	0.00

Table A.39.: Patient 9, LPV

Case	Rescan no.	motion period	motion starting phase	Margin	D5-D95	V95	V107
RESCANNING	5	6s	0	0mm	7.70	93.97	0.00
RESCANNING	10	6s	0	0mm	7.91	93.89	0.00
RESCANNING	15	6s	0	0mm	7.64	94.30	0.00
RESCANNING	20	6s	0	0mm	7.98	94.30	0.00
RESCANNING	5	6s	90	0mm	7.86	93.97	0.08
RESCANNING	10	6s	90	0mm	7.80	93.97	0.00
RESCANNING	15	6s	90	0mm	7.66	94.30	0.00
RESCANNING	20	6s	90	0mm	7.93	94.30	0.00
RESCANNING	5	8s	0	0mm	8.73	94.30	0.00
RESCANNING	10	8s	0	0mm	8.39	93.81	0.08
RESCANNING	15	8s	0	0mm	8.75	93.56	0.08
RESCANNING	20	8s	0	0mm	7.96	94.38	0.08
RESCANNING	5	8s	90	0mm	8.57	94.30	0.00
RESCANNING	10	8s	90	0mm	8.70	93.97	0.08
RESCANNING	15	8s	90	0mm	7.46	94.30	0.08
RESCANNING	20	8s	90	0mm	8.03	94.80	0.08
RESCANNING	5	6s	0	3mm	3.86	100.00	0.00
RESCANNING	10	6s	0	3mm	4.06	100.00	0.00
RESCANNING	15	6s	0	3mm	3.75	100.00	0.00
RESCANNING	20	6s	0	3mm	3.69	100.00	0.00
RESCANNING	5	6s	90	3mm	3.83	100.00	0.00
RESCANNING	10	6s	90	3mm	4.10	100.00	0.00
RESCANNING	15	6s	90	3mm	3.74	100.00	0.00
RESCANNING	20	6s	90	3mm	3.70	100.00	0.00
RESCANNING	5	8s	0	3mm	4.26	100.00	0.00
RESCANNING	10	8s	0	3mm	3.92	100.00	0.00
RESCANNING	15	8s	0	3mm	3.93	100.00	0.00
RESCANNING	20	8s	0	3mm	4.08	100.00	0.00
RESCANNING	5	8s	90	3mm	4.26	100.00	0.00
RESCANNING	10	8s	90	3mm	3.96	100.00	0.00
RESCANNING	15	8s	90	3mm	4.02	99.92	0.00
RESCANNING	20	8s	90	3mm	3.89	100.00	0.00
RESCANNING	5	6s	0	5mm	3.73	100.00	0.00
RESCANNING	10	6s	0	5mm	3.61	100.00	0.00
RESCANNING	15	6s	0	5mm	3.50	100.00	0.00
RESCANNING	20	6s	0	5mm	3.65	100.00	0.00
RESCANNING	5	6s	90	5mm	3.73	100.00	0.00
RESCANNING	10	6s	90	5mm	3.63	100.00	0.00
RESCANNING	15	6s	90	5mm	3.52	100.00	0.00
RESCANNING	20	6s	90	5mm	3.67	100.00	0.00
RESCANNING	5	8s	0	5mm	3.73	100.00	0.00
RESCANNING	10	8s	0	5mm	3.63	100.00	0.00
RESCANNING	15	8s	0	5mm	3.59	100.00	0.00
RESCANNING	20	8s	0	5mm	3.58	100.00	0.00
RESCANNING	5	8s	90	5mm	3.73	100.00	0.00
RESCANNING	10	8s	90	5mm	3.68	100.00	0.00
RESCANNING	15	8s	90	5mm	3.61	100.00	0.00
RESCANNING	20	8s	90	5mm	3.58	100.00	0.00
RESCANNING	5	6s	0	7mm	3.89	100.00	0.00
RESCANNING	10	6s	0	7mm	3.45	100.00	0.00
RESCANNING	15	6s	0	7mm	3.19	100.00	0.00
RESCANNING	20	6s	0	7mm	3.22	100.00	0.00
RESCANNING	5	6s	90	7mm	3.83	100.00	0.00
RESCANNING	10	6s	90	7mm	3.45	100.00	0.00
RESCANNING	15	6s	90	7mm	3.16	100.00	0.00
RESCANNING	20	6s	90	7mm	3.23	100.00	0.00
RESCANNING	5	8s	0	7mm	3.56	100.00	0.00
RESCANNING	10	8s	0	7mm	3.81	100.00	0.00
RESCANNING	15	8s	0	7mm	3.48	100.00	0.00
RESCANNING	20	8s	0	7mm	3.34	100.00	0.00
RESCANNING	5	8s	90	7mm	3.77	100.00	0.00
RESCANNING	10	8s	90	7mm	3.61	100.00	0.00
RESCANNING	15	8s	90	7mm	3.41	100.00	0.00
RESCANNING	20	8s	90	7mm	3.42	100.00	0.00

Table A.40.: Patient 9, RPV

Case	Rescan no.	motion period	motion starting phase	Margin	D5-D95	V95	V107
RESCANNING	5	6s	0	0mm	4.72	99.26	0.00
RESCANNING	10	6s	0	0mm	4.48	99.26	0.00
RESCANNING	15	6s	0	0mm	4.22	99.35	0.00
RESCANNING	20	6s	0	0mm	4.07	99.17	0.00
RESCANNING	5	6s	90	0mm	4.81	99.26	0.00
RESCANNING	10	6s	90	0mm	4.47	99.26	0.00
RESCANNING	15	6s	90	0mm	4.31	99.17	0.00
RESCANNING	20	6s	90	0mm	3.98	99.17	0.00
RESCANNING	5	8s	0	0mm	4.94	99.07	0.00
RESCANNING	10	8s	0	0mm	4.68	98.70	0.00
RESCANNING	15	8s	0	0mm	4.50	99.17	0.00
RESCANNING	20	8s	0	0mm	4.50	99.17	0.00
RESCANNING	5	8s	90	0mm	5.11	99.17	0.00
RESCANNING	10	8s	90	0mm	4.63	98.89	0.00
RESCANNING	15	8s	90	0mm	4.27	99.17	0.00
RESCANNING	20	8s	90	0mm	4.58	99.17	0.00
RESCANNING	5	6s	0	3mm	3.93	100.00	0.00
RESCANNING	10	6s	0	3mm	3.64	100.00	0.00
RESCANNING	15	6s	0	3mm	3.47	100.00	0.00
RESCANNING	20	6s	0	3mm	3.60	100.00	0.00
RESCANNING	5	6s	90	3mm	3.94	100.00	0.00
RESCANNING	10	6s	90	3mm	3.64	100.00	0.00
RESCANNING	15	6s	90	3mm	3.49	100.00	0.00
RESCANNING	20	6s	90	3mm	3.57	100.00	0.00
RESCANNING	5	8s	0	3mm	3.94	99.91	0.00
RESCANNING	10	8s	0	3mm	3.75	100.00	0.00
RESCANNING	15	8s	0	3mm	3.84	100.00	0.00
RESCANNING	20	8s	0	3mm	4.03	100.00	0.00
RESCANNING	5	8s	90	3mm	4.05	100.00	0.00
RESCANNING	10	8s	90	3mm	3.69	100.00	0.00
RESCANNING	15	8s	90	3mm	3.63	100.00	0.00
RESCANNING	20	8s	90	3mm	3.59	100.00	0.00
RESCANNING	5	6s	0	5mm	3.60	100.00	0.00
RESCANNING	10	6s	0	5mm	3.11	100.00	0.00
RESCANNING	15	6s	0	5mm	3.06	100.00	0.00
RESCANNING	20	6s	0	5mm	3.20	100.00	0.00
RESCANNING	5	6s	90	5mm	3.61	100.00	0.00
RESCANNING	10	6s	90	5mm	3.16	100.00	0.00
RESCANNING	15	6s	90	5mm	3.22	100.00	0.00
RESCANNING	20	6s	90	5mm	3.19	100.00	0.00
RESCANNING	5	8s	0	5mm	3.75	100.00	0.00
RESCANNING	10	8s	0	5mm	2.97	100.00	0.00
RESCANNING	15	8s	0	5mm	3.69	100.00	0.00
RESCANNING	20	8s	0	5mm	2.93	100.00	0.00
RESCANNING	5	8s	90	5mm	3.78	100.00	0.00
RESCANNING	10	8s	90	5mm	3.48	100.00	0.00
RESCANNING	15	8s	90	5mm	3.71	100.00	0.00
RESCANNING	20	8s	90	5mm	4.15	100.00	0.00
RESCANNING	5	6s	0	7mm	3.74	100.00	0.00
RESCANNING	10	6s	0	7mm	3.58	100.00	0.00
RESCANNING	15	6s	0	7mm	3.43	100.00	0.00
RESCANNING	20	6s	0	7mm	3.42	100.00	0.00
RESCANNING	5	6s	90	7mm	3.74	100.00	0.00
RESCANNING	10	6s	90	7mm	3.58	100.00	0.00
RESCANNING	15	6s	90	7mm	3.45	100.00	0.00
RESCANNING	20	6s	90	7mm	3.43	100.00	0.00
RESCANNING	5	8s	0	7mm	3.57	100.00	0.00
RESCANNING	10	8s	0	7mm	3.51	100.00	0.00
RESCANNING	15	8s	0	7mm	3.61	100.00	0.00
RESCANNING	20	8s	0	7mm	3.57	100.00	0.00
RESCANNING	5	8s	90	7mm	3.61	100.00	0.00
RESCANNING	10	8s	90	7mm	3.47	100.00	0.00
RESCANNING	15	8s	90	7mm	3.55	100.00	0.00
RESCANNING	20	8s	90	7mm	3.31	100.00	0.00



B Appendix of chapter 3

B.1 Motion of PV due to heartbeat

The mean relative displacement and standard deviation of the target volumes (LPV and RPV) to the reference phase zero will be shown for the three studied motion directions (SI: superior-inferior, AP: anterior-posterior, LR: left-right) and the absolute (ABS) displacement.

Table B.1.: Patient 1, LPV: Mean and standard deviation of target motion in all phases of the heartbeat, relative to the reference phase.

motion phase	ABS [mm]	SI [mm]	AP [mm]	LR [mm]
01	0.62 ± 0.27	-0.22 ± 0.15	0.39 ± 0.26	-0.28 ± 0.30
02	1.78 ± 0.81	-1.00 ± 0.48	0.97 ± 0.62	-0.86 ± 0.71
03	2.79 ± 0.98	-1.65 ± 0.78	1.55 ± 1.03	-1.08 ± 0.87
04	3.15 ± 1.22	-1.61 ± 1.11	1.78 ± 1.19	-1.48 ± 0.91
05	3.36 ± 1.28	-0.79 ± 0.93	2.32 ± 1.39	-1.83 ± 0.90
06	4.50 ± 1.72	-0.27 ± 1.13	3.25 ± 1.49	-2.76 ± 1.19
07	4.39 ± 1.68	0.26 ± 0.93	3.05 ± 1.56	-2.84 ± 1.15
08	4.17 ± 1.82	-0.32 ± 1.02	2.95 ± 1.58	-2.64 ± 1.19
09	4.39 ± 1.68	0.26 ± 0.93	3.05 ± 1.56	-2.84 ± 1.15
10	2.85 ± 1.26	-1.81 ± 0.88	1.61 ± 1.42	-0.82 ± 0.61
11	2.76 ± 1.08	-2.30 ± 0.98	1.18 ± 1.04	0.02 ± 0.24
12	2.68 ± 1.02	-2.16 ± 1.05	1.31 ± 0.82	0.06 ± 0.29
13	2.11 ± 0.71	-1.53 ± 0.89	0.88 ± 0.82	-0.28 ± 0.56
14	2.44 ± 1.02	-2.01 ± 0.99	0.66 ± 0.86	-0.65 ± 0.61
15	2.58 ± 1.16	-2.29 ± 1.12	0.39 ± 0.88	-0.46 ± 0.59
16	2.49 ± 1.23	-2.25 ± 1.18	0.36 ± 0.85	-0.24 ± 0.57
17	2.15 ± 1.20	-1.91 ± 1.06	0.33 ± 0.85	0.44 ± 0.48
18	1.61 ± 0.41	-0.88 ± 0.38	-0.26 ± 0.60	1.15 ± 0.33
19	0.60 ± 0.20	0.32 ± 0.19	-0.18 ± 0.21	0.39 ± 0.20

Table B.2.: Patient 1, RPV: Mean and standard deviation of target motion in all phases of the heartbeat, relative to the reference phase.

motion phase	ABS [mm]	SI [mm]	AP [mm]	LR [mm]
01	0.25 ± 0.13	-0.03 ± 0.12	-0.02 ± 0.14	0.18 ± 0.11
02	0.62 ± 0.20	-0.23 ± 0.33	0.06 ± 0.37	0.31 ± 0.17
03	1.68 ± 0.31	-1.28 ± 0.42	0.73 ± 0.40	0.61 ± 0.24
04	2.22 ± 0.42	-1.18 ± 0.73	1.26 ± 0.65	0.91 ± 0.54
05	2.77 ± 0.76	-1.11 ± 0.77	2.05 ± 1.02	0.57 ± 0.94
06	3.99 ± 1.40	-0.35 ± 0.90	3.63 ± 1.57	0.65 ± 0.93
07	3.70 ± 1.24	0.04 ± 0.80	3.36 ± 1.41	0.51 ± 1.02
08	3.10 ± 1.12	0.12 ± 0.72	2.68 ± 1.31	0.79 ± 0.92
09	3.70 ± 1.24	0.04 ± 0.80	3.36 ± 1.41	0.51 ± 1.02
10	2.77 ± 0.71	-1.52 ± 0.52	1.77 ± 1.01	0.95 ± 0.74
11	2.08 ± 0.34	-1.51 ± 0.61	0.49 ± 0.77	0.87 ± 0.47
12	1.93 ± 0.45	-1.64 ± 0.62	0.20 ± 0.53	0.64 ± 0.31
13	1.42 ± 0.44	-1.25 ± 0.57	-0.02 ± 0.45	0.18 ± 0.31
14	1.99 ± 0.41	-1.68 ± 0.63	0.13 ± 0.64	0.55 ± 0.45
15	2.18 ± 0.49	-1.87 ± 0.72	0.05 ± 0.62	0.59 ± 0.49
16	2.27 ± 0.74	-1.90 ± 1.00	0.04 ± 0.75	0.57 ± 0.45
17	1.98 ± 0.40	-1.25 ± 0.69	0.46 ± 0.73	1.11 ± 0.26
18	1.14 ± 0.51	-0.27 ± 0.38	0.58 ± 0.59	0.68 ± 0.42
19	0.48 ± 0.21	0.18 ± 0.24	0.28 ± 0.23	0.20 ± 0.13

Table B.3.: Patient 2, LPV: Mean and standard deviation of target motion in all phases of the heartbeat, relative to the reference phase.

motion phase	ABS [mm]	SI [mm]	AP [mm]	LR [mm]
01	0.67 ± 0.48	-0.03 ± 0.21	-0.10 ± 0.17	-0.38 ± 0.67
02	1.86 ± 0.88	-0.62 ± 0.66	-0.32 ± 0.59	-1.31 ± 1.12
03	2.62 ± 1.20	1.43 ± 1.41	0.59 ± 1.06	-1.39 ± 0.94
04	3.94 ± 1.86	2.46 ± 1.71	1.68 ± 0.92	-2.35 ± 0.92
05	5.21 ± 1.80	3.52 ± 1.90	1.82 ± 0.61	-3.03 ± 1.23
06	5.26 ± 1.92	3.21 ± 1.58	1.51 ± 0.58	-3.65 ± 1.62
07	4.64 ± 1.94	2.25 ± 1.77	0.44 ± 0.76	-3.74 ± 1.53
08	4.52 ± 1.72	1.78 ± 1.84	0.57 ± 0.82	-3.71 ± 1.47
09	4.64 ± 1.94	2.25 ± 1.77	0.44 ± 0.76	-3.74 ± 1.53
10	2.68 ± 0.70	1.66 ± 0.59	0.90 ± 0.27	-1.84 ± 0.56
11	2.03 ± 0.61	1.39 ± 0.70	0.96 ± 0.28	-0.89 ± 0.51
12	1.43 ± 0.38	1.03 ± 0.53	0.78 ± 0.24	-0.32 ± 0.28
13	1.03 ± 0.28	0.53 ± 0.47	0.70 ± 0.25	0.06 ± 0.27
14	0.84 ± 0.28	0.48 ± 0.42	0.52 ± 0.12	-0.09 ± 0.28
15	0.75 ± 0.27	0.47 ± 0.42	0.37 ± 0.09	-0.19 ± 0.23
16	0.52 ± 0.10	0.18 ± 0.27	0.35 ± 0.07	-0.16 ± 0.15
17	0.47 ± 0.13	0.13 ± 0.23	0.35 ± 0.11	0.07 ± 0.16
18	0.56 ± 0.49	-0.19 ± 0.29	0.28 ± 0.23	0.36 ± 0.42
19	0.26 ± 0.09	0.05 ± 0.15	0.11 ± 0.12	0.07 ± 0.13

Table B.4.: Patient 2, RPV: Mean and standard deviation of target motion in all phases of the heartbeat, relative to the reference phase.

motion phase	ABS [mm]	SI [mm]	AP [mm]	LR [mm]
01	0.56 ± 0.32	0.07 ± 0.25	0.34 ± 0.40	-0.12 ± 0.23
02	2.62 ± 0.87	0.69 ± 1.07	1.66 ± 0.66	-1.49 ± 0.76
03	4.17 ± 1.55	0.83 ± 1.87	1.84 ± 0.84	-3.05 ± 1.48
04	5.20 ± 1.80	1.48 ± 1.70	2.55 ± 1.36	-3.92 ± 1.22
05	5.04 ± 2.35	1.61 ± 1.93	2.77 ± 1.69	-3.25 ± 1.87
06	4.88 ± 1.71	1.36 ± 1.64	2.76 ± 1.54	-3.22 ± 1.35
07	3.82 ± 1.83	1.02 ± 1.17	2.09 ± 1.57	-2.45 ± 1.64
08	3.52 ± 2.09	0.89 ± 1.11	2.04 ± 2.08	-1.80 ± 1.74
09	3.82 ± 1.83	1.02 ± 1.17	2.09 ± 1.57	-2.45 ± 1.64
10	2.08 ± 1.40	0.89 ± 1.53	0.76 ± 1.27	-0.67 ± 0.74
11	1.72 ± 1.17	0.86 ± 1.40	0.24 ± 1.03	-0.42 ± 0.59
12	1.34 ± 0.86	0.77 ± 1.11	-0.07 ± 0.76	-0.14 ± 0.34
13	1.04 ± 0.66	0.53 ± 0.83	0.05 ± 0.65	0.09 ± 0.36
14	0.79 ± 0.44	0.42 ± 0.59	-0.08 ± 0.46	0.01 ± 0.26
15	0.64 ± 0.33	0.37 ± 0.41	-0.15 ± 0.36	-0.05 ± 0.26
16	0.54 ± 0.29	0.31 ± 0.36	-0.18 ± 0.25	-0.06 ± 0.22
17	0.38 ± 0.23	0.19 ± 0.25	-0.17 ± 0.21	0.04 ± 0.15
18	0.24 ± 0.14	0.04 ± 0.13	-0.10 ± 0.18	0.07 ± 0.10
19	0.39 ± 0.15	-0.06 ± 0.15	-0.23 ± 0.14	0.23 ± 0.14

Table B.5.: Patient 3, LPV: Mean and standard deviation of target motion in all phases of the heartbeat, relative to the reference phase.

motion phase	ABS [mm]	SI [mm]	AP [mm]	LR [mm]
01	0.72 ± 0.48	-0.29 ± 0.51	0.09 ± 0.19	-0.33 ± 0.50
02	1.59 ± 1.12	-0.24 ± 0.70	0.48 ± 0.32	-1.17 ± 1.25
03	2.04 ± 1.34	0.09 ± 0.52	1.43 ± 0.61	-0.82 ± 1.61
04	3.06 ± 1.79	0.83 ± 0.92	1.89 ± 0.75	-1.42 ± 2.21
05	3.23 ± 1.73	0.74 ± 0.88	2.02 ± 0.67	-1.75 ± 2.13
06	3.22 ± 1.82	1.17 ± 1.24	1.73 ± 0.88	-1.26 ± 2.32
07	3.26 ± 2.06	1.01 ± 1.32	1.55 ± 0.82	-1.79 ± 2.42
08	3.39 ± 2.24	0.44 ± 1.17	1.62 ± 0.84	-2.38 ± 2.44
09	3.26 ± 2.06	1.01 ± 1.32	1.55 ± 0.82	-1.79 ± 2.42
10	2.91 ± 2.37	-1.26 ± 1.25	0.58 ± 0.80	-1.98 ± 2.45
11	2.73 ± 2.11	-1.43 ± 1.32	0.25 ± 0.98	-1.54 ± 2.16
12	2.47 ± 1.92	-1.09 ± 1.12	0.12 ± 0.95	-1.33 ± 2.15
13	2.55 ± 1.94	-1.43 ± 1.22	-0.42 ± 0.96	-1.42 ± 1.91
14	2.68 ± 2.02	-1.72 ± 1.25	-0.46 ± 0.88	-1.37 ± 1.96
15	2.82 ± 2.07	-1.70 ± 1.33	-0.50 ± 1.01	-1.46 ± 2.05
16	2.63 ± 1.99	-1.80 ± 1.11	-0.47 ± 0.86	-1.18 ± 2.02
17	1.86 ± 1.19	-0.83 ± 0.47	-0.67 ± 0.80	-0.55 ± 1.61
18	1.99 ± 0.66	-0.76 ± 1.20	-0.45 ± 0.75	0.60 ± 1.13
19	0.80 ± 0.62	0.48 ± 0.50	-0.06 ± 0.28	0.45 ± 0.51

Table B.6.: Patient 3, RPV: Mean and standard deviation of target motion in all phases of the heartbeat, relative to the reference phase.

motion phase	ABS [mm]	SI [mm]	AP [mm]	LR [mm]
01	1.06 ± 0.66	-0.40 ± 0.92	0.12 ± 0.67	0.21 ± 0.25
02	1.30 ± 0.85	-0.39 ± 1.21	0.01 ± 0.82	-0.09 ± 0.31
03	1.97 ± 1.01	0.52 ± 1.01	0.68 ± 1.52	-0.48 ± 0.80
04	2.38 ± 1.18	0.66 ± 1.18	0.85 ± 1.80	-0.58 ± 0.95
05	2.38 ± 1.34	0.56 ± 1.10	1.21 ± 1.82	-0.92 ± 0.56
06	2.45 ± 1.40	0.71 ± 1.53	1.30 ± 1.75	-0.35 ± 0.52
07	2.66 ± 1.57	0.82 ± 1.55	1.42 ± 2.04	-0.30 ± 0.47
08	2.54 ± 1.73	0.81 ± 1.60	1.35 ± 2.03	0.23 ± 0.55
09	2.66 ± 1.57	0.82 ± 1.55	1.42 ± 2.04	-0.30 ± 0.47
10	2.62 ± 1.51	0.03 ± 1.29	0.65 ± 2.33	1.06 ± 0.73
11	2.93 ± 1.35	-0.28 ± 1.35	0.54 ± 2.45	1.21 ± 0.86
12	2.92 ± 1.29	-0.15 ± 1.38	0.38 ± 2.48	1.06 ± 0.93
13	2.62 ± 0.98	-0.14 ± 1.35	-0.06 ± 2.01	1.08 ± 0.85
14	2.53 ± 1.11	-0.10 ± 1.38	0.03 ± 2.01	0.99 ± 0.82
15	2.62 ± 1.10	-0.27 ± 1.42	-0.12 ± 2.03	1.15 ± 0.75
16	2.09 ± 0.92	-0.12 ± 0.93	-0.14 ± 1.60	1.15 ± 0.63
17	1.49 ± 0.63	0.53 ± 0.57	-0.10 ± 0.82	0.99 ± 0.58
18	1.97 ± 0.91	0.49 ± 1.03	0.03 ± 0.53	1.39 ± 1.10
19	0.99 ± 0.64	0.23 ± 0.74	0.08 ± 0.74	-0.12 ± 0.47

Table B.7.: Patient 4, LPV: Mean and standard deviation of target motion in all phases of the heartbeat, relative to the reference phase.

motion phase	ABS [mm]	SI [mm]	AP [mm]	LR [mm]
01	1.31 ± 0.54	-1.07 ± 0.67	0.23 ± 0.28	-0.36 ± 0.39
02	2.73 ± 0.90	-2.06 ± 1.06	0.46 ± 0.68	-1.04 ± 1.07
03	4.04 ± 1.73	-3.06 ± 1.69	1.09 ± 0.96	-1.07 ± 1.96
04	4.54 ± 2.11	-3.38 ± 1.91	1.13 ± 1.20	-0.93 ± 2.53
05	4.41 ± 2.41	-2.97 ± 2.01	1.08 ± 1.34	-1.37 ± 2.76
06	4.94 ± 2.74	-3.27 ± 2.29	1.29 ± 1.43	-1.97 ± 2.90
07	5.13 ± 3.09	-3.52 ± 2.40	1.27 ± 1.82	-2.00 ± 2.96
08	5.39 ± 3.44	-3.66 ± 2.89	0.68 ± 1.97	-1.63 ± 3.48
09	5.13 ± 3.09	-3.52 ± 2.40	1.27 ± 1.82	-2.00 ± 2.96
10	5.87 ± 3.53	-4.43 ± 3.15	0.27 ± 2.13	-1.49 ± 3.25
11	5.52 ± 3.06	-4.39 ± 2.94	0.18 ± 1.81	-0.27 ± 2.93
12	5.09 ± 2.83	-3.82 ± 3.15	-0.16 ± 1.64	-0.26 ± 2.58
13	4.87 ± 2.87	-3.73 ± 3.16	-0.24 ± 1.37	-0.32 ± 2.45
14	4.84 ± 2.83	-3.64 ± 3.22	-0.43 ± 1.28	-0.21 ± 2.45
15	4.94 ± 2.95	-3.78 ± 3.30	-0.20 ± 1.27	-0.40 ± 2.49
16	5.10 ± 2.90	-3.73 ± 3.35	-0.35 ± 1.42	-0.21 ± 2.68
17	4.32 ± 2.42	-3.06 ± 2.76	-0.36 ± 1.44	0.09 ± 2.32
18	2.57 ± 0.99	-1.23 ± 1.34	-0.63 ± 1.30	0.44 ± 1.43
19	0.47 ± 0.24	-0.01 ± 0.26	-0.07 ± 0.22	0.26 ± 0.30

Table B.8.: Patient 4, RPV: Mean and standard deviation of target motion in all phases of the heartbeat, relative to the reference phase.

motion phase	ABS [mm]	SI [mm]	AP [mm]	LR [mm]
01	1.31 ± 0.92	-0.85 ± 1.17	0.03 ± 0.62	0.21 ± 0.19
02	2.07 ± 1.03	-0.90 ± 1.66	0.65 ± 1.04	0.43 ± 0.34
03	3.56 ± 2.05	-1.50 ± 2.11	1.99 ± 2.11	1.24 ± 0.48
04	4.59 ± 2.44	1.82 ± 2.81	2.28 ± 2.68	1.71 ± 0.70
05	4.76 ± 2.66	-1.30 ± 2.81	2.62 ± 3.11	1.72 ± 0.84
06	5.30 ± 3.05	-1.59 ± 3.20	2.90 ± 3.48	1.68 ± 1.13
07	5.82 ± 3.35	-1.63 ± 3.51	3.30 ± 3.75	1.70 ± 1.50
08	6.18 ± 3.19	-1.78 ± 3.93	3.02 ± 3.74	2.10 ± 1.51
09	5.82 ± 3.35	-1.63 ± 3.51	3.30 ± 3.75	1.70 ± 1.50
10	6.49 ± 3.00	-1.78 ± 4.11	2.68 ± 3.85	2.70 ± 1.38
11	6.43 ± 2.55	-2.25 ± 3.95	2.20 ± 3.41	3.14 ± 0.98
12	5.94 ± 2.18	-2.32 ± 3.65	1.52 ± 3.11	2.94 ± 0.87
13	5.54 ± 2.05	-2.35 ± 3.58	1.12 ± 2.76	2.67 ± 0.75
14	5.23 ± 2.13	-2.34 ± 3.58	0.73 ± 2.57	2.41 ± 0.81
15	5.25 ± 2.25	-2.42 ± 3.69	0.63 ± 2.73	2.22 ± 0.61
16	5.62 ± 2.23	-2.35 ± 3.81	0.93 ± 2.86	2.61 ± 0.84
17	4.61 ± 1.70	-1.80 ± 3.02	1.03 ± 2.56	1.88 ± 0.82
18	2.66 ± 0.54	-1.03 ± 1.15	0.72 ± 1.19	1.64 ± 0.60
19	0.62 ± 0.33	-0.20 ± 0.47	0.06 ± 0.33	0.17 ± 0.30

Table B.9.: Patient 5, LPV: Mean and standard deviation of target motion in all phases of the heartbeat, relative to the reference phase.

motion phase	ABS [mm]	SI [mm]	AP [mm]	LR [mm]
01	0.38 ± 0.23	0.12 ± 0.29	0.03 ± 0.25	0.09 ± 0.17
02	1.13 ± 0.51	0.32 ± 0.80	0.07 ± 0.68	0.20 ± 0.52
03	1.63 ± 0.64	-0.03 ± 1.23	0.35 ± 0.79	-0.53 ± 0.73
04	1.86 ± 0.72	0.03 ± 1.22	0.49 ± 0.85	-0.59 ± 1.10
05	1.77 ± 0.69	0.04 ± 1.20	0.43 ± 0.87	-0.51 ± 0.98
06	2.12 ± 1.25	0.30 ± 1.18	0.73 ± 1.28	-1.03 ± 1.17
07	2.46 ± 1.33	0.05 ± 1.34	0.85 ± 1.68	-1.27 ± 0.92
08	2.76 ± 1.27	-0.11 ± 1.19	0.98 ± 1.86	-1.63 ± 0.88
09	2.46 ± 1.33	0.05 ± 1.34	0.85 ± 1.68	-1.27 ± 0.92
10	2.58 ± 1.56	-1.13 ± 1.57	1.32 ± 1.60	-0.43 ± 0.94
11	2.56 ± 1.37	-1.31 ± 1.85	0.98 ± 0.99	-0.31 ± 1.12
12	2.68 ± 1.58	-1.58 ± 2.07	0.84 ± 0.91	-0.06 ± 1.17
13	2.73 ± 1.68	-1.62 ± 2.11	0.77 ± 0.92	0.46 ± 1.24
14	2.48 ± 1.46	-1.63 ± 1.78	0.70 ± 0.93	0.36 ± 0.97
15	2.70 ± 1.55	-1.90 ± 1.83	0.90 ± 0.95	0.38 ± 0.91
16	2.92 ± 1.54	-2.16 ± 1.72	0.91 ± 0.94	0.44 ± 1.17
17	2.70 ± 1.63	-2.10 ± 1.61	0.97 ± 0.90	0.56 ± 0.94
18	2.13 ± 0.90	-1.15 ± 1.03	0.52 ± 0.94	1.13 ± 0.72
19	0.84 ± 0.47	-0.38 ± 0.37	0.08 ± 0.32	0.53 ± 0.52

Table B.10.: Patient 5, RPV: Mean and standard deviation of target motion in all phases of the heartbeat, relative to the reference phase.

motion phase	ABS [mm]	SI [mm]	AP [mm]	LR [mm]
01	0.61 ± 0.33	0.22 ± 0.50	0.04 ± 0.22	0.17 ± 0.32
02	1.56 ± 0.82	0.61 ± 1.15	0.10 ± 0.57	0.63 ± 0.82
03	2.21 ± 1.10	0.77 ± 1.61	0.22 ± 0.67	0.95 ± 1.24
04	2.42 ± 1.48	1.12 ± 1.37	0.60 ± 0.89	1.49 ± 1.23
05	2.69 ± 2.22	1.27 ± 1.62	1.23 ± 1.26	1.29 ± 1.78
06	2.89 ± 2.15	1.32 ± 1.23	1.75 ± 1.81	0.85 ± 1.65
07	3.08 ± 2.12	1.29 ± 1.54	1.87 ± 1.69	0.89 ± 1.69
08	3.14 ± 2.11	1.17 ± 1.59	1.96 ± 1.85	0.50 ± 1.69
09	3.08 ± 2.12	1.29 ± 1.54	1.87 ± 1.69	0.89 ± 1.69
10	3.05 ± 1.96	0.79 ± 1.99	1.75 ± 1.60	0.94 ± 1.44
11	2.98 ± 1.74	0.12 ± 1.99	1.24 ± 1.29	1.34 ± 1.73
12	3.24 ± 1.63	-0.15 ± 2.09	1.19 ± 1.36	1.96 ± 1.28
13	3.61 ± 1.58	-0.28 ± 2.26	1.09 ± 1.30	2.48 ± 1.15
14	3.73 ± 1.97	-0.78 ± 2.57	1.01 ± 1.16	2.49 ± 1.41
15	3.95 ± 2.27	-1.16 ± 2.83	0.92 ± 1.15	2.54 ± 1.68
16	3.65 ± 1.84	-1.11 ± 2.18	0.94 ± 1.14	2.46 ± 1.59
17	3.54 ± 1.95	-1.11 ± 2.06	1.02 ± 1.18	2.39 ± 1.65
18	2.53 ± 0.93	-0.77 ± 1.02	0.53 ± 0.85	2.00 ± 0.81
19	0.74 ± 0.45	-0.35 ± 0.32	0.17 ± 0.33	0.31 ± 0.54

B.2 Values of dose analysis parameters for all patients

In the following the D5-D95, V95 and V107 values will be presented for all patient data sets (patient 1 to 5) and target volumes (LPV and RPV). All studied techniques (static, interplay and rescanning with five, ten, fifteen and twenty rescans) will be shown for four different motion patterns and all studied safety margins (0mm, 3mm, 5mm, 7mm).

Table B.11.: Patient 1, LPV

Case	motion period	motion starting phase	Margin	rescan no.	D5-D95 [%]	V95 [%]	V107 [%]
STATIC	-	-	0mm	-	5.94	98.16	0.00
STATIC	-	-	3mm	-	3.31	100.00	0.00
STATIC	-	-	5mm	-	3.32	100.00	0.00
STATIC	-	-	7mm	-	3.06	100.00	0.26
INTERPLAY	1s	0	0mm	-	14.84	87.93	6.30
INTERPLAY	1s	90	0mm	-	12.05	91.86	2.89
INTERPLAY	0.7s	0	0mm	-	12.16	91.60	2.10
INTERPLAY	0.7s	90	0mm	-	10.54	93.44	0.52
INTERPLAY	1s	0	3mm	-	13.68	91.34	5.25
INTERPLAY	1s	90	3mm	-	14.30	86.88	5.25
INTERPLAY	0.7s	0	3mm	-	10.45	93.18	1.31
INTERPLAY	0.7s	90	3mm	-	9.04	97.38	1.05
INTERPLAY	1s	0	5mm	-	7.59	98.43	0.00
INTERPLAY	1s	90	5mm	-	7.45	99.48	0.79
INTERPLAY	0.7s	0	5mm	-	10.24	95.01	1.31
INTERPLAY	0.7s	90	5mm	-	9.22	96.85	0.52
INTERPLAY	1s	0	7mm	-	7.46	98.16	0.00
INTERPLAY	1s	90	7mm	-	7.48	98.95	0.79
INTERPLAY	0.7s	0	7mm	-	9.67	95.54	1.05
INTERPLAY	0.7s	90	7mm	-	9.29	97.38	0.79
RESCANNING	1s	0	0mm	5	9.07	97.38	0.79
RESCANNING	1s	0	0mm	10	8.28	98.16	0.00
RESCANNING	1s	0	0mm	15	7.95	97.64	0.00
RESCANNING	1s	0	0mm	20	7.49	97.90	0.00
RESCANNING	1s	90	0mm	5	8.34	96.06	0.26
RESCANNING	1s	90	0mm	10	7.37	98.43	0.26
RESCANNING	1s	90	0mm	15	7.12	98.95	0.26
RESCANNING	1s	90	0mm	20	6.75	98.43	0.26
RESCANNING	0.7s	0	0mm	5	7.71	97.64	0.26
RESCANNING	0.7s	0	0mm	10	5.79	99.48	0.00
RESCANNING	0.7s	0	0mm	15	6.43	99.21	0.00
RESCANNING	0.7s	0	0mm	20	5.90	99.21	0.00
RESCANNING	0.7s	90	0mm	5	7.29	96.59	0.00
RESCANNING	0.7s	90	0mm	10	6.46	99.21	0.00
RESCANNING	0.7s	90	0mm	15	5.82	98.95	0.00
RESCANNING	0.7s	90	0mm	20	6.08	98.95	0.00
RESCANNING	1s	0	3mm	5	7.52	100.00	1.05
RESCANNING	1s	0	3mm	10	5.41	100.00	0.00
RESCANNING	1s	0	3mm	15	4.63	100.00	0.00
RESCANNING	1s	0	3mm	20	5.22	100.00	0.00
RESCANNING	1s	90	3mm	5	8.83	93.18	0.00
RESCANNING	1s	90	3mm	10	6.19	99.21	0.00
RESCANNING	1s	90	3mm	15	5.40	100.00	0.00
RESCANNING	1s	90	3mm	20	5.17	100.00	0.00
RESCANNING	0.7s	0	3mm	5	5.68	100.00	0.00
RESCANNING	0.7s	0	3mm	10	4.49	100.00	0.00
RESCANNING	0.7s	0	3mm	15	3.95	100.00	0.00
RESCANNING	0.7s	0	3mm	20	3.59	100.00	0.00
RESCANNING	0.7s	90	3mm	5	6.34	99.74	0.00
RESCANNING	0.7s	90	3mm	10	3.98	100.00	0.00
RESCANNING	0.7s	90	3mm	15	3.53	100.00	0.00
RESCANNING	0.7s	90	3mm	20	3.47	100.00	0.00
RESCANNING	1s	0	5mm	5	6.49	100.00	0.00
RESCANNING	1s	0	5mm	10	4.21	100.00	0.00
RESCANNING	1s	0	5mm	15	4.11	100.00	0.00
RESCANNING	1s	0	5mm	20	3.26	100.00	0.00
RESCANNING	1s	90	5mm	5	9.00	98.16	1.05
RESCANNING	1s	90	5mm	10	7.27	100.00	0.00
RESCANNING	1s	90	5mm	15	6.34	100.00	0.26
RESCANNING	1s	90	5mm	20	6.26	100.00	0.26
RESCANNING	0.7s	0	5mm	5	6.45	99.74	0.00
RESCANNING	0.7s	0	5mm	10	3.77	100.00	0.00
RESCANNING	0.7s	0	5mm	15	2.77	100.00	0.00
RESCANNING	0.7s	0	5mm	20	2.54	100.00	0.00
RESCANNING	0.7s	90	5mm	5	5.04	100.00	0.00
RESCANNING	0.7s	90	5mm	10	3.75	100.00	0.00
RESCANNING	0.7s	90	5mm	15	2.88	100.00	0.00
RESCANNING	0.7s	90	5mm	20	3.00	100.00	0.00
RESCANNING	1s	0	7mm	5	5.35	100.00	0.00
RESCANNING	1s	0	7mm	10	4.10	100.00	0.00
RESCANNING	1s	0	7mm	15	3.74	100.00	0.00
RESCANNING	1s	0	7mm	20	3.69	100.00	0.00
RESCANNING	1s	90	7mm	5	7.05	96.85	0.00
RESCANNING	1s	90	7mm	10	7.30	97.11	0.00
RESCANNING	1s	90	7mm	15	5.47	100.00	0.00
RESCANNING	1s	90	7mm	20	4.97	100.00	0.00
RESCANNING	0.7s	0	7mm	5	5.60	99.48	0.00
RESCANNING	0.7s	0	7mm	10	3.41	100.00	0.00
RESCANNING	0.7s	0	7mm	15	3.18	100.00	0.00
RESCANNING	0.7s	0	7mm	20	2.72	100.00	0.00
RESCANNING	0.7s	90	7mm	5	5.61	100.00	0.00
RESCANNING	0.7s	90	7mm	10	3.90	100.00	0.00
RESCANNING	0.7s	90	7mm	15	3.35	100.00	0.00
RESCANNING	0.7s	90	7mm	20	2.87	100.00	0.00

Table B.12.: Patient 1, RPV

Case	motion period	motion starting phase	Margin	rescan no.	D5-D95 [%]	V95 [%]	V107 [%]
STATIC	-	-	0mm	-	4.86	98.88	0.00
STATIC	-	-	3mm	-	3.63	100.00	0.00
STATIC	-	-	5mm	-	3.08	100.00	0.00
STATIC	-	-	7mm	-	3.23	100.00	0.00
INTERPLAY	1s	0	0mm	-	12.50	89.29	3.57
INTERPLAY	1s	90	0mm	-	11.64	91.74	1.12
INTERPLAY	0.7s	0	0mm	-	11.57	90.40	2.01
INTERPLAY	0.7s	90	0mm	-	9.08	96.43	0.22
INTERPLAY	1s	0	3mm	-	11.01	92.63	1.56
INTERPLAY	1s	90	3mm	-	10.40	96.65	1.56
INTERPLAY	0.7s	0	3mm	-	10.55	94.64	1.12
INTERPLAY	0.7s	90	3mm	-	8.24	97.77	0.00
INTERPLAY	1s	0	5mm	-	9.34	95.98	0.00
INTERPLAY	1s	90	5mm	-	7.92	98.66	0.22
INTERPLAY	0.7s	0	5mm	-	6.41	98.88	0.00
INTERPLAY	0.7s	90	5mm	-	6.07	100.00	0.00
INTERPLAY	1s	0	7mm	-	9.21	95.76	0.00
INTERPLAY	1s	90	7mm	-	7.78	98.21	0.00
INTERPLAY	0.7s	0	7mm	-	6.20	98.44	0.00
INTERPLAY	0.7s	90	7mm	-	6.10	99.78	0.00
RESCANNING	1s	0	0mm	5	8.32	95.09	0.00
RESCANNING	1s	0	0mm	10	6.81	96.88	0.00
RESCANNING	1s	0	0mm	15	7.15	96.43	0.00
RESCANNING	1s	0	0mm	20	6.85	96.43	0.00
RESCANNING	1s	90	0mm	5	8.61	94.64	0.00
RESCANNING	1s	90	0mm	10	6.91	96.65	0.00
RESCANNING	1s	90	0mm	15	7.26	96.21	0.22
RESCANNING	1s	90	0mm	20	7.45	96.21	0.00
RESCANNING	0.7s	0	0mm	5	7.96	96.65	0.22
RESCANNING	0.7s	0	0mm	10	6.70	96.21	0.00
RESCANNING	0.7s	0	0mm	15	6.52	96.88	0.00
RESCANNING	0.7s	0	0mm	20	6.52	96.43	0.00
RESCANNING	0.7s	90	0mm	5	8.30	93.97	0.00
RESCANNING	0.7s	90	0mm	10	7.46	94.87	0.00
RESCANNING	0.7s	90	0mm	15	6.28	97.10	0.00
RESCANNING	0.7s	90	0mm	20	6.28	96.43	0.00
RESCANNING	1s	0	3mm	5	5.59	100.00	0.00
RESCANNING	1s	0	3mm	10	4.61	100.00	0.00
RESCANNING	1s	0	3mm	15	3.90	100.00	0.00
RESCANNING	1s	0	3mm	20	3.94	100.00	0.00
RESCANNING	1s	90	3mm	5	6.41	100.00	0.00
RESCANNING	1s	90	3mm	10	4.90	99.78	0.00
RESCANNING	1s	90	3mm	15	4.24	100.00	0.00
RESCANNING	1s	90	3mm	20	4.36	100.00	0.00
RESCANNING	0.7s	0	3mm	5	5.79	100.00	0.00
RESCANNING	0.7s	0	3mm	10	3.75	100.00	0.00
RESCANNING	0.7s	0	3mm	15	3.54	100.00	0.00
RESCANNING	0.7s	0	3mm	20	3.67	100.00	0.00
RESCANNING	0.7s	90	3mm	5	5.59	99.33	0.00
RESCANNING	0.7s	90	3mm	10	4.18	100.00	0.00
RESCANNING	0.7s	90	3mm	15	3.67	100.00	0.00
RESCANNING	0.7s	90	3mm	20	3.48	100.00	0.00
RESCANNING	1s	0	5mm	5	6.01	100.00	0.00
RESCANNING	1s	0	5mm	10	4.16	100.00	0.00
RESCANNING	1s	0	5mm	15	3.96	100.00	0.00
RESCANNING	1s	0	5mm	20	3.86	100.00	0.00
RESCANNING	1s	90	5mm	5	6.67	97.99	0.00
RESCANNING	1s	90	5mm	10	4.37	100.00	0.00
RESCANNING	1s	90	5mm	15	4.00	100.00	0.00
RESCANNING	1s	90	5mm	20	4.01	100.00	0.00
RESCANNING	0.7s	0	5mm	5	4.21	100.00	0.00
RESCANNING	0.7s	0	5mm	10	3.52	100.00	0.00
RESCANNING	0.7s	0	5mm	15	2.79	100.00	0.00
RESCANNING	0.7s	0	5mm	20	3.02	100.00	0.00
RESCANNING	0.7s	90	5mm	5	4.83	100.00	0.00
RESCANNING	0.7s	90	5mm	10	3.38	100.00	0.00
RESCANNING	0.7s	90	5mm	15	3.00	100.00	0.00
RESCANNING	0.7s	90	5mm	20	2.54	100.00	0.00
RESCANNING	1s	0	7mm	5	5.61	100.00	0.22
RESCANNING	1s	0	7mm	10	4.34	100.00	0.00
RESCANNING	1s	0	7mm	15	4.10	100.00	0.00
RESCANNING	1s	0	7mm	20	3.71	100.00	0.00
RESCANNING	1s	90	7mm	5	6.77	98.44	0.00
RESCANNING	1s	90	7mm	10	3.75	100.00	0.00
RESCANNING	1s	90	7mm	15	3.80	100.00	0.00
RESCANNING	1s	90	7mm	20	3.74	100.00	0.00
RESCANNING	0.7s	0	7mm	5	5.37	100.00	0.00
RESCANNING	0.7s	0	7mm	10	3.22	100.00	0.00
RESCANNING	0.7s	0	7mm	15	2.75	100.00	0.00
RESCANNING	0.7s	0	7mm	20	2.20	100.00	0.00
RESCANNING	0.7s	90	7mm	5	5.23	100.00	0.00
RESCANNING	0.7s	90	7mm	10	3.33	100.00	0.00
RESCANNING	0.7s	90	7mm	15	2.74	100.00	0.00
RESCANNING	0.7s	90	7mm	20	2.09	100.00	0.00

Table B.13.: Patient 2, LPV

Case	motion period	motion starting phase	Margin	rescan no.	D5-D95 [%]	V95 [%]	V107 [%]
STATIC	-	-	0mm	-	14.19	89.75	0.00
STATIC	-	-	3mm	-	2.93	100.00	0.00
STATIC	-	-	5mm	-	2.64	100.00	0.00
STATIC	-	-	7mm	-	2.42	100.00	0.00
INTERPLAY	1s	0	0mm	-	8.27	96.93	0.41
INTERPLAY	1s	90	0mm	-	9.61	95.29	2.66
INTERPLAY	0.7s	0	0mm	-	9.22	94.88	0.82
INTERPLAY	0.7s	90	0mm	-	6.65	99.39	0.20
INTERPLAY	1s	0	3mm	-	11.75	93.65	2.87
INTERPLAY	1s	90	3mm	-	11.56	94.88	3.89
INTERPLAY	0.7s	0	3mm	-	7.90	99.80	1.64
INTERPLAY	0.7s	90	3mm	-	7.07	99.80	0.20
INTERPLAY	1s	0	5mm	-	8.06	97.75	0.20
INTERPLAY	1s	90	5mm	-	9.78	95.49	2.66
INTERPLAY	0.7s	0	5mm	-	8.89	95.29	0.82
INTERPLAY	0.7s	90	5mm	-	6.54	98.98	0.00
INTERPLAY	1s	0	7mm	-	6.78	98.16	0.00
INTERPLAY	1s	90	7mm	-	7.06	99.59	0.20
INTERPLAY	0.7s	0	7mm	-	8.90	95.08	1.02
INTERPLAY	0.7s	90	7mm	-	6.41	99.18	0.20
RESCANNING	1s	0	0mm	5	17.86	89.55	7.99
RESCANNING	1s	0	0mm	10	13.98	90.78	2.87
RESCANNING	1s	0	0mm	15	13.00	90.57	0.20
RESCANNING	1s	0	0mm	20	12.15	90.57	0.20
RESCANNING	1s	90	0mm	5	10.86	87.30	0.00
RESCANNING	1s	90	0mm	10	11.21	88.93	0.00
RESCANNING	1s	90	0mm	15	10.70	88.73	0.00
RESCANNING	1s	90	0mm	20	10.65	88.93	0.00
RESCANNING	0.7s	0	0mm	5	11.05	91.80	0.20
RESCANNING	0.7s	0	0mm	10	10.21	90.98	0.00
RESCANNING	0.7s	0	0mm	15	10.46	90.98	0.00
RESCANNING	0.7s	0	0mm	20	10.29	90.78	0.00
RESCANNING	0.7s	90	0mm	5	11.30	91.39	0.20
RESCANNING	0.7s	90	0mm	10	10.28	91.39	0.00
RESCANNING	0.7s	90	0mm	15	10.33	90.98	0.00
RESCANNING	0.7s	90	0mm	20	10.18	91.39	0.00
RESCANNING	1s	0	3mm	5	6.72	100.00	0.20
RESCANNING	1s	0	3mm	10	5.28	100.00	0.00
RESCANNING	1s	0	3mm	15	4.54	100.00	0.00
RESCANNING	1s	0	3mm	20	4.41	100.00	0.00
RESCANNING	1s	90	3mm	5	5.67	98.57	0.00
RESCANNING	1s	90	3mm	10	4.67	100.00	0.00
RESCANNING	1s	90	3mm	15	4.33	100.00	0.00
RESCANNING	1s	90	3mm	20	4.34	100.00	0.00
RESCANNING	0.7s	0	3mm	5	4.89	99.39	0.00
RESCANNING	0.7s	0	3mm	10	4.09	100.00	0.00
RESCANNING	0.7s	0	3mm	15	3.13	100.00	0.00
RESCANNING	0.7s	0	3mm	20	2.79	100.00	0.00
RESCANNING	0.7s	90	3mm	5	6.72	100.00	0.41
RESCANNING	0.7s	90	3mm	10	4.54	99.80	0.00
RESCANNING	0.7s	90	3mm	15	2.94	100.00	0.00
RESCANNING	0.7s	90	3mm	20	2.91	100.00	0.00
RESCANNING	1s	0	5mm	5	5.50	100.00	0.00
RESCANNING	1s	0	5mm	10	3.87	100.00	0.00
RESCANNING	1s	0	5mm	15	3.43	100.00	0.00
RESCANNING	1s	0	5mm	20	2.92	100.00	0.00
RESCANNING	1s	90	5mm	5	5.31	99.59	0.00
RESCANNING	1s	90	5mm	10	4.35	100.00	0.00
RESCANNING	1s	90	5mm	15	3.63	100.00	0.00
RESCANNING	1s	90	5mm	20	3.53	100.00	0.00
RESCANNING	0.7s	0	5mm	5	5.23	100.00	0.00
RESCANNING	0.7s	0	5mm	10	3.65	100.00	0.00
RESCANNING	0.7s	0	5mm	15	3.03	100.00	0.00
RESCANNING	0.7s	0	5mm	20	2.88	100.00	0.00
RESCANNING	0.7s	90	5mm	5	4.18	100.00	0.00
RESCANNING	0.7s	90	5mm	10	3.17	100.00	0.00
RESCANNING	0.7s	90	5mm	15	2.73	100.00	0.00
RESCANNING	0.7s	90	5mm	20	2.12	100.00	0.00
RESCANNING	1s	0	7mm	5	5.42	100.00	0.00
RESCANNING	1s	0	7mm	10	2.90	100.00	0.00
RESCANNING	1s	0	7mm	15	3.26	100.00	0.00
RESCANNING	1s	0	7mm	20	2.51	100.00	0.00
RESCANNING	1s	90	7mm	5	5.85	99.59	0.00
RESCANNING	1s	90	7mm	10	3.76	100.00	0.00
RESCANNING	1s	90	7mm	15	3.32	100.00	0.00
RESCANNING	1s	90	7mm	20	3.73	100.00	0.00
RESCANNING	0.7s	0	7mm	5	3.68	100.00	0.00
RESCANNING	0.7s	0	7mm	10	2.89	100.00	0.00
RESCANNING	0.7s	0	7mm	15	3.01	100.00	0.00
RESCANNING	0.7s	0	7mm	20	2.16	100.00	0.00
RESCANNING	0.7s	90	7mm	5	4.56	100.00	0.00
RESCANNING	0.7s	90	7mm	10	3.22	100.00	0.00
RESCANNING	0.7s	90	7mm	15	2.51	100.00	0.00
RESCANNING	0.7s	90	7mm	20	2.07	100.00	0.00

Table B.14.: Patient 2, RPV

Case	motion period	motion starting phase	Margin	rescan no.	D5-D95 [%]	V95 [%]	V107 [%]
STATIC	-	-	0mm	-	12.37	89.27	0.00
STATIC	-	-	3mm	-	3.47	99.58	0.00
STATIC	-	-	5mm	-	3.17	99.79	0.00
STATIC	-	-	7mm	-	3.18	99.79	0.00
INTERPLAY	1s	0	0mm	-	9.41	94.38	1.15
INTERPLAY	1s	90	0mm	-	10.47	92.19	1.15
INTERPLAY	0.7s	0	0mm	-	8.64	97.71	0.31
INTERPLAY	0.7s	90	0mm	-	7.85	98.54	0.10
INTERPLAY	1s	0	3mm	-	11.05	93.33	1.67
INTERPLAY	1s	90	3mm	-	11.73	91.15	1.46
INTERPLAY	0.7s	0	3mm	-	9.84	92.08	0.73
INTERPLAY	0.7s	90	3mm	-	9.66	95.10	0.73
INTERPLAY	1s	0	5mm	-	9.29	94.38	1.15
INTERPLAY	1s	90	5mm	-	10.39	91.98	1.25
INTERPLAY	0.7s	0	5mm	-	8.71	98.23	0.52
INTERPLAY	0.7s	90	5mm	-	7.74	99.06	0.10
INTERPLAY	1s	0	7mm	-	8.48	97.40	0.42
INTERPLAY	1s	90	7mm	-	9.19	95.94	0.10
INTERPLAY	0.7s	0	7mm	-	8.91	97.60	0.73
INTERPLAY	0.7s	90	7mm	-	7.87	98.54	0.31
RESCANNING	1s	0	0mm	5	12.09	86.35	0.21
RESCANNING	1s	0	0mm	10	10.92	88.02	0.00
RESCANNING	1s	0	0mm	15	10.94	87.40	0.00
RESCANNING	1s	0	0mm	20	10.60	88.65	0.00
RESCANNING	1s	90	0mm	5	12.14	84.58	0.31
RESCANNING	1s	90	0mm	10	12.24	87.60	0.00
RESCANNING	1s	90	0mm	15	11.13	87.71	0.00
RESCANNING	1s	90	0mm	20	11.21	88.96	0.00
RESCANNING	0.7s	0	0mm	5	12.06	87.40	0.10
RESCANNING	0.7s	0	0mm	10	11.01	90.10	0.00
RESCANNING	0.7s	0	0mm	15	10.87	90.42	0.00
RESCANNING	0.7s	0	0mm	20	10.12	91.25	0.00
RESCANNING	0.7s	90	0mm	5	12.50	89.27	0.62
RESCANNING	0.7s	90	0mm	10	10.91	90.42	0.00
RESCANNING	0.7s	90	0mm	15	10.45	90.83	0.00
RESCANNING	0.7s	90	0mm	20	10.35	90.62	0.00
RESCANNING	1s	0	3mm	5	8.82	94.69	0.10
RESCANNING	1s	0	3mm	10	5.45	99.06	0.00
RESCANNING	1s	0	3mm	15	4.74	99.58	0.00
RESCANNING	1s	0	3mm	20	4.63	99.58	0.00
RESCANNING	1s	90	3mm	5	7.45	97.50	0.00
RESCANNING	1s	90	3mm	10	6.43	99.69	0.00
RESCANNING	1s	90	3mm	15	5.33	99.38	0.00
RESCANNING	1s	90	3mm	20	5.09	99.48	0.00
RESCANNING	0.7s	0	3mm	5	5.78	99.27	0.21
RESCANNING	0.7s	0	3mm	10	4.53	99.58	0.00
RESCANNING	0.7s	0	3mm	15	3.91	99.48	0.00
RESCANNING	0.7s	0	3mm	20	3.50	99.58	0.00
RESCANNING	0.7s	90	3mm	5	5.88	99.06	0.00
RESCANNING	0.7s	90	3mm	10	4.34	99.79	0.10
RESCANNING	0.7s	90	3mm	15	4.35	99.38	0.00
RESCANNING	0.7s	90	3mm	20	3.66	99.58	0.00
RESCANNING	1s	0	5mm	5	9.22	99.06	3.02
RESCANNING	1s	0	5mm	10	5.18	99.58	0.00
RESCANNING	1s	0	5mm	15	4.89	99.79	0.00
RESCANNING	1s	0	5mm	20	4.16	99.79	0.00
RESCANNING	1s	90	5mm	5	7.67	99.58	0.73
RESCANNING	1s	90	5mm	10	5.36	99.69	0.00
RESCANNING	1s	90	5mm	15	4.88	99.79	0.00
RESCANNING	1s	90	5mm	20	4.62	99.79	0.00
RESCANNING	0.7s	0	5mm	5	6.76	99.06	0.10
RESCANNING	0.7s	0	5mm	10	4.43	99.90	0.00
RESCANNING	0.7s	0	5mm	15	3.87	99.69	0.00
RESCANNING	0.7s	0	5mm	20	3.35	99.69	0.00
RESCANNING	0.7s	90	5mm	5	5.31	99.38	0.00
RESCANNING	0.7s	90	5mm	10	4.33	99.69	0.00
RESCANNING	0.7s	90	5mm	15	3.49	99.79	0.00
RESCANNING	0.7s	90	5mm	20	3.28	99.90	0.00
RESCANNING	1s	0	7mm	5	6.68	99.48	0.00
RESCANNING	1s	0	7mm	10	5.61	99.58	0.10
RESCANNING	1s	0	7mm	15	3.83	99.79	0.00
RESCANNING	1s	0	7mm	20	4.13	99.90	0.00
RESCANNING	1s	90	7mm	5	8.62	99.17	1.04
RESCANNING	1s	90	7mm	10	5.34	99.58	0.00
RESCANNING	1s	90	7mm	15	3.79	100.00	0.00
RESCANNING	1s	90	7mm	20	4.22	99.90	0.00
RESCANNING	0.7s	0	7mm	5	5.92	99.79	0.00
RESCANNING	0.7s	0	7mm	10	4.01	99.90	0.00
RESCANNING	0.7s	0	7mm	15	3.75	99.90	0.00
RESCANNING	0.7s	0	7mm	20	3.35	99.79	0.00
RESCANNING	0.7s	90	7mm	5	5.60	99.79	0.00
RESCANNING	0.7s	90	7mm	10	4.37	99.69	0.00
RESCANNING	0.7s	90	7mm	15	3.70	99.90	0.00
RESCANNING	0.7s	90	7mm	20	2.96	100.00	0.00

Table B.15.: Patient 3, LPV

Case	motion period	motion starting phase	Margin	rescan no.	D5-D95 [%]	V95 [%]	V107 [%]
STATIC	-	-	0mm	-	4.67	100.00	0.29
STATIC	-	-	3mm	-	4.14	100.00	0.00
STATIC	-	-	5mm	-	3.47	100.00	0.00
STATIC	-	-	7mm	-	3.08	100.00	0.00
INTERPLAY	1s	0	0mm	-	13.88	87.71	2.00
INTERPLAY	1s	90	0mm	-	10.18	77.14	0.00
INTERPLAY	0.7s	0	0mm	-	10.92	89.14	1.43
INTERPLAY	0.7s	90	0mm	-	10.96	86.57	0.29
INTERPLAY	1s	0	3mm	-	7.79	100.00	0.86
INTERPLAY	1s	90	3mm	-	8.30	97.14	0.00
INTERPLAY	0.7s	0	3mm	-	9.59	95.71	0.29
INTERPLAY	0.7s	90	3mm	-	7.41	99.43	2.00
INTERPLAY	1s	0	5mm	-	7.79	100.00	1.14
INTERPLAY	1s	90	5mm	-	8.40	96.86	0.00
INTERPLAY	0.7s	0	5mm	-	9.47	95.71	0.00
INTERPLAY	0.7s	90	5mm	-	7.55	99.43	1.14
INTERPLAY	1s	0	7mm	-	7.82	100.00	1.43
INTERPLAY	1s	90	7mm	-	8.33	96.57	0.00
INTERPLAY	0.7s	0	7mm	-	9.42	96.00	0.29
INTERPLAY	0.7s	90	7mm	-	7.81	98.86	1.14
RESCANNING	1s	0	0mm	5	8.88	96.00	0.29
RESCANNING	1s	0	0mm	10	8.90	95.71	0.00
RESCANNING	1s	0	0mm	15	8.63	96.86	0.29
RESCANNING	1s	0	0mm	20	8.46	97.43	0.29
RESCANNING	1s	90	0mm	5	9.42	92.00	0.57
RESCANNING	1s	90	0mm	10	9.27	93.71	0.00
RESCANNING	1s	90	0mm	15	8.93	94.00	0.29
RESCANNING	1s	90	0mm	20	8.35	93.71	0.00
RESCANNING	0.7s	0	0mm	5	8.86	92.00	0.00
RESCANNING	0.7s	0	0mm	10	8.19	95.71	0.00
RESCANNING	0.7s	0	0mm	15	7.61	95.14	0.00
RESCANNING	0.7s	0	0mm	20	7.36	96.29	0.00
RESCANNING	0.7s	90	0mm	5	8.88	94.00	0.00
RESCANNING	0.7s	90	0mm	10	6.94	95.71	0.00
RESCANNING	0.7s	90	0mm	15	6.40	97.14	0.00
RESCANNING	0.7s	90	0mm	20	5.96	98.00	0.00
RESCANNING	1s	0	3mm	5	6.57	100.00	0.29
RESCANNING	1s	0	3mm	10	6.50	100.00	0.57
RESCANNING	1s	0	3mm	15	5.61	100.00	0.00
RESCANNING	1s	0	3mm	20	5.32	100.00	0.00
RESCANNING	1s	90	3mm	5	6.86	100.00	0.29
RESCANNING	1s	90	3mm	10	5.89	100.00	0.00
RESCANNING	1s	90	3mm	15	5.94	100.00	0.29
RESCANNING	1s	90	3mm	20	5.17	100.00	0.00
RESCANNING	0.7s	0	3mm	5	5.78	99.43	0.00
RESCANNING	0.7s	0	3mm	10	4.23	99.71	0.00
RESCANNING	0.7s	0	3mm	15	3.69	99.71	0.00
RESCANNING	0.7s	0	3mm	20	3.34	99.71	0.00
RESCANNING	0.7s	90	3mm	5	5.85	99.43	0.00
RESCANNING	0.7s	90	3mm	10	4.57	99.71	0.00
RESCANNING	0.7s	90	3mm	15	4.14	100.00	0.00
RESCANNING	0.7s	90	3mm	20	3.62	99.71	0.00
RESCANNING	1s	0	5mm	5	8.21	100.00	3.71
RESCANNING	1s	0	5mm	10	4.89	100.00	0.00
RESCANNING	1s	0	5mm	15	4.73	100.00	0.00
RESCANNING	1s	0	5mm	20	4.20	100.00	0.00
RESCANNING	1s	90	5mm	5	7.77	99.14	0.86
RESCANNING	1s	90	5mm	10	5.17	100.00	0.00
RESCANNING	1s	90	5mm	15	4.91	100.00	0.00
RESCANNING	1s	90	5mm	20	4.08	100.00	0.00
RESCANNING	0.7s	0	5mm	5	5.81	100.00	0.00
RESCANNING	0.7s	0	5mm	10	4.83	100.00	0.00
RESCANNING	0.7s	0	5mm	15	4.02	100.00	0.00
RESCANNING	0.7s	0	5mm	20	4.23	100.00	0.00
RESCANNING	0.7s	90	5mm	5	5.57	100.00	0.00
RESCANNING	0.7s	90	5mm	10	4.37	100.00	0.00
RESCANNING	0.7s	90	5mm	15	4.52	100.00	0.00
RESCANNING	0.7s	90	5mm	20	4.65	100.00	0.00
RESCANNING	1s	0	7mm	5	5.24	100.00	0.00
RESCANNING	1s	0	7mm	10	6.37	100.00	0.00
RESCANNING	1s	0	7mm	15	5.31	100.00	0.00
RESCANNING	1s	0	7mm	20	5.39	100.00	0.00
RESCANNING	1s	90	7mm	5	5.87	99.43	0.00
RESCANNING	1s	90	7mm	10	5.61	99.71	0.00
RESCANNING	1s	90	7mm	15	5.35	100.00	0.00
RESCANNING	1s	90	7mm	20	5.19	99.71	0.00
RESCANNING	0.7s	0	7mm	5	5.89	100.00	0.00
RESCANNING	0.7s	0	7mm	10	4.29	100.00	0.00
RESCANNING	0.7s	0	7mm	15	3.90	100.00	0.00
RESCANNING	0.7s	0	7mm	20	3.84	100.00	0.00
RESCANNING	0.7s	90	7mm	5	5.72	100.00	0.00
RESCANNING	0.7s	90	7mm	10	4.22	100.00	0.00
RESCANNING	0.7s	90	7mm	15	3.62	100.00	0.00
RESCANNING	0.7s	90	7mm	20	3.75	100.00	0.00

Table B.16.: Patient 3, RPV

Case	motion period	motion starting phase	Margin	rscan no.	D5-D95 [%]	V95 [%]	V107 [%]
STATIC	-	-	0mm	-	3.87	98.81	0.10
STATIC	-	-	3mm	-	1.99	100.00	0.00
STATIC	-	-	5mm	-	2.14	100.00	0.00
STATIC	-	-	7mm	-	1.94	99.90	0.00
INTERPLAY	1s	0	0mm	-	9.50	95.03	0.50
INTERPLAY	1s	90	0mm	-	10.30	95.53	1.79
INTERPLAY	0.7s	0	0mm	-	8.79	93.35	0.10
INTERPLAY	0.7s	90	0mm	-	9.74	94.64	0.20
INTERPLAY	1s	0	3mm	-	6.12	99.90	0.10
INTERPLAY	1s	90	3mm	-	7.18	99.60	0.79
INTERPLAY	0.7s	0	3mm	-	6.07	100.00	0.10
INTERPLAY	0.7s	90	3mm	-	6.56	100.00	0.79
INTERPLAY	1s	0	5mm	-	6.09	99.60	0.00
INTERPLAY	1s	90	5mm	-	7.27	99.60	0.70
INTERPLAY	0.7s	0	5mm	-	6.09	100.00	0.10
INTERPLAY	0.7s	90	5mm	-	6.46	100.00	0.60
INTERPLAY	1s	0	7mm	-	6.15	99.70	0.00
INTERPLAY	1s	90	7mm	-	7.26	99.50	0.30
INTERPLAY	0.7s	0	7mm	-	6.20	99.90	0.40
INTERPLAY	0.7s	90	7mm	-	6.47	100.00	0.50
RESCANNING	1s	0	0mm	5	8.60	94.64	0.20
RESCANNING	1s	0	0mm	10	6.64	98.21	0.00
RESCANNING	1s	0	0mm	15	6.30	98.61	0.00
RESCANNING	1s	0	0mm	20	6.18	98.71	0.00
RESCANNING	1s	90	0mm	5	8.73	95.73	0.60
RESCANNING	1s	90	0mm	10	7.11	97.32	0.00
RESCANNING	1s	90	0mm	15	6.55	98.21	0.00
RESCANNING	1s	90	0mm	20	6.29	98.61	0.00
RESCANNING	0.7s	0	0mm	5	6.89	95.63	0.00
RESCANNING	0.7s	0	0mm	10	4.98	99.01	0.00
RESCANNING	0.7s	0	0mm	15	4.31	99.11	0.00
RESCANNING	0.7s	0	0mm	20	4.33	99.30	0.00
RESCANNING	0.7s	90	0mm	5	7.03	97.42	0.00
RESCANNING	0.7s	90	0mm	10	5.39	98.51	0.00
RESCANNING	0.7s	90	0mm	15	4.66	99.40	0.00
RESCANNING	0.7s	90	0mm	20	4.55	99.21	0.00
RESCANNING	1s	0	3mm	5	6.94	99.90	0.79
RESCANNING	1s	0	3mm	10	4.55	99.90	0.00
RESCANNING	1s	0	3mm	15	3.88	99.90	0.00
RESCANNING	1s	0	3mm	20	4.00	99.90	0.00
RESCANNING	1s	90	3mm	5	5.86	99.70	0.00
RESCANNING	1s	90	3mm	10	4.82	100.00	0.00
RESCANNING	1s	90	3mm	15	4.19	100.00	0.00
RESCANNING	1s	90	3mm	20	4.05	100.00	0.00
RESCANNING	0.7s	0	3mm	5	4.87	99.90	0.10
RESCANNING	0.7s	0	3mm	10	3.82	100.00	0.00
RESCANNING	0.7s	0	3mm	15	3.17	100.00	0.00
RESCANNING	0.7s	0	3mm	20	2.93	100.00	0.00
RESCANNING	0.7s	90	3mm	5	5.65	98.81	0.00
RESCANNING	0.7s	90	3mm	10	4.50	100.00	0.00
RESCANNING	0.7s	90	3mm	15	3.36	100.00	0.00
RESCANNING	0.7s	90	3mm	20	2.65	100.00	0.00
RESCANNING	1s	0	5mm	5	7.18	100.00	1.49
RESCANNING	1s	0	5mm	10	4.62	100.00	0.00
RESCANNING	1s	0	5mm	15	3.76	100.00	0.00
RESCANNING	1s	0	5mm	20	3.66	100.00	0.00
RESCANNING	1s	90	5mm	5	4.85	100.00	0.00
RESCANNING	1s	90	5mm	10	4.30	100.00	0.00
RESCANNING	1s	90	5mm	15	4.07	100.00	0.00
RESCANNING	1s	90	5mm	20	3.39	100.00	0.00
RESCANNING	0.7s	0	5mm	5	4.97	100.00	0.00
RESCANNING	0.7s	0	5mm	10	4.12	100.00	0.00
RESCANNING	0.7s	0	5mm	15	3.10	100.00	0.00
RESCANNING	0.7s	0	5mm	20	2.98	100.00	0.00
RESCANNING	0.7s	90	5mm	5	5.46	100.00	0.00
RESCANNING	0.7s	90	5mm	10	3.85	100.00	0.00
RESCANNING	0.7s	90	5mm	15	3.19	100.00	0.00
RESCANNING	0.7s	90	5mm	20	3.02	100.00	0.00
RESCANNING	1s	0	7mm	5	8.50	100.00	0.30
RESCANNING	1s	0	7mm	10	4.30	100.00	0.00
RESCANNING	1s	0	7mm	15	4.59	100.00	0.00
RESCANNING	1s	0	7mm	20	4.32	100.00	0.00
RESCANNING	1s	90	7mm	5	6.61	100.00	0.50
RESCANNING	1s	90	7mm	10	4.42	100.00	0.00
RESCANNING	1s	90	7mm	15	3.73	100.00	0.00
RESCANNING	1s	90	7mm	20	3.71	100.00	0.00
RESCANNING	0.7s	0	7mm	5	4.93	100.00	0.00
RESCANNING	0.7s	0	7mm	10	3.53	100.00	0.00
RESCANNING	0.7s	0	7mm	15	3.24	100.00	0.00
RESCANNING	0.7s	0	7mm	20	3.16	100.00	0.00
RESCANNING	0.7s	90	7mm	5	4.64	100.00	0.10
RESCANNING	0.7s	90	7mm	10	3.53	100.00	0.00
RESCANNING	0.7s	90	7mm	15	3.36	100.00	0.00
RESCANNING	0.7s	90	7mm	20	3.16	100.00	0.00

Table B.17.: Patient 4, LPV

Case	motion period	motion starting phase	Margin	rescan no.	D5-D95 [%]	V95 [%]	V107 [%]
STATIC	-	-	0mm	-	7.36	95.76	0.25
STATIC	-	-	3mm	-	3.92	99.75	0.00
STATIC	-	-	5mm	-	3.63	100.00	0.00
STATIC	-	-	7mm	-	3.49	100.00	0.00
INTERPLAY	1s	0	0mm	-	13.55	89.03	2.99
INTERPLAY	1s	90	0mm	-	14.82	80.30	1.00
INTERPLAY	0.7s	0	0mm	-	14.10	84.79	1.75
INTERPLAY	0.7s	90	0mm	-	10.66	91.27	1.25
INTERPLAY	1s	0	3mm	-	7.73	99.25	0.25
INTERPLAY	1s	90	3mm	-	10.01	95.76	0.75
INTERPLAY	0.7s	0	3mm	-	9.86	90.02	0.00
INTERPLAY	0.7s	90	3mm	-	9.94	95.76	1.75
INTERPLAY	1s	0	5mm	-	9.38	98.50	0.25
INTERPLAY	1s	90	5mm	-	9.57	95.26	0.75
INTERPLAY	0.7s	0	5mm	-	7.35	98.75	0.00
INTERPLAY	0.7s	90	5mm	-	6.73	98.25	0.00
INTERPLAY	1s	0	7mm	-	11.59	91.77	2.49
INTERPLAY	1s	90	7mm	-	10.69	89.03	0.25
INTERPLAY	0.7s	0	7mm	-	8.97	94.26	0.00
INTERPLAY	0.7s	90	7mm	-	7.44	98.25	0.00
RESCANNING	1s	0	0mm	5	9.37	94.01	0.25
RESCANNING	1s	0	0mm	10	9.43	88.03	0.00
RESCANNING	1s	0	0mm	15	8.56	86.78	0.00
RESCANNING	1s	0	0mm	20	8.89	85.79	0.00
RESCANNING	1s	90	0mm	5	8.74	91.27	0.50
RESCANNING	1s	90	0mm	10	8.88	91.77	0.00
RESCANNING	1s	90	0mm	15	8.54	92.77	0.00
RESCANNING	1s	90	0mm	20	8.46	92.77	0.00
RESCANNING	0.7s	0	0mm	5	8.87	91.27	0.25
RESCANNING	0.7s	0	0mm	10	8.20	92.27	0.00
RESCANNING	0.7s	0	0mm	15	7.89	91.02	0.00
RESCANNING	0.7s	0	0mm	20	8.08	91.77	0.00
RESCANNING	0.7s	90	0mm	5	10.18	89.03	0.25
RESCANNING	0.7s	90	0mm	10	8.33	93.27	0.00
RESCANNING	0.7s	90	0mm	15	7.59	94.76	0.00
RESCANNING	0.7s	90	0mm	20	7.85	94.26	0.00
RESCANNING	1s	0	3mm	5	6.77	98.50	0.00
RESCANNING	1s	0	3mm	10	5.30	99.25	0.00
RESCANNING	1s	0	3mm	15	5.27	99.00	0.00
RESCANNING	1s	0	3mm	20	4.75	99.50	0.00
RESCANNING	1s	90	3mm	5	7.77	99.50	2.00
RESCANNING	1s	90	3mm	10	5.94	99.50	0.00
RESCANNING	1s	90	3mm	15	6.11	99.50	0.00
RESCANNING	1s	90	3mm	20	5.90	99.50	0.00
RESCANNING	0.7s	0	3mm	5	5.52	99.75	0.00
RESCANNING	0.7s	0	3mm	10	4.62	99.75	0.00
RESCANNING	0.7s	0	3mm	15	4.44	100.00	0.00
RESCANNING	0.7s	0	3mm	20	3.93	100.00	0.00
RESCANNING	0.7s	90	3mm	5	5.50	99.25	0.00
RESCANNING	0.7s	90	3mm	10	4.21	99.25	0.00
RESCANNING	0.7s	90	3mm	15	4.85	99.50	0.00
RESCANNING	0.7s	90	3mm	20	3.72	99.50	0.00
RESCANNING	1s	0	5mm	5	6.45	100.00	0.00
RESCANNING	1s	0	5mm	10	5.15	99.75	0.00
RESCANNING	1s	0	5mm	15	4.70	99.75	0.00
RESCANNING	1s	0	5mm	20	4.27	99.75	0.00
RESCANNING	1s	90	5mm	5	8.63	92.02	0.00
RESCANNING	1s	90	5mm	10	6.15	97.51	0.00
RESCANNING	1s	90	5mm	15	5.18	99.50	0.00
RESCANNING	1s	90	5mm	20	5.93	99.50	0.00
RESCANNING	0.7s	0	5mm	5	5.61	99.50	0.00
RESCANNING	0.7s	0	5mm	10	3.64	99.50	0.00
RESCANNING	0.7s	0	5mm	15	3.47	99.75	0.00
RESCANNING	0.7s	0	5mm	20	3.23	99.50	0.00
RESCANNING	0.7s	90	5mm	5	5.07	99.50	0.00
RESCANNING	0.7s	90	5mm	10	4.18	99.50	0.00
RESCANNING	0.7s	90	5mm	15	3.63	99.25	0.00
RESCANNING	0.7s	90	5mm	20	3.30	99.50	0.00
RESCANNING	1s	0	7mm	5	5.26	100.00	0.00
RESCANNING	1s	0	7mm	10	4.14	100.00	0.00
RESCANNING	1s	0	7mm	15	4.03	100.00	0.00
RESCANNING	1s	0	7mm	20	4.15	100.00	0.00
RESCANNING	1s	90	7mm	5	5.59	99.25	0.00
RESCANNING	1s	90	7mm	10	5.34	99.75	0.00
RESCANNING	1s	90	7mm	15	4.57	100.00	0.00
RESCANNING	1s	90	7mm	20	4.35	99.75	0.00
RESCANNING	0.7s	0	7mm	5	5.00	99.75	0.00
RESCANNING	0.7s	0	7mm	10	3.66	99.75	0.00
RESCANNING	0.7s	0	7mm	15	3.28	100.00	0.00
RESCANNING	0.7s	0	7mm	20	3.41	100.00	0.00
RESCANNING	0.7s	90	7mm	5	4.74	99.75	0.00
RESCANNING	0.7s	90	7mm	10	3.04	99.75	0.00
RESCANNING	0.7s	90	7mm	15	3.12	100.00	0.00
RESCANNING	0.7s	90	7mm	20	2.76	100.00	0.00

Table B.18.: Patient 4, RPV

Case	motion period	motion starting phase	Margin	rscan no.	D5-D95 [%]	V95 [%]	V107 [%]
STATIC	-	-	0mm	-	5.46	97.80	0.00
STATIC	-	-	3mm	-	3.65	100.00	0.00
STATIC	-	-	5mm	-	3.07	100.00	0.00
STATIC	-	-	7mm	-	2.63	99.40	0.00
INTERPLAY	1s	0	0mm	-	11.43	89.80	0.40
INTERPLAY	1s	90	0mm	-	11.22	94.00	2.00
INTERPLAY	0.7s	0	0mm	-	11.12	94.60	2.00
INTERPLAY	0.7s	90	0mm	-	13.29	84.20	1.80
INTERPLAY	1s	0	3mm	-	9.67	95.20	0.60
INTERPLAY	1s	90	3mm	-	9.16	96.60	0.20
INTERPLAY	0.7s	0	3mm	-	9.68	97.00	1.20
INTERPLAY	0.7s	90	3mm	-	9.55	96.80	0.40
INTERPLAY	1s	0	5mm	-	8.83	96.80	0.40
INTERPLAY	1s	90	5mm	-	8.88	92.20	0.00
INTERPLAY	0.7s	0	5mm	-	8.56	96.80	0.00
INTERPLAY	0.7s	90	5mm	-	7.55	99.60	0.40
INTERPLAY	1s	0	7mm	-	8.88	98.80	1.60
INTERPLAY	1s	90	7mm	-	8.05	97.60	0.00
INTERPLAY	0.7s	0	7mm	-	7.81	97.00	0.00
INTERPLAY	0.7s	90	7mm	-	7.66	99.80	0.20
RESCANNING	1s	0	0mm	5	10.05	94.00	0.80
RESCANNING	1s	0	0mm	10	8.77	94.80	0.40
RESCANNING	1s	0	0mm	15	8.47	94.40	0.00
RESCANNING	1s	0	0mm	20	8.27	94.60	0.20
RESCANNING	1s	90	0mm	5	9.65	95.20	1.00
RESCANNING	1s	90	0mm	10	9.35	95.80	0.40
RESCANNING	1s	90	0mm	15	8.28	96.00	0.40
RESCANNING	1s	90	0mm	20	8.35	96.40	0.20
RESCANNING	0.7s	0	0mm	5	8.51	94.00	0.00
RESCANNING	0.7s	0	0mm	10	7.67	95.80	0.00
RESCANNING	0.7s	0	0mm	15	7.24	96.20	0.00
RESCANNING	0.7s	0	0mm	20	7.13	95.80	0.00
RESCANNING	0.7s	90	0mm	5	8.77	94.60	0.20
RESCANNING	0.7s	90	0mm	10	6.86	96.20	0.00
RESCANNING	0.7s	90	0mm	15	6.98	96.60	0.20
RESCANNING	0.7s	90	0mm	20	6.46	96.40	0.20
RESCANNING	1s	0	3mm	5	7.05	99.40	0.00
RESCANNING	1s	0	3mm	10	5.62	100.00	0.00
RESCANNING	1s	0	3mm	15	5.10	100.00	0.00
RESCANNING	1s	0	3mm	20	4.86	99.80	0.00
RESCANNING	1s	90	3mm	5	5.56	99.60	0.00
RESCANNING	1s	90	3mm	10	5.62	100.00	0.20
RESCANNING	1s	90	3mm	15	5.14	99.80	0.00
RESCANNING	1s	90	3mm	20	5.36	100.00	0.00
RESCANNING	0.7s	0	3mm	5	5.69	100.00	0.00
RESCANNING	0.7s	0	3mm	10	3.71	100.00	0.00
RESCANNING	0.7s	0	3mm	15	3.54	100.00	0.00
RESCANNING	0.7s	0	3mm	20	3.59	100.00	0.00
RESCANNING	0.7s	90	3mm	5	6.53	99.60	0.00
RESCANNING	0.7s	90	3mm	10	4.21	100.00	0.00
RESCANNING	0.7s	90	3mm	15	4.37	100.00	0.00
RESCANNING	0.7s	90	3mm	20	4.23	100.00	0.00
RESCANNING	1s	0	5mm	5	7.82	100.00	1.80
RESCANNING	1s	0	5mm	10	4.77	100.00	0.20
RESCANNING	1s	0	5mm	15	4.98	100.00	0.00
RESCANNING	1s	0	5mm	20	5.16	100.00	0.00
RESCANNING	1s	90	5mm	5	7.26	94.20	0.00
RESCANNING	1s	90	5mm	10	5.12	99.60	0.00
RESCANNING	1s	90	5mm	15	5.27	100.00	0.00
RESCANNING	1s	90	5mm	20	4.74	100.00	0.00
RESCANNING	0.7s	0	5mm	5	5.87	100.00	0.00
RESCANNING	0.7s	0	5mm	10	3.72	100.00	0.00
RESCANNING	0.7s	0	5mm	15	3.09	100.00	0.00
RESCANNING	0.7s	0	5mm	20	3.14	100.00	0.00
RESCANNING	0.7s	90	5mm	5	5.34	99.80	0.00
RESCANNING	0.7s	90	5mm	10	3.52	100.00	0.00
RESCANNING	0.7s	90	5mm	15	3.53	100.00	0.00
RESCANNING	0.7s	90	5mm	20	2.93	100.00	0.00
RESCANNING	1s	0	7mm	5	5.44	100.00	0.20
RESCANNING	1s	0	7mm	10	4.23	100.00	0.20
RESCANNING	1s	0	7mm	15	3.95	99.80	0.00
RESCANNING	1s	0	7mm	20	3.84	100.00	0.00
RESCANNING	1s	90	7mm	5	6.29	99.20	0.20
RESCANNING	1s	90	7mm	10	5.31	100.00	0.00
RESCANNING	1s	90	7mm	15	4.04	100.00	0.00
RESCANNING	1s	90	7mm	20	3.69	100.00	0.00
RESCANNING	0.7s	0	7mm	5	5.03	100.00	0.00
RESCANNING	0.7s	0	7mm	10	4.37	100.00	0.00
RESCANNING	0.7s	0	7mm	15	3.03	100.00	0.00
RESCANNING	0.7s	0	7mm	20	2.81	100.00	0.00
RESCANNING	0.7s	90	7mm	5	4.49	100.00	0.00
RESCANNING	0.7s	90	7mm	10	3.68	100.00	0.00
RESCANNING	0.7s	90	7mm	15	3.62	100.00	0.00
RESCANNING	0.7s	90	7mm	20	3.12	100.00	0.00

Table B.19.: Patient 5, LPV

Case	motion period	motion starting phase	Margin	rescan no.	D5-D95 [%]	V95 [%]	V107 [%]
STATIC	-	-	0mm	-	4.65	100.00	0.00
STATIC	-	-	3mm	-	2.52	100.00	0.00
STATIC	-	-	5mm	-	2.95	100.00	0.00
STATIC	-	-	7mm	-	4.29	100.00	0.00
INTERPLAY	1s	0	0mm	-	10.55	93.41	0.94
INTERPLAY	1s	90	0mm	-	10.79	93.68	0.94
INTERPLAY	0.7s	0	0mm	-	9.18	91.40	0.27
INTERPLAY	0.7s	90	0mm	-	9.34	89.65	0.00
INTERPLAY	1s	0	3mm	-	8.09	97.31	0.27
INTERPLAY	1s	90	3mm	-	9.60	98.39	2.55
INTERPLAY	0.7s	0	3mm	-	7.84	95.43	0.13
INTERPLAY	0.7s	90	3mm	-	7.95	97.85	0.13
INTERPLAY	1s	0	5mm	-	6.48	99.73	0.81
INTERPLAY	1s	90	5mm	-	7.43	95.97	0.13
INTERPLAY	0.7s	0	5mm	-	6.99	97.58	0.00
INTERPLAY	0.7s	90	5mm	-	8.00	99.87	0.40
INTERPLAY	1s	0	7mm	-	6.71	99.46	0.13
INTERPLAY	1s	90	7mm	-	9.40	96.24	0.81
INTERPLAY	0.7s	0	7mm	-	8.18	93.95	0.00
INTERPLAY	0.7s	90	7mm	-	7.38	98.25	0.00
RESCANNING	1s	0	0mm	5	9.34	88.58	0.00
RESCANNING	1s	0	0mm	10	7.44	91.94	0.00
RESCANNING	1s	0	0mm	15	6.78	94.89	0.00
RESCANNING	1s	0	0mm	20	6.57	95.30	0.00
RESCANNING	1s	90	0mm	5	8.62	97.04	1.61
RESCANNING	1s	90	0mm	10	8.47	96.51	0.54
RESCANNING	1s	90	0mm	15	6.67	97.72	0.13
RESCANNING	1s	90	0mm	20	6.82	97.58	0.27
RESCANNING	0.7s	0	0mm	5	7.95	96.10	0.00
RESCANNING	0.7s	0	0mm	10	6.38	98.12	0.00
RESCANNING	0.7s	0	0mm	15	6.20	97.98	0.00
RESCANNING	0.7s	0	0mm	20	5.74	97.98	0.00
RESCANNING	0.7s	90	0mm	5	7.87	95.16	0.13
RESCANNING	0.7s	90	0mm	10	6.10	96.77	0.00
RESCANNING	0.7s	90	0mm	15	6.01	97.18	0.00
RESCANNING	0.7s	90	0mm	20	5.84	96.37	0.00
RESCANNING	1s	0	3mm	5	5.44	99.87	0.00
RESCANNING	1s	0	3mm	10	4.47	100.00	0.00
RESCANNING	1s	0	3mm	15	3.79	100.00	0.00
RESCANNING	1s	0	3mm	20	3.33	100.00	0.00
RESCANNING	1s	90	3mm	5	7.74	91.94	0.00
RESCANNING	1s	90	3mm	10	4.42	99.87	0.00
RESCANNING	1s	90	3mm	15	3.67	100.00	0.00
RESCANNING	1s	90	3mm	20	3.78	100.00	0.00
RESCANNING	0.7s	0	3mm	5	5.64	99.87	0.00
RESCANNING	0.7s	0	3mm	10	4.74	100.00	0.00
RESCANNING	0.7s	0	3mm	15	3.68	100.00	0.00
RESCANNING	0.7s	0	3mm	20	3.45	100.00	0.00
RESCANNING	0.7s	90	3mm	5	5.58	99.73	0.00
RESCANNING	0.7s	90	3mm	10	3.86	99.87	0.00
RESCANNING	0.7s	90	3mm	15	3.46	100.00	0.00
RESCANNING	0.7s	90	3mm	20	3.38	100.00	0.00
RESCANNING	1s	0	5mm	5	6.69	99.06	0.00
RESCANNING	1s	0	5mm	10	4.19	100.00	0.00
RESCANNING	1s	0	5mm	15	3.85	100.00	0.00
RESCANNING	1s	0	5mm	20	3.67	100.00	0.00
RESCANNING	1s	90	5mm	5	4.90	99.60	0.00
RESCANNING	1s	90	5mm	10	4.63	99.87	0.00
RESCANNING	1s	90	5mm	15	3.60	100.00	0.00
RESCANNING	1s	90	5mm	20	3.49	100.00	0.00
RESCANNING	0.7s	0	5mm	5	4.64	100.00	0.00
RESCANNING	0.7s	0	5mm	10	3.83	100.00	0.00
RESCANNING	0.7s	0	5mm	15	3.25	100.00	0.00
RESCANNING	0.7s	0	5mm	20	2.60	100.00	0.00
RESCANNING	0.7s	90	5mm	5	5.04	100.00	0.00
RESCANNING	0.7s	90	5mm	10	3.66	99.73	0.00
RESCANNING	0.7s	90	5mm	15	2.97	100.00	0.00
RESCANNING	0.7s	90	5mm	20	2.58	100.00	0.00
RESCANNING	1s	0	7mm	5	5.11	100.00	0.00
RESCANNING	1s	0	7mm	10	5.04	99.73	0.00
RESCANNING	1s	0	7mm	15	3.86	100.00	0.00
RESCANNING	1s	0	7mm	20	4.02	100.00	0.00
RESCANNING	1s	90	7mm	5	6.23	98.52	0.00
RESCANNING	1s	90	7mm	10	5.25	98.12	0.00
RESCANNING	1s	90	7mm	15	5.12	98.39	0.00
RESCANNING	1s	90	7mm	20	4.80	98.52	0.00
RESCANNING	0.7s	0	7mm	5	4.98	99.87	0.00
RESCANNING	0.7s	0	7mm	10	4.18	99.87	0.00
RESCANNING	0.7s	0	7mm	15	4.29	99.33	0.00
RESCANNING	0.7s	0	7mm	20	3.64	100.00	0.00
RESCANNING	0.7s	90	7mm	5	5.45	99.46	0.00
RESCANNING	0.7s	90	7mm	10	4.10	99.60	0.00
RESCANNING	0.7s	90	7mm	15	3.74	100.00	0.00
RESCANNING	0.7s	90	7mm	20	3.51	99.87	0.00

Table B.20.: Patient 5, RPV

Case	motion period	motion starting phase	Margin	rescan no.	D5-D95 [%]	V95 [%]	V107 [%]
STATIC	-	-	0mm	-	3.94	99.85	0.00
STATIC	-	-	3mm	-	2.26	100.00	0.00
STATIC	-	-	5mm	-	2.46	100.00	0.00
STATIC	-	-	7mm	-	2.83	100.00	0.00
INTERPLAY	1s	0	0mm	-	12.04	90.52	0.87
INTERPLAY	1s	90	0mm	-	9.83	94.02	1.17
INTERPLAY	0.7s	0	0mm	-	10.12	96.79	2.19
INTERPLAY	0.7s	90	0mm	-	9.12	92.57	0.15
INTERPLAY	1s	0	3mm	-	7.44	99.42	0.00
INTERPLAY	1s	90	3mm	-	7.43	97.67	0.00
INTERPLAY	0.7s	0	3mm	-	6.13	99.71	0.00
INTERPLAY	0.7s	90	3mm	-	8.35	96.21	0.15
INTERPLAY	1s	0	5mm	-	7.34	98.83	0.00
INTERPLAY	1s	90	5mm	-	8.23	98.11	0.87
INTERPLAY	0.7s	0	5mm	-	5.79	99.27	0.00
INTERPLAY	0.7s	90	5mm	-	7.86	97.52	0.00
INTERPLAY	1s	0	7mm	-	6.45	99.13	0.15
INTERPLAY	1s	90	7mm	-	8.99	94.90	0.15
INTERPLAY	0.7s	0	7mm	-	6.18	97.38	0.00
INTERPLAY	0.7s	90	7mm	-	6.82	99.85	0.00
RESCANNING	1s	0	0mm	5	8.32	91.55	0.15
RESCANNING	1s	0	0mm	10	8.53	88.48	0.00
RESCANNING	1s	0	0mm	15	8.04	91.55	0.00
RESCANNING	1s	0	0mm	20	8.30	90.52	0.00
RESCANNING	1s	90	0mm	5	8.14	99.13	0.58
RESCANNING	1s	90	0mm	10	7.53	99.56	0.73
RESCANNING	1s	90	0mm	15	8.16	97.81	0.44
RESCANNING	1s	90	0mm	20	7.82	98.69	0.44
RESCANNING	0.7s	0	0mm	5	7.65	92.57	0.00
RESCANNING	0.7s	0	0mm	10	6.75	95.34	0.00
RESCANNING	0.7s	0	0mm	15	6.24	96.21	0.00
RESCANNING	0.7s	0	0mm	20	6.19	95.77	0.00
RESCANNING	0.7s	90	0mm	5	8.18	97.23	0.15
RESCANNING	0.7s	90	0mm	10	6.45	97.81	0.00
RESCANNING	0.7s	90	0mm	15	6.04	97.38	0.00
RESCANNING	0.7s	90	0mm	20	5.46	97.96	0.00
RESCANNING	1s	0	3mm	5	6.04	100.00	0.00
RESCANNING	1s	0	3mm	10	4.16	100.00	0.00
RESCANNING	1s	0	3mm	15	4.39	100.00	0.00
RESCANNING	1s	0	3mm	20	4.21	100.00	0.00
RESCANNING	1s	90	3mm	5	6.01	98.69	0.00
RESCANNING	1s	90	3mm	10	5.38	100.00	0.15
RESCANNING	1s	90	3mm	15	4.65	100.00	0.29
RESCANNING	1s	90	3mm	20	4.65	100.00	0.00
RESCANNING	0.7s	0	3mm	5	5.52	100.00	0.00
RESCANNING	0.7s	0	3mm	10	4.20	100.00	0.00
RESCANNING	0.7s	0	3mm	15	3.12	100.00	0.00
RESCANNING	0.7s	0	3mm	20	2.99	100.00	0.00
RESCANNING	0.7s	90	3mm	5	5.10	99.85	0.00
RESCANNING	0.7s	90	3mm	10	3.49	100.00	0.00
RESCANNING	0.7s	90	3mm	15	2.83	100.00	0.00
RESCANNING	0.7s	90	3mm	20	2.85	100.00	0.00
RESCANNING	1s	0	5mm	5	4.83	100.00	0.00
RESCANNING	1s	0	5mm	10	4.56	100.00	0.00
RESCANNING	1s	0	5mm	15	3.96	100.00	0.00
RESCANNING	1s	0	5mm	20	3.87	100.00	0.00
RESCANNING	1s	90	5mm	5	6.37	96.94	0.00
RESCANNING	1s	90	5mm	10	4.26	99.85	0.00
RESCANNING	1s	90	5mm	15	4.18	100.00	0.00
RESCANNING	1s	90	5mm	20	3.94	100.00	0.00
RESCANNING	0.7s	0	5mm	5	4.21	100.00	0.00
RESCANNING	0.7s	0	5mm	10	3.38	100.00	0.00
RESCANNING	0.7s	0	5mm	15	3.24	100.00	0.00
RESCANNING	0.7s	0	5mm	20	2.66	100.00	0.00
RESCANNING	0.7s	90	5mm	5	4.47	100.00	0.00
RESCANNING	0.7s	90	5mm	10	3.26	100.00	0.00
RESCANNING	0.7s	90	5mm	15	2.93	100.00	0.00
RESCANNING	0.7s	90	5mm	20	2.37	100.00	0.00
RESCANNING	1s	0	7mm	5	5.23	100.00	0.00
RESCANNING	1s	0	7mm	10	4.50	99.42	0.00
RESCANNING	1s	0	7mm	15	4.01	100.00	0.00
RESCANNING	1s	0	7mm	20	4.29	100.00	0.00
RESCANNING	1s	90	7mm	5	5.15	99.27	0.00
RESCANNING	1s	90	7mm	10	4.81	99.42	0.00
RESCANNING	1s	90	7mm	15	4.47	98.54	0.00
RESCANNING	1s	90	7mm	20	4.44	98.83	0.00
RESCANNING	0.7s	0	7mm	5	5.04	100.00	0.00
RESCANNING	0.7s	0	7mm	10	3.43	99.85	0.00
RESCANNING	0.7s	0	7mm	15	3.04	99.71	0.00
RESCANNING	0.7s	0	7mm	20	2.84	100.00	0.00
RESCANNING	0.7s	90	7mm	5	4.58	100.00	0.00
RESCANNING	0.7s	90	7mm	10	3.81	99.42	0.00
RESCANNING	0.7s	90	7mm	15	3.53	100.00	0.00
RESCANNING	0.7s	90	7mm	20	3.23	99.71	0.00

C Appendix of chapter 4

C.1 Motion of target volumes in contrast enhanced CT scans

The mean relative displacement and standard deviation of the target volumes (PVs, CTI and AV node) to the reference phase zero of the contrast enhanced CT scans will be shown for the three studied motion directions (SI: superior-inferior, AP: anterior-posterior, LR: left-right) and the absolute (ABS) displacement.

Table C.1.: PV: Mean and standard deviation of target motion in all phases of the heartbeat, relative to the reference phase. The values are taken from the contrast CTs of Pig 1.

motion phase	ABS [mm]	SI [mm]	AP [mm]	LR [mm]
01	0.43 ± 0.23	0.30 ± 0.25	0.03 ± 0.13	-0.10 ± 0.24
02	1.76 ± 0.52	0.49 ± 0.28	1.29 ± 0.33	-0.79 ± 0.79
03	2.61 ± 0.30	0.62 ± 0.39	2.00 ± 0.49	-1.16 ± 0.89
04	3.10 ± 0.28	0.51 ± 0.41	2.47 ± 0.68	-1.27 ± 1.03
05	3.46 ± 0.39	0.40 ± 0.57	2.77 ± 0.90	-1.42 ± 1.07
06	3.52 ± 0.59	0.54 ± 0.64	2.78 ± 1.09	-1.31 ± 1.19
07	3.80 ± 0.77	0.46 ± 0.86	3.06 ± 1.32	-1.32 ± 1.12
08	3.85 ± 0.98	0.34 ± 1.04	3.04 ± 1.60	-1.13 ± 1.23
09	3.80 ± 0.77	0.46 ± 0.86	3.06 ± 1.32	-1.32 ± 1.12
10	4.02 ± 1.09	0.10 ± 1.42	2.88 ± 1.85	-1.01 ± 1.62
11	4.04 ± 1.14	0.25 ± 1.57	2.66 ± 2.09	-1.11 ± 1.56
12	4.12 ± 1.13	0.48 ± 1.68	2.49 ± 2.25	-1.16 ± 1.61
13	4.22 ± 1.07	0.79 ± 1.56	2.42 ± 2.22	-1.40 ± 1.79
14	3.83 ± 0.88	0.31 ± 1.76	2.26 ± 1.58	-1.77 ± 1.26
15	2.97 ± 0.72	-0.00 ± 1.16	2.02 ± 1.08	-1.46 ± 0.77
16	1.94 ± 0.76	-0.01 ± 0.75	1.37 ± 0.79	-1.01 ± 0.53
17	1.67 ± 0.55	-0.60 ± 0.43	1.12 ± 0.37	-0.79 ± 0.72
18	1.17 ± 0.46	-0.58 ± 0.30	0.69 ± 0.39	-0.34 ± 0.65
19	0.48 ± 0.23	-0.36 ± 0.20	0.05 ± 0.24	-0.04 ± 0.23

Table C.2.: CTI: Mean and standard deviation of target motion in all phases of the heartbeat, relative to the reference phase. The values are taken from the contrast CTs of Pig 1.

motion phase	ABS [mm]	SI [mm]	AP [mm]	LR [mm]
01	0.49 ± 0.21	-0.02 ± 0.13	0.20 ± 0.23	0.39 ± 0.16
02	0.87 ± 0.26	0.46 ± 0.24	0.04 ± 0.43	0.55 ± 0.28
03	1.75 ± 0.66	1.35 ± 0.53	0.70 ± 0.48	0.61 ± 0.54
04	1.92 ± 0.62	1.18 ± 0.45	0.99 ± 0.51	0.91 ± 0.63
05	2.82 ± 0.94	0.93 ± 0.57	2.00 ± 0.58	1.56 ± 0.93
06	5.05 ± 0.80	0.39 ± 0.45	4.20 ± 0.66	2.63 ± 0.93
07	5.79 ± 0.98	0.62 ± 0.58	4.48 ± 0.73	3.47 ± 1.06
08	5.36 ± 1.06	0.42 ± 0.60	3.95 ± 1.31	3.31 ± 0.99
09	5.79 ± 0.98	0.62 ± 0.58	4.48 ± 0.73	3.47 ± 1.06
10	5.73 ± 0.94	-0.20 ± 0.66	4.92 ± 0.81	2.58 ± 1.29
11	5.40 ± 1.01	0.75 ± 0.65	4.60 ± 1.13	2.46 ± 0.82
12	5.67 ± 1.07	0.84 ± 0.98	4.90 ± 1.20	2.37 ± 0.70
13	5.25 ± 1.14	0.80 ± 1.11	4.60 ± 1.30	1.82 ± 0.91
14	3.83 ± 1.10	1.43 ± 0.95	2.92 ± 1.38	0.86 ± 1.35
15	3.78 ± 0.83	1.92 ± 1.71	2.32 ± 0.76	0.76 ± 1.35
16	3.29 ± 0.44	1.46 ± 1.52	1.28 ± 0.74	1.56 ± 1.40
17	1.97 ± 0.60	0.70 ± 1.30	-0.80 ± 0.47	0.62 ± 0.90
18	1.82 ± 0.43	0.31 ± 0.71	-1.46 ± 0.30	-0.76 ± 0.33
19	0.76 ± 0.37	-0.01 ± 0.17	-0.60 ± 0.32	-0.40 ± 0.23

Table C.3.: AV node: Mean and standard deviation of target motion in all phases of the heart-beat, relative to the reference phase. The values are taken from the contrast CTs of Pig 1.

motion phase	ABS [mm]	SI [mm]	AP [mm]	LR [mm]
01	0.15 ± 0.09	-0.01 ± 0.06	-0.01 ± 0.04	0.12 ± 0.10
02	0.66 ± 0.27	-0.01 ± 0.14	0.51 ± 0.12	-0.08 ± 0.46
03	2.38 ± 0.24	0.52 ± 0.31	2.25 ± 0.21	-0.28 ± 0.41
04	2.95 ± 0.34	0.87 ± 0.11	2.80 ± 0.37	-0.25 ± 0.18
05	3.12 ± 0.40	0.79 ± 0.60	2.90 ± 0.56	-0.42 ± 0.21
06	3.60 ± 0.53	0.64 ± 0.38	3.46 ± 0.62	-0.44 ± 0.36
07	3.79 ± 0.56	0.33 ± 0.55	3.62 ± 0.70	-0.63 ± 0.50
08	4.14 ± 0.69	0.29 ± 0.39	4.03 ± 0.80	-0.44 ± 0.56
09	3.79 ± 0.56	0.33 ± 0.55	3.62 ± 0.70	-0.63 ± 0.50
10	4.25 ± 0.66	0.36 ± 0.33	4.10 ± 0.80	-0.64 ± 0.63
11	4.33 ± 0.57	0.54 ± 0.39	4.08 ± 0.76	-1.06 ± 0.56
12	4.67 ± 0.29	0.49 ± 0.40	4.43 ± 0.41	-1.21 ± 0.50
13	4.93 ± 0.26	1.70 ± 0.35	4.46 ± 0.39	-1.11 ± 0.27
14	4.27 ± 0.30	0.00 ± 0.44	3.84 ± 0.34	-1.76 ± 0.31
15	3.57 ± 0.24	0.03 ± 0.42	3.33 ± 0.23	-1.20 ± 0.15
16	2.25 ± 0.21	1.00 ± 0.46	1.86 ± 0.28	-0.56 ± 0.27
17	1.91 ± 0.35	-0.30 ± 0.78	-0.41 ± 0.40	-1.61 ± 0.38
18	1.14 ± 0.40	-0.29 ± 0.41	-0.32 ± 0.25	-0.88 ± 0.51
19	0.37 ± 0.15	0.06 ± 0.06	-0.27 ± 0.12	-0.14 ± 0.22

Table C.4.: PV: Mean and standard deviation of target motion in all phases of the heartbeat, relative to the reference phase. The values are taken from the contrast CTs of Pig 2.

motion phase	ABS [mm]	SI [mm]	AP [mm]	LR [mm]
01	0.37 ± 0.25	0.02 ± 0.27	0.14 ± 0.20	-0.10 ± 0.24
02	1.16 ± 0.69	0.40 ± 0.42	0.78 ± 0.58	-0.43 ± 0.60
03	2.06 ± 0.57	0.73 ± 0.47	1.61 ± 0.63	-0.61 ± 0.69
04	2.26 ± 0.64	0.79 ± 0.47	1.74 ± 0.75	-0.77 ± 0.69
05	2.50 ± 0.66	1.09 ± 0.65	1.82 ± 0.80	-0.61 ± 0.89
06	2.71 ± 0.96	1.26 ± 0.85	1.89 ± 1.04	-0.51 ± 1.02
07	3.02 ± 1.11	1.33 ± 0.95	2.14 ± 1.35	-0.67 ± 0.91
08	3.09 ± 1.22	1.20 ± 0.96	2.18 ± 1.50	-0.47 ± 1.22
09	3.02 ± 1.11	1.33 ± 0.95	2.14 ± 1.35	-0.67 ± 0.91
10	3.30 ± 1.12	1.21 ± 1.24	1.81 ± 1.72	-0.64 ± 1.57
11	3.24 ± 1.14	1.33 ± 1.33	1.60 ± 1.68	-0.68 ± 1.57
12	3.71 ± 1.55	1.50 ± 1.46	2.08 ± 2.05	-0.81 ± 1.61
13	3.37 ± 1.23	1.67 ± 1.41	1.62 ± 1.58	-0.92 ± 1.46
14	2.92 ± 1.11	1.55 ± 1.26	1.42 ± 1.25	-0.97 ± 1.12
15	2.19 ± 1.00	1.12 ± 1.00	1.27 ± 0.87	-0.70 ± 0.83
16	1.80 ± 0.70	0.10 ± 0.61	0.87 ± 0.86	-1.01 ± 0.90
17	1.52 ± 0.69	-0.19 ± 0.61	0.72 ± 0.71	-0.86 ± 0.79
18	1.11 ± 0.57	-0.23 ± 0.58	0.21 ± 0.65	-0.50 ± 0.66
19	0.39 ± 0.25	-0.04 ± 0.32	0.10 ± 0.21	-0.03 ± 0.23

Table C.5.: CTI: Mean and standard deviation of target motion in all phases of the heartbeat, relative to the reference phase. The values are taken from the contrast CTs of Pig 2.

motion phase	ABS [mm]	SI [mm]	AP [mm]	LR [mm]
01	0.29 ± 0.13	-0.00 ± 0.13	0.19 ± 0.11	0.16 ± 0.11
02	1.89 ± 0.49	0.25 ± 0.87	1.55 ± 0.56	0.25 ± 0.48
03	2.21 ± 0.55	0.48 ± 0.85	1.79 ± 0.46	0.51 ± 0.72
04	2.17 ± 0.43	0.84 ± 0.65	1.56 ± 0.39	-0.49 ± 0.98
05	4.12 ± 1.29	2.00 ± 1.31	3.40 ± 0.82	0.01 ± 0.85
06	4.43 ± 0.60	0.07 ± 1.42	4.10 ± 0.55	0.66 ± 0.68
07	4.92 ± 0.57	-0.75 ± 1.49	4.26 ± 0.54	1.47 ± 1.06
08	6.34 ± 0.54	1.26 ± 1.32	5.09 ± 0.60	3.04 ± 1.25
09	4.92 ± 0.57	-0.75 ± 1.49	4.26 ± 0.54	1.47 ± 1.06
10	4.33 ± 1.08	1.28 ± 1.14	3.50 ± 0.80	1.46 ± 1.38
11	4.41 ± 1.19	1.72 ± 1.11	3.45 ± 0.72	1.41 ± 1.51
12	4.89 ± 0.95	2.34 ± 0.86	3.68 ± 0.48	0.76 ± 2.06
13	5.53 ± 0.80	3.12 ± 0.96	4.11 ± 0.34	0.23 ± 1.87
14	4.70 ± 1.00	3.17 ± 0.96	3.03 ± 0.57	0.26 ± 1.60
15	4.31 ± 0.67	3.22 ± 0.81	2.45 ± 0.73	-0.19 ± 1.20
16	2.03 ± 0.77	0.89 ± 0.94	0.65 ± 0.62	-1.00 ± 1.12
17	2.35 ± 0.99	-0.70 ± 0.64	-0.63 ± 0.27	-2.01 ± 1.04
18	2.09 ± 0.78	-0.41 ± 0.60	-0.88 ± 0.25	-1.67 ± 0.92
19	0.71 ± 0.23	0.28 ± 0.18	-0.48 ± 0.18	-0.39 ± 0.19

Table C.6.: AV node: Mean and standard deviation of target motion in all phases of the heart-beat, relative to the reference phase. The values are taken from the contrast CTs of Pig 2.

motion phase	ABS [mm]	SI [mm]	AP [mm]	LR [mm]
01	0.53 ± 0.10	0.34 ± 0.09	0.40 ± 0.07	-0.04 ± 0.05
02	1.83 ± 0.49	0.08 ± 0.10	1.73 ± 0.42	0.46 ± 0.46
03	2.10 ± 0.08	0.68 ± 0.25	1.97 ± 0.14	0.06 ± 0.09
04	3.32 ± 0.17	1.62 ± 0.37	2.86 ± 0.09	-0.11 ± 0.30
05	3.95 ± 0.29	1.35 ± 0.20	3.68 ± 0.33	0.12 ± 0.37
06	3.94 ± 0.28	1.56 ± 0.30	3.56 ± 0.20	-0.56 ± 0.20
07	4.89 ± 0.36	2.48 ± 0.23	4.20 ± 0.41	-0.09 ± 0.24
08	5.44 ± 0.25	2.68 ± 0.37	4.71 ± 0.33	0.14 ± 0.27
09	4.89 ± 0.36	2.48 ± 0.23	4.20 ± 0.41	-0.09 ± 0.24
10	5.83 ± 0.25	2.79 ± 0.41	5.08 ± 0.11	-0.21 ± 0.49
11	6.04 ± 0.19	3.71 ± 0.36	4.71 ± 0.17	-0.38 ± 0.51
12	5.86 ± 0.23	3.27 ± 0.28	4.85 ± 0.11	0.12 ± 0.22
13	5.47 ± 0.46	3.55 ± 0.56	4.13 ± 0.21	0.07 ± 0.21
14	5.25 ± 0.53	3.01 ± 0.51	4.25 ± 0.35	0.23 ± 0.50
15	4.15 ± 0.48	1.99 ± 0.28	3.52 ± 0.34	0.56 ± 0.76
16	2.98 ± 0.43	1.82 ± 0.40	2.30 ± 0.26	0.30 ± 0.36
17	2.52 ± 0.53	1.84 ± 0.45	1.45 ± 0.23	0.89 ± 0.28
18	1.05 ± 0.61	0.70 ± 0.46	0.21 ± 0.24	0.73 ± 0.38
19	0.21 ± 0.06	-0.10 ± 0.06	-0.03 ± 0.08	-0.14 ± 0.09

Table C.7.: PV: Mean and standard deviation of target motion in all phases of the heartbeat, relative to the reference phase. The values are taken from the contrast CTs of Pig 3.

motion phase	ABS [mm]	SI [mm]	AP [mm]	LR [mm]
01	0.59 ± 0.27	0.05 ± 0.22	-0.07 ± 0.42	0.25 ± 0.35
02	1.39 ± 0.85	-0.21 ± 0.41	1.13 ± 0.85	0.46 ± 0.50
03	2.09 ± 0.80	-0.15 ± 0.48	1.67 ± 0.70	0.69 ± 1.01
04	2.17 ± 0.85	-0.27 ± 0.50	1.64 ± 0.73	0.81 ± 1.11
05	2.21 ± 0.89	-0.41 ± 0.57	1.94 ± 0.81	0.41 ± 0.79
06	2.39 ± 0.89	-0.48 ± 0.58	2.10 ± 0.80	0.42 ± 0.85
07	2.36 ± 0.91	-0.48 ± 0.65	2.00 ± 0.83	0.44 ± 0.92
08	2.23 ± 0.97	-0.55 ± 0.67	1.77 ± 0.89	0.47 ± 1.01
09	2.36 ± 0.91	-0.48 ± 0.65	2.00 ± 0.83	0.44 ± 0.92
10	1.79 ± 0.74	-0.19 ± 0.54	1.29 ± 0.77	0.32 ± 1.03
11	1.61 ± 0.76	0.06 ± 0.56	0.92 ± 0.85	0.16 ± 1.12
12	1.54 ± 0.57	-0.13 ± 0.43	0.53 ± 1.03	-0.17 ± 1.07
13	1.21 ± 0.52	0.01 ± 0.41	0.31 ± 0.82	-0.44 ± 0.77
14	1.53 ± 0.59	0.09 ± 0.45	-0.52 ± 1.31	-0.42 ± 0.58
15	1.38 ± 0.59	-0.13 ± 0.49	-0.52 ± 1.09	-0.59 ± 0.46
16	1.58 ± 0.77	-0.16 ± 0.59	-0.80 ± 1.21	-0.56 ± 0.53
17	1.76 ± 1.05	-0.13 ± 0.76	-1.08 ± 1.35	-0.54 ± 0.60
18	1.65 ± 0.98	-0.11 ± 0.81	-1.12 ± 1.15	-0.25 ± 0.59
19	0.63 ± 0.43	0.03 ± 0.36	-0.22 ± 0.33	-0.29 ± 0.47

Table C.8.: CTI: Mean and standard deviation of target motion in all phases of the heartbeat, relative to the reference phase. The values are taken from the contrast CTs of Pig 3.

motion phase	ABS [mm]	SI [mm]	AP [mm]	LR [mm]
01	0.40 ± 0.16	0.26 ± 0.21	-0.08 ± 0.18	0.10 ± 0.15
02	1.30 ± 0.59	-0.85 ± 0.50	0.84 ± 0.43	0.20 ± 0.38
03	1.59 ± 0.38	-0.56 ± 0.45	1.37 ± 0.32	0.05 ± 0.40
04	1.63 ± 0.43	-0.16 ± 0.60	1.41 ± 0.52	0.02 ± 0.45
05	1.84 ± 0.70	0.37 ± 0.82	1.53 ± 0.74	0.19 ± 0.36
06	1.58 ± 0.67	0.08 ± 0.64	1.26 ± 0.82	0.02 ± 0.53
07	1.73 ± 0.78	-0.02 ± 0.46	1.54 ± 0.91	0.28 ± 0.36
08	1.66 ± 0.63	0.19 ± 0.47	1.08 ± 1.22	0.39 ± 0.31
09	1.73 ± 0.78	-0.02 ± 0.46	1.54 ± 0.91	0.28 ± 0.36
10	1.92 ± 0.58	0.36 ± 0.38	1.44 ± 1.17	0.04 ± 0.56
11	2.23 ± 0.63	0.89 ± 0.46	1.30 ± 0.79	1.16 ± 0.83
12	2.08 ± 0.58	0.09 ± 0.55	1.45 ± 0.42	1.03 ± 0.99
13	1.44 ± 0.55	0.90 ± 0.51	0.48 ± 0.35	0.60 ± 0.76
14	1.83 ± 0.69	1.50 ± 0.73	-0.06 ± 0.49	0.16 ± 0.86
15	1.43 ± 0.49	1.06 ± 0.49	-0.00 ± 0.46	0.17 ± 0.83
16	1.60 ± 0.29	1.25 ± 0.41	-0.48 ± 0.48	-0.10 ± 0.67
17	1.97 ± 0.40	1.48 ± 0.43	-0.68 ± 0.46	-0.88 ± 0.45
18	1.10 ± 0.48	0.77 ± 0.41	-0.44 ± 0.19	-0.44 ± 0.51
19	0.42 ± 0.14	0.08 ± 0.18	-0.22 ± 0.14	-0.12 ± 0.27

Table C.9.: AV node: Mean and standard deviation of target motion in all phases of the heart-beat, relative to the reference phase. The values are taken from the contrast CTs of Pig 3.

motion phase	ABS [mm]	SI [mm]	AP [mm]	LR [mm]
01	0.97 ± 0.23	0.25 ± 0.24	-0.58 ± 0.14	-0.66 ± 0.30
02	3.86 ± 0.24	-0.46 ± 0.45	3.19 ± 0.54	-1.72 ± 1.06
03	3.38 ± 0.23	-0.62 ± 0.41	3.06 ± 0.18	-1.15 ± 0.48
04	2.87 ± 0.48	0.15 ± 0.20	1.97 ± 0.33	-2.06 ± 0.43
05	4.35 ± 0.10	-0.30 ± 0.41	3.88 ± 0.23	-1.85 ± 0.42
06	4.15 ± 0.14	0.08 ± 0.40	3.60 ± 0.26	-1.94 ± 0.54
07	3.84 ± 0.16	0.02 ± 0.31	3.40 ± 0.29	-1.68 ± 0.41
08	3.17 ± 0.17	0.04 ± 0.24	2.71 ± 0.24	-1.51 ± 0.55
09	3.84 ± 0.16	0.02 ± 0.31	3.40 ± 0.29	-1.68 ± 0.41
10	3.16 ± 0.13	0.28 ± 0.13	2.85 ± 0.20	-1.18 ± 0.59
11	3.40 ± 0.26	1.46 ± 0.54	2.18 ± 0.52	-1.91 ± 0.76
12	2.47 ± 0.37	0.04 ± 0.20	2.26 ± 0.20	-0.79 ± 0.68
13	1.56 ± 0.43	0.24 ± 0.39	1.24 ± 0.23	-0.70 ± 0.57
14	2.07 ± 0.44	0.06 ± 0.23	1.80 ± 0.30	-0.68 ± 0.78
15	2.30 ± 0.65	0.04 ± 0.26	0.60 ± 0.17	-2.20 ± 0.66
16	2.49 ± 0.63	-0.07 ± 0.17	0.19 ± 0.18	-2.47 ± 0.64
17	2.89 ± 0.74	-0.10 ± 0.13	0.41 ± 0.17	-2.84 ± 0.76
18	1.26 ± 0.26	-0.22 ± 0.11	0.73 ± 0.17	0.72 ± 0.72
19	0.85 ± 0.12	-0.18 ± 0.28	0.67 ± 0.14	0.34 ± 0.21

Table C.10.: PV: Mean and standard deviation of target motion in all phases of the heartbeat, relative to the reference phase. The values are taken from the contrast CTs of Pig 4.

motion phase	ABS [mm]	SI [mm]	AP [mm]	LR [mm]
01	0.52 ± 0.31	0.22 ± 0.31	0.29 ± 0.27	-0.07 ± 0.22
02	1.72 ± 0.39	0.09 ± 0.27	1.56 ± 0.32	-0.44 ± 0.53
03	2.21 ± 0.28	0.07 ± 0.29	1.96 ± 0.22	-0.73 ± 0.66
04	2.39 ± 0.23	0.22 ± 0.32	2.14 ± 0.33	-0.63 ± 0.75
05	2.48 ± 0.38	0.14 ± 0.34	2.24 ± 0.53	-0.37 ± 0.86
06	2.48 ± 0.56	0.14 ± 0.33	2.24 ± 0.71	-0.23 ± 0.86
07	2.38 ± 0.68	0.29 ± 0.33	2.12 ± 0.86	-0.25 ± 0.80
08	2.34 ± 0.80	0.41 ± 0.38	1.99 ± 1.00	-0.30 ± 0.86
09	2.38 ± 0.68	0.29 ± 0.33	2.12 ± 0.86	-0.25 ± 0.80
10	3.05 ± 1.06	0.70 ± 0.59	2.45 ± 1.36	-0.59 ± 1.19
11	3.13 ± 1.03	0.81 ± 0.67	2.64 ± 1.17	-0.49 ± 1.09
12	2.82 ± 0.80	0.80 ± 0.63	2.44 ± 0.84	-0.37 ± 0.87
13	2.38 ± 0.74	0.56 ± 0.62	2.19 ± 0.68	-0.08 ± 0.51
14	2.17 ± 0.63	0.45 ± 0.52	2.02 ± 0.58	0.13 ± 0.48
15	2.05 ± 0.45	0.22 ± 0.37	1.92 ± 0.46	0.30 ± 0.47
16	1.98 ± 0.41	-0.10 ± 0.43	1.79 ± 0.37	0.32 ± 0.68
17	1.68 ± 0.51	-0.03 ± 0.56	1.42 ± 0.41	0.41 ± 0.64
18	1.12 ± 0.43	-0.02 ± 0.32	0.87 ± 0.39	0.37 ± 0.54
19	0.48 ± 0.22	-0.11 ± 0.19	0.29 ± 0.29	0.09 ± 0.22

Table C.11.: CTI: Mean and standard deviation of target motion in all phases of the heartbeat, relative to the reference phase. The values are taken from the contrast CTs of Pig 4.

motion phase	ABS [mm]	SI [mm]	AP [mm]	LR [mm]
01	0.24 ± 0.07	0.11 ± 0.16	0.01 ± 0.11	0.07 ± 0.07
02	0.73 ± 0.16	0.55 ± 0.20	0.26 ± 0.29	-0.10 ± 0.24
03	1.47 ± 0.47	0.41 ± 0.41	1.19 ± 0.36	-0.59 ± 0.39
04	1.66 ± 0.47	0.50 ± 0.34	1.46 ± 0.37	-0.09 ± 0.59
05	2.18 ± 0.34	0.44 ± 0.26	2.04 ± 0.31	0.20 ± 0.54
06	2.64 ± 0.36	0.09 ± 0.13	2.55 ± 0.40	0.53 ± 0.39
07	2.63 ± 0.43	0.07 ± 0.26	2.54 ± 0.41	0.51 ± 0.43
08	2.70 ± 0.61	0.46 ± 0.48	2.56 ± 0.56	0.26 ± 0.52
09	2.63 ± 0.43	0.07 ± 0.26	2.54 ± 0.41	0.51 ± 0.43
10	3.52 ± 0.53	1.76 ± 0.65	2.86 ± 0.58	0.12 ± 0.75
11	3.52 ± 0.49	2.02 ± 0.56	2.71 ± 0.56	0.10 ± 0.74
12	3.67 ± 0.63	1.97 ± 0.51	2.96 ± 0.59	0.47 ± 0.64
13	3.95 ± 0.83	2.27 ± 0.59	3.12 ± 0.77	0.36 ± 0.57
14	3.11 ± 0.69	1.72 ± 0.66	2.44 ± 0.75	-0.17 ± 0.43
15	1.98 ± 0.40	0.98 ± 0.37	1.56 ± 0.51	-0.16 ± 0.53
16	1.42 ± 0.32	0.70 ± 0.29	1.05 ± 0.49	-0.34 ± 0.29
17	1.19 ± 0.32	0.55 ± 0.28	0.55 ± 0.38	-0.69 ± 0.46
18	0.94 ± 0.23	0.66 ± 0.25	0.02 ± 0.24	-0.54 ± 0.30
19	0.46 ± 0.20	0.12 ± 0.07	0.12 ± 0.20	-0.29 ± 0.31

Table C.12.: AV node: Mean and standard deviation of target motion in all phases of the heartbeat, relative to the reference phase. The values are taken from the contrast CTs of Pig 4.

motion phase	ABS [mm]	SI [mm]	AP [mm]	LR [mm]
01	0.27 ± 0.08	0.17 ± 0.05	-0.17 ± 0.12	0.01 ± 0.07
02	0.52 ± 0.18	0.11 ± 0.04	0.16 ± 0.25	-0.36 ± 0.27
03	2.19 ± 0.21	0.13 ± 0.17	1.99 ± 0.18	-0.82 ± 0.38
04	2.30 ± 0.23	0.17 ± 0.12	2.16 ± 0.22	-0.71 ± 0.27
05	2.30 ± 0.23	0.17 ± 0.08	2.22 ± 0.24	-0.52 ± 0.22
06	2.52 ± 0.32	0.24 ± 0.17	2.44 ± 0.32	-0.40 ± 0.36
07	2.42 ± 0.37	0.28 ± 0.10	2.32 ± 0.39	-0.50 ± 0.36
08	3.05 ± 0.33	0.42 ± 0.13	2.84 ± 0.40	-0.86 ± 0.52
09	2.42 ± 0.37	0.28 ± 0.10	2.32 ± 0.39	-0.50 ± 0.36
10	3.63 ± 0.67	0.77 ± 0.22	3.18 ± 0.44	-1.43 ± 0.81
11	3.49 ± 0.55	0.98 ± 0.20	3.16 ± 0.47	-0.95 ± 0.62
12	2.92 ± 0.60	1.03 ± 0.30	2.59 ± 0.47	-0.66 ± 0.59
13	2.39 ± 0.55	0.75 ± 0.31	2.16 ± 0.42	-0.56 ± 0.48
14	1.96 ± 0.40	0.65 ± 0.18	1.72 ± 0.34	-0.54 ± 0.41
15	2.04 ± 0.46	0.40 ± 0.21	1.67 ± 0.28	-1.04 ± 0.48
16	2.01 ± 0.39	0.69 ± 0.27	1.37 ± 0.25	-1.24 ± 0.40
17	1.31 ± 0.38	0.64 ± 0.24	0.62 ± 0.20	-0.89 ± 0.41
18	0.74 ± 0.40	0.55 ± 0.31	0.09 ± 0.27	-0.36 ± 0.31
19	0.41 ± 0.15	0.13 ± 0.09	-0.06 ± 0.19	-0.26 ± 0.25

C.2 Motion of AV node in native CT scan

The mean relative displacement of the AV node to the reference phase zero of the native CT scan of Pig 3 will be shown for the three studied motion directions (SI: superior-inferior, AP: anterior-posterior, LR: left-right) and the absolute (ABS) displacement.

Table C.13.: AV node: Mean and standard deviation of target motion in all phases of the heart-beat, relative to the reference phase. The values are taken from the native CTs of Pig 3.

motion phase	ABS [mm]	SI [mm]	AP [mm]	LR [mm]
01	0.07 ± 0.02	0.01 ± 0.03	-0.03 ± 0.03	-0.02 ± 0.03
02	0.12 ± 0.06	0.09 ± 0.06	0.04 ± 0.04	-0.04 ± 0.03
03	0.09 ± 0.05	-0.02 ± 0.03	0.05 ± 0.05	-0.01 ± 0.06
04	0.19 ± 0.07	0.13 ± 0.07	0.09 ± 0.08	0.03 ± 0.05
05	0.16 ± 0.07	0.05 ± 0.07	0.11 ± 0.08	-0.00 ± 0.06
06	0.18 ± 0.08	0.12 ± 0.10	0.06 ± 0.08	-0.01 ± 0.05
07	0.19 ± 0.08	0.16 ± 0.09	0.03 ± 0.05	-0.04 ± 0.05
08	0.13 ± 0.05	0.06 ± 0.08	-0.01 ± 0.05	-0.06 ± 0.06
09	0.19 ± 0.08	0.16 ± 0.09	0.03 ± 0.05	-0.04 ± 0.05
10	0.17 ± 0.05	0.10 ± 0.05	-0.10 ± 0.08	-0.03 ± 0.07
11	0.16 ± 0.07	0.05 ± 0.03	-0.12 ± 0.08	0.05 ± 0.05
12	0.23 ± 0.08	0.11 ± 0.03	-0.14 ± 0.09	0.11 ± 0.06
13	0.13 ± 0.04	-0.00 ± 0.05	-0.06 ± 0.08	0.06 ± 0.05
14	0.10 ± 0.04	-0.05 ± 0.02	0.01 ± 0.07	0.03 ± 0.06
15	0.11 ± 0.05	0.01 ± 0.04	0.01 ± 0.07	-0.01 ± 0.09
16	0.12 ± 0.06	0.03 ± 0.03	0.04 ± 0.07	-0.02 ± 0.10
17	0.08 ± 0.04	-0.01 ± 0.03	0.01 ± 0.07	-0.01 ± 0.04
18	0.10 ± 0.04	-0.06 ± 0.03	-0.00 ± 0.06	-0.03 ± 0.03
19	0.05 ± 0.02	0.01 ± 0.03	-0.02 ± 0.04	-0.00 ± 0.03

Values of dose analysis parameters for all pigs

In the following the D5-D95, V95 and V107 values will be presented for the irradiation of the AV node in all porcine data sets (pig 1 to 4). All studied techniques (static, interplay and rescanning with five, ten and fifteen rescans) will be shown for four different motion patterns and for the studied safety margin of 5mm.

Table C.14.: Pig 1, AV node: Dose analysis parameters D5-D95 (dose homogeneity), V95 (dose coverage) and V107 (over dosage) for all studied techniques and motion patterns for an irradiation with 5mm margin.

Case	motion period	motion starting phase	Margin	rescan no.	D5-D95 [%]	V95 [%]	V107 [%]
STATIC	-	-	5mm	-	5.66	100.00	0.00
INTERPLAY	0.7s	0	5mm	-	13.94	100.00	51.85
INTERPLAY	0.7s	90	5mm	-	13.64	90.74	6.67
INTERPLAY	0.5s	0	5mm	-	16.37	73.33	4.81
INTERPLAY	0.5s	90	5mm	-	8.19	100.00	32.96
RESCANNING	0.7s	0	5mm	5	11.09	100.00	9.63
RESCANNING	0.7s	90	5mm	5	7.08	100.00	0.00
RESCANNING	0.5s	0	5mm	5	8.55	93.70	0.00
RESCANNING	0.5s	90	5mm	5	11.01	97.41	3.33
RESCANNING	0.7s	0	5mm	10	6.26	100.00	0.00
RESCANNING	0.7s	90	5mm	10	4.70	100.00	0.00
RESCANNING	0.5s	0	5mm	10	5.79	100.00	0.00
RESCANNING	0.5s	90	5mm	10	4.24	100.00	0.00
RESCANNING	0.7s	0	5mm	15	4.88	100.00	0.00
RESCANNING	0.7s	90	5mm	15	3.91	100.00	0.00
RESCANNING	0.5s	0	5mm	15	5.37	100.00	0.00
RESCANNING	0.5s	90	5mm	15	5.80	100.00	0.00

Table C.15.: Pig 2, AV node: Dose analysis parameters D5-D95 (dose homogeneity), V95 (dose coverage) and V107 (over dosage) for all studied techniques and motion patterns for an irradiation with 5mm margin.

Case	motion period	motion starting phase	Margin	rescan no.	D5-D95 [%]	V95 [%]	V107 [%]
STATIC	-	-	5mm	-	4.41	100.00	0.00
INTERPLAY	0.7s	0	5mm	-	7.20	97.55	0.00
INTERPLAY	0.7s	90	5mm	-	6.19	99.02	0.00
INTERPLAY	0.5s	0	5mm	-	9.33	91.18	0.00
INTERPLAY	0.5s	90	5mm	-	10.90	99.51	4.90
RESCANNING	0.7s	0	5mm	5	5.65	100.00	3.43
RESCANNING	0.7s	90	5mm	5	8.20	43.63	0.00
RESCANNING	0.5s	0	5mm	5	5.66	100.00	0.00
RESCANNING	0.5s	90	5mm	5	7.24	99.51	0.00
RESCANNING	0.7s	0	5mm	10	3.66	100.00	0.00
RESCANNING	0.7s	90	5mm	10	7.90	98.53	0.00
RESCANNING	0.5s	0	5mm	10	6.20	100.00	9.31
RESCANNING	0.5s	90	5mm	10	4.03	100.00	0.00
RESCANNING	0.7s	0	5mm	15	4.35	100.00	0.00
RESCANNING	0.7s	90	5mm	15	6.98	100.00	0.00
RESCANNING	0.5s	0	5mm	15	7.27	99.51	0.00
RESCANNING	0.5s	90	5mm	15	3.61	100.00	0.00

Table C.16.: Pig 3, AV node: Dose analysis parameters D5-D95 (dose homogeneity), V95 (dose coverage) and V107 (over dosage) for all studied techniques and motion patterns for an irradiation with 5mm margin.

Case	motion period	motion starting phase	Margin	rescan no.	D5-D95 [%]	V95 [%]	V107 [%]
STATIC	-	-	5mm	-	2.20	100.00	0.00
INTERPLAY	0.7s	0	5mm	-	5.64	55.88	0.00
INTERPLAY	0.7s	90	5mm	-	6.98	100.00	0.00
INTERPLAY	0.5s	0	5mm	-	8.83	92.94	0.00
INTERPLAY	0.5s	90	5mm	-	5.22	100.00	0.00
RESCANNING	0.7s	0	5mm	5	8.49	98.24	0.00
RESCANNING	0.7s	90	5mm	5	7.13	100.00	0.00
RESCANNING	0.5s	0	5mm	5	5.68	100.00	77.65
RESCANNING	0.5s	90	5mm	5	4.27	51.76	0.00
RESCANNING	0.7s	0	5mm	10	4.89	100.00	0.00
RESCANNING	0.7s	90	5mm	10	6.22	100.00	0.00
RESCANNING	0.5s	0	5mm	10	4.42	100.00	0.00
RESCANNING	0.5s	90	5mm	10	3.42	100.00	0.00
RESCANNING	0.7s	0	5mm	15	5.85	99.41	0.00
RESCANNING	0.7s	90	5mm	15	5.57	100.00	0.00
RESCANNING	0.5s	0	5mm	15	4.70	100.00	0.00
RESCANNING	0.5s	90	5mm	15	5.38	100.00	0.00

Table C.17.: Pig 4, AV node: Dose analysis parameters D5-D95 (dose homogeneity), V95 (dose coverage) and V107 (over dosage) for all studied techniques and motion patterns for an irradiation with 5mm margin.

Case	motion period	motion starting phase	Margin	rescan no.	D5-D95 [%]	V95 [%]	V107 [%]
STATIC	-	-	5mm	-	5.53	100.00	0.00
INTERPLAY	0.7s	0	5mm	-	13.82	83.67	0.00
INTERPLAY	0.7s	90	5mm	-	12.81	74.29	0.41
INTERPLAY	0.5s	0	5mm	-	17.58	80.61	17.14
INTERPLAY	0.5s	90	5mm	-	21.75	44.49	0.00
RESCANNING	0.7s	0	5mm	5	6.79	100.00	0.00
RESCANNING	0.7s	90	5mm	5	7.08	96.73	0.00
RESCANNING	0.5s	0	5mm	5	4.90	86.33	0.00
RESCANNING	0.5s	90	5mm	5	7.90	100.00	3.47
RESCANNING	0.7s	0	5mm	10	5.25	100.00	0.00
RESCANNING	0.7s	90	5mm	10	5.95	97.76	0.00
RESCANNING	0.5s	0	5mm	10	5.09	100.00	0.20
RESCANNING	0.5s	90	5mm	10	5.44	98.37	0.00
RESCANNING	0.7s	0	5mm	15	4.99	100.00	0.00
RESCANNING	0.7s	90	5mm	15	5.55	100.00	0.00
RESCANNING	0.5s	0	5mm	15	2.96	100.00	0.00
RESCANNING	0.5s	90	5mm	15	4.69	100.00	0.00



Bibliography

- [AAPM10] Benedict SH, Yenice KM, Followill D, Galvin JM, Hinson W, Kavanagh B, Keall P, Lovelock M, Meeks S, Papiez L, Purdie T, Sadagopan R, Schell MC, Salter B, Schlesinger DJ, Shiu AS, Solberg T, Song DY, Stieber V, Timmerman R, Tome WA, Verellen D, Wang L, Yin FF: Stereotactic body radiation therapy: the report of AAPM Task Group 101; *Med. Phys.*; 37(8); 2010
- [ACC06] Bonow RO et al: ACC/AHA 2006 Guidelines for the Management of Patients With Valvular Heart Disease; *J. Am. Coll. Cardiol.*; 48(3); 2006
- [afib] Atrial fibrillation Resources for patients, a-fib.com
- [Ahl80] Ahlen SP: Theoretical and experimental aspects of the energy loss of relativistic heavily ionizing particles; *Rev. Mod. Phys.*; 52(1); 121; 1980
- [Alp98] Alpen EL: Radiation Biophysics; Academic Press; 2nd edition; 1998
- [Ama04] Amaldia U: CNAO - the Italian centre for light ion therapy; *Radiother. Oncol.*; 73(Supplement 2); 191-201; 2004
- [amc] Arthur's Medical Clipart, arthursclipart.org
- [Ami06] Amino M, Yoshioka K, Tanabe T, Tanaka E, Mori H, Furusawa Y, Zareba W, Yamazaki M, Nakagawa H, Honjo H, Yasui K, Kamiya K, Kodama I: Heavy ion radiation up-regulates Cx43 and ameliorates arrhythmogenic substrates in hearts after myocardial infarction; *Cardiovasc. Res.*; 72(3); 412-421; 2006
- [Ami10] Amino M, Yoshioka K, Fujibayashi D, Hashida T, Furusawa Y, Zareba W, Ikari Y, Tanaka E, Mori H, Inokuchi S, Kodama I, Tanabe T: Year-long upregulation of connexin43 in rabbit hearts by heavy ion irradiation; *Am. J. Physiol. Heart Circ. Physiol.*; 298(3); H1014-21; 2010
- [Aok04] Aoka Y, Kamada T, Kawana M, Yamada Y, Nishikawa T, Kasanuki H and Tsujii H: Primary cardiac angiosarcoma treated with carbon-ion radiotherapy; *Lancet Oncol.*; 5(10); 636-638; 2004
- [Bar63] Barkas H.W.: Nuclear Research Emulsions; Vol.I; Academic Press New York and London; 1963

- [Ben98] Benjamin EJ, Wolf PA, D'Agostino RB, Silbershatz H, Kannel WB, Levy D. Impact of atrial fibrillation on the risk of death: the Framingham Heart Study; *Circulation*; 98(10); 946-952; 1998
- [Bent12] Bentefour el H, Shikui T, Prieels D, Lu HM: Effect of tissue heterogeneity on an in vivo range verification technique for proton therapy; *Phys. Med. Biol.*; 57(17); 5473-5484; 2012
- [Ber05] Bert C, Metheny KG, Doppke K, Chen GT: A phantom evaluation of a stereovision surface imaging system for radiotherapy patient setup; *Med. Phys.*; 32(9); 2753-2762; 2005
- [Ber06] Bert C: Bestrahlungsplanung für bewegte Zielvolumina in der Tumortherapie mit gescanntem Kohlenstoffstrahl; Dissertation; TU Darmstadt; 2006
- [Ber07] Bert C, Saito N, Schmidt A, Chaudhri N, Schardt D and Rietzel E: Target motion tracking with a scanned particle beam; *Med. Phys.*; 34(12); 4768-4771; 2007
- [Ber07b] Bert C and Rietzel E: 4D treatment planning for scanned carbon ion beams; *Radiat. Oncol.*; 2(24); 2007
- [Ber08] Bert C, Groezinger SO and Rietzel E: Quantification of interplay effects of scanned particle beams and moving targets; *Phys. Med. Biol.*; 53(9); 2253-2265; 2008
- [Ber09] Bert C, Gemmel A, Saito N and Rietzel E: Gated irradiation with scanned particle beams; *Int. J. Radiat. Oncol. Biol. Phys.*; 73(4); 1270-1275; 2009
- [Ber09b] Bert C, Gemmel A, Chaudhri N, Lüechtenborg R, Saito N, Durante M and Rietzel E: Rescanning to mitigate the impact of motion in scanned particle therapy; *GSI Scientific Report*; 397; 2008
- [Ber10] Bert C, Gemmel A, Saito N, Chaudhri N, Schardt D, Durante M, Kraft G and Rietzel E: Dosimetric precision of an ion beam tracking system; *Radiat. Oncol.*; 5(1); 61; 2010
- [Ber11] Bert C and Durante M: Motion in radiotherapy: particle therapy; *Phys. Med. Biol.*; 56(16); 2011
- [Ber12] Bert C, Engenhart-Cabillic R and Durante M: Particle therapy for noncancer diseases; *Med. Phys.*; 39(4); 2012
- [Bet30] Bethe H: Zur Theorie des Durchgangs schneller Korpuskularstrahlung durch Materie; *Annalen der Physik*; 5(5); 325-400; 1930

- [Bik11] Bikou O, Thomas D, Trappe K, Lugenbiel P, Kelemen K, Koch M, Soucek R, Voss F, Becker R, Katus HA, Bauer A: Connexin 43 gene therapy prevents persistent atrial fibrillation in a porcine model; *Cardiovasc. Res.*; 92(2); 2011
- [Bis65] Bishop VS, Stone HL, Yates J, Simek J, Davis JA: Effects of external irradiation of the heart on cardiac output, venous pressure and arterial pressure; *J. Nucl. Med.*; 6(9); 1965
- [Bla13] Blanck O, Bode F, Gebhard M, Hunold P, Brandt S, Bruder R, Schweikard A, Grossherr M, Rades D and Dunst J: Radiochirurgisch erzeugte Läsionen im Antrum der Pulmonarvenen: Vorläufige Ergebnisse im Tiermodell und mögliche Implikationen für die Behandlung von Vorhofflimmern [abstract]; DEGRO 2013
- [Blo33] Block F: Bremsvermögen von Atomen mit mehreren Elektronen; *Zeitschrift der Physik A Hadrons and Nuclei*; 81(5); 285-321; 1933
- [Boe12] Boersma LV et al.: Atrial fibrillation catheter ablation vs. surgical ablation treatment (FAST): a 2-center randomized clinical trial; *Circulation*; 125(1); 23-30; 2005
- [Bor11] Borian G et al.: Italian AT-500 Registry Investigators. Improving stroke risk stratification using the CHADS₂ and CHADS₂-VASc risk score in patients with paroxysmal atrial fibrillation by continuous arrhythmia burden monitoring; *Stroke*; 42(6); 1768-1770; 2011
- [Bor40] Bohr N: Scattering and stopping of fission fragments; *Phys.Rev.*; 58(7); 654-655; 1940
- [Bro07] Brock et al.: Image Registration in IMRT, IGRT and SBRT; in C. Meyer (ed): *IMRT-IGRT-SBRT*; *Front. Radiat. Ther. Oncol.*; Karger; 2007
- [Bro10] Brock KK: Results of multi-institution deformable registration accuracy study (midras); *Int. J. Radiat. Oncol. Biol. Phys.*; 76(2); 538-596; 2010
- [Buc05] Bucci MK, Bevan A and Roach M: Advances in radiation therapy: Conventional to 3D, to IMRT, to 4D, and beyond; *CA: A Cancer Journal for Clinicians*; 55(2); 117-134; 2005
- [bw] <http://www.biosensewebster.com/cart3.php>
- [Cap05] Cappato R et al: Worldwide Survey on the Methods, Efficacy, and Safety of Catheter Ablation for Human Atrial Fibrillation; *Circulation*; 111(9); 1100-1105; 2005
- [Cap10] Cappato R, Calkins H, Chen SA, Davies W, Iesaka Y, Kalman J, Kim YH, Klein G, Natale A, Packer D, Skanes A, Ambrogi F and Biganzoli E: Updated Worldwide Sur-

- vey on the Methods, Efficacy, and Safety of Catheter Ablation for Human Atrial Fibrillation; *Circ. Arrhythm. Electrophysiol.*; 3(1); 32-38; 2010
- [Car76] Carmel RJ, Kaplan HS: Mantle irradiation in Hodgkin's disease. An analysis of technique, tumor eradication, and complications; *Cancer*; 37(6); 1976
- [Cara07] Carabe-Fernandez A, Dale RG and Jones B: The incorporation of the concept of minimum RBE (RbEmin) into the linear-quadratic model and the potential for improved radiobiological analysis of high-LET treatments; *Int. J. Radiat. Biol.*; 83(1); 27-39; 2007
- [CE09] Zipes and Jalife: *Cardiac Electrophysiology: From Cell to Bedside*; Saunders Elsevier; 5th Edition; 2009
- [Cha76] Chatterjee A and Schaefer HJ: Microdosimetric structure of heavy ion tracks in tissue; *Radiat. Environ. Biophys.*; 13(3); 215-227; 1976
- [Chr13] Christodouleas JP, Tang S, Susil RC, McNutt TR, Song DY, Bekelman J, Deville C, Vapiwala N, Deweese TL, Lu HM, Both S: The effect of anterior proton beams in the setting of a prostate-rectum spacer; *Med. Dosim.*; 38(3); 2013
- [Chu93] Chu WT, Ludewigt BA and Renner TR: Instrumentation for treatment of cancer using protons and light-ion beams; *Rev. Sci. Instrum.*; 64; 2055; 1993
- [Com10] Combs SE, Jäkel O, Haberer T, Debus J: Particle therapy at the Heidelberg Ion Therapy Center (HIT) - Integrated research-driven university-hospital-based radiation oncology service in Heidelberg, Germany; *Radiother. Oncol.*; 95(1); 41-44; 2010
- [Com11] Combs SE, Habermehl D, Ganter T, Schmidt J, Edler L, Burkholder I, Jäkel O, Haberer T and Debus J: Phase i study evaluating the treatment of patients with hepatocellular carcinoma (HCC) with carbon ion radiotherapy: The PROMETHEUS-01 trial; *BMC Cancer*; 11; 2011
- [Coo91] Cooper DKC, Ye Y, Rolf LL, Zuhdi N: The pig as potential organ donor for man. In *Xenotransplantation: The Transplantation of Organs and Tissues Between Species* (ed. Cooper DKC, Kemp E, Reemtsma K, White DJG); pp. 480-500; Springer; 1991
- [Cot05] Cotton JM, Rance K, Patil A and Thomas MR: Intracoronary brachytherapy for the treatment of complex in-stent restenosis; *Heart*; 91(2); 231-231; 2005
- [Cri98] Crick SJ, Sheppard MN, Ho SY, Gebstein L, Anderson RH: Anatomy of the pig heart: comparisons with normal human cardiac structure; *J. Anat.*; 193(Pt 1); 105-119; 1998

- [CTS13] cts.usc.edu/mazeprocedure.html; Cardiothoracic surgery, University of Southern Carolina Keck School of Medicine; 2013
- [Dar13] Darby SC, Ewertz M, McGale P, Bennet AM, Blom-Goldman U, Brnnum D, Correa C, Cutter D, Gagliardi G, Gigante B, Jensen MB, Nisbet A, Peto R, Rahimi K, Taylor C, Hall P: Risk of ischemic heart disease in women after radiotherapy for breast cancer; *N. Engl. J. Med.*; 368(11); 2013
- [Dou72] Douglas WR: Of pigs and men and research: a review of applications and analogies of the pig, *Sus scrofa*, in human medical research; *Space Life Sciences*; 3(3); 226-234; 1972
- [Doug06] Douglas YL, Jongbloed MR, Gittenbergerde Groot AC et al: Histology of vascular myocardial wall of left atrial body after pulmonary venous incorporation; *Am. J. Cardiol.*; 97(5); 662-670; 2006
- [Ect08] Ector J, De Buck S, Loeckx D, Coudyzer W, Maes F, Dymarkowski S, Bogaert J, Heidbüchel H: Changes in left atrial anatomy due to respiration: impact on three-dimensional image integration during atrial fibrillation ablation; *J. Cardiovasc. Electrophysiol.*; 19(8); 828-34; 2008
- [Efs56] Efskind D: The Effect of Massive X-ray Doses to the Mediastinum, Especially the Heart; Norsk Hydro's Institute for Cancer Research Report 1954-1956; pp. 13-14; 1956
- [Ele12] Eley J, Graeff C, Lüchtenborg R, Durante M, Howell R, Newhauser W and Bert C: 4D Optimization for Scanned Ion Beam Tracking Therapy for Moving Tumors; *Med. Phys.*; 39(6); 3970; 2012
- [Ema91] Emami B, Lyman J, Brown A, Coia L, Goitein M, Munzenrider JE, Shank B, Solin LJ, Wesson M: Tolerance of normal tissue to therapeutic irradiation; *Int. J. Radiat. Oncol. Biol. Phys.*; 21(1); 1991
- [Eng11] Engelsman M and Bert C: Precision and Uncertainties in Proton Therapy for Moving Targets; in Paganetti H: Proton Therapy Physics; Taylor & Francis; 2011
- [Eva08] Evans PM: Anatomical imaging for radiotherapy; *Phys. Med. Bio.*; 53(12); 151-191; 2008
- [ESC10] ESC Guidelines for the management of atrial fibrillation: The task force for the Management of Atrial Fibrillation of the European Society of Cardiology (ESC); *Eur. Heart J.*; 31; 2369-2429; 2010

- [ESC12] 2012 focused update of the ESC Guidelines for the management of atrial fibrillation: An update of the 2010 ESC Guidelines for the management of atrial fibrillation; Eur. Heart J.; 33(21); 2719-472; 2012
- [Faj70] Fajardo LF and Stewart JR: Capillary Injury Preceding Radiation-Induced Myocardial Fibrosis; Radiology; 101; 1971
- [Faj73] Fajardo LF and Stewart JR: Pathogenesis of radiation-induced myocardial fibrosis; Laboratory Investigation; 29(2); 244; 1973
- [Fie10] Fiedler F, Shakirin G, Skowron J, Braess H, Crespo P, Kunath D, Pawelke J, Pönisch F and Enghardt W: On the effectiveness of ion range determination from in-beam PET data; Phys. Med. Bio.; 55(7); 2010
- [Fle] <http://flexikon.doccheck.com/de/CHA2DS2-VASc-Score>
- [Fok04] Fokdal L et al.: Impact of changes in bladder and rectal filling volume n organ motion and dose distribution of the bladder in radiotherapy for urinary bladder cancer; Int. J. Radiat. Oncol. Biol. Phys.; 59(2); 436-444; 2004
- [Fox09] Fox CS et al.: Parental atrial fibrillation as a risk factor for atrial fibrillation in offspring; JAMA 291; 2851-2855; 2004
- [Fri12] Friberg L et al.: Evaluation of risk stratification schemes for ischemic stroke and bleeding in 182 678 patients with atrial fibrillation: the Swedish Atrial Fibrillation Cohort study; Eur. Heart J.; 33(12); 1500-1510; 2012
- [Frie12] Friedmann PA: Hitting a moving target: Catheter ablation and respiration; Heart Rhythm; 9(7); 1048-1049; 2012
- [Fried13] Friedrich T, Grün R, Scholz U, Elsässer T, Durante M and Scholz M: Sensitivity analysis of the relative biological effectiveness predicted by the local effect model; Phys. Med. Biol.; 58(19); 6827-6849; 2013
- [Fur05] Furukawa T, Noda K, Uesugi TH, Naruse T, Shibuya S: Intensity control in RF-knockout extraction for scanning irradiation; Nucl. Inst & Meth. in Phys. Res. B; 240(1); 32-35; 2005
- [Fur07] Furukawa T, Inaniwa T, Sato S, Tomitani T, Minohara S, Noda K and Kanai T: Design study of a raster scanning system for moving target irradiation in heavy-ion radiotherapy; Med. Phys.; 34(3); 1085-1097; 2007
- [Fus06] Fuster V, Ryden LE, Cannom DS et al.: ACC/AHA/ESC 2006 guidelines for the management of patients with atrial fibrillation; Europace; 8(9); 651-745; 2006

- [Gag10] Gagliardi G, Constine LS, Moiseenko V, Correa C, Pierce LJ, Allen AM and Marks LB: Radiation dose-volume effects in the heart; *Int. J. Radiat. Oncol. Biol. Phys.*; 76(3 Suppl); 2010
- [Gai10] Gaita F, Caponi D, Pianelli M, Scaglione M, Toso E, Cesarani F, Boffano C, Gandini G, Valentini MC, De Ponti R, Halimi F and Leclercq JF: Radiofrequency catheter ablation of atrial fibrillation: A cause of silent thromboembolism? Magnetic resonance imaging assessment of cerebral thromboembolism in patients undergoing ablation of atrial fibrillation; *Circulation*; 122(17); 1667-1673; 2010
- [Gem11] Gemmel A, Rietzel E, Kraft G, Durante M and Bert C: Calculation and experimental verification of the RBE-weighted dose for scanned ion beams in the presence of target motion; *Phys. Med. Biol.*; 56(23); 2011
- [Gra12] Graeff C, Durante M and Bert C: Motion mitigation in intensity modulated particle therapy by internal target volumes covering range changes; *Med. Phys.*; 39(10); 6004-6013; 2012
- [Gra13] Graeff C, Constantinescu A, Lüchtenborg R, Durante M and Bert C: Multigating: 4D optimized beam tracking in scanned ion beam therapy; *Technol. Cancer Res. Treat.*, Epub ahead of print; 2013
- [Gri11] Grimm J, LaCouture T, Croce R, Yeo I, Zhu Y and Xue J: Dose tolerance limits and dose volume histogram evaluation for stereotactic body radiotherapy; *J. Appl. Clin. Med. Phys.*; 12(2); 2011
- [Gro04] Groezinger SO: Volume conformal irradiation of moving target volumes with scanned ion beams; Dissertation; TU Darmstadt; 2004
- [Gru12] Grün R, Friedrich T, Elsässer T, Krämer M, Zink K, Karger CP, Durante M, Engenhart-Cabillic R, Scholz M: Impact of enhancements in the local effect model (LEM) on the predicted RBE-weighted target dose distribution in carbon ion therapy; *Phys Med Biol.*; 57(22); 2012
- [Gys14] van Gysen K, Kneebone A, Alfieri F, Guo L, Eade T: Feasibility of and rectal dosimetry improvement with the use of SpaceOAR® hydrogel for dose-escalated prostate cancer radiotherapy; *J. Med. Imaging Radiat. Oncol.*; 2014
- [Hab93] Haberer T et al.: Magnetic Scanning System for Heavy Ion Therapy; *Nucl. Inst & Meth. in Phys. Res. A*; 330(1-2); 296-305; 1993
- [Hai98] Haïssagurre M, Jais P, Shah DC et al.: Spontaneous initiation of atrial fibrillation by ectopic beats originating in the pulmonary veins; *N. Engl. J. Med.*; 339(10); 659-666; 1998

- [Hai04] Haïssaguerre M, Sanders P, Hocini M, et al.: Changes in atrial fibrillation cycle length and inducibility during catheter ablation and their relation to outcome; *Circulation*; 109(24); 3007-3013; 2004
- [Hai05] Haïssaguerre M, Hocini M, Sanders P, et al.: Catheter ablation of long-lasting persistent atrial fibrillation: Clinical outcome and mechanisms of subsequent arrhythmias; *J. Cardiovasc. Electrophysiol.*; 16(11); 1138-1147; 2005
- [Hal06] Hall EJ and Giaccia AJ: Radiobiology for the Radiologist; Lippincott Williams & Wilkins; 6th Edition; 2006
- [Han93] Hancock SL, Tucker MA and Hoppe RT: Factors affecting late mortality from heart disease after treatment of Hodgkin's disease; *JAMA*; 270(16); 1993
- [Hanl99] Hanley J et al.: Deep inspiration breath-hold technique for lung tumors: the potential value of target immobilisation and reduced lung density in dose escalation; *Int. J. Radiat. Oncol. Biol. Phys.*; 45(3); 603-611; 1999
- [Has06] Hashimoto T et al.: Repeated proton beam therapy for hepatocellular carcinoma; *Int. J. Radiat. Oncol. Biol. Phys.*; 65(1); 196-202; 2006
- [Her13] Herm J et al.: Neuropsychological Effects of MRI-Detected Brain Lesions after Left Atrial Catheter Ablation for Atrial Fibrillation: Long Term Results of the MACPAF Study; *Circ. Arrhythm. Electrophysiol.*; 6(5); 843-50; 2013
- [Hil09] Hild S, Krämer M, Durante M and Bert C: Display functionality for TRIP; GSI Scientific Report; 492; 2009
- [Hof03] Hof H et al.: Stereotactic single-dose radiotherapy of stage I non-small cell lung cancer (nsclc); *Int. J. Radiat. Oncol. Biol. Phys.*; 56(2); 335-341; 2003
- [Hoo07] Hooning MJ, Botma A, Aleman BM, Baaijens MH, Bartelink H, Klijn JG, Taylor CW, van Leeuwen FE: Long-term risk of cardiovascular disease in 10-year survivors of breast cancer; *J. Natl. Cancer Inst.*; 99(5); 2007
- [Hug86] Hughes HC: Swine in cardiovascular research; *Laboratory Animal Science*; 36(4); 348-350; 1986
- [ICRU93] Quantities and units in radiation protection dosimetry; ICRU report 51
- [ICRU93a] Prescribing, Recording and Reporting Photon Beam Therapy; ICRU report 50
- [ICRU99] Prescribing, Recording and Reporting Photon Beam Therapy (Supplement to ICRU report 50); ICRU report 62

- [Inf05] Tumortherapie mit schweren Ionen, Physikalische und biologische Grundlagen, Technische Realisierung an der GSI, klinische Ergebnisse; Informationen für Studenten, Ärzte und Patienten; 2005
- [Iwa10] Iwata et al.: High-dose proton therapy and carbon-ion therapy for stage I non-small cell lung cancer; *Cancer*; 116(110); 2476-2485; 2010
- [Iwa10b] Iwata Y, Kadowaki T, Uchiyama H, Fujimoto T, Takada E, Shirai T, Furukawa T, Mizushima K, Takeshita E, Katagiri K, Sato S, Sano Y, Noda K: Multiple-energy operation with extended flattops at HIMAC; *Nucl. Inst & Meth. in Phys. Res. A*; 624(1); 2010
- [Jong05] Jongbloed MR, Dirksen MS, Bax JJ et al.: Atrial fibrillation: multi-detector row CT of pulmonary vein anatomy prior to radiofrequency catheter ablation - initial experience; *Radiology*; 234(3); 702-709; 2005
- [Kad12] Kaderka R, Schardt D, Durante M, Berger T, Ramm U, Licher J and La Tessa C: Out-of-field dose measurements in a water phantom using different radiotherapy modalities; *Phys. Med. Biol.*; 57(16); 5059-5074; 2012
- [Kea01] Kaell PJ, Kini VR, Vedem SS and Mohan R: Motion adaptive x-ray therapy: a feasibility study; *Phys. Med. Biol.*; 46(1); 1-10; 2001
- [Kea06] Keall PJ, Mageras GS, Balter JM, Emery RS, Forster KM, Jiang SB, Kapatoes JM, Low DA, Murphy MJ, Murray BR, Ramsey CR, Van Herk MB, Vedam SS, Wong JW, Yorke E: The management of respiratory motion in radiation oncology report of AAPM Task Group 76; *Med. Phys.*; 33(10); 2006
- [Kan04] Kanagaratnam P, Cherian A, Stanbridge RD, Glenville B, Severs NJ, Peters NS: Relationship between connexins and atrial activation during human atrial fibrillation; *J. Cardiovasc. Electrophysiol.*; 15(2); 206-216; 2004
- [Kat99] Katz R and Cucinotta E: Tracks to therapy; *Radiat. Meas.*; 31(1-6); 379-388; 1999
- [Kha10] Khan FM: The physics of radiation therapy; 4th edition; Lippincott Williams & Wilkins; 2010
- [Kie86] Kiefer J and Straaten H: A model of ion track structure based on classical collision dynamics; *Phys. Med. Biol.*; 31(11); 1201-1209; 1986
- [Kne08] Knecht S, Oelschlager C, Duning T, Lohmann H, Albers J, Stehling C, Heindel W, Breithardt G, Berger G, Ringelstein EB, Kirchhof P, Wersching H: Atrial fibrillation in stroke-free patients is associated with memory impairment and hippocampal atrophy; *Eur. Heart J.*; 29(17); 2125-2132; 2008

- [Kra92] Kraft G, Kraemer M, Scholz M: LET, track structure and models. A review; Radiat. Environ. Biophys.; 31(3); 161-180; 1992
- [Kra00] Kraft G: Tumor therapie with heavy charged particles; Progress in Particle and Nuclear Physics; 45; 473; 2000
- [Krae00] Krämer M, Jäkel O, Haberer T, Kraft G, Schardt D and Weber U: Treatment planning for heavy-ion radiotherapy: a physical beam model and dose optimization; Phys. Med. Biol.; 45(11); 3299-3317; 2000
- [Krae00b] Krämer M and Scholz M: Treatment planning for heavy-ion radiotherapy: calculation and optimization of biologically effective dose; Phys. Med. Biol.; 45(11); 3319-3330; 2000
- [Krae03] Krämer M et al.: The increased biological effectiveness of heavy charged particles: from radiobiology to treatment planning; Technol. Cancer. Res. Treat.; 2(5); 427-36; 2003
- [Krae10] Krämer M and Durante M: Ion beam transport calculations and treatment plans in particle therapy; Eur. Phys. J. D; 60; 195-202; 2010
- [Kub96] Kubo HD and Hill BC: Respiration gated radiotherapy treatment: a technical study; Phys. Med. Biol.; 41(1); 83-91; 1996
- [Kum12] Kumar S, Morton JB, Halloran K, Spence SJ, Wong MCG, Kistler PM and Kalman JM: Effect of respiration on catheter-tissue contact force during ablation of atrial arrhythmias; Heart Rhythm; 9(7); 2012
- [Lan01] Langen KM and Jones DTL: Organ motion and its management; Int. J. Radiat. Oncol. Biol. Phys.; 50(1); 265-278; 2001
- [Li06] Li T, Thorndyke B, Schreibmann E, Yang Y and Xing L: Model-based image reconstruction for four-dimensional PET; Med. Phys.; 33(5); 1288-1298; 2006
- [Lic05] Lickfett L, Dickfeld T, Kato R, Tandri H, Vasamreddy CR, Berger R, Bluemke D, Luderitz B, Halperin H, Calkins H: Changes of pulmonary vein orifice size and location throughout the cardiac cycle: dynamic analysis using magnetic resonance cine imaging; J. Cardiovasc. Electrophysiol.; 16(6); 2005
- [Lic06] Lickfett L, Hackenbroch M, Lewalter T, Selbach S, Schwab JO, Yang A, Balta O, Schrickel J, Bitzen A, Lüderitz B, Sommer T: Cerebral diffusion-weighted magnetic imaging: A tool to monitor the thrombogenicity of left atrial catheter ablation; J. Cardiovasc. Electrophysiol.; 17(1); 1-71 2006

- [Lil06] Lilley J: Nuclear Physics - Principles and Applications; Wiley; 2006
- [Lin12] Linz U: Ion Beam Therapy - Fundamentals, Technology and Clinical Applications; Springer; chapter 31: Online Irradiation Control by Mean of PET by Fiedler F, Kunath D, Priegnitz M and Enghardt W; p.535; 2012
- [Lip11] Lip GY: Stroke in atrial atrial fibrillation: epidemiology and thromboprophylaxis; *J. Thromb. Hearnost.*; 107; 1053-1065; 2011
- [Loe13] Loeffler JS and Durante M: Charged particle therapy–optimization, challenges and future directions; *Nat. Rev. Clin. Oncol.*; 10(7); 411-24; 2013
- [Lue12] Lüchtenborg R: Real-time dose compensation methods for scanned ion beam therapy of moving tumors; Dissertation; TU Darmstadt; 2012
- [Luj99] Lujan AE, Larsen EW, Balter JM and Haken RKT: A method for incorporating organ motion due to breathing into 3D dose calculations; *Med. Phys.*; 26(5); 1999
- [Lum66] Lumb GD: Experimentally induced cardiac failure in swine: pathological changes; *Swine in Biomedical Research* (ed. Bustad LK, McClellan RO); pp. 389-403; Pacific Northwest Laboratory, Seattle, Washington: Batelle Memorial Institute; 1966
- [Mad14] Madhavan M, Lehmann HI, Swale MK, Johnson SB, Parker KD, Curley M, Hindricks G and Packer DL: Impact of a Novel Heated Saline Augmented Needle Tip Catheter on Improving Ablative Lesion Penetration and Eliminating Deep Tissue Conducting Channels in Canine Infarcts; [abstract] (PO05-162); HRS Scientific Session; 2014
- [Mag11] Maguire P, Gardner E, Jack A, Zei P, Al-Ahmed A, Fajardo L, Ladich E and Takeda P: Cardiac radiosurgery (CyberHeart) for treatment of arrhythmia: physiologic and histopathologic correlation in the porcine model; *Cureus*; 3(8); 2011
- [Mar98] Martel MK, Sahijdak WM, Ten Haken RK, Kessler ML, Turrisi AT: Fraction size and dose parameters related to the incidence of pericardial effusions; *Int. J. Radiat. Oncol. Biol. Phys.*; 40(1); 1998
- [Marti13] Martinek M et al.: Asymptomatic cerebral lesions during pulmonary vein isolation under uninterrupted oral anticoagulation; *Europace*; 15(3); 325-331; 2013
- [Mayo] Atrial fibrillation: Health information, mayoclinic.com
- [Med] Seeley R.R., Stephans T.D and Tate P: Essentials of Anatomy and Physiology, McGraw-Hill International Edition; 6th edition; 2007
- [Med13] Medi C, Evered L, Silbert B, The A, Halloran K, Morton J, Kistler P, Kalman J: Subtle Post-Procedural Cognitive Dysfunction following Atrial Fibrillation Ablation; *J. Am. Coll. Cardiol.*; 62(6); 2013

- [Min00] Minohara S, Kanai T, Endo M, Noda K and Kanazawa M: Respiratory gated irradiation system for heavy-ion radiotherapy; *Int. J. Radiat. Oncol. Biol. Phys.*; 47(4); 1097-1103; 2000
- [Miy06] Miyasak Y, Barnes ME, Gersh BJ et al: Secular trends in incidences of atrial fibrillation in Olmsted County, Minnesota, 1980 to 2000, and implications on the projection for future prevalence; *Circulation*; 114(2); 119-125; 2006
- [Mol48] Molière G: Theorie der Streuung schneller geladener Teilchen II, Mehrfach- und Vielfachstreuung; *Zeitschrift für Naturforschung*; 3a; 78-97; 1948
- [Mon08] Monz M, Küfer KH, Bortfeld TR, Thieke C: Pareto navigation: algorithmic foundation of interactive multi-criteria IMRT planning; *Phys. Med. Biol.*; 53(4); 2008
- [Mor09] Mori S, Lu H, Wolfgang JA, Choi NC and Chen GTY: Effects of interfractional anatomical changes on water-equivalent pathlength in charged-particle radiotherapy of lung cancer; *J. Radiat. Res.*; 50(6); 513-519; 2009
- [Mue14] Muessig D: Re-scanning in scanned ion beam therapy in the presence of organ motion; Dissertation; TU Darmstadt; 2014
- [Nab09] Nabauer M et al.: The registry of the German Competence Network on atrial fibrillation: patient characteristics and initial management; *Eurospace*; 11(4); 423-434; 2009
- [Nak10] Nakamura K and Particle Data Group: Review of particle physics; *Journal of Physics G: Nuclear and Particle Physics*; 37(7A); 2010
- [Nat99] Nath R, Amols H, Coffey C, Duggan D, Jani S, Li Z, Schell M, Soares C, Whiting J, Cole PE, Crocker I and Schwartz R: Intravascular brachytherapy physics: Report of the AAPM Radiation Therapy Committee Task Group No. 60; *Med. Phys.*; 26(2); 1999
- [Neg01] Negoro Y et al: The effectiveness of an immobilization device in conformal radiotherapy for lung tumor: reduction of respiratory tumor movement and evaluation of the daily setup accuracy; *Int. J. Radiat. Oncol. Biol. Phys.*; 65(1); 107-111; 2001
- [Nie07] Nieder C, Schill S, Kneschaurek P, Molls M: Influence of different treatment techniques on radiation dose to the LAD coronary artery; *Radiat Oncol.*; 2:20; 2007
- [Nod96] Noda K, Kanazawa AI, Takada E, Torikoshi M, Araki N, Yoshizawa J, Sate K, Yamada S, Ogawa H, Itoh H, Noda A, Tomizawa M, Yoshizawa M: Slow beam extraction by a transverse RF field with AM and FM; *Nucl. Inst & Meth. in Phys. Res. A*; 374; 269-277; 1996

- [Nos05] Noseworthy PA, Malchano ZJ, Ahmed J, Holmvang G, Ruskin JN, and Reddy VY: The impact of respiration on left atrial and pulmonary venous anatomy: Implications for image-guided intervention; *Heart Rhythm*; 2(11); 1173-1178; 2005
- [Ole11] Olesen JB et al.: Validation of the risk stratification schemes for predicting stroke and thromboembolism in patients with atrial fibrillation: nationwide cohort study; *Br. Med. J.*; 342; 2011
- [Ole12] Olesen JB et al.: The value of the CHADS₂-VASc score for refining stroke risk stratification in patients with atrial fibrillation with a CHADS₂ score 0-1: a nationwide cohort study; *J. Thromb. Haernost.*; 107; 1172-1179; 2012
- [Oles62] Olesen KH: The natural history of 271 patients with mitral stenosis under medical treatment; *Br. Heart. J.*; 24(3); 349-357; 1962
- [Ora02] Oral H, Ozaydin M, Tada H, et al.: Mechanistic significance of intermittent pulmonary vein tachycardia in patients with atrial fibrillation; *J. Cardiovasc. Electrophysiol.*; 13(7); 645-650; 2002
- [Ora03] Oral H, Scharf C, Chugh A, et al.: Catheter ablation for paroxysmal atrial fibrillation: Segmental pulmonary vein ostial ablation versus left atrial ablation; *Circulation*; 108(19); 2355-2360; 2003
- [Ora04] Oral H, Chugh A, Lemola K, et al.: Noninducibility of atrial fibrillation as an end point of left atrial circumferential ablation for paroxysmal atrial fibrillation: A randomized study; *Circulation*; 110; 2797-2801; 2004
- [Ora06] Oral H, Pappone C, Chugh A, et al.: Circumferential pulmonary-vein ablation for chronic atrial fibrillation; *N. Engl. J. Med.*; 354; 934-941; 2006
- [Ouy04] Ouyang D, Bansch D, Ernst S, et al.: Complete isolation of left atrium surrounding the pulmonary veins: New insights from the double-Lasso technique in paroxysmal atrial fibrillation; *Circulation*; 110; 2090-2096; 2004
- [Ozh08] Ozhasoglu SC, Chen H, et al: Synchrony-CyberKnife respiratory compensation technology; *Med. Dosim.*; 33 (2); 117-123; 2008
- [Pat08] Patel AR, Fatemi O, Norton PT, West JJ, Helms AS, Kramer CM, Ferguson JD: Cardiac cycle-dependent left atrial dynamics: implications for catheter ablation of atrial fibrillation; *Heart Rhythm*; 5(6); 2008
- [Ped95] Pedroni E et al: The 200 MeV proton therapy project at the Paul Scherer Institute: conceptual design and practical realization; *Med. Phys*; 22(1); 37-53; 1995

- [Ped04] Pedroni E, Bearpark R, Bhringer T, Coray A, Duppich J, Forss S, George D, Grossmann M, Goitein G, Hilbes C, Jermann M, Lin S, Lomax A, Negrazus M, Schippers M, Kotle G: The PSI Gantry 2: a second generation proton scanning gantry; *Z Med Phys.*; 14(1); 25-34; 2004
- [Per06] Pérez-Castellano N et al.: Pathological effects of pulmonary vein β -radiation in a swine model; *J. Cardiovasc. Electrophysiol.*; 17; 662-669; 2006
- [Phil64] Phillips SJ, Reid JA and Rugh R: Electrocardiographic and pathologic changes after cardiac X-irradiation in dogs; *Am. Heart J.*; 68; 1964
- [Phi92] Phillips MH, Pedroni E, Blattmann H, Boehringer T, Corey A and Scheib S: Effects of respiratory motion on dose uniformity with a charged particle scanning method; *Phys. Med. Biol.*; 37(1); 223-233; 1992
- [Pol01] Polontchouk L, Haefliger J-A, Ebelt B, Schafer T, Stuhlmann D, Mehlhorn U et al: Effects of chronic atrial fibrillation on gap junction distribution in human and rat atria; *J. Am. Coll. Cardiol.*; 38; 883-891; 2001
- [Pra12] Prall M, Kaderka R, Jenne J, Saito N, Sarti C, Schwaab J and Bert C: Ion beam tracking using ultrasound motion detection; *GSI Scientific Report*; 2012
- [PTCOG13] <http://ptcog.web.psi.ch/ptcentres.html>; Overview of particle centers; 2013
- [Pot12] Potpara TS et al.: Reliable identification of 'truly low' thromboembolic risk in patients initially diagnosed with 'lone' atrial fibrillation: the Belgrade Atrial Fibrillation Study; *Circ. Arrhythm. Electrophysiol.*; 5; 319-326; 2012
- [QUANTEC10] Bentzen SM, Constine LS, Deasy JO, Eisbruch A, Jackson A, Marks LB, Ten Haken RK, Yorke ED: Quantitative Analyses of Normal Tissue Effects in the Clinic (QUANTEC): an introduction to the scientific issues; *Int. J. Radiat. Oncol. Biol. Phys.*; 76 (3 Suppl); 2010
- [Red11] Reddy VY, Neuzil P, Kautzner J, et al.: Low catheter-tissue contact force results in late PV reconnection - initial results from EFFICAS I [abstract]; *Heart Rhythm*; 8; S26; 2011
- [Ric13] Richter D, Schwarzkopf A, Trautmann J, Krämer M, Durante M, Jäkel O, Bert C: Upgrade and benchmarking of a 4D treatment planning system for scanned ion beam therapy; *Med. Phys.*; 40(5); 2013
- [Rie05] Rietzel E, Pan T and Chen GTY: Four-dimensional computed tomography: Image formation and clinical protocol; *Med. Phys.*; 32(4); 874-889; 2005

-
- [Rie10] Rietzel E and Bert C: Respiratory motion management in particle radiotherapy; Med. Phys.; 37(2); 449-460; 2010
- [Ric12] Richter D: Treatment planning for tumors with residual motion in scanned ion beam therapy; Dissertation; TU Darmstadt; 2012
- [Ric13] Richter D, Schwarzkopf A, Trautmann J, Krämer M, Durante M, Jäkel O, Bert C: Upgrade and benchmarking of a 4D treatment planning system for scanned ion beam therapy; Med. Phys.; 40(5); 2013
- [RPTC12] Erfahrungsbericht zweiter Monat klinischer Betrieb RPTC; Mai 2009; Internet Communication
- [RTOG] <http://www.rtog.org/>
- [RTOG0631] RTOG 0631 Protocol Information: Phase II/III Study of Image-Guided Radio-surgery/SBRT for Localized Spine Metastasis; 2011
- [RTOG0915] RTOG 0915 Protocol Information: A Randomized Phase II Study Comparing 2 Stereotactic Body Radiation Therapy (SBRT) Schedules for Medically Inoperable Patients with Stage I Peripheral Non-Small Cell Lung Cancer; 2010
- [Ruc13] Ruciński A, Bauer J, Campbell P, Brons S, Unholtz D, Habl G, Herfarth K, Debus J, Bert C, Parodi K, Jäkel O, Haberer T: Preclinical investigations towards the first spacer gel application in prostate cancer treatment during particle therapy at HIT; Radiat. Oncol.; 8:134; 2013
- [Sai09] Saito N, Bert C, Chaudhri N, Gemmel A, Schardt D and Rietzel E: Speed and accuracy of a beam tracking system for treatment of moving targets with scanned ion beams; Phys. Med. Biol.; 54; 4849-4862; 2009
- [Sch10] Schardt D, Elsaesser T and Schulz-Ertner D: Heavy ion tumor therapy: Physical and radiobiological benefits; Rev. Mod. Phys; 82(1); 383; 2010
- [Schl01] Schlegel W and Mahr A: 3D Conformal Radiation Therapy: Multimedia Introduction to Methods and Techniques; Springer; 2001
- [Scho94] Scholz M and Kraft G: Calculation of heavy ion inactivation probabilities based on track structure, x ray sensitivity and target size; Radiat. Prot. Dosim.; 52; 1-4; 1994
- [Scho96] Scholz M and Kraft G: Track structure and the calculation of biological effects of heavy charged particles; Adv. Space Res.; 18; 5-14; 1996
- [Schoe11] Schoemers C, Feldmeier E, Haberer T, Naumann J, Panse R and Peters A: Implementation of an intensity feedback-loop for an ion-therapy synchrotron; Prcoeedings of IPAC 2011; 2851-22853

-
- [Schu07] Schulz-Ertner D et al: Effectiveness of carbon ion radiotherapy in the treatment of skull-base chordomas; *Int. J. Radiat. Oncol. Biol. Phys.*; 68(2); 449-457; 2007
- [Schr10] Schrickel JW, Lickfett L, Lewalter T, Mittman-Braun E, Selbach S, Strach K, Nahle CP, Schwab JO, Linhart M, Andrie R, Nickenig G, Sommer T: Incidence and predictors of silent cerebral embolism during pulmonary vein catheter ablation for atrial fibrillation; *Europace*; 12; 52-57; 2010
- [Schw04] Schweikard A, Shiomi H and Adler J: Respiration tracking in radiosurgery; *Med. Phys.*; 31(10); 2738-2741; 2004
- [Sec09] Seco J, Robertson D, Trofimov A, Paganetti H: Breathing interplay effects during proton beam scanning: simulation and statistical analysis; *Phys. Med. Biol.*; 54(14); 2009
- [Ser13] Seregni M, Kaderka R, Fattori G, Riboldi M, Pella A, Constantinescu A, Saito N, Durante M, Cerveri P, Bert C, Baroni G: Tumor tracking based on correlation models in scanned ion beam therapy: an experimental study; *Phys. Med. Biol.*; 58(13); 2013
- [Sev04] Severs NJ, Coppen SR, Dupont E, Yeh H-I, Ko Y-S, Matsushita T: Gap junction alterations in human cardiac disease; *Cardiovas. Res.*; 62(2); 368-377; 2004
- [Sev08] Severs NJ, Bruce AF, Dupont E and Rothery S: Remodelling of gap junctions and connexin expression in diseased myocardium; *Cardiovas. Res.*; 80(1); 9-19; 2008
- [Sha10] Sharma A, Wong D, Weidlich G, Fogarty T, Jack A, Sumanaweera T, Maguire P: Noninvasive stereotactic radiosurgery (CyberHeart) for creation of ablation lesions in the atrium; *Heart Rhythm*; 7(6); 802-810; 2010
- [Shack10] Shackleford JA, Kandasamy N and Sharp GC: On developing B-spline registration algorithms for multi-core processors; *Phys. Med. Biol.*; 55(21); 2010
- [Shah10] Shah DC, Lambert H, Nakagawa H, Langenkamp A, Aeby N, Leo G: Area under the real-time contact force curve (force-time integral) predicts radiofrequency lesion size in an in vitro contractile model; *J. Cardiovasc. Electrophysiol.*; 21; 1038-1043; 2010
- [Shah11] Shah DC, Reddy VY, Kautzner J, et al.: Contact force during ablation predicts AF recurrence at 12 months [abstract]; *Heart Rhythm*; 8; S447-S448; 2011
- [Shar07] Sharp CG, Kandasamy N, Singh H and Folkert M: GPU-based streaming architectures for fast cone-beam CT image reconstruction and demons deformable registration; *Phys. Med. Biol.*; 52(19); 5771-5783; 2007

- [Sharp07] Sharp CG, Kandasamy N, Singh H and Folkert M: GPU-based streaming architectures for fast cone-beam CT image reconstruction and demons deformable registration; *Phys. Med. Biol.*; 52(19); 5771-5783; 2007
- [Son08] Sonke JJ, Lebesque J and van Herk M: Variability of four-dimensional computed tomography patient models; *Int. J. Radiat. Oncol. Biol. Phys.*; 70(2); 590-598; 2008
- [Song14] Song L, Lehmann HI, Cusma JT, Christner JA, Misiri J, Johnson SB, Parker KD, Takami M, Miller RC, Herman MG and Packer DL: Intensity Modulated Proton Therapy using Pencil Beam Scanning as a Catheter-free Ablation Approach: A 4D Treatment Planning Study in the Porcine Model; *HRS [abstract]*; 2014
- [Ste68] Stewart JR, Fajardo LF, Cohn K and Page V: Experimental Radiation-Induced Heart Disease in Rabbits; *Radiology*; 91; 1968
- [Tad98] Tada T et al.: Lung cancer: intermittent irradiation synchronized with respiratory motion - results of a pilot study; *Radiology*; 207; 779-783; 1998
- [Tay07] Taylor CW, Nisbet A, McGale P and Darby SC: Cardiac exposures in breast cancer radiotherapy: 1950s-1990s; *Int. J. Radiat. Oncol. Biol. Phys.*; 69(5); 2007
- [Tay08] Taylor CW, Povall JM, McGale P, Nisbet A, Dodwell D, Smith JT, Darby SC: Cardiac dose from tangential breast cancer radiotherapy in the year 2006; *Int. J. Radiat. Oncol. Biol. Phys.*; 72(2); 2008
- [Tia14] Tian J, Jeudy J, Smith MF, Jimenez A, Yin X, Bruce PA, Lei P, Turgeman A, Abbo A, Shekhar R, Saba M, Shorofsky S, Dickfeld T: Three-Dimensional Contrast-Enhanced Multidetector CT for Anatomic, Dynamic, and Perfusion Characterization of Abnormal Myocardium To Guide Ventricular Tachycardia Ablations; *Circ. Arrhythm. Electrophysiol.*; 3; 2010
- [Til14] Tilz RR, Makimoto H, Lin T, Rillig A, Deiss S, Wissner E, Mathew S, Metzner A, Rausch P, Kuck KH, Ouyang F: Electrical isolation of a substrate after myocardial infarction: a novel ablation strategy for unmappable ventricular tachycardias—feasibility and clinical outcome; *Europace*; Epub ahead of print; 2014
- [Tob58] Tobias CA et al: Pituitary irradiation with high energy proton beams: a preliminary report; *Cancer Research*; 18(2); 121-134; 1958
- [Tsu08] Tsunashima Y, Vedam S, Dong L, Umezawa M, Sakae T, Bues M, Balter P, Smith A, Mohan R: Efficiency of respiratory-gated delivery of synchrotron-based pulsed proton irradiation; *Phys. Med. Biol.*; 53(7); 2008

- [Van11] Van Staa TP et al.: A comparison of risk stratification schemes for stroke in 79,884 atrial fibrillation patients in general practice; *J. Thromb. Haernost.*; 9(1); 39-48; 2011
- [Vij10] Vijaykumar R, Locke AH, Ahmed H, Neuzil P, Lambert H, Reddy VY: Novel visualisation of catheter-tissue contact force during pulmonary vein isolation [abstract]. *Heart Rhythm*; 7; S100-S101; 2010
- [Vis13] Viswanathan AN, Damato AL, Nguyen PL: Novel use of a hydrogel spacer permits reirradiation in otherwise incurable recurrent gynecologic cancers; *J. Clin. Oncol.*; 31(34); 2013
- [Wat09] van de Water S, Kreuger R, Zenklusen S, Hug E and Lomax AJ: Tumour tracking with scanned proton beams: assessing the accuracy and practicalities; *Phys. Med. Biol.*; 54(21); 6549-6563; 2009
- [Web99] Weber U and Kraft G: Design and construction of a ripple filter for a smoothed depth dose distribution in conformal particle therapy. *Phys. Med. Biol.*; 44(11); 2765-2775; 1999
- [Wei08] Wei X, Liu HH, Tucker SL, Wang S, Mohan R, Cox JD, Komaki R, Liao Z: Risk factors for pericardial effusion in inoperable esophageal cancer patients treated with definitive chemoradiation therapy; *Int. J. Radiat. Oncol. Biol. Phys.*; 70(3); 2008
- [Wer04] Wertz H and Jäkel O: Influence of iodine contrast agent on the range of ion beams for radiotherapy; *Med Phys.*; 31(4); 767-73; 2004
- [Whi93] White D, Wallwork J: Xenografting: probability, possibility, or pipe-dream?; *Lancet*, 342(8876); 879-880; 1993
- [Wil46] Wilson RR: Radiobiological use of fast protons; *Radiology*; 47; 487-491; 1946
- [Woe11] Wölfelschneider J: Fraktionierte Bestrahlung bewegter Tumoren mit gescannten Schwerionen; Diplomarbeit; Technische Hochschule Mittelhessen; 2011
- [Wol91] Wolf PA, Abbott RD, Kannel WB: Atrial fibrillation as an independent risk factor for stroke: the Framingham study; *Stroke*; 22; 938-988; 1991
- [Yeh01] Yeh H-I, Lai Y-J, Lee S-H, Lee Y-N, Ko Y-S, Chen S-A et al: Heterogeneity of myocardial sleeve morphology and gap junctions in canine superior vena cava; *Circulation*; 104; 3152-3157; 2001
- [Yok08] Yokoyama K, Nakagawa H, Shah DC, et al.: Novel contact force sensor incorporated in irrigated radiofrequency ablation catheter predicts lesion size and incidence of steam pop and thrombus; *Circ. Arrhythm. Electrophysiol.*; 1; 354-362; 2008

-
- [Zen10] Zenklusen SM, Pedroni E and Meer D: A study on repainting strategies for treating moderately moving targets with proton pencil beam scanning at the new gantry 2 at PSI; *Phys. Med. Biol.*; 55(17); 5103-5121; 2010



Lebenslauf

Persönliche Daten

Name Anna Constantinescu
Geburtstag 31. August 1984
Geburtsort Bukarest, Rumänien
Nationalität Deutsch

Universitäre Ausbildung

- seit 11/2010 Mitglied der Helmholtz Graduate School for Hadron and Ion Research (HGS-HIRe)
- seit 11/2010 **TU Darmstadt**
Promotion (Durchführung an der GSI)
- 07/2007–07/2010 **TU Darmstadt**
Master of Science in Physik
Titel der Masterarbeit: (Durchführung an der GSI)
Optimisation of the ion range adaptation method for moving tumour treatment with ion beam tracking
- 07/2007–06/2008 **NTNU Trondheim**
Austausch im Rahmen des ERASMUS Programms
- 04/2004–07/2007 **TU Darmstadt**
Bachelor of Science in Physik
Titel der Bachelorarbeit:
Untersuchung der Ablenkeigenschaften eines Dipolmagneten und Entwicklung eines Teilchen-Raytracer

Schulische Ausbildung

- 08/1995–06/2004 **Gymnasium Gernsheim**, Gernsheim
08/1991–07/1995 **Insel Kühkopf Schule**, Stockstadt



Danksagungen

Ich möchte mich herzlich bei allen bedanken, die zum Gelingen dieser Arbeit beigetragen haben und die mich auf diesem Weg unterstützt haben. Prof. Gerhard Kraft danke ich für die Aufnahme in die Biophysik Abteilung, in der ich so viel gelernt habe und in der ich mich all die Jahre sehr wohl gefühlt habe. Prof. Marco Durante möchte ich für die Möglichkeit danken an diesem aufregenden Thema forschen zu dürfen. Des Weiteren möchte ich ihm für die Unterstützung und das Verständnis danken, die er mir auch in persönlich schweren Zeiten entgegen gebracht hat und in denen er mich ermutigt hat weiter zu machen. Prof. Christoph Bert danke ich für seine Betreuung und die lehrreichen und interessanten Jahre. Danke für die vielen Anmerkungen und Anregungen die entscheidend zum Gelingen dieser Arbeit beigetragen haben. Bei Dr. Christian Graeff möchte ich mich für die neue Leitung des "motion teams" bedanken, die die anregende Arbeitsatmosphäre erhalten hat. Außerdem danke ich ihm für die Hilfe und Anmerkungen bei der Entstehung dieser Arbeit, seine Crashkurse in statistischer Auswertung und für sein stets offenes Ohr. Ich danke auch PD Dr. Michael Krämer, ohne den all die Simulationen nie so schnell fertig geworden wären.

I would like to thank Dr. Douglas Packer and his team and colleagues from Mayo Clinic for the productive collaboration and the opportunity to work on this innovative idea. I especially thank Dr. Immo Lehmann for teaching me so much about cardiology as well as for his prompt answers and for all his support. Thank you to Dr. Limin Song and Dr. Amanda Deisher for their contributing work on photon treatments.

Natürlich bedanke ich mich auch bei der gesamten Biophysik und speziell bei unserer Arbeitsgruppe für die tolle Arbeitsatmosphäre. Das gilt natürlich auch für alle ehemaligen Mitglieder. Jeder einzelne von euch hat mich in diesen Jahren ein wenig geprägt und es war mir eine Freude euch kennenzulernen. Robert Kaderka und Matthias Prall danke ich für das sorgfältige Gelesen dieser Arbeit. Kristjan Anderle danke ich für das geduldige Einweisen in Slicer. Danke euch allen dafür, dass ich mich jeden Morgen gefreut habe in unser Büro zu kommen. Natürlich danke ich auch Daniel Richter und Sebastian Hild für ihre Hilfe in Softwarefragen. Außerdem danke ich allen, die mich in dieser arbeitsintensiven Zeit mit Süßigkeiten versorgt haben.

Besonders möchte ich mich auch bei meinen Eltern bedanken, die mich immer unterstützt haben und die mir mit ihren Ratschlägen weitergeholfen haben. Meinen Freunden, allen voran Matthias Holl, danke ich für die vielen lustigen Stunden.



Erklärung zur Dissertation

Hiermit versichere ich, die vorliegende Dissertation ohne Hilfe Dritter nur mit den angegebenen Quellen und Hilfsmitteln angefertigt zu haben. Alle Stellen, die aus Quellen entnommen wurden, sind als solche kenntlich gemacht. Diese Arbeit hat in gleicher oder ähnlicher Form noch keiner Prüfungsbehörde vorgelegen.

Darmstadt, den 23. April 2014

(Anna Constantinescu)

